JYVÄSKYLÄ STUDIES IN COMPUTING
198

Matti Kurki

The Stress-Strain State and Stabilization of Viscoelastoplastic, Imperfect Moving Web Continuum

JYVÄSKYLÄN YLIOPISTO

JYVÄSKYLÄ STUDIES IN COMPUTING 198

Matti Kurki

The Stress-Strain State and Stabilization of Viscoelastoplastic, Imperfect Moving Web Continuum

Esitetään Jyväskylän yliopiston informaatioteknologian tiedekunnan suostumuksella
julkisesti tarkastettavaksi yliopiston Agora-rakennuksen Gamma-salissa
lokakuun 24. päivänä 2014 kello 14.

Academic dissertation to be publicly discussed, by permission of
the Faculty of Information Technology of the University of Jyväskylä,
in building Agora, auditorium Gamma, on October 24, 2014 at 14 o'clock.

UNIVERSITY OF JYVÄSKYLÄ

JYVÄSKYLÄ 2014

The Stress-Strain State and Stabilization of Viscoelastoplastic, Imperfect Moving Web Continuum

JYVÄSKYLÄ STUDIES IN COMPUTING 198

Matti Kurki

The Stress-Strain State and Stabilization of Viscoelastoplastic, Imperfect Moving Web Continuum

UNIVERSITY OF JYVÄSKYLÄ

JYVÄSKYLÄ 2014

Editors
Timo Männikkö
Department of Mathematical Information Technology, University of Jyväskylä
Pekka Olsbo, Ville Korkiakangas
Publishing Unit, University Library of Jyväskylä

URN:ISBN:978-951-39-5856-5
ISBN 978-951-39-5856-5 (PDF)

ISBN 978-951-39-5855-8 (nid.)
ISSN 1456-5390

Jyväskylä University Printing House, Jyväskylä 2014

ABSTRACT

Kurki, Matti
The Stress-Strain State and Stabilization of Viscoelastoplastic, Imperfect Moving Web Continuum
Jyväskylä: University of Jyväskylä, 2014, 78 p.(+included articles)
(Jyväskylä Studies in Computing
ISSN 1456-5390; 198)
ISBN 978-951-39-5855-8 (nid.)
ISBN 978-951-39-5856-5 (PDF)
Finnish summary
Diss.

Successful handling of different web-like materials is the key issue in their production industry. The thesis completes the area of moving web research by introducing a continuation, where cross-scientific web handling issues are presented.

A fundamental aspect in all moving webs is their stress-strain behavior. A new theory for moving, viscoelastic web continuum is introduced. A system of third-order partial differential equations is developed modelling the moving solid continuum. The results show that strain distribution of the viscoelastic web is no longer constant. The two-dimensional solution is always nonlinear since the contraction couples the in-plane velocities U_x and U_y.

The effects of stress state to the divergence velocity limit of orthotropic moving web is presented. The minimal eigenvalue and the corresponding out-of-buckling mode and velocity are found. The buckling modes are localized at the edge areas of the web depending on the level of orthotropic properties. A new model of a coupled web-fluid environment utlizing steady-state potential fluid flow is also presented giving good results compared to the wind tunnel tests.

The thesis includes the effects of web edge imperfections on production efficiency. A new model for the fatigue life of a moving elastic web is introduced. An optimization procedure for web stress has been developed in order to find the optimum for maximizing the production performance of the web handling line.

In practice, the utilization of the web's stress-strain capability is limited by the web strength and the amount of irrecoverable strains. Additionally, a stress relaxation occurs in web materials. A measurement method for viscoelastic materials is introduced. Results show that relaxation of the web increases the irrecoverable strain of the web decreasing the strain potential for upcoming processes.

An example of an adaptive web stabilization using specialized roll is included in thesis. The air flow forming boundary layers to roll and fabric surfaces are utilized creating a underpressurizing suction through the fabric. This type of the roll enables a more simple web supporting arrangements.

Keywords: modelling, solid mechanics, moving continuum, continuum mechanics, viscoelasticity, stability, fluid-structure, runnability

Author

Matti Kurki
School of Technology
Jyväskylä University of Applied Sciences
Finland

Supervisors

Professor Pekka Neittaanmäki
Department of Mathematical Information Technology
University of Jyväskylä
Finland

Ph.D Juha Jeronen
Department of Mathematical Information Technology
University of Jyväskylä
Finland

Reviewers

Professor Emeritus Heikki Koivo
Department of Automation and Systems Technology
Aalto University
Finland

TkT Jouko Yli-Kauppila
Valmet Technologies Oy
Finland

Opponent

Professor Tetsu Uesaka
Department of Chemical Engineering
Mid Sweden University
Sundswall
Sweden

PREFACE

The scientific activities presented in this work were conceived during the author's employment at VTT Jyvãskylã and continued in Valmet AIR unit and later in Metso Paper Inc. between 1996 and 2007. One of the first tasks in Valmet Corp. was the speeding up the development of the runnability components for Valmet AIR for high-speed paper machines. At that time, the Valmet's Web Handling Competence Group (WHCG) was formed to improve the research of various kinds of web handling problems and to distribute that knowledge within the company. The group, lead by the author, included selected specialists throughout the Valmet Corp. Their expertise covered entire web handling line: from the raw materials and furnish optimization, through web elasticity enhancement, to the efficiency studies of different high speed printing machines.

During that time, new material measurement methods for web rheology were developed along with the extensive usage of different numerical tools, especially the CFD (Computational Fluid Dynamics). In several projects the numerical models developed increased the fundamental understanding of moving web behavior thus shortening significantly the development work for physical products. In several cases, the results given by the models allowed a complete realization of selected paper machinery components without the traditional (and expensive) physical prototype testing.

The topic of this research is motivated by a desire to understand better the basics of viscoelastic stress-strain behavior and to create a contribution to efficient production of various kinds of flat, web-like materials, where both the mechanical stability and the efficient use of raw materials play an important role. This thesis extends the previous work of the research group on web handling continuance, where different cross-scientific web handling items are thematically connected together by using their common contributor, the web stress state.

New insights to the questions of stress-strain state of the moving viscoelastic web, web stability, imperfectness, its viscoelastoplastic properties and adaptive stabilization technology are generated. These items are the building blocks of a thematic web handling continuance, which includes some of the most important items for successful, high-efficiency web production.

ACKNOWLEDGEMENTS

The body of this work was conceived at the University of Jyväskylä, Department of Mathematical Information Technology. The work, which orginally started 2010, was carried out in a research group lead by Professor Pekka Neittaanmäki from the University of Jyväskylä and Professor Nikolay Banichuk from the Russian Academy of Sciences. Other researchers in the group included Maria Tirronen M.Sc. and Doctors Juha Jeronen, Tytti Saksa, and Tero Tuovinen. Professor Neittaanmäki and Dr. Jeronen supervised this thesis.

A sincere Thank You to all the people who had contributed to this work. In the science and research there are basically only two things which one must remember:

"Tietä käyden tien on vanki,
vapaa on vain umpihanki"

– Aaro Hellaakoski

"Jos et kykene vaihtamaan mielipidettäsi,
et kykene oppimaan uusia asioitakaan"

– Prof. Arto Verho

NOMENCLATURE

Notation

$\mathcal{L}(w)$: $= D_1 \frac{\partial^4 w}{\partial x^4} + 2D_3 \frac{\partial^4 w}{\partial x^2 \partial y^2} + D_2 \frac{\partial^4 w}{\partial y^4}$
flexural stiffness of the orthotropic plate.

$\frac{\partial u}{\partial x}$: partial derivative of u with respect to x

$\frac{\mathrm{d}u(x,t)}{\mathrm{d}t} := \frac{\partial u(x,t)}{\partial t} + \frac{\mathrm{d}x}{\mathrm{d}t}\frac{\partial u(x,t)}{\partial x}$
total (material, Lagrange) derivative of $u(x,t)$ with respect to t, here often $\mathrm{d}x/\mathrm{d}t = V_0$ is constant

∇: $= \frac{\partial}{\partial \mathrm{x}} i + \frac{\partial}{\partial \mathrm{y}} j + \frac{\partial}{\partial \mathrm{z}} k$, gradient

ΔT: (small) change of T, variation of T

$(...)^T$: matrix transpose

Latin symbols

A: area. Unit $[A] = \mathrm{m}^2$

A_1: area at the begin state. Unit $[A_1] = \mathrm{m}^2$

A_2: area at the end state. Unit $[A_2] = \mathrm{m}^2$

a: length of edge crack. Unit $[a] = \mathrm{m}$

a_0: initial length of edge crack. Unit $[a_0] = \mathrm{m}$

a^{cr}: critical length of edge crack. Unit $[a^{cr}] = \mathrm{m}$

b: width of panel or half-width of plate. Unit $[b] = \mathrm{m}$

C_{11}: elasticity coefficient in x-direction. Unit $[C_{11}] = \mathrm{N/m}^2$

C_{22}: elasticity coefficient in y-direction. Unit $[C_{22}] = \mathrm{N/m}^2$

C_{12}: orthotropic elasticity coefficient. Unit $[C_{12}] = \mathrm{N/m}^2$

C_{21}: orthotropic elasticity coefficient. Unit $[C_{21}] = \mathrm{N/m}^2$

C_{66}: shear elasticity coefficient. Unit $[C_{66}] = \mathrm{N/m}^2$

D: flexural stiffness. For panel, $D = Eh^3/(12(1-\nu^2))$. Unit $[D] = \mathrm{N\ m}$

D_1: flexural stiffness in x-direction. Unit $[D_1] = \mathrm{N\ m}$

D_2: flexural stiffness in y-direction. Unit $[D_2] = \mathrm{N\ m}$

D_3: flexural shear stiffness in xy-plane. Unit $[D_3] = \mathrm{N\ m}$

E: Young's modulus of isotropic plate or panel. Unit $[E] = \mathrm{N/m}^2$

E_{11}: Young's modulus of orthotropic plate in x-direction. Unit $[E_{11}] = \mathrm{N/m}^2$

E_{22}: Young's modulus of orthotropic plate in y-direction. Unit $[E_{22}] = \mathrm{N/m}^2$

$F(x)$: functional describing out-of-displacement. Unit $[F(x)] = \mathrm{m}$

F_x: body force in x-direction. Unit $[F_x] = \mathrm{N/m}^3$

F_y: body force in y-direction. Unit $[F_y] = \mathrm{N/m}^3$

G_{12}: in-plane shear modulus of orthotropic plate in xy plane. Unit $[G_{12}] = \mathrm{N/m}^2$

G_H: in-plane shear modulus of orthotropic plate in xy plane (geometric mean from E_1 and E_1). Unit $[G_H] = \mathrm{N/m^2}$

H_1: nondimensional flexural stiffness in x-direction.

H_2: nondimensional flexural stiffness in y-direction.

H_3: nondimensional flexural shear stiffness in xy-plane.

h: thickness. Unit $[h] = \mathrm{m}$

K: stress intensity factor. Unit $[K] = \mathrm{Pa}\sqrt{\mathrm{m}}$

K_C: fracture toughness. Unit $[K] = \mathrm{Pa}\sqrt{\mathrm{m}}$

K_{11}: viscosity coefficient in x-direction. Unit $[K_{11}] = \mathrm{Pa \cdot s}$

K_{12}: orthotropic viscosity coefficient. Unit $[K_{12}] = \mathrm{Pa \cdot s}$

K_{21}: orthotropic viscosity coefficient. Unit $[K_{21}] = \mathrm{Pa \cdot s}$

K_{22}: viscosity coefficient in y-direction. Unit $[K_{22}] = \mathrm{Pa \cdot s}$

K_{66}: shear viscosity coefficient. Unit $[K_{66}] = \mathrm{Pa \cdot s}$

k: material constant in Paris law

ℓ: free span length parameter. For the panel submerged in flowing fluid, the free span is taken to be $x \in (-\ell, \ell)$. Otherwise, as $x \in (0, \ell)$. Unit $[\ell] = \mathrm{m}$

M: bending moment per unit length or total mass or critical mass. Unit for bending moment $[M] = \mathrm{N\,m/m}$. Unit for mass $[M] = \mathrm{kg}$

m: mass per unit area. Unit $[m] = \mathrm{kg/m^2}$

N: normal for out-of-plane direction

n: number of loading cycles

n^{cr}: critical number of loading cycles due to fatigue fracture

n_x: unit normal in x-direction. Unit $[n_x] = \mathrm{m}$

n_y: unit normal in y-direction. Unit $[n_y] = \mathrm{m}$

$\mathbf{n}$: unit normal vector. Unit $[\mathbf{n}] = \mathrm{m}$

q_{f}: aerodynamic reaction pressure. Unit $[q_{\mathrm{f}}] = \mathrm{N/m^2}$

T: tension. Unit $[T] = \mathrm{N/m}$

T_0: constant (homogeneous) tension. Unit $[T_0] = \mathrm{N/m}$

T_{xx}: tension in x-direction. Unit $[T_{xx}] = \mathrm{N/m}$

T_{yy}: tension in y-direction. Unit $[T_{yy}] = \mathrm{N/m}$

T_{xy}: shear tension in xy-plane. Unit $[T_{xy}] = \mathrm{N/m}$

t: time. Unit $[t] = \mathrm{s}$

U: longitudinal transport velocity. Unit $[U] = \mathrm{m/s}$

U_1: transport velocity at beginning state. Unit $[U_1] = \mathrm{m/s}$

U_2: transport velocity at end state. Unit $[U_2] = \mathrm{m/s}$

$\mathbf{U}$: velocity vector. Unit $[U] = \mathrm{m/s}$

U_x: velocity in x-direction. Unit $[U_x] = \mathrm{m/s}$

U_y: velocity in y-direction. Unit $[U_y] = \mathrm{m/s}$

V: volume. Unit $[V] = \mathrm{m^3}$

V_0: axial velocity of panel or plate or initial volume.
Unit $[V_0] = \mathrm{m/s}$ for velocity.
Unit $[V_0] = \mathrm{m}^3$ for volume

V_0^{cr}: critical velocity of elastic instability of travelling panel or plate

V_∞: free-stream velocity of surrounding fluid. Unit $[V_\infty] = \mathrm{m/s}$

w: z-directional, out-of-plane displacement. Unit $[w] = \mathrm{m}$

x: x-coordinate. Unit $[x] = \mathrm{m}$

y: y-coordinate. Unit $[y] = \mathrm{m}$

z: z-coordinate. Unit $[z] = \mathrm{m}$

Greek symbols

α: nondimensional variable for calculating the root γ_0^2 or
nondimensional web velocity for fluid-structure calculation.

β: nondimensional flexural stiffness in fluid-structure calculation.

β_1: Poisson ratio $\beta_1 = \nu_{12}$ or
nondimensional flexural stiffness in fluid-structure calculation or
geometric factor for edge crack.

β_2: modified Poisson ratio. $\beta_2 = \nu_{12} + \frac{4\,G_{12}}{E_2}(1 - \nu_{12}\nu_{21})$

γ: nondimensional fluid mass in fluid-structure calculation.

γ_{xy}: shear strain. $\gamma_{xy} = -2z(\partial^2 w/\partial x \partial y)$ or $\gamma_{xy} = \varepsilon_{xy} + \varepsilon_{yx}$

γ_{xy}: shear strain. $\gamma_{xy} = -2z(\partial^2 w/\partial x \partial y)$ or $\gamma_{xy} = \varepsilon_{xy} + \varepsilon_{yx}$

Γ: edge of the domain.

ε_T: total strain applied.

ε_{xx}: x-directional component of strain. $\varepsilon_{xx} = -z(\partial^2 w/\partial x^2)$ or $\varepsilon_{xx} = \partial u/\partial x$

ε_{xy}: xy-shear strain component in xy-plane. $\varepsilon_{xy} = \partial u/\partial y$

ε_{yx}: yx-shear strain component in xy-plane. $\varepsilon_{xy} = \partial v/\partial x$

ε_{yy}: y-directional component of strain. $\varepsilon_{yy} = -z(\partial^2 w/\partial y^2)$ or $\varepsilon_{yy} = \partial v/\partial y$

ε_{zz}: z-directional component of strain. $\varepsilon_{ww} = \partial w/\partial z$

η_{11}: viscous damping coefficient in x-direction.
Unit $[\eta_{11}] = \mathrm{N\,s/m^2} = \mathrm{Pa \cdot s}$

η_{22}: viscous damping coefficient in y-direction.
Unit $[\eta_{22}] = \mathrm{N\,s/m^2} = \mathrm{Pa \cdot s}$

θ: nondimensional fluid velocity for fluid-structure calculation.

κ: nondimensional variable for calculating eigenfunction.

λ: nondimensional bending stiffness parameter.

Π: viscous shear constant. Unit $[\Pi] = \mathrm{N\,s/m^2} = \mathrm{Pa \cdot s}$

ρ: density. Unit $[\rho] = \mathrm{kg/m^3}$

ρ_f: density of fluid. Unit $[\rho_f] = \mathrm{kg/m^3}$

ρ_0: density at initial state. Unit $[\rho_0] = \mathrm{kg/m^3}$

ρ_1: density at the begin state. Unit $[\rho_1] = \mathrm{kg/m^3}$

ρ_2: density at the end state. Unit $[\rho_2] = \mathrm{kg/m^3}$

ν: Poisson ratio of isotropic plate or panel (nondimensional).

ν_{12}: Poisson ratio for orthotropic material. When stretched along axis 1 (x), ν_{12} is the contraction factor along axis 2 (y).

ν_{13}: Poisson ratio for orthotropic material. When stretched along axis 1 (x), ν_{13} is the contraction factor along axis 3 (z).

ν_{21}: Poisson ratio for orthotropic plate. When stretched along axis 2 (y), ν_{21} is the contraction factor along axis 1 (x).

σ_{xx}: normal stress in x-direction. Unit $[\sigma_{xx}] = \mathrm{N/m^2}$

σ_{yy}: normal stress in y-direction. Unit $[\sigma_{yy}] = \mathrm{N/m^2}$

τ_{xy}: shear stress in xy-plane. Unit $[\tau_{xy}] = \mathrm{N/m^2}$

ϕ: continuous test function (vector).

φ_{12}: viscous Poisson ratio for orthotropic material. When stretched along axis 1 (x), ν_{12} is the contraction factor along axis 2 (y).

φ_{21}: viscous Poisson ratio for orthotropic material. When stretched along axis 2 (x), ν_{21} is the contraction factor along axis 1 (y).

Φ: nondimensional variable for calculating eigenfunction.

Ψ: continuous function for describing out-of-plane displacement or nondimensional variable for calculating eigenfunction.

Ω: domain of the governing equation (connected open set).

LIST OF FIGURES

CONTENTS

INCLUDED ARTICLES

PI Matti Kurki, Juha Jeronen, Tytti Saksa and Tero Tuovinen. Strain Field Theory for Viscoelastic Continuous High-speed Webs with Plane Stress Behavior. *European Congress on Computational Methods in Applied Sciences and Engineering, (ECCOMAS)*, 2012.

PII Matti Kurki, Juha Jeronen, Tytti Saksa and Tero Tuovinen. On Displacement-Velocity Coupling and the Origin of In-plane Stresses in Orthotropic Moving Continua. *Reports of the Department of Mathematical Information Technology Series B, Scientific Computing, ISBN 978-951-39-5742-1, ISSN 1456-436X*, 2014.

PIII Nikolay Banichuk, Juha Jeronen, Matti Kurki, Pekka Neittaanmäki, Tytti Saksa and Tero Tuovinen. On the limit velocity and buckling phenomena of axially moving orthotropic membranes and plates. *International Journal of Solids and Structures, Vol. 48, pp. 2015-2025*, 2011.

PIV Nikolay Banichuk, Matti Kurki, Pekka Neittaanmãki, Tytti Saksa, Maria Tirronen And Tero Tuovinen. Optimization and Analysis of Processes With Moving Materials Subjected to Fatigue Fracture and Instability. *Mechanics Based Design of Structures and Machines, Vol. 41, Issue 2, pp. 146-167, DOI:10.1080/15397734.2012.708630*, 2013.

PV Matti Kurki, Pasi Kekko and Jarmo Kouko. Laboratory Scale Measurement Procedure of Paper Machine Wet Web Runnability: Part 1. *Paper and Timber (Paperi ja Puu), Vol. 86, No. 4*, 2004.

PVI Jarmo Kouko, Kristian Salminen and Matti Kurki. Laboratory Scale Measurement Procedure of Paper Machine Wet Web Runnability: Part 2. *Paper and Timber (Paperi ja Puu), Vol. 89, No. 7–8*, 2007.

PVII Matti Kurki and Pekka Martikainen. Roll in a Paper Or Board Machine And a Dryer Group in a Paper Or Board Machine. *United States Patent US20050075229*, 2008.

For this thesis, the emphasis in papers **PI** and **PII** is on the introduction of a new theory for continuous, moving viscoelastic web. This theory is developed by the author, and the solution of both the one-dimensional and two-dimensional equations using FEM with different elements and boundary conditions were realized as a group effort with the co-authors.

In paper **PIII**, the author's contribution was to suggest and develop realistic calculation cases for the developed orthotropic model, which was targeted more closely to the practical high-velocity web handling environment where different web handling geometries and orthotropic material parameters, especially, are important.

The edges in the web handling are under intensive research of this group. In paper **PIV**, the author suggests and develops the first approaches of the fracture mechanics to be utilized in moving web modelling. Special emphasis is placed on edge cracks and the nature of cyclic tension since those are common in web handling lines. The calculation applications and the multi-criteria optimization methodology were developed by the co-authors.

Papers **PV** and **PVI** are connected, consisting of parts 1 and 2. The publications are the first reliable results of the web material rheology research perfomed at VTT (Technical Research Center of Finland). The author contributed by initializing this research in VTT and by designing the first measurement devices. Later, the author supervised this research at Metso Paper Corporation.

Final paper **PVII** is author's the patent US7351309 accepted at 2008. The patent consists of self-amplifying, adaptive roll for web handling purposes in high-velocity environments. This adaptive roll patent is a succession to PCT Patent WO/98/27274, and its main purpose is, essentially, to guarantee the immaterial rights for utilizing optimized roll structure to create self-amplifying underpressure. The research, CFD calculations and measurements were designed by the author. CFD calulations were carried out by Process Flow Ltd., and measurements were done in VTT. This roll has been the subject of a separate Ph.D. thesis by Simo Nurmi [77]. His thesis was done independently without author's participation.

1 INTRODUCTION

The fundamental stress-strain behavior of continuous moving webs forms an interesting area, which is relatively well- studied, but still includes aspects which are not well-understood. Axially moving materials, such as strings, belts, beams, membranes and plates have many applications in industry, e.g. in paper production, and their out-of-plane mechanics have been studied widely. In processing of different kinds of thin, laterally moving solid webs, challenges such as the efficiency of production and effects due to instability caused by high velocity are being met. These challenges are tightly connected to the overall behavior of the stresses and strains appearing in moving solid continua. [36, 32, 33, 59, 117].

This thesis aims to give comprehensive insight to the different sections of web handling continuation, including theoretical stress-strain behavior of moving webs, the stabilization criteria for coupled web-air systems, the significance of the web imperfections and edge cracks, the effects and nature of viscoelastoplastic materials and the principles of external stabilization applications for high velocities. This approach will give a new, distinctive and cross-scientific structure to this thesis, as it takes account both the theoretical and practical aspects of the web handling in different velocity and efficiency environments.

1.1 Structure of the Thesis

The structure of this thesis is based on the cross-scientific approach described in the introduction in Chapter 1. The principle of this thesis is to create thematic continuance for web handling (Figure 1). Mathematical theory is followed by the modelling of the constitutive physical features, stabilization principles and the fatigue life of the web, this leads to the investigation of the effects of the viscoelastoplastic material properties, which contribute to the web's behavior, and finally the process is concluded with a web handling application in a high-velocity web transport environment.

These stages include essential components, which cover the creation of the

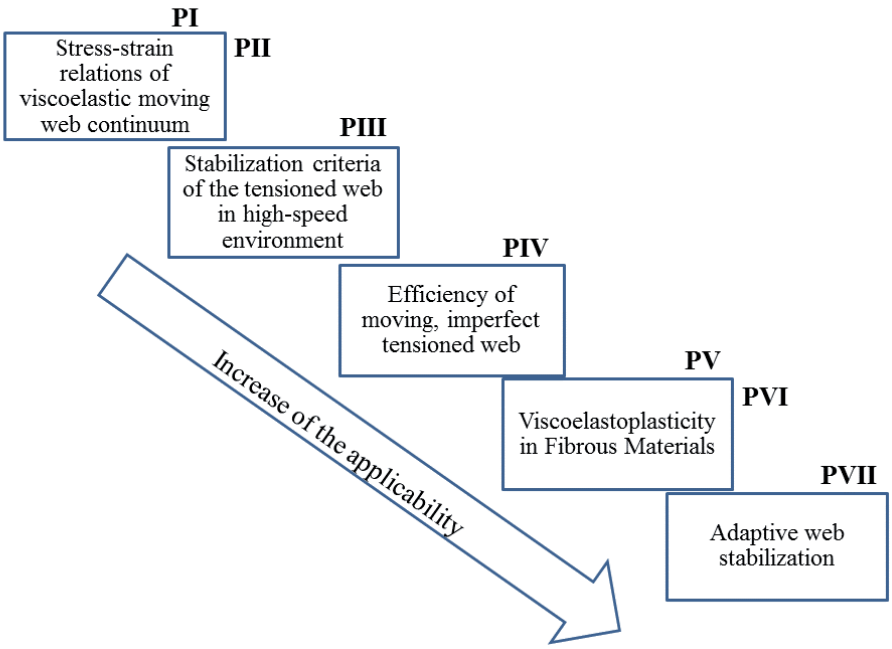

FIGURE 1 Web handling continuance: the structure and cross-scientific nature of this thesis including the publications **PI** - **PVII** thematically located along the continuance.

stress state inside the web thickness due to relative velocity differences used in various continuous web handling environments. Further, the stress-strain model for viscoelastic moving web continuum connetcs both viscous and velocity properties in moving web [52, 57]. These properties provide additional features to the physics of the moving web: both velocity and viscoelasticity are contributing to the in-plane stress distribution and thus also to the planar stress distribution of the moving medium [59].

The great majority of moving webs in different practical environments are arranged, unsupported, between the rollers that are usually the only supporting surfaces along the web handling line. In a situation of this kind, web stress plays an essential role in web stabilization [52, 75, 85, 3, 106].

The quality of the final fibrous product, during process the moving web, is tightly connected to the production efficiency. The effect of the sharp geometrical shapes to the stress concentrations of the structures is well known [105]. In practical web handling environments, these geometrical disturbances at the web edges are common contributors to the efficiency. All geometrical disturbances appearing on the edges of the web will increase the stress peaks around the disturbances. Further, this will increase the probability of web breaks when the tension values and fracture stiffness values are approaching the critical limit values of the mate-

rial itself [95, 94, 39, 105, 34, 40, 5].

In practical high-velocity web handling, one very likely web instability contributor is the viscous behavior of the air. To prevent the web detachment from supporting or guiding surface at the closing pocket area of the contacting web and roll, the excess, over-pressurized air must be removed [22, 27, 61, 53].

This thesis introduces a more recent adaptive air-control method, where air removal is handled using special groove geometry in the roll mantle. The geometry of the grooves is designed so that the flow at both closing and opening pockets create an active closures at the both ends of the web-roll contact (wrap) area. The stabilizing, contact-ensuring negative pressure (suction) is adaptive: the self-adjusting process depends on roll surface velocity, which, when increasing, increases both the sealing and the suction effect with velocity increase. This property is useful especially at places where the web stabilization is essential. The alignment of the application space and roll alignment are tightly controlled and can be difficult to realize with traditional web stabilizing methods using external suction fan installation.

The structure of this thesis presented in Figure 1 illustrates only one possible path starting from the theoretical foundation of the web's stress-strain behavior and leading to the actual application of web stabilization by using external forces directed against the web. Especially at the latter part of the path there exist many different web handling applications for the needs of the web material and web handling process [53]. The creation of the stress inside the moving web, however, is a common contributor in all web handling applications.

1.2 Objectives

The main objective of this thesis is to create and demonstrate a conceptual web handling continuance using mathematical modelling approaches for moving viscoelastic, possibly imperfect web continuum. The common contributor of this continuance is web stress σ (or web tension T).

In Figure 2, an exemplary web tension level T_{web} is created using the relative speed difference. This usage for the purpose of stability is mandatory in open, unsupported web spans, but if uncontrolled, this method can cause decreased efficiency. Therefore, a new adaptive web stabilizing application is introduced to supported web handling environments to reduce the dependence from the web stress.

The benefit of this cross-scientific approach is to bring front the developmental path from theory to practice forwarded by finding how theoretical considerations and practical applications are affecting in real-life web handling environments. Additionally, with the help of new principles of continuum modelling, it is possible to find similarities between other transport phenomena where fluid is the transport medium.

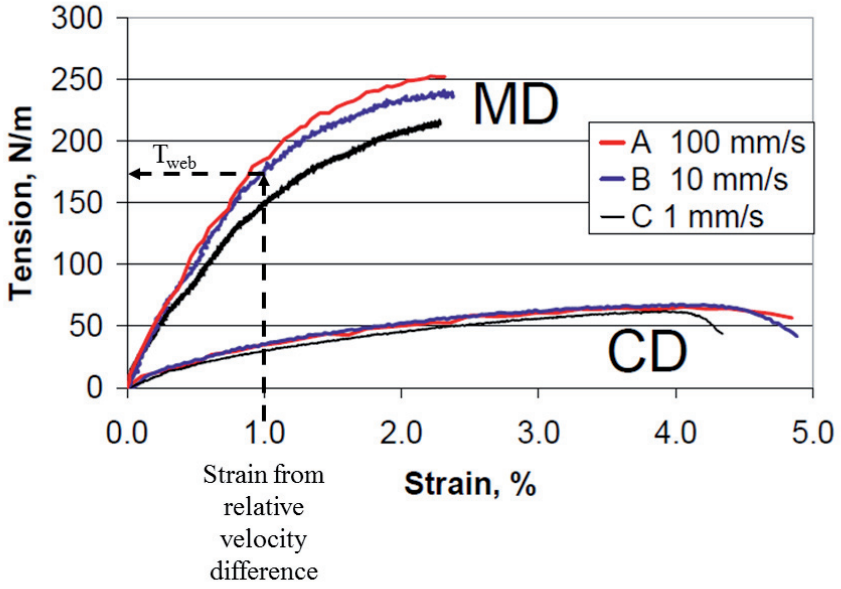

FIGURE 2 The creation of web tension in MD (Machine Direction) in wet LWC paper with 1.0% strain. Redraw from **PVI** .

2 LITERATURE REVIEW AND CONTRIBUTION OF THE PUBLICATIONS

2.1 Stress-strain relations of viscoelastic moving web continuum

The origin and structure of the in-plane tension distribution in a moving solid web seems to be an area of which very little is known. The models that are often used with the heterogenous web materials are based on assumptions of isotropic or orthotropic material properties [24, 69, 86, 82]. Also, the web materials are often considered as viscoelastic or viscoplastic but there is no coupling between in-plane strain and web velocity effects.

The building up of the stress and strain in moving solids is closely related to the advance of the strain waves inside the solids. In this area, valuable work has been performed by Mann et al. who studied the advance of waves in fibrous materials. In their case, the main focus was in the determination of elastic constants of the fibrous materials [69]. Time-dependent, in-plane vibrations of a moving continuous membrane were studied by Shin et al. [96]. In their work, in-plane vibration modes of an isotropic web were studied between the traction lines. Also Guan et. al. have studied viscoelastic web behavior in both steady-state and unsteady-state cases [32, 33].

Usually, in the viscoelastic constitutive relations, instead of the material derivative the partial time derivative is used. The first applications using the material derivatives with the in-plane moving web continuum were presented by Kurki [52]. Later, Mockensturm and Guo suggested that the material derivative should be used [72]. In their work, non-linear, out-of-plane vibrations and dynamic response of axially moving viscoelastic strings was studied. Kurki and Lehtinen suggested, independently, that the material derivative in the constitutive relations should be used in their study concerning the in-plane displacement field of a travelling viscoelastic plate [59] which is also one of the main themes in **PI** and **PII**. In the study by Chen et al., the material derivative was used in the viscoelastic constitutive relations [14]. They studied parametric, out-of-plane vibration of axially accelerating viscoelastic strings. Chen and Ding studied the

stability of axially accelerating viscoelastic beams using the method of multiple scales and the material derivative in the viscoelastic constitutive relations [16]. Chen and Wang the studied stability of axially accelerating viscoelastic beams using asymptotic perturbation analysis and the material derivative in the viscoelastic relations [17]. In a recent research by Chen and Ding, the material derivative was also used to study the dynamic response of vibrations of axially moving viscoelastic beams [16]. In their study, a non-linear model was used and the coupling of the transverse displacement with the longitudinal (in-plane) displacement was taken into account. However, their main focus was on the out-of-plane bending behavior of the beam.

2.2 Stabilization criteria of the tensioned web in high-speed environment

Studies performed on the area of web handling are usually connected with the time-dependent behavior of out-of-plane displacements of the moving webs. Research on vibrations of travelling elastic materials goes back to 1890's when Skutch made the first models dealing with tensioned, ideal strings [99]. In the 1950's, Sack [88] as well as Archibald and Emslie [3] studied transverse vibrations in a traveling string. In the 1960's and 70's, many researchers continued studies on moving strings and beams concentrating mainly on various aspects of free and forced transverse vibrations [71, 106, 74, 73, 109].

Stability of small, out-of-plane vibrations of travelling two-dimensional rectangular membranes and plates has been studied by Ulsoy and Mote [114]. When the web is advancing through its various processes without an external support, the inertial forces depending on the web velocity are coupled with web tension [88, 3]. Pramila et. al. showed that the transverse behavior of the web and the response in the flowing fluid (air) surrounding the web are coupled if the density of the web material is low (see e.g. [85, 12]). Lin and Mote studied an axially moving membrane in a 2D formulation, predicting the equilibrium displacement and stress distributions under transverse loading [66]. Later, the same authors studied the wrinkling of axially moving rectangular webs with a small flexural stiffness [67].

One of the first studies on transverse vibration of travelling viscoelastic material was carried out by Fung et al. using a string model [29]. Extending their work in their later research, they studied the effects of viscous damping [30]. Viscoelastic strings and beams have recently been studied extensively, see e.g. [19, 14, 15]. Using the spectral element method, Oh et al. studied critical velocities, eigenvalues and natural modes of the transverse displacement of axially moving viscoelastic beams [78, 63].

Chen and Zhao [20] presented a modified finite difference method to simplify a non-linear model of an axially moving string. They studied numerically the free transverse vibrations of both elastic and viscoelastic strings. Chen and

Yang studied free vibrations of viscoelastic beams travelling between simple supports with torsion strings [18]. They studied the viscoelastic effect by perturbing a similar elastic problem and using the method of multiple scales. Recently, Yang et al. have studied vibrations, bifurcation, and chaos of axially moving viscoelastic plates using finite differences and a non-linear model for transverse displacements [21].

2.3 Production Efficiency with Moving, Imperfect Tensioned Web

Production efficiency has been and still is very important item in different web handling environments and becomes emphasized when web velocities are high. This is closely linked with the tension levels used in order to improve the web stability. Essentially, the core of the efficiency problem is often with the edges of the web. After web forming, the edges are corrected first time with edge trimming, high-pressure water jets are cutting a narrow strips from the edges. This, largely unstudied area gives rise to one of the many edge handling problems, especially in paper- and board making. These problems become even more apparent later at the production line when the paper dries and advances to the finishing stage.

Problems in the edge trimming are usually visible only with the use high-speed imaging together with an appropriate lighting system [103]. Edge trimming can have significant effect in the creation of edge cracks leading to possible fractures and web breaks. Figure 3 clearly reveals these effects often unseen with bare eyes. One of the main items contributing on this is the web's stress behavior at the roll contact areas, especially where roll friction prevents the web from contracting in cross direction, thus creating stress peaks in longitudinal transport direction at the roll-web detachment area [37].

The field of fracture mechanics was developed by Irwin [43], whose research was based on the early papers of Inglis, Griffith, and Westergaard [42, 31, 120]. Linear elastic fracture mechanics was first applied to paper materials by Seth and Page, who measured fracture toughness for different paper materials [94]. Swinehart and Broek determined the fracture toughness of paper with the help of both the stress intensity factor and the strain energy release rate [105]. They found that the measured crack length and fracture toughness were in a good agreement with the LEFM theory.

Wathén has discussed how paper that has undergone damage affects the web breaks in paper making [119]. Tryding has studied crack growth evolution in paper material using experiments and a cohesive crack model with finite element analysis [112]. Fatigue of wood-pulp fibers on micro-structural level has been studied by Hamad [35, 34].

Various analyses of vibrations and stability of stationary beams and plates exists in the literature. An extensive review of fractures in cracked materials and of challenges in such models was carried out by Dimarogonas [23]. Finite element analysis has often been applied to analyze the vibrations and stability of cracked

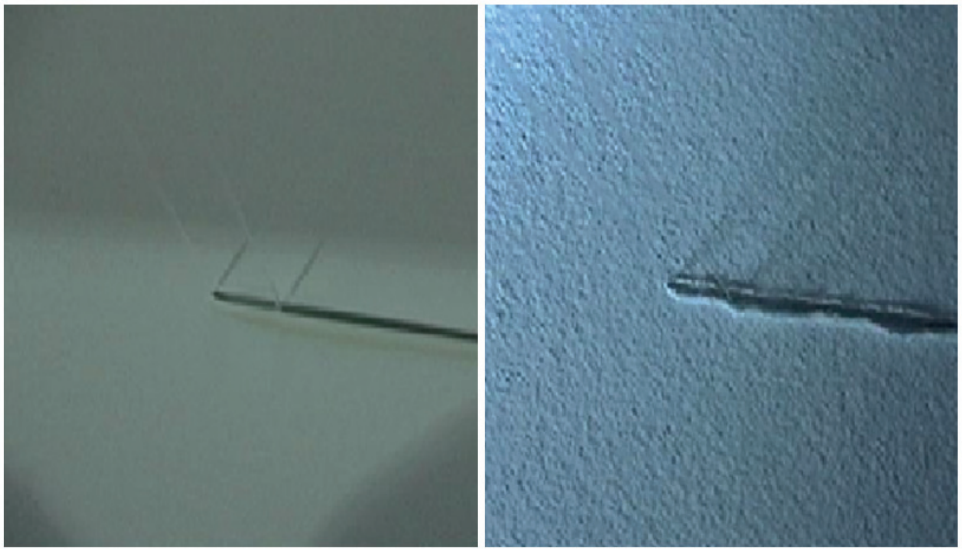

a b

FIGURE 3 Edge trimming quality photographed with long exposure time a) and using high-speed imaging b) [103].

rectangular plates in the case centre- or edge-located cracks. Bachene et al. used the extended finite element method and Liew et al. developed an efficient decomposition method to study vibrations of cracked plates [4, 64]. Brighenti examined buckling failure of cracked plates for different crack orientations with the help of finite element analysis [9]. Both buckling and vibration analysis were covered in the finite element studies of cracked plates by Prabhakara and Datta [83, 84].

With the help of dual series equations, Stahl and Keer studied vibrations and stability of rectangular plates [102]. Vafai et al. studied parametric instability of plates having one crack at an edge [115]. They considered simply supported rectangular plates under periodic loadings using an integral equation method. Effects of cracks on the eigenfrequencies and eigenmodes of axially moving beams at sub-critical transport velocities was studied by Murphy and Zhang [76].

Hristopulos and Uesaka studied the variations in web velocity that cause fluctuations in the relative velocity difference responsible for creating the strain and stress to the web. These were found to be important for web breaks and production efficiency where the high strain fluctuations appear due to large out-of-roll deformations [40].

2.4 Viscoelastoplasticity in Fibrous Web Materials

Many real-life amorphous materials do not behave according to linear elasticity, and depending on the level of the loading, the degree of nonlinear elasticity increases. Especially with fibrous materials such as paper, the nature of the elastoplasticity depends both of the connections between the fibers, i.e. the bonds, and on the fiber elasticity itself [1].

Generally, different possibilities to the topochemical modification of fibers using different mechanical or chemical aids are myriad and will not be discussed here. Briefly we can state that both paper elasticity and strength are based on fibrillar structure of fiber cell wall, which is essentially a structure of cellulose chains. These chains are linear polymers of D-glucose residues bound together with beta-(1,4) glycosidic linkages and these are also responsible for the attachments (bonds) between the fiber surfaces [48, 118].

Strength and elasticity properties are further modified by the fiber network structure. Vainio studied both fiber segments between the bonding areas and their alignment which are contributing to the overall elastoplastic behavior of the paper through a fiber activation process [116].

Both nonlinear elasticity and viscoelasticity of different polymers have been known for a long time. First known studies on paper viscoelasticity has made Andersson et al. who measured basic viscoelastic properties of paper using different strain rates [2]. Basic studies on nonlinear plasticity in fibrous, wood-based materials have been carried out by Sanborn [91]. Skowronski et al. continued the research of irrecoverable strains and in their study one of the important findings was the coupling between the time-dependent creep and the increase of plastic irrecoverable strain in material [98]. Additionally, the modelling of nonlinear orthotropic behavior of the fibrous materials has been studied by Ostoja-Starzewski et al. However, the models developed by several authors do not include the irrecoverable properties of the material. [113, 108, 46, 10, 101, 89]. From the modelling point of view, an important finding was reported by Subramanian et al. showed that geometrical mean of in-plane orthotropic moduli of elasticity does not change even if the anisotropy of the paper changes [104].

An important connection between the viscoelasticity and stress behavior is brought up in **PV** and **PVI**. The emphasis of the research was on fast, step-like straining of the fibrous, paper structures. During the production, a paper web undergoes different velocity increase steps in order to create the adequate strain and stress levels for web stability. In these occasions, viscoelastic stress response has a significant effect on stress levels that appear in different web handling processes [37]. A special emphasis in these studies was on the determination of viscoelastoplastic properties of a paper web when which had not been dried completely and the strength of which in wet state was only 15...30% of the final dried paper [68, 56, 53, 26].

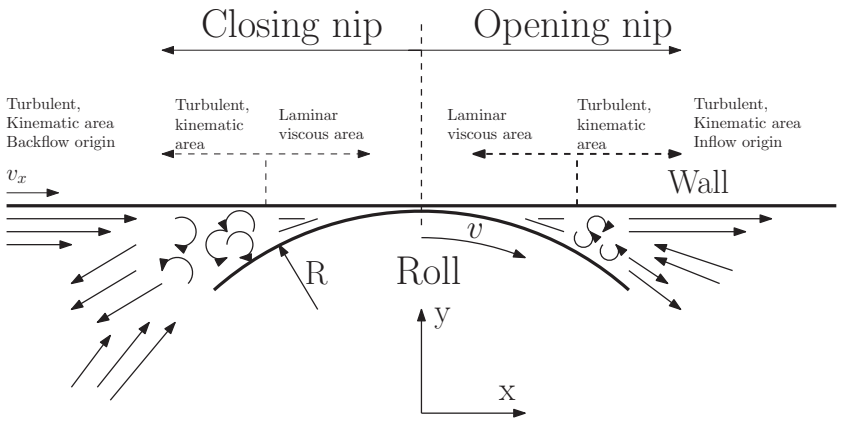

FIGURE 4 Air flows at closing and opening pockets [57, 77].

2.5 Adaptive web stabilization

Aerodynamical over- and underpressure effects in the paper machine are one of the key contributors to the development of runnability disturbances at high web velocity levels. The origin of these effects is the viscosity of the surrounding air which further causes the formation of turbulent boundary layers [93, 22, 27, 49, 61].

Web forms both closing and opening pockets with different types of rolls throughout the web processing line. Due to transported air by the boundary layers, an excess air flows out from the closing pockets, which causes overpressure effects (see Figure 4). At the opening pocket area, the detachment of the web from the roll forms a closed, sharp pocket area, from where the forming boundary layers transport air away, creating an underpressure. Furthermore, these pressures cause web displacements, which can be divergent, apparently steady-state -type stable deflections or unstable time-dependent web flutter [22, 75, 107, 13].

Web stabilization is always needed in fast web handling environments whenever the elasticity or the strength of the web is at low level. Moreover, in the case of paper making, low elasticity leads to high strain levels which further can cause the quality degradation to finished, dry paper [39, 53]. In paper making, web velocities were increasing over 1000 m/min at the end of 1980's [107, 11, 49]. At that time, web detachment and runnability disturbances were becoming more common restricting the increase of production velocities.

To overcome these difficulties, several different inventions were made to ensure the attachment between the web and the roll. Kankaanpãã et. al. made the first approach to eliminate the effect of overpressurizing closing the pocket area; they created an additional space for the excess air by grooving the roll surface [50, 11].

The development of the overpressure in the closing pocket area is approximately quadratically dependent on the web velocity, and therefore an additonal

stabilization technique was needed for web velocities approaching 1200 m/min [51, 49]. The next step in the development was the implementation of active air removal from the pocket area by using an external, blower-assisted vacuum system, which is still the most common web stabilization installation in high velocity paper and board machines. This air removal is made possible by a drilled roll mantle or a grooved roll with the drillings at the bottom of the grooves. Suction can be arranged through the axle of the roll or with the help of a separate suction box attached in the immediate vicinity of the roll [50, 11]. However, since the overpressure levels in the pocket areas between the roll and the web are increasing quadratically with respect to web velocity, also the fan power used for creating the necessary suction increases rapidly.

The first application of the adaptive, self-underpressurizing roll was developed during 1990's. In that construction, the special feature was the arrangement of parallel discs and the hollow center area of the roll so that the opening area for air penetration in the closing pocket to groove volume area is high enough. This roll was capable of creating its own underpressure when used with permeable dryer fabric but the groove structure of the roll was not optimized [87].

3 STRESS-STRAIN RELATIONS OF A VISCOELASTIC MOVING WEB CONTINUUM

3.1 The continuum of the moving web

A continuous, moving web creates a solid continuum which can be treated as a flowing medium. In this derivation, the web continuum is assumed to be under a stress state, which is caused by a strain state and can be expressed in terms of the velocity difference between supporting rollers, by the means of a mass conservation law.

Let us consider an orthotropic material with initial (i.e. in the undeformed state) constant density ρ_0, undergoing steady-state longitudinal transport at velocity $\mathbf{U} = (U_x, 0, 0)$, depicted in Figure 5. Let us assume that the material axes 1, 2 and 3 are aligned with the x, y and z axes, respectively. The continuity equation, in the Eulerian frame, is

$$\frac{\partial \rho}{\partial t} + \nabla \cdot (\rho \mathbf{U}) = 0 \,, \tag{1}$$

which, in a steady state, reduces to

$$\nabla \cdot (\rho \mathbf{U}) = 0 \,. \tag{2}$$

Mass conservation requires that the flow rates at the incoming and outgoing flow control areas are equal; this requirement is readily obtained from equation (2). Let us consider a stationary control volume

$$\Omega = \{ \, (x, y, z) : \, 0 < x < \ell \,, \; 0 < y < b \,, \; 0 < z < h \, \}$$

where ℓ is the length of the span between the rollers, b is the width of the span, and h is the thickness of the sheet of material. Integrating equation (2) over the control volume Ω, applying the divergence theorem, and noting that ρ is a scalar, we have

$$\int_\Omega \nabla \cdot (\rho \mathbf{U}) \, \mathrm{d}\Omega = \int_{\partial\Omega} \rho \, (\mathbf{n} \cdot \mathbf{U}) \, \mathrm{d}\Gamma \,. \tag{3}$$

Material flows in and out of the control volume only occur at the surfaces A_1

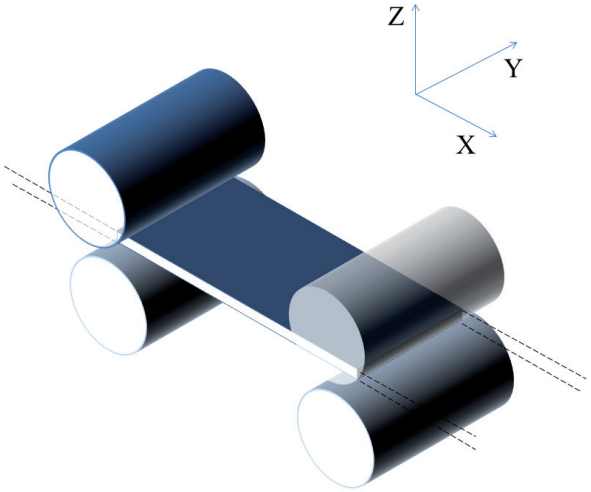

FIGURE 5 Schematic representation of the setup for modelling a moving viscoelastic web, stressed at the traction lines represented by the rollers form **PI**. The arrows depict axial motion.

and A_2 (see Figure 6). Let us assume that ρ and $\mathbf{U}$ are constant across these inflow and outflow surfaces, but that their values may change between these surfaces. In practice, there always are small variations in the velocity at the outlet due to technical difficulties of realizing accurate velocity, but for small strains and high velocity, constant velocity along these surfaces is a reasonable approximation [40]. Under these assumptions, the mass balance becomes

$$-\rho_1 A_1 U_1 + \rho_2 A_2 U_2 = 0\,. \tag{4}$$

The subscripts 1 and 2 for ρ and U refer to the (constant) values on the surfaces A_1 and A_2, respectively. Note the form of the velocity field, $\mathbf{U} = (U_x, 0, 0)$. Finally, it is convenient to rewrite (4) as

$$U_1\,(\rho_1/\rho_2)\,(A_1/A_2) - U_2 = 0\,. \tag{5}$$

In order to manipulate equation (5) further, we must consider the ratios of the densities and the cross-sectional areas. When subjected to a small-displacement deformation $\mathbf{u} = (u, v, w)$, the volume V of a differential element initially (in the undeformed state) having volume V_0 becomes

$$V = V_0\big[1 + \nabla \cdot \mathbf{u}\big] \equiv V_0\big[1 + \varepsilon_{xx} + \varepsilon_{yy} + \varepsilon_{zz}\big]\,, \tag{6}$$

as is known from the theory of elasticity. Because the total mass M of the differential element is conserved in the small deformation, it follows for the density ρ

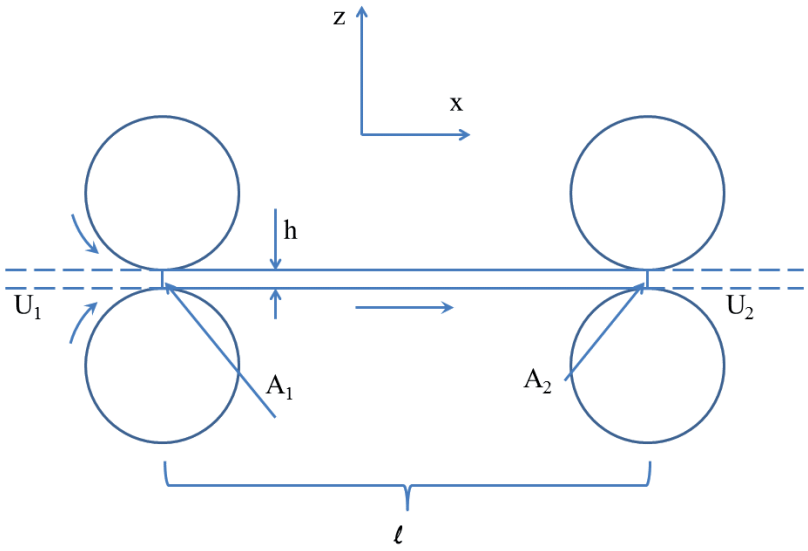

FIGURE 6 Solid web continuum flowing between the incoming and outgoing flow control areas (two-dimensional surfaces) A_1 and A_2 at longitudinal velocities U_1 and U_2 at the beginning and ending traction lines respectively (from **PI**) .

that

$$\rho \equiv \frac{M}{V} = \frac{1}{V_0}\frac{M}{V/V_0} = \frac{M}{V_0}\frac{1}{V/V_0} = \rho_0\left[1+\varepsilon_{xx}+\varepsilon_{yy}+\varepsilon_{zz}\right]^{-1}, \tag{7}$$

where (6) and the definition $\rho_0 \equiv M/V_0$ have been used. Let us assume that the material is subjected to pure axial stress. This induces an axial strain ε_x, and via the Poisson effect, also the strains ε_y and ε_z in the two orthogonal directions:

$$\varepsilon_{yy} = -\check{\nu}_{12}\varepsilon_{xx}\,, \quad \varepsilon_{zz} = -\check{\nu}_{13}\varepsilon_{xx}\,. \tag{8}$$

where $\check{\nu}_{12}$ and $\check{\nu}_{13}$ are Poisson parameters including both elastic and viscoelastic effects. The cross-sectional area of the web is

$$A \;=\; (1+\varepsilon_{zz})h(1+\varepsilon_{yy})b \;\approx\; bh\,(\,1+\varepsilon_{yy}+\varepsilon_{zz}\,)\,, \tag{9}$$

where second-order small terms have been neglected. Combining (8) and (9), we have

$$A \approx bh\,(\,1-(\check{\nu}_{12}+\check{\nu}_{13})\varepsilon_{xx}\,) \equiv bh\,(\,1-\nu_{1A}\varepsilon_{xx}\,)\,, \tag{10}$$

where the effective Poisson ratio for change of cross-sectional area, when stretched along material axis 1, is defined as

$$\nu_{1A} \equiv \check{\nu}_{12}+\check{\nu}_{13}\,. \tag{11}$$

Note that it also follows from (6) and (8) that

$$V = V_0\big[1 + (1 - \nu_{1A})\varepsilon_{xx}\big] \,. \tag{12}$$

The effective Poisson ratio contains the material parameters $\check{\nu}_{12}$ and $\check{\nu}_{13}$. Finally, for the density, by combining (7), (8) and (11), we obtain

$$\rho = \rho_0\big[1 + (1 - \nu_{1A})\varepsilon_{xx}\big]^{-1} = \rho_0\big[\varepsilon_{xx} + (1 - \nu_{1A}\varepsilon_{xx})\big]^{-1} \,, \tag{13}$$

where ρ_0 is the density in the initial (unstressed) state.

In the following, we will assume that the material, subjected to constant axial tension at the rollers (traction lines), has zero strain at A_1, and experiences some nonzero axial strain ε_{xx} at A_2, due to the applied axial stress. Preliminary one-dimensional results indicate that such a strain state occurs at least for an axially travelling Kelvin–Voigt viscoelastic material (see the section concerning the one-dimensional case further below). By (10), the cross-sectional areas become

$$A_1 = bh \,, \qquad A_2 = bh(1 - \nu_{1A}\varepsilon_{xx}) \,, \tag{14}$$

and by (14), the densities are:

$$\rho_1 = \rho_0 \,, \qquad \rho_2 = \frac{\rho_0}{\big[1 + (1 - \nu_{1A})\varepsilon_{xx}\big]} \,. \tag{15}$$

By inserting (14) and (15) into the mass balance (4), simplifying, and solving for ε_{xx}, we obtain the result

$$\varepsilon_{xx} = \frac{\dfrac{U_2}{U_1} - 1}{1 + \left[\dfrac{U_2}{U_1} - 1\right]\nu_{1A}} \,. \tag{16}$$

Equation (16) can be used for setting up a strain-based boundary condition (at the traction line at $x = \ell$) for the problem of in-plane (visco-)elastic deformation, corresponding to given roller velocities U_1 and U_2. Obviously, in order for the model to remain valid, the given velocities must be such that the strain according to (16) remains in the small-deformation range.

The transport velocity of the flowing solid continuum in the above case is assumed to be controlled only in the x (longitudinal) direction; all in-plane deformations in the y (widthwise) direction are determined by the viscoelastic response. It should also be kept in mind that equation (16) only applies in a steady-state flow, i.e. when the web flows smoothly without time-dependent disturbances [33].

The traction lines at the cross-sectional areas A_1 and A_2 affect only the surfaces of the web, which implies that stress and strain waves advancing inside the web thickness can cross the traction lines. Therefore in the boundary conditions of moving continuous webs, in reality, one should consider rather complicated friction-based force transmission phenomena at web-roll contact areas [57].

3.2 Constitutive equations

In this section we will define the stresses and strains, deformations, material assumptions and velocity dependent in-plane inertial forces for moving web. This leads to both one- and two-dimensional equations for the moving viscoelastic continuum.

A usual approach for describing structural deformations is the Lagrangean description. However, longitudinally moving in-plane deformations are more challenging. One possibility is to actually move the medium at the desired velocity, and update the boundary conditions at each timestep [100]. Another possibility is to use an 'Eulerian' flow description, and then the actual deformation of the moving continuum can be handled using a mixed Lagrange–Euler description [54]. The Eulerian description is a standard approach in fluid dynamics where the observer is 'watching' a control volume, where possible deformations will appear [100, 62].

In this thesis, we consider two-dimensional in-plane membrane behavior. Based on Figure 7, one can derive the following well-known force balance [110]:

$$\frac{\partial \sigma_x}{\partial x} + \frac{\partial \tau_{yx}}{\partial y} - F_x = 0 \qquad \text{in } \Omega \tag{17}$$

$$\frac{\partial \sigma_y}{\partial y} + \frac{\partial \tau_{xy}}{\partial x} - F_y = 0 \qquad \text{in } \Omega \tag{18}$$

where Ω is an open, connected set in $\mathbb{R}^2$. The linear Cauchy strains are

$$\varepsilon_{xx} = \frac{\partial u}{\partial x}\,,\ \ \varepsilon_{yy} = \frac{\partial v}{\partial y}\,,\ \ \varepsilon_{xy} = \frac{\partial u}{\partial y}\,,\ \ \varepsilon_{yx} = \frac{\partial v}{\partial x}\,,\ \ \gamma_{xy} = \left(\frac{\partial u}{\partial y} + \frac{\partial v}{\partial x}\right)\,. \tag{19}$$

In the mixed Lagrange–Euler description, the strains

$$\varepsilon_{ij} = \varepsilon_{ij}\,(x, y, t) \tag{20}$$

are written as

$$\begin{aligned} \frac{\mathrm{d}\varepsilon_{ij}}{\mathrm{d}t} &= \frac{\partial \varepsilon_{ij}}{\partial t} + \frac{\partial \varepsilon_{ij}}{\partial x}\frac{\mathrm{d}x}{\mathrm{d}t} + \frac{\partial \varepsilon_{ij}}{\partial y}\frac{\mathrm{d}y}{\mathrm{d}t} \\ &= \frac{\partial \varepsilon_{ij}}{\partial t} + \frac{\partial \varepsilon_{ij}}{\partial x}U_x + \frac{\partial \varepsilon_{ij}}{\partial y}U_y\,, \end{aligned} \tag{21}$$

where (U_x, U_y) is the velocity field and the indexes i and j refer to spatial coordinates. We will use the material assumption of orthotropic viscoelasticity. With fibrous, composite-type materials, the elastic properties are the result of complicated material preprocessing, which further results in orthotropic anisotropy and material time-dependency (see e.g. [69, 113, 46, 82, 10, 116]).

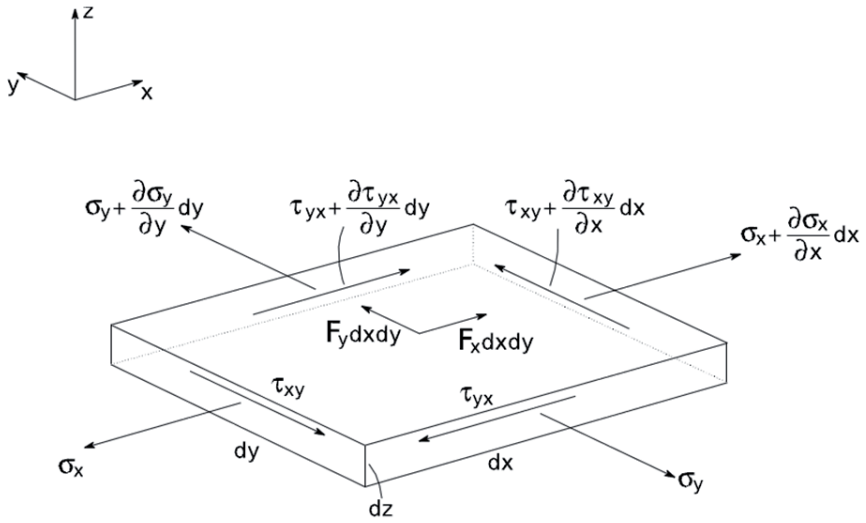

FIGURE 7 Differential parallelepiped and assumed stresses acting in the in-plane directions x and y, from **PI**.

It is possible to derive a vast number of different rheological models for time-dependent material behavior, but the fundamental behavior of continuous flow of a solid viscoelastic web can be analyzed using the simple Kelvin–Voigt model shown in Figure 8. More complicated rheological models rapidly increase the complexity of the continuum model without additional benefit.

The stress-strain behavior of one-dimensional Kelvin-Voigt material (see e.g. [28]) is:

$$\sigma = E\varepsilon + \eta \frac{\mathrm{d}\varepsilon}{\mathrm{d}t} \,. \tag{22}$$

Based on observations mentioned in previous chapters of fibrous web materials, we will apply a two-dimensional, orthotropic plane stress extension of the above model [108, 113]:

$$\sigma_x = \frac{E_{11}}{1-\nu_{12}\nu_{21}} \left(\varepsilon_{xx} + \nu_{21}\varepsilon_{yy}\right) + \frac{\eta_{11}}{1-\varphi_{12}\varphi_{21}} \left(\frac{\mathrm{d}\varepsilon_{xx}}{\mathrm{d}t} + \varphi_{21}\frac{\mathrm{d}\varepsilon_{yy}}{\mathrm{d}t}\right) \tag{23}$$

$$\sigma_y = \frac{E_{22}}{1-\nu_{12}\nu_{21}} \left(\varepsilon_{yy} + \nu_{12}\varepsilon_{xx}\right) + \frac{\eta_{22}}{1-\varphi_{12}\varphi_{21}} \left(\frac{\mathrm{d}\varepsilon_{yy}}{\mathrm{d}t} + \varphi_{12}\frac{\mathrm{d}\varepsilon_{xx}}{\mathrm{d}t}\right) \tag{24}$$

$$\tau_{yx} = \tau_{xy} = G_{12}\gamma_{xy} + \Pi\frac{\mathrm{d}\gamma_{xy}}{\mathrm{d}t} \tag{25}$$

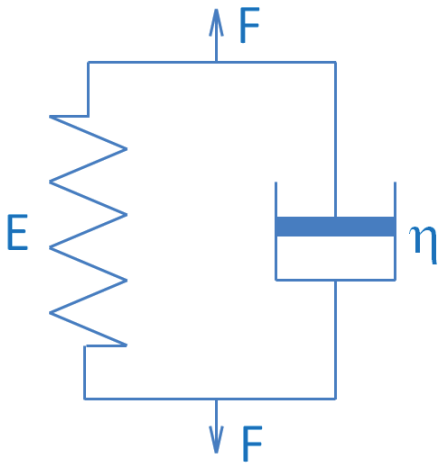

FIGURE 8 Schematic representation of the classical Kelvin-Voigt rheological model in one dimension. E is Young's modulus, η is the material viscosity, from **PI**.

Here φ_{12} and φ_{21} are the viscous analogues of the orthotropic in-plane Poisson ratios ν_{12} and ν_{21}, and Π is the shear viscosity of the material. We assume for simplicity, that the main axes of the orthotropic material coincide with the main axes of the control volume Ω.

Often, plane stress applications are written using only an elastic model, involving the moduli of elasticity E_{11} and E_{22}, and the strain variables ε_{xx} and ε_{yy}. However, in practice all the elastic-related material properties are measured with some definite velocity, and therefore apparent elasticity includes both elastic and viscous material properties [28]. Fundamentally, all materials exhibit some form of viscoelasticity, typically measured by normal and complex moduli E and E', respectively. It should also be pointed out that the viscoelastic Poisson ratios φ_{12} and φ_{21} cannot be calculated using compliances from the theory of elasticity [38].

The force balance equations (17) and (18) include also the body forces F_x and F_y, which are important especially with fibrous cellulose-based materials. Moisture-dependent dimension changes can be significant: they generate stresses in addition to those related to the strains based on external velocity differences, as was presented in equation (16) [44].

According to the D'alembert's principle, time-dependent kinematic behavior always includes inertial forces. Two-dimensional force balance in in-plane membrane behavior can be presented with the following equilibrium equations (see e.g. [97]):

$$\frac{\partial \sigma_x}{\partial x} + \frac{\partial \tau_{yx}}{\partial y} - F_x = \rho \frac{\mathrm{d}^2 u}{\mathrm{d}t^2} \tag{26}$$

$$\frac{\partial \sigma_y}{\partial y} + \frac{\partial \tau_{xy}}{\partial x} - F_y = \rho \frac{\mathrm{d}^2 v}{\mathrm{d}t^2} \tag{27}$$

Note that the operator $\mathrm{d}^2/\mathrm{d}t^2$ describes the inertial behavior in the Lagrangean

reference frame. Thus the inertial terms depending on the displacements u and v, in the Eulerian frame, must be presented by using the material derivative:

$$\frac{\mathrm{d}u}{\mathrm{d}t} = \frac{\partial u}{\partial t} + \sum_{i=1,2} \frac{\partial u}{\partial x_i}\frac{\mathrm{d}x_i}{\mathrm{d}t} \tag{28}$$

$$\frac{\mathrm{d}v}{\mathrm{d}t} = \frac{\partial v}{\partial t} + \sum_{j=1,2} \frac{\partial v}{\partial x_j}\frac{\mathrm{d}x_j}{\mathrm{d}t} \tag{29}$$

In above equations 28 and 29 above, both i and j are indexes referring to spatial coordinates. The second material derivatives of the displacements u and v are

$$\begin{aligned}\frac{\mathrm{d}^2u}{\mathrm{d}t^2} = \frac{\partial^2 u}{\partial t^2} + 2U_x\frac{\partial^2 u}{\partial x\partial t} + 2U_y\frac{\partial^2 u}{\partial y\partial t} + U_x^2\frac{\partial^2 u}{\partial x^2} + 2U_xU_y\frac{\partial^2 u}{\partial x\partial y} + U_y^2\frac{\partial^2 u}{\partial y^2} + \\ \frac{\partial u}{\partial x}\left(\frac{\partial U_x}{\partial x}U_x + \frac{\partial U_x}{\partial y}U_y + \frac{\partial U_x}{\partial t}\right) + \frac{\partial u}{\partial y}\left(\frac{\partial U_y}{\partial x}U_x + \frac{\partial U_y}{\partial y}U_y + \frac{\partial U_y}{\partial t}\right)\end{aligned} \tag{30}$$

$$\begin{aligned}\frac{\mathrm{d}^2v}{\mathrm{d}t^2} = \frac{\partial^2 v}{\partial t^2} + 2U_x\frac{\partial^2 v}{\partial x\partial t} + 2U_y\frac{\partial^2 v}{\partial y\partial t} + U_x^2\frac{\partial^2 v}{\partial x^2} + 2U_xU_y\frac{\partial^2 v}{\partial x\partial y} + U_y^2\frac{\partial^2 v}{\partial y^2} + \\ \frac{\partial v}{\partial x}\left(\frac{\partial U_x}{\partial x}U_x + \frac{\partial U_x}{\partial y}U_y + \frac{\partial U_x}{\partial t}\right) + \frac{\partial v}{\partial y}\left(\frac{\partial U_y}{\partial x}U_x + \frac{\partial U_y}{\partial y}U_y + \frac{\partial U_y}{\partial t}\right)\end{aligned} \tag{31}$$

By substituting (30) – (31) and (23) – (25) into equations (26) and (27), we will obtain the final, time-dependent two-dimensional equations for the in-plane, plane stress membrane behavior of the moving viscoelastic web:

$$\begin{aligned}\left(C_{11} - \rho U_x^2\right)\frac{\partial^2 u}{\partial x^2} + \left(C_{66} - \rho U_y^2\right)\frac{\partial^2 u}{\partial y^2} + C_{12}\frac{\partial^2 v}{\partial x\partial y} + C_{66}\frac{\partial^2 v}{\partial x\partial y} + \\ K_{11}U_x\frac{\partial^3 u}{\partial x^3} + K_{11}U_y\frac{\partial^3 u}{\partial x^2\partial y} + K_{11}\frac{\partial^3 u}{\partial x^2\partial t} + \left(K_{12} + K_{66}\right)U_y\frac{\partial^3 v}{\partial x\partial y^2} + \\ K_{66}U_y\frac{\partial^3 u}{\partial y^3} + \left(K_{12} + K_{66}\right)U_x\frac{\partial^3 v}{\partial x^2\partial y} + \left(K_{12} + K_{66}\right)\frac{\partial^3 v}{\partial x\partial y\partial t} + K_{66}U_x\frac{\partial^3 u}{\partial x\partial y^2} + \\ K_{66}\frac{\partial^3 u}{\partial y^2\partial t} - F_x \quad = \quad \rho\frac{\partial^2 u}{\partial t^2} + 2\rho U_xU_y\frac{\partial^2 u}{\partial x\partial y} + 2\rho U_x\frac{\partial^2 u}{\partial x\partial t} + 2\rho U_y\frac{\partial^2 u}{\partial y\partial t} + \\ \rho\frac{\partial u}{\partial x}\left(\frac{\partial U_x}{\partial x}U_x + \frac{\partial U_x}{\partial y}U_y + \frac{\partial U_x}{\partial t}\right) + \rho\frac{\partial u}{\partial y}\left(\frac{\partial U_y}{\partial x}U_x + \frac{\partial U_y}{\partial y}U_y + \frac{\partial U_y}{\partial t}\right)\end{aligned} \tag{32}$$

and:

$$\left(C_{22}-\rho U_y^2\right)\frac{\partial^2 v}{\partial y^2}+\left(C_{66}-\rho U_x^2\right)\frac{\partial^2 v}{\partial x^2}+C_{21}\frac{\partial^2 u}{\partial x\partial y}+C_{66}\frac{\partial^2 v}{\partial x\partial y}+ \tag{33}$$
$$K_{22}U_y\frac{\partial^3 v}{\partial y^3}+K_{22}U_x\frac{\partial^3 v}{\partial x^2\partial y}+K_{22}\frac{\partial^3 v}{\partial x^2\partial t}+\left(K_{21}+K_{66}\right)U_x\frac{\partial^3 u}{\partial x^2\partial y}+$$
$$K_{66}U_x\frac{\partial^3 v}{\partial x^3}+\left(K_{21}+K_{66}\right)U_y\frac{\partial^3 u}{\partial x\partial y^2}+\left(K_{21}+K_{66}\right)\frac{\partial^3 u}{\partial x\partial y\partial t}+K_{66}U_y\frac{\partial^3 v}{\partial x^2\partial y}+$$
$$K_{66}\frac{\partial^3 v}{\partial y^2\partial t}-F_y \quad = \quad \rho\frac{\partial^2 v}{\partial t^2}+2\rho U_xU_y\frac{\partial^2 v}{\partial x\partial y}+2\rho U_x\frac{\partial^2 v}{\partial x\partial t}+2\rho U_y\frac{\partial^2 v}{\partial y\partial t}+$$
$$\rho\frac{\partial v}{\partial x}\left(\frac{\partial U_x}{\partial x}U_x+\frac{\partial U_x}{\partial y}U_y+\frac{\partial U_x}{\partial t}\right)+\rho\frac{\partial v}{\partial y}\left(\frac{\partial U_y}{\partial x}U_x+\frac{\partial U_y}{\partial y}U_y+\frac{\partial U_y}{\partial t}\right),$$

The orthotropic coefficients are:

$$C_{11}=\frac{E_{11}}{1-\nu_{12}\nu_{21}},\quad C_{22}=\frac{E_{22}}{1-\nu_{12}\nu_{21}}, \tag{34}$$
$$C_{12}=C_{11}\nu_{21}=C_{22}\nu_{12}=C_{21},\quad C_{66}=G_{12}, \tag{35}$$
$$K_{11}=\frac{\eta_{11}}{1-\varphi_{12}\varphi_{21}},\quad K_{22}=\frac{\eta_{22}}{1-\varphi_{12}\varphi_{21}}, \tag{36}$$
$$K_{12}=K_{11}\varphi_{21}=K_{22}\varphi_{12}=K_{21},\quad K_{66}=\Pi. \tag{37}$$

Equations (32) and (33) are nonlinear. Nonlinearity appears in the velocity U_y, which is dependent on the contraction controlled by both elastic and viscous Poisson's ratios. There are also nonlinear Navier–Stokes type convection terms, the significance of which is small if the strains defined in the equation (19) can be considered small Cauchy strains.

The steady-state solution describing the movement of smooth, undisturbed web is possible to obtain by omitting the time-dependent terms from equations (32) and (33):

$$\left(C_{11}-\rho U_x^2\right)\frac{\partial^2 u}{\partial x^2}+\left(C_{66}-\rho U_y^2\right)\frac{\partial^2 u}{\partial y^2}+C_{12}\frac{\partial^2 v}{\partial x\partial y}+C_{66}\frac{\partial^2 v}{\partial x\partial y}+ \tag{38}$$
$$K_{11}U_x\frac{\partial^3 u}{\partial x^3}+K_{11}U_y\frac{\partial^3 u}{\partial x^2\partial y}+\left(K_{12}+K_{66}\right)U_y\frac{\partial^3 v}{\partial x\partial y^2}+K_{66}U_y\frac{\partial^3 u}{\partial y^3}+$$
$$\left(K_{12}+K_{66}\right)U_x\frac{\partial^3 v}{\partial x^2\partial y}+K_{66}U_x\frac{\partial^3 u}{\partial x\partial y^2}-F_x=$$
$$2\rho U_xU_y\frac{\partial^2 u}{\partial x\partial y}+\rho\frac{\partial u}{\partial x}\left(\frac{\partial U_x}{\partial x}U_x+\frac{\partial U_x}{\partial y}U_y\right)+\rho\frac{\partial u}{\partial y}\left(\frac{\partial U_y}{\partial x}U_x+\frac{\partial U_y}{\partial y}U_y\right)$$

and:

$$\left(C_{22}-\rho U_y^2\right)\frac{\partial^2 v}{\partial y^2}+\left(C_{66}-\rho U_x^2\right)\frac{\partial^2 v}{\partial x^2}+C_{21}\frac{\partial^2 u}{\partial x\partial y}+C_{66}\frac{\partial^2 v}{\partial x\partial y}+ \tag{39}$$
$$K_{22}U_y\frac{\partial^3 v}{\partial y^3}+K_{22}U_x\frac{\partial^3 v}{\partial x\partial y}^2+\left(K_{21}+K_{66}\right)U_x\frac{\partial^3 u}{\partial x^2\partial y}+K_{66}U_x\frac{\partial^3 v}{\partial x^3}+$$
$$+\left(K_{21}+K_{66}\right)U_y\frac{\partial^3 u}{\partial x\partial y^2}+K_{66}U_y\frac{\partial^3 v}{\partial x^2\partial y}-F_y=$$
$$2\rho U_xU_y\frac{\partial^2 v}{\partial x\partial y}+\rho\frac{\partial v}{\partial x}\left(\frac{\partial U_x}{\partial x}U_x+\frac{\partial U_x}{\partial y}U_y\right)+\rho\frac{\partial v}{\partial y}\left(\frac{\partial U_y}{\partial x}U_x+\frac{\partial U_y}{\partial y}U_y\right).$$

Often a good understanding of the basic physical behavior of the modeled system can be achieved by one-dimensional approach. Using (32), one-dimensional, time-dependent equation for viscoelastic moving web in x-direction is:

$$\left(C_{11}-\rho U_x^2\right)\frac{\partial^2 u}{\partial x^2}+K_{11}U_x\frac{\partial^3 u}{\partial x^3}+K_{11}\frac{\partial^3 u}{\partial x^2\partial t}-F_x= \tag{40}$$
$$\rho\frac{\partial^2 u}{\partial t^2}+2\rho U_x\frac{\partial^2 u}{\partial x\partial t}+\rho\frac{\partial u}{\partial x}\left(\frac{\partial U_x}{\partial x}U_x+\frac{\partial U_x}{\partial t}\right)$$

Further, the steady-state form of the above equation is:

$$\left(C_{11}-\rho U_x^2\right)\frac{\partial^2 u}{\partial x^2}+K_{11}U_x\frac{\partial^3 u}{\partial x^3}-F_x-\rho\frac{\partial u}{\partial x}\frac{\partial U_x}{\partial x}U_x=0 \tag{41}$$

The interpretation of displacements u and v in equations (32) and (33) are a in vital part of understanding of the nature of the displacements in a moving web. Displacements should be understood as instantaneous snapshots of a specific situation in an Eulerian coordinate system. They are changing the magnitude at each situation according to the transfer velocities U_x and U_y.

3.3 Solution and results of the in-plane equations

As mentioned earlier, the presented in-plane equations are nonlinear since there exist in certain terms velocity U_y, which is further dependent on the y-directional displacement v. An analytical solution is presented in **PI**. It is possible to achieve that solution with a linearized, one-dimensional equation formed with the help of equation (42):

$$\left(C_{11}-\rho U_x^2\right)\frac{\partial^2 u}{\partial x^2}+K_{11}U_x\frac{\partial^3 u}{\partial x^3}-F_x=0 \tag{42}$$

This is a third-order linear differential equation, with a convective nature, including an internal body force F_x.

3.3.1 Analytical solution of 1-D viscoelastic equations

Recall (19), which states that $\varepsilon_{xx} = \partial u/\partial x$. The form of the equation (42) without the body force term $F_x$will be:

$$\eta_{11} U_x \frac{\partial^2 \varepsilon_{xx}}{\partial x^2} + \left(C_{11} - \rho U_x^2\right) \frac{\partial \varepsilon_{xx}}{\partial x} = 0 \,. \tag{43}$$

Equation (43) can be solved with analytical methods. First, as a special case, if only pure elasticity is present ($\eta_{11} = 0$), the solution is of the form:

$$\left(C_{11} - \rho U_x^2\right) \varepsilon_{xx} = C \,. \tag{44}$$

In this case the solution describes Hookean behavior, i.e., the strain ε_{xx} is constant along the whole span regardless of the magnitude of the transport velocity U_x. Now, consider the general case with nonzero viscosity η_{11}, which is the more natural case since majority of solid materials possess viscous properties. Equation (43) becomes,

$$\frac{\partial^2 \varepsilon_{xx}}{\partial x^2} + \left(\frac{C_{11} - \rho U_x^2}{\eta_{11} U_x}\right) \frac{\partial \varepsilon_{xx}}{\partial x} = 0 \,. \tag{45}$$

With the boundary conditions $\varepsilon_{xx}(0) = 0$ and $\varepsilon_{xx}(\ell) = \varepsilon_T$, the analytical solution of equation (46) is [57, 59]:

$$\varepsilon_{xx}(x) = \varepsilon_T \frac{1 - e^{-kx}}{1 - e^{-k\ell}} \,, \qquad \text{where} \qquad k = \frac{E_{11} - \rho U_x^2}{\eta_{11} U_x} \,. \tag{46}$$

That is, for a moving viscoelastic material loaded only by tension at the ends of the span, the strain is not constant, but grows logarithmically along the span. Finally, let us find the corresponding x-directional stress field.

The stress is a superposition of elastic and viscous stress components:

$$\sigma_x = C_{11} \varepsilon_{xx} + \eta_{11} \frac{\mathrm{d}\varepsilon_{xx}}{\mathrm{d}t} \,. \tag{47}$$

A straightforward analytical solution of the stress is easy to obtain only in a the linearized, one-dimensional, steady-state case. Using equations (20) and (22), the time derivative of the strain, in mixed Lagrange–Euler form, can be written for the steady-state solution as follows:

$$\frac{\mathrm{d}\varepsilon_{xx}}{\mathrm{d}t} = \frac{\partial \varepsilon_{xx}}{\partial x} U_x \,. \tag{48}$$

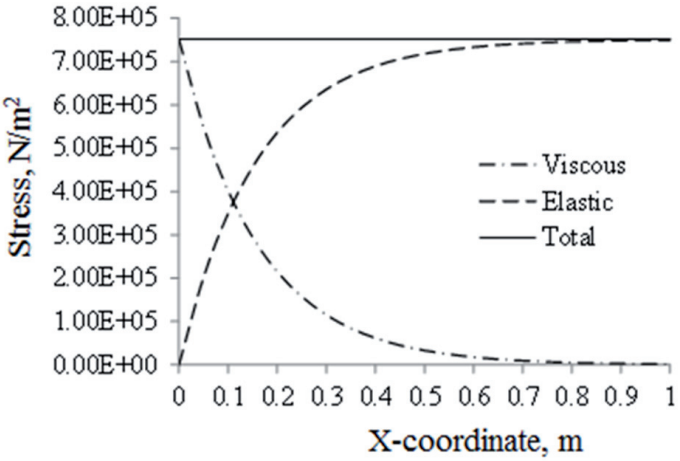

FIGURE 9 Stresses of the one-dimensional, viscoelastic web with span length $\ell = 1.0$m and with applied strain ϵ_T, from **PI**.

Using (46) in (48), and then inserting (47), we obtain the stress field as

$$\sigma_x = C_{11}\varepsilon_T \frac{1 - e^{-kx}}{1 - e^{-k\ell}} + \eta_{11} U_x \varepsilon_T \frac{k e^{-kx}}{1 - e^{-k\ell}} \,. \tag{49}$$

Expanding the k in the second term of (49) by using (46) obtains

$$\sigma_x = \frac{\varepsilon_T}{1 - e^{-k\ell}} \left(E_{11} - \rho U_x^2 e^{-kx} \right). \tag{50}$$

An example solution of equation (50) is presented in Figure 9. Total stress appearing in the web (span length = 1.0 m) is due to elastic and viscous components. Even though the stress appears to be constant, it has slightly increasing tendency (not visible in Figure 9) due the acceleration from velocity increase between starting and ending points (see also Equation (17)).

A numerical FEM solution of the nonlinear equation (42) is presented in **PI**.

3.3.2 Numerical solution of 2-D elastic equations

A numerical solution for the two-dimensional, orthotropic, elastic moving continuum plane stress problem was realized with the help of the finite element method (FEM). Although the above treatment was extremely useful for handling the one-dimensional case, a correct derivation requires tensor derivation in a Cartesian coordinate system.

Starting from (32) and (33) in a Cartesian tensor form we will get:

$$\rho \frac{\mathrm{d}^2 \mathbf{u}}{\mathrm{d}t^2} - \nabla \cdot \boldsymbol{\sigma}^{\mathrm{T}} = \mathbf{F} \,, \tag{51}$$

where $(\dots)^{\mathrm{T}}$ denotes the transpose of a rank-2 tensor. The second material derivative expands as:

$$\frac{\mathrm{d}^2 \mathbf{u}}{\mathrm{d}t^2} = \frac{\mathrm{d}}{\mathrm{d}t}\left(\frac{\partial \mathbf{u}}{\partial t} + \mathbf{U}\cdot\nabla\mathbf{u}\right) = \frac{\partial^2 \mathbf{u}}{\partial t^2} + 2\mathbf{U}\cdot\nabla\left(\frac{\partial \mathbf{u}}{\partial t}\right) + (\mathbf{U}\cdot\nabla)(\mathbf{U}\cdot\nabla\mathbf{u}) \,. \tag{52}$$

In steady state, only the last term remains. Hence (51), for a steady state, becomes

$$\rho\,(\mathbf{U}\cdot\nabla)(\mathbf{U}\cdot\nabla\mathbf{u}) - \nabla\cdot\boldsymbol{\sigma}^{\mathrm{T}} = \mathbf{F} \,. \tag{53}$$

Next, we will use the principle of virtual work. Let us take the dot product of (53) with a vector-valued test function (virtual displacement) $\boldsymbol{\phi}$, and integrate the equation over the two-dimensional domain

$$\Omega \equiv \{\, (x,y) : 0 < x < \ell \,,\; 0 < y < b \,\} \,. \tag{54}$$

Assuming that ρ can be approximated as a constant (i.e. that the small strains do not significantly affect the density), we obtain:

$$\rho \int_\Omega \boldsymbol{\phi}\cdot(\mathbf{U}\cdot\nabla)(\mathbf{U}\cdot\nabla\mathbf{u})\,\mathrm{d}\Omega - \int_\Omega \boldsymbol{\phi}\cdot[\nabla\cdot\boldsymbol{\sigma}^{\mathrm{T}}]\,\mathrm{d}\Omega = \int_\Omega \boldsymbol{\phi}\cdot\mathbf{F}\,\mathrm{d}\Omega \,. \tag{55}$$

In order to integrate by parts in (55), we make use of the following two identities:

$$\int_\Omega \boldsymbol{\phi}\cdot[\nabla\cdot\boldsymbol{\sigma}^{\mathrm{T}}]\,\mathrm{d}\Omega = \int_{\partial\Omega} \boldsymbol{\phi}\cdot(\mathbf{n}\cdot\boldsymbol{\sigma}^{\mathrm{T}})\,\mathrm{d}\Gamma - \int_\Omega \nabla\boldsymbol{\phi} : \boldsymbol{\sigma}\,\mathrm{d}\Omega \,, \tag{56}$$

$$\begin{aligned}\int_\Omega \boldsymbol{\phi}\cdot(\mathbf{U}\cdot\nabla)(\mathbf{U}\cdot\nabla\mathbf{u}) &= \int_{\partial\Omega} \mathbf{n}\cdot[(\mathbf{U}\cdot\nabla\mathbf{u})\cdot(\boldsymbol{\phi}\otimes\mathbf{U})]\,\mathrm{d}\Gamma \\ &\quad - \int_\Omega (\mathbf{U}\cdot\nabla\mathbf{u})\cdot[\nabla\cdot(\mathbf{U}\otimes\boldsymbol{\phi})]\,\mathrm{d}\Omega \,.\end{aligned} \tag{57}$$

where $\mathbf{n}$ is the outer unit normal, and the notational conventions are

$$(\nabla\mathbf{a})_{ij} \equiv \partial_i a_j \,, \quad (\nabla\cdot\mathbf{A})_j \equiv \partial_i A_{ij} \quad (\mathbf{a}\otimes\mathbf{b})_{ij} = a_i b_j \,, \quad \mathbf{A}:\mathbf{B} \equiv A_{ij}B_{ji} \,. \tag{58}$$

Here $\mathbf{a}$ and $\mathbf{b}$ are vectors, and $\mathbf{A}$ and $\mathbf{B}$ are rank-2 tensors. The summation convention for repeated indices applies. The integration-by-parts formula (56) is standard in the theory of elasticity, but the formula (57) is new and must be handled in the following manner:

Observe that for any differentiable vector fields $\mathbf{a}$, $\mathbf{b}$ and $\mathbf{c}$,

$$\nabla\cdot(\mathbf{a}\cdot(\mathbf{b}\otimes\mathbf{c})) = \mathbf{b}\cdot(\mathbf{c}\cdot\nabla\mathbf{a}) + \mathbf{a}\cdot(\nabla\cdot(\mathbf{c}\otimes\mathbf{b})) \,. \tag{59}$$

By integrating (58) over Ω, applying the divergence theorem to the left-hand side, and choosing $\mathbf{a} = (\mathbf{U}\cdot\nabla\mathbf{u})$, $\mathbf{b} = \boldsymbol{\phi}$, and $\mathbf{c} = \mathbf{U}$, relation (57) follows. Using (56) and (57) in (55), we obtain

$$\begin{aligned}&-\rho\int_\Omega (\mathbf{U}\cdot\nabla\mathbf{u})\cdot[\nabla\cdot(\mathbf{U}\otimes\boldsymbol{\phi})]\,\mathrm{d}\Omega + \int_\Omega \nabla\boldsymbol{\phi}:\boldsymbol{\sigma}\,\mathrm{d}\Omega \\ &+\rho\int_{\partial\Omega}\mathbf{n}\cdot[(\mathbf{U}\cdot\nabla\mathbf{u})\cdot(\boldsymbol{\phi}\otimes\mathbf{U})]\,\mathrm{d}\Gamma - \int_{\partial\Omega}\boldsymbol{\phi}\cdot(\mathbf{n}\cdot\boldsymbol{\sigma}^{\mathrm{T}})\,\mathrm{d}\Gamma = \int_\Omega \boldsymbol{\phi}\cdot\mathbf{F}\,\mathrm{d}\Omega \,.\end{aligned} \tag{60}$$

By using the identity

$$\nabla \cdot (\mathbf{U} \otimes \boldsymbol{\phi}) = (\nabla \cdot \mathbf{U})\boldsymbol{\phi} + \mathbf{U} \cdot \nabla \boldsymbol{\phi} \tag{61}$$

we will obtain the final form:

$$\begin{aligned} &-\rho \int_\Omega (\mathbf{U} \cdot \nabla \mathbf{u}) \cdot [(\nabla \cdot \mathbf{U})\boldsymbol{\phi} + \mathbf{U} \cdot \nabla \boldsymbol{\phi}] \, \mathrm{d}\Omega + \int_\Omega \nabla \boldsymbol{\phi} : \boldsymbol{\sigma} \, \mathrm{d}\Omega \\ &+\rho \int_{\partial\Omega} \mathbf{n} \cdot \left[\, (\mathbf{U} \cdot \nabla \mathbf{u}) \cdot (\boldsymbol{\phi} \otimes \mathbf{U}) \right] \mathrm{d}\Gamma - \int_{\partial\Omega} \boldsymbol{\phi} \, (\mathbf{n} \cdot \boldsymbol{\sigma}^{\mathrm{T}}) \, \mathrm{d}\Gamma = \int_\Omega \boldsymbol{\phi} \cdot \mathbf{F} \, \mathrm{d}\Omega \, . \end{aligned} \tag{62}$$

Note that (62) also gives the natural boundary conditions, when the boundary terms are gathered under one integral sign.

When expanded to the component form, (62) gives following two equations:

$$\begin{aligned} &\int_\Omega \left[-\sigma_x + \rho U_x^2 \frac{\partial u}{\partial x} + \rho U_y U_x \frac{\partial u}{\partial y} \right] \frac{\partial \phi}{\partial x} \, \mathrm{d}\Omega \\ &+ \int_\Omega \left[-\tau_{xy} + \rho U_x U_y \frac{\partial u}{\partial x} + \rho U_y^2 \frac{\partial u}{\partial y} \right] \frac{\partial \phi}{\partial y} \, \mathrm{d}\Omega \\ &+\rho \int_\Omega \left\{ \left[U_x \frac{\partial u}{\partial x} + U_y \frac{\partial u}{\partial y} \right] \left[\frac{\partial U_x}{\partial x} + \frac{\partial U_y}{\partial y} \right] \right\} \phi \, \mathrm{d}\Omega \\ &+ \int_{\partial\Omega} n_x \left[\sigma_x - \rho U_x^2 \frac{\partial u}{\partial x} - \rho U_y U_x \frac{\partial u}{\partial y} \right] \phi \, \mathrm{d}\Gamma \\ &+ \int_{\partial\Omega} n_y \left[\tau_{xy} - \rho U_x U_y \frac{\partial u}{\partial x} - \rho U_y^2 \frac{\partial u}{\partial y} \right] \phi \, \mathrm{d}\Gamma \\ &+ \int_\Omega F_x \phi = 0 \, . \end{aligned} \tag{63}$$

and

$$\begin{aligned} &\int_\Omega \left[-\tau_{yx} + \rho U_x^2 \frac{\partial v}{\partial x} + \rho U_y U_x \frac{\partial v}{\partial y} \right] \frac{\partial \psi}{\partial x} \, \mathrm{d}\Omega \\ &+ \int_\Omega \left[-\sigma_y + \rho U_x U_y \frac{\partial v}{\partial x} + \rho U_y^2 \frac{\partial v}{\partial y} \right] \frac{\partial \psi}{\partial y} \, \mathrm{d}\Omega \\ &+\rho \int_\Omega \left\{ \left[U_x \frac{\partial v}{\partial x} + U_y \frac{\partial v}{\partial y} \right] \left[\frac{\partial U_x}{\partial x} + \frac{\partial U_y}{\partial y} \right] \right\} \psi \, \mathrm{d}\Omega \\ &+ \int_{\partial\Omega} n_x \left[\tau_{yx} - \rho U_x^2 \frac{\partial v}{\partial x} - \rho U_y U_x \frac{\partial v}{\partial y} \right] \psi \, \mathrm{d}\Gamma \\ &+ \int_{\partial\Omega} n_y \left[\sigma_y - \rho U_x U_y \frac{\partial v}{\partial x} - \rho U_y^2 \frac{\partial v}{\partial y} \right] \psi \, \mathrm{d}\Gamma \\ &+ \int_\Omega F_y \phi = 0 \, , \end{aligned} \tag{64}$$

where the outer unit normal $\mathbf{n}$ has the components $\mathbf{n} = (\, n_x \, , n_y \,)$. We now have moved all terms to the left-hand side and multiplied each equation by -1.

Equations (63) and (64) represent the two-dimensional steady-state equation of any moving Lagrangian-Euler continuum. Applying pure orthotropic elasticity we will get the following equations in a weak form:

$$\begin{aligned}
&\int_\Omega \left[-\left[C_{11}\frac{\partial u}{\partial x} + C_{12}\frac{\partial v}{\partial y} \right] + \rho U_x^2 \frac{\partial u}{\partial x} + \rho U_y U_x \frac{\partial u}{\partial y} \right] \frac{\partial \phi}{\partial x}\, \mathrm{d}\Omega \\
&+ \int_\Omega \left[-\left[C_{66}\left(\frac{\partial u}{\partial y} + \frac{\partial v}{\partial x}\right) \right] + \rho U_x U_y \frac{\partial u}{\partial x} + \rho U_y^2 \frac{\partial u}{\partial y} \right] \frac{\partial \phi}{\partial y}\, \mathrm{d}\Omega \\
&\qquad + \rho \int_\Omega \left\{ \left[U_x \frac{\partial u}{\partial x} + U_y \frac{\partial u}{\partial y} \right] \left[\frac{\partial U_x}{\partial x} + \frac{\partial U_y}{\partial y} \right] \right\} \phi\, \mathrm{d}\Omega \\
&+ \int_{\partial\Omega} n_x \left[\left[C_{11}\frac{\partial u}{\partial x} + C_{12}\frac{\partial v}{\partial y} \right] - \rho U_x^2 \frac{\partial u}{\partial x} - \rho U_y U_x \frac{\partial u}{\partial y} \right] \phi\, \mathrm{d}\Gamma \\
&+ \int_{\partial\Omega} n_y \left[\left[C_{66}\left(\frac{\partial u}{\partial y} + \frac{\partial v}{\partial x}\right) \right] - \rho U_x U_y \frac{\partial u}{\partial x} - \rho U_y^2 \frac{\partial u}{\partial y} \right] \phi\, \mathrm{d}\Gamma \\
&\qquad + \int_\Omega F_x \phi\, \mathrm{d}\Omega = 0
\end{aligned} \tag{65}$$

and

$$\begin{aligned}
&\int_\Omega \left[-\left[C_{66}\left(\frac{\partial u}{\partial y} + \frac{\partial v}{\partial x}\right) \right] + \rho U_x^2 \frac{\partial v}{\partial x} + \rho U_y U_x \frac{\partial v}{\partial y} \right] \frac{\partial \psi}{\partial x}\, \mathrm{d}\Omega \\
&+ \int_\Omega \left[-\left[C_{21}\frac{\partial u}{\partial x} + C_{22}\frac{\partial v}{\partial y} \right] + \rho U_x U_y \frac{\partial v}{\partial x} + \rho U_y^2 \frac{\partial v}{\partial y} \right] \frac{\partial \psi}{\partial y}\, \mathrm{d}\Omega \\
&\qquad + \rho \int_\Omega \left\{ \left[U_x \frac{\partial v}{\partial x} + U_y \frac{\partial v}{\partial y} \right] \left[\frac{\partial U_x}{\partial x} + \frac{\partial U_y}{\partial y} \right] \right\} \psi\, \mathrm{d}\Omega \\
&+ \int_{\partial\Omega} n_x \left[\left[C_{66}\left(\frac{\partial u}{\partial y} + \frac{\partial v}{\partial x}\right) \right] - \rho U_x^2 \frac{\partial v}{\partial x} - \rho U_y U_x \frac{\partial v}{\partial y} \right] \psi\, \mathrm{d}\Gamma \\
&+ \int_{\partial\Omega} n_y \left[\left[C_{21}\frac{\partial u}{\partial x} + C_{22}\frac{\partial v}{\partial y} \right] - \rho U_x U_y \frac{\partial v}{\partial x} - \rho U_y^2 \frac{\partial v}{\partial y} \right] \psi\, \mathrm{d}\Gamma \\
&\qquad + \int_\Omega F_y \phi\, \mathrm{d}\Omega = 0\,.
\end{aligned} \tag{66}$$

For the results presented, we use the numerical finite element method. In the examples, the simulation area is 1.0 m $\times$ 1.0 m and Dirichlet boundary conditions $u = 0$ and $u = 0.03$ are applied at the vertical incoming and outgoing edges respectively; upper and lower edges are assumed to be free (zero Neumann condition).

In the case of isotropic material assumption, the modulus of elasticity is $E = E_{11} = E_{22} = 2.5 \cdot 10^7\ \mathrm{N/m^2}$ and $\nu = \nu_{12} = \nu_{21} = 0.3$ describing the properties of isotropic wet paper. The basis weight of the wet paper is $m = 0.18\ \mathrm{kg/m^2}$ and the thickness of the web is 0.2 mm.

With orthotropic assumption, the Maxwell law of orthotropic materials is assumed to be apply here even though it is known that paper or board does not satisfy this rule completely [57]:

$$\frac{\nu_{12}}{E_{11}} = \frac{\nu_{21}}{E_{22}} \tag{67}$$

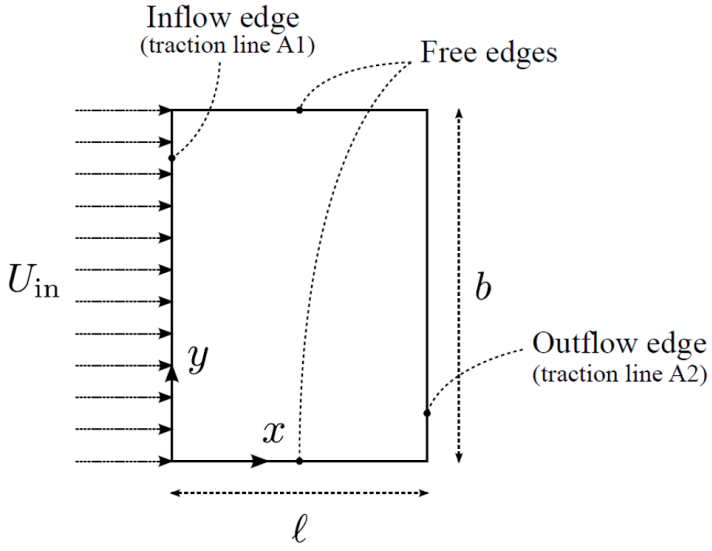

FIGURE 10 Setup for the two-dimensional numerical investigation. Elastic material flows in from the left at velocity U_{in}. From **PII**.

Thus, the orthotropic material values here are chosen so that the geometric mean of the values E_{11} and E_{22} is equal with isotropic material values. If the elasticity ratio $E_{11}/E_{22} = 4.0$, then $E_{11} = 5.0 \cdot 10^7$ N/m^2, $E_{22} = 1.25 \cdot 10^7$ N/m^2 at the x- and y-direction respectively. The Poisson's ratios, $\nu_{12} = 0.6$ and $\nu_{21} = 0.15$, are following same Maxwell law of orthotropic materials.

The two-dimensional setup for numerical analysis is presented in Figure 10. Web flows in at speed U_{in} from the left side through traction line A1, where the Dirichlet boundary conditions $u = v = 0$ are assigned. Since the area under observation is open, unsupported, two-dimensional web span, both upper and lower edges are free.

The coupling between the Eulerian displacements and velocity field can be presented using the Cauchy strains. In this case, we obtain for velocities U_x and U_y:

$$\begin{aligned} U_X &= (1 + \frac{\partial u}{\partial x})U_x + \frac{\partial u}{\partial y}U_y \,, \\ U_Y &= \frac{\partial v}{\partial x}U_x + (1 + \frac{\partial v}{\partial y})U_y \,. \end{aligned} \tag{68}$$

At the outflow edge, edge contraction in y-direction must be allowed since the transport velocity $\|U\|$ affecting in the area contributes not only to the web contraction along the normal in-plane contraction, but also constantly regenerates the web material in the span. The web, therefore, is capable to perform v-directional displacements.

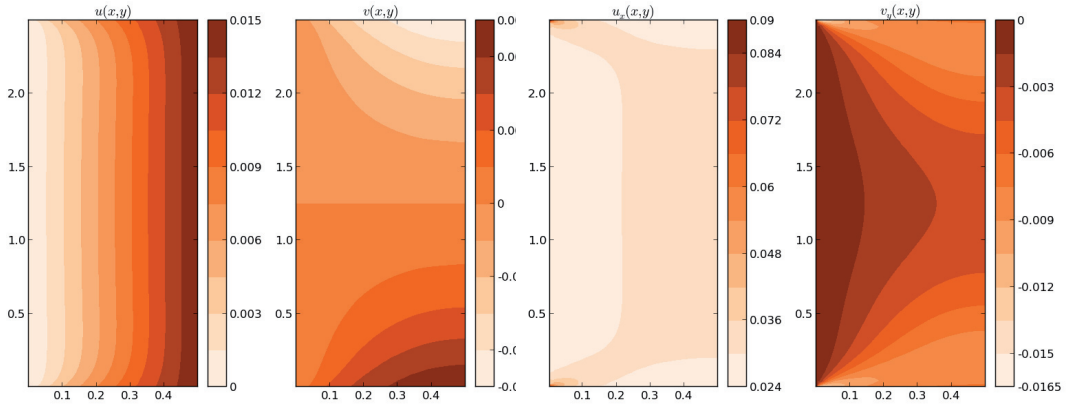

FIGURE 11 Reference behavior of 2-dimensional, unsupported web with $U_{in} = 0$. Aspect ratio $b/\ell = 5$. From left to right: Displacement u, displacement v, strain $\partial u/\partial x$ and strain $\partial v/\partial y$.

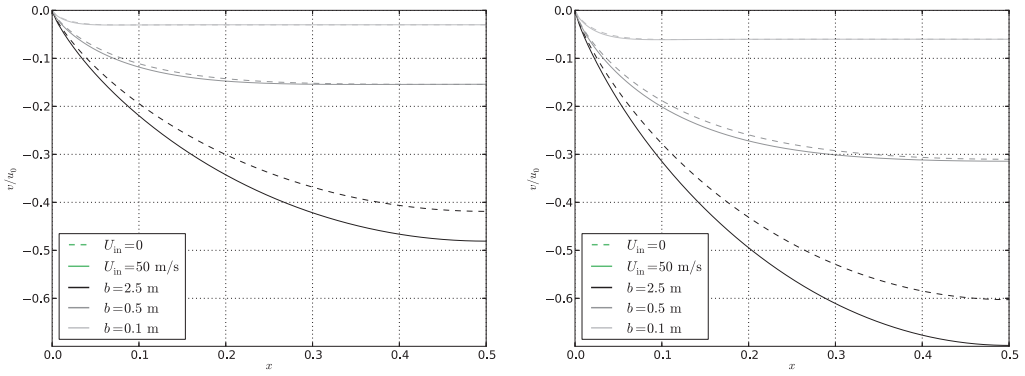

FIGURE 12 Displacement v, normalized to u_{f}, along the free edge $0 < x < \ell$, $y = b$. *Left*: isotropic. *Right*: orthotropic. Line style indicates inflow velocity U_{in}, darkness indicates span width b. From **PII**.

The numerical results are presented in Figures 11 – 14. In Figure 11 typical displacements and strain fields become apparent with the boundary conditions used; the computed values are (must be) symmetrical according to the x-axis at the centerline of the web height.

Figure 12 shows the effect of the inflow velocity: the contraction of the web in y-direction increases with a higher web width, but also the velocity accelerates this contraction. This effect is easy to understand since the also the y-directional velocity component U_y increases with contraction levels through increased centrifugal force appearing on the web plane.

The consequences of the increased centrifugal force are visible in Figure 13. The velocity-assisted contraction decreases web stress in y-direction, softening

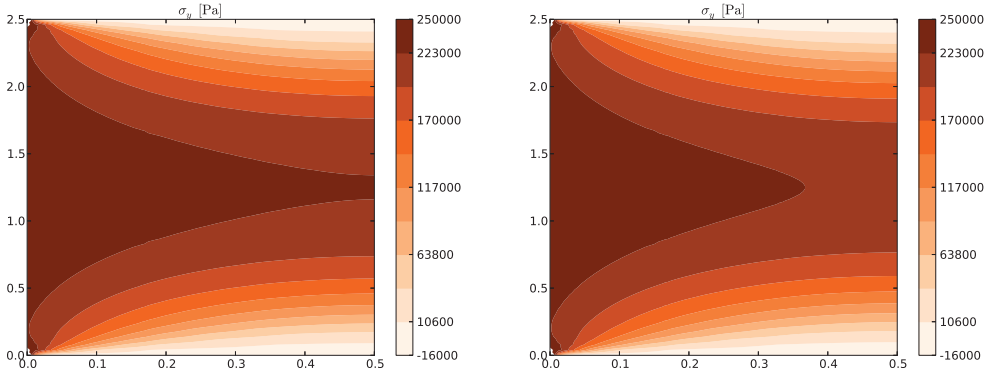

FIGURE 13 Stress σ_y in orthotropic web with aspect ratio $b/\ell = 5$. *Left*: $U_{in} = 0\,m/s$. *Right*: $U_{in} = 25\,m/s$. From **PII**.

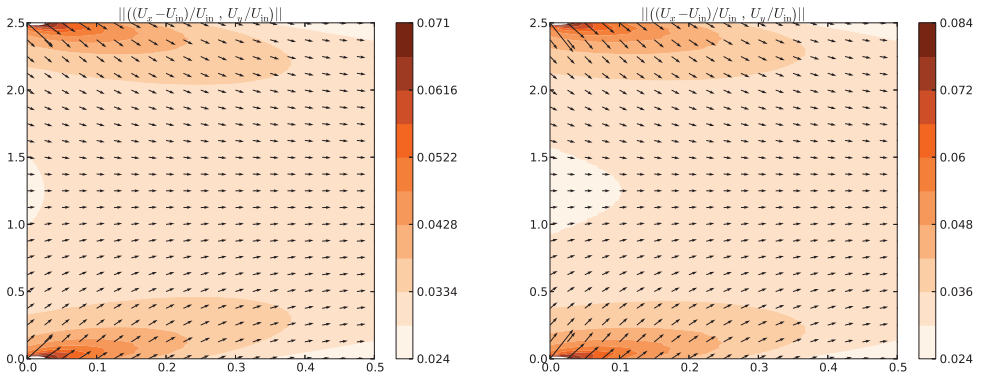

FIGURE 14 Relative velocity field U_{rel} as vector plot, normalized to $U_{in} = 50\,m/s$. Aspect ratio $b/\ell = 5$. *Left*: Isotropic. *Right*: Orthotropic. From **PII**.

the web, thus slightly increasing the low-stress areas at web edges.

Finally, the velocity field appearing in the moving continua is presented in Figure 14. The highest relative velocity values are reached at the corner areas where the contraction gradient is highest. A small difference exists between isotropic and orthotropic material assumptions; lower y-directional elasticity with orthotropic material is contributing to higher contraction but also slightly higher relative velocity values towards the centerline of the web.

4 STABILIZATION AND PRODUCTION EFFICIENCY OF THE TENSIONED IMPERFECT WEB IN HIGH VELOCITY ENVIRONMENT

One of the most fundamental web handling problem arises from the stressing of the web. By applying the relative velocity difference to the extremes of an open web span, one can increase the tension, thus improving the stability of the web. However, this tensioning has an upper limit. Web break probability increases rapidly as a function of this straining [40]. In this chapter we discuss two important but severely contradictory items related to web stability and production efficiency of the web.

4.1 Stability of a tensioned, orthotropic web in high velocity environment

Moving, low-grammage webs in high velocity board and paper making are susceptible to stability loss. Web behavior in unsupported, open draws is well known but often the studies have focused on coupled, time-dependent air-web frequency behavior [85, 12]. In **PIII**, the main focus is on the primary limit velocity analysis of stability loss of an orthotropic web. Additionally, the importance of the fluid coupling with the web and its effects to the buckling speed are brought up [58].

Consider an elastic, orthotropic web moving with constant velocity V_0 in the x-direction supported by the rollers located at $x = 0$ and $x = \ell$ in cartesian coordinate system presented in Figure 15:

$$\Omega \equiv \{(x, y) \in \mathbb{R}^2 : 0 < x < \ell,\ -b < y < b\} \tag{69}$$

The web is represented by a rectangular elastic orthotropic plate with bending rigidities D_1, D_2 and D_3, or by a rectangular orthotropic membrane with zero bending rigidities. The ”1” axis of the orthotropic material is aligned with the x direction, while the ”2” axis is aligned with the y direction (see Figure 15). The

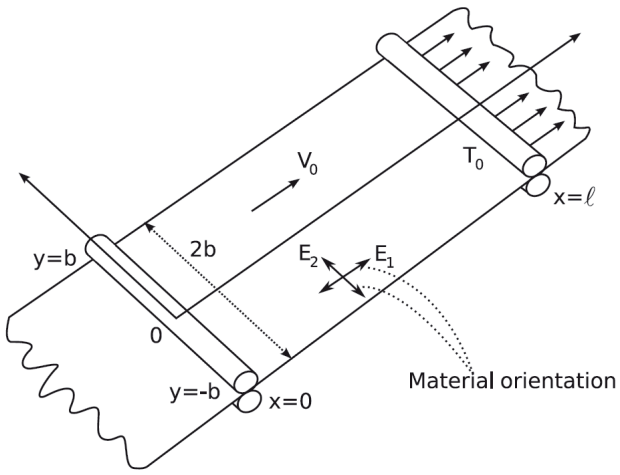

FIGURE 15 Axially moving elastic orthotropic web under homogenous tension from **PIII**.

web is subjected to homogeneous tension, acting in the x direction. The sides of the band $x = 0$, $-b \leq y \leq b$ and $x = \ell$, $-b \leq y \leq b$ are simply supported, and the sides $y = -b$, $0 \leq x \leq \ell$ and $y = b$, $0 \leq x \leq \ell$ are free of tractions.

The transverse displacement of the travelling band is described by the deflection function w, which depends on the coordinates x and y and time t. The differential equation for small transverse vibrations has the form

$$m\left(\frac{\partial^2 w}{\partial t^2} + 2V_0\frac{\partial^2 w}{\partial x \partial t} + V_0^2\frac{\partial^2 w}{\partial x^2}\right) = T_{xx}\frac{\partial^2 w}{\partial x^2} + 2T_{xy}\frac{\partial^2 w}{\partial x \partial y} + T_{yy}\frac{\partial^2 w}{\partial y^2} - \mathcal{L}(w) \quad (70)$$

where

$$\mathcal{L}(w) = D_1\frac{\partial^4 w}{\partial x^4} + 2D_3\frac{\partial^4 w}{\partial x^2 \partial y^2} + D_2\frac{\partial^4 w}{\partial y^4}\,, \quad (71)$$

in the case of a plate. For the bending rigidities in (71), we have the expressions [111]

$$D_1 = \frac{h^3}{12}C_{11}\,, \quad D_2 = \frac{h^3}{12}C_{22}\,, \quad D_3 = \frac{h^3}{12}\left(C_{12} + 2\,C_{66}\right)\,, \quad (72)$$

where C_{ij} are the elastic moduli. These can be expressed in terms of the Young moduli E_1, E_2 and Poisson's ratios ν_{12}, ν_{21} (see also equations (34) - (35)).

$$C_{11} = \frac{E_1}{1-\nu_{12}\nu_{21}}\,,\; C_{22} = \frac{E_2}{1-\nu_{12}\nu_{21}}\,,\; C_{12} = C_{21} = \frac{\nu_{12}E_2}{1-\nu_{12}\nu_{21}}\,,\; C_{66} = G_{12}\,. \quad (73)$$

We assume that the deflection function w and its partial derivatives are small, and that they satisfy the boundary conditions corresponding to simply supported

boundaries at $x = 0$, $-b \leq y \leq b$ and $x = \ell$, $-b \leq y \leq b$, and free boundaries at $-b \leq y \leq b$, $0 \leq x \leq \ell$. In the case of an orthotropic plate, the boundary conditions read

$$(w)_{x=0,\ell} = 0, \qquad \left(\frac{\partial^2 w}{\partial x^2}\right)_{x=0,\ell} = 0\,, \qquad -b \leq y \leq b\,, \tag{74}$$

$$\left(\frac{\partial^2 w}{\partial y^2} + \beta_1 \frac{\partial^2 w}{\partial x^2}\right)_{y=\pm b} = 0\,, \qquad 0 \leq x \leq \ell\,, \tag{75}$$

$$\left(\frac{\partial^3 w}{\partial y^3} + \beta_2 \frac{\partial^3 w}{\partial x^2 \partial y}\right)_{y=\pm b} = 0, \qquad 0 \leq x \leq \ell\,, \tag{76}$$

where β_1 and β_2 are mechanical parameters defined as

$$\beta_1 = \nu_{12}\,, \qquad \beta_2 = \nu_{12} + \frac{4\,G_{12}}{E_2}(1 - \nu_{12}\nu_{21})\,. \tag{77}$$

As is well known, in the isotropic case we have $E_1 = E_2 = E$, $\nu_{12} = \nu_{21} = \nu$, $G_{12} = G = E/(2(1+\nu))$ and, consequently, $\beta_1 = \nu$ and $\beta_2 = 2 - \nu$.

If the material is orthotropic, then the shear modulus G_{12} is possible to approximate using the geometric average G_H developed by Huber [41]:

$$G_H \equiv \frac{\sqrt{E_1 E_2}}{2(1 + \sqrt{\nu_{12}\nu_{21}})}\,, \tag{78}$$

The in-plane stresses in **PIII** are the same as in **PII**, namely, σ_{xx}, τ_{xy} and σ_{yy} and they are assumed to satisfy the standard equilibrium equations (17) - (18) where body forces F_x and F_y are assumed to be zero:

Now the boundary conditions are:

$$(\sigma_{xx})_{x=0,\,\ell} = T_0\,, \qquad (\tau_{xy})_{x=0,\,\ell} = 0\,, \qquad -b \leq y \leq b\,, \tag{79}$$

$$(\sigma_{yy})_{y=\pm b} = 0\,, \qquad (\tau_{xy})_{y=\pm b} = 0\,, \qquad 0 \leq x \leq \ell\,, \tag{80}$$

where tension T_0 creating the stabilizing stress in the web is:

$$T_0 = h\frac{u_0}{\ell}\left(C_{11} - \frac{C_{12}^2}{C_{22}}\right) = h\frac{u_0}{\ell}E_1\,. \tag{81}$$

The equation for solving the minimal eigenvalue problem of the moving, steady-state plate (from **PIII**) is:

$$\left(mV_0^2 - T_0\right)\frac{\partial^2 w}{\partial x^2} + D_1\mathcal{L}_0(w) = 0. \tag{82}$$

Using the boundary conditions (74) - (76), the minimal eigenvalue is [7]:

$$\lambda = \gamma^2 = \frac{\ell^2}{\pi^2 D_1}\left(mV_0^2 - T_0\right) \ . \tag{83}$$

The corresponding eigenfunction can be found by assuming that the solution for (82) is:

$$w = w(x,y) = f(y)\ \sin\left(\frac{\pi x}{\ell}\right) \ , \tag{84}$$

where $f\,(y)$ is an unknown function.

The root of the nondimensional form of the (82) is (see **PIII**):

$$\gamma_0^2 = \frac{1}{2}\left((\beta_2 - \beta_1)\ \alpha + 2\,H_1 - \left({\beta_1}^2 - 4\,\beta_1\,\beta_2 + {\beta_2}^2\right)\ H_2 - 4\,\beta_1\,H_3\right) \ . \tag{85}$$

where

$$\alpha \equiv \sqrt{8\,\beta_1\,H_2\,H_3 + \left({\beta_1}^2 - 6\,\beta_1\,\beta_2 + {\beta_2}^2\right)\ {H_2}^2} \, . \tag{86}$$

and

$$H_1 = \frac{D_1}{D_1}, \qquad H_2 = \frac{D_2}{D_1}, \qquad H_3 = \frac{D_3}{D_1} \, . \tag{87}$$

The numerical solution process is based below Equations depending on the nature of the eigenfunctions (symmetric or antisymmetric):

$$\Phi - \Psi = 0 \ \text{ or } \ \Phi - \frac{1}{\Psi} = 0 \tag{88}$$

where

$$\Phi \ = \ \tanh\frac{\kappa-}{\mu}\coth\frac{\kappa_+}{\mu} \, , \tag{89}$$

$$\Psi \ = \ \frac{\kappa_+(\kappa_+^2 - \beta_2)(\kappa_-^2 - \beta_1)}{\kappa_-(\kappa_+^2 - \beta_1)(\kappa_-^2 - \beta_2)} \, , \tag{90}$$

and

$$\kappa_\pm^2 = \frac{H_3}{H_2}\left(1 \pm \sqrt{1 - \frac{H_2(1-\lambda)}{H_3^2}}\right) \ , \tag{91}$$

Finally, the shape of the eigenfunction is found by using the nondimensional form of (84).

Results showing the effect of the orthotropic material properties one the shape of the web are presented in Figures 16 and 17.

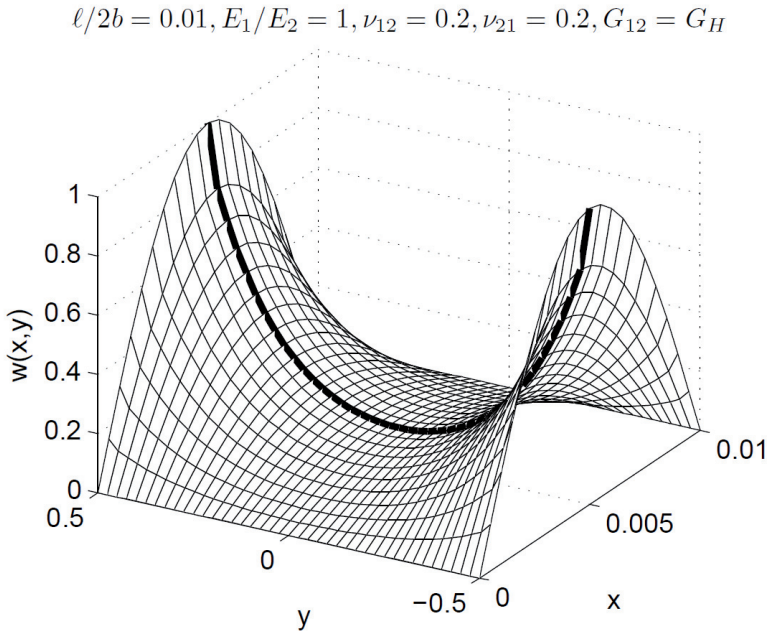

FIGURE 16 Symmetric buckling shape for isotropic material, $E = 5$ GPa and $\nu = 0.2$. Aspect ratio $\ell/2b = 0.01$, from **PIII**.

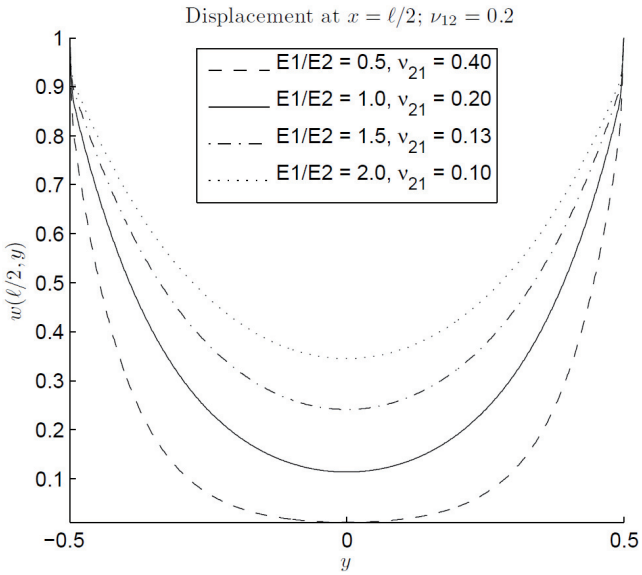

FIGURE 17 Shape of the profile on the bold line of the Figure 16. The solid line corresponds to the picture on the left. The dotted lines show the shape of the resulting profile if the isotropic material is replaced with an orthotropic one, while keeping $E_1 = 5$ GPa and $\nu_{12} = 0.2$, from **PIII**.

The free, unsupported edges are the basis of the shape of the buckled web; the buckling displacements are concentrating at the edges even though the length-width aspect ratio of the two-dimensional web is quite small, $\ell/2b = 0.01$. The increase of the elasticity E_1 using the same strain ε_x (see equation (81)) results in higher web stress in x-direction and thus in lower absolute $w(x, y)$ displacement field.

If the coupling effect with the fluid surrounding the moving web is included to the buckling analysis, fundamental stability studies use one-dimensional tensioned web. The web's tension is assumed to be constant and the effect of the surrounding air during out-of-plane movement is described as reaction force q_f [8]. Now the problem can be simplified using equation (82) [58, 45]:

$$\left(mV_0^2 - T\right)\frac{\partial^2 w}{\partial x^2} + D\frac{\partial^4 w}{\partial x^4} = q_f, \tag{92}$$

where D is the flexural rigidity of the web:

$$D = \frac{E_{11}h^3}{12\left(1-\nu^2\right)}. \tag{93}$$

Reaction force q_f can be further presented as aerodynamic lift:

$$q_f = -\rho_f V_\infty^2 \frac{\partial F(x)}{\partial x} = -\rho_f V_\infty^2 \frac{\partial}{\partial x}\int_{-1}^{1} N(\xi, x)\frac{\mathrm{d}w(\xi)}{\mathrm{d}x}\,\mathrm{d}\xi. \tag{94}$$

In equation (94) $N(\xi, x)$ is a kernel function describing local aerodynamic force directed to the web. Combining (92) and (94) we will get [8, 58, 45]:

$$\left(mV_0^2 - T\right)\frac{\partial^2 w}{\partial x^2} + D\frac{\partial^4 w}{\partial x^4} = -\rho_f V_\infty^2 \frac{\partial}{\partial x}\int_{-1}^{1} N(\xi, x)\frac{\mathrm{d}w(\xi)}{\mathrm{d}x}\,\mathrm{d}\xi. \tag{95}$$

Equation (95) describes a situation, where a web moving with velocity V_0 is immersed in fluid with the density of ρ_f and velocity V_∞. The lift force q_f is quadratically proportional to fluid velocity V_∞. Basically, the right side of the (95) is a Bernoulli-type dynamical fluid pressure, where functional $F(x)$ in (95) takes into account the local shape of the web. Thus, equation (95) predicts a local lift force using $N(\xi, x)$ for pressure effect at a local slope of the web $\mathrm{d}w/\mathrm{d}x$.

Equation (95) can not be solved analytically. One solution possibility is to

apply the Galerkin numerical method by assuming that the shape of the web is some continuous function Ψ_n [8, 58, 45]:

$$w(x) = \sum_{1}^{n} f_n \Psi_n(x), \tag{96}$$

where

$$\Psi_n(x) = \sin\left(\frac{n\pi}{2}(x+1)\right). \tag{97}$$

If we scale the solving area according to (95) to $-1 \leq x \leq 1$, substitute (96) and (97) to (95) and perform the integration, we will obtain:

$$\left(S + \beta K - \gamma \theta^2 N\right) f = \left(\left(S + \gamma N\right)\alpha^2\right) - 2\gamma\theta N\alpha\Big) f, \tag{98}$$

where matrices S, K and N are:

$$S_{jn} = \int_{-1}^{1} \frac{d\Psi_j}{dx}\frac{d\Psi_n}{dx}dx = \left(\frac{j\pi}{2}\right)^2 \delta_{jn} \tag{99}$$

$$K_{jn} = \int_{-1}^{1} \frac{d^2\Psi_j}{dx^2}\frac{d^2\Psi_n}{dx^2}dx = \left(\frac{j\pi}{2}\right)^4 \delta_{jn} \tag{100}$$

$$N_{jn} = \int_{-1}^{1} dx \int_{-1}^{1} \frac{d\Psi_n(\xi)}{dx} N(\xi, x) \frac{d\Psi_j(x)}{dx} d\xi. \tag{101}$$

In equations (99) – (101) δ_{jn} is the Kronecker delta and indexes j and n are referring to the usage of the delta value (0 or 1). The nondimensional parameters in (98) α, β, γ and θ are:

$$\alpha = \frac{V_0}{\sqrt{\frac{T}{m}}}, \beta = \frac{D}{T\ell^2}, \gamma = \frac{\ell\rho_f}{m}, \theta = \frac{V_\infty}{\sqrt{\frac{T}{m}}} \tag{102}$$

The applicability of (98) was tested with wind tunnel measurements carried out by Chang et. al. in [12]. In Figure 18 presents a comparison between the experimental results and the two theories.

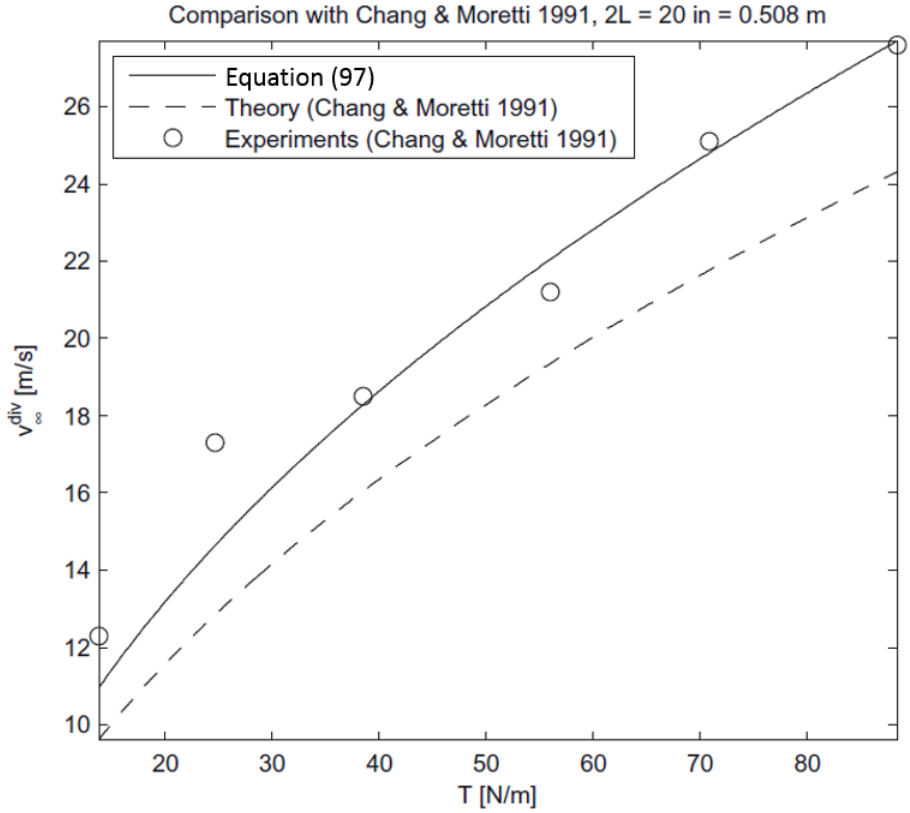

FIGURE 18 Wind tunnel test results of limit divergence velocity V_{div}, and thoretical predictions from [12] and Equation (98) [58, 45].

4.2 Efficiency optimization of moving, imperfect tensioned web

Successful web handling creates contradictory demands to the controlling variables of the we handling environment. On one hand, there must be a high enough stress (tension) level enough to stabilize the web but, on the other, the level must be optimized according to the web breaks. Depending on the parameters to be used, there are many different means to overcome this problem [57, 53, 90, 79]. When seeking the optimal value of tension while having opposing objectives, we encounter a multi-objective optimization problem, which usually has no unique optimal solution but a set of "equally optimal", Pareto optimal solutions. In this optimization analysis, we may apply the solutions from stability analysis for the critical velocities.

The critical velocity corresponding to the loss of stability of the transverse

vibrations of the web is analyzed here by the linearized Kirchhoff plate theory, in which we assume that the transverse vibrations are small [111]. The critical velocity can be found by solving the buckling problem for dynamic transverse deflections of the plate [65]. Each span Ω_i is defined as

$$\Omega_i = \{\, (x,y) : i\ell < x < (i+1)\ell\,, -b < y < b\,\}, i = 1,2,3,\dots \tag{103}$$

Consider an axially moving elastic isotropic plate, travelling at a constant velocity V_0 and having an initial crack, between a system of subsequent supports (rollers). The plate undergoes open draws between the supports, the open draws being assumed to be equal in length.

For each span there are tensions T acting at simply supported sides in x-direction:

$$\begin{aligned} \Gamma_{i,\ell} &= \{\, x = i\ell\,, -b \le y \le b\,\} \quad \text{and} \\ \Gamma_{i,r} &= \{\, x = (i+1)\ell\,, -b \le y \le b\,\} \end{aligned} \tag{104}$$

In y-direction, the span edges are assumed to be free:

$$\begin{aligned} \Gamma_{i,-} &= \{\, y = -b\,, i\ell \le x \le (i+1)\ell\,\} \quad \text{and} \\ \Gamma_{i,+} &= \{\, y = b\,, i\ell \le x \le (i+1)\ell\,\} \end{aligned} \tag{105}$$

For the problem setup, see Figure 19. Stationary equations describing the behavior of the web with applied boundary conditions form the following eigenvalue problem (a buckling problem):

$$\begin{aligned} (mV_0^2 - T_0)\frac{\partial^2 w}{\partial x^2} + D\left(\frac{\partial^4 w}{\partial x^4} + 2\frac{\partial^4 w}{\partial x^2 \partial y^2} + \frac{\partial^4 w}{\partial y^4}\right) = 0\,, &\qquad \text{in } \Omega_i \\ w = 0\,, \quad \frac{\partial^2 w}{\partial x^2} = 0\,, &\qquad \text{on } \Gamma_{i,\ell} \text{ and } \Gamma_{i,r}\,, \\ \frac{\partial^2 w}{\partial y^2} + \nu\frac{\partial^2 w}{\partial x^2} = 0\,, &\qquad \text{on } \Gamma_{i,-} \text{ and } \Gamma_{i,+}\,, \\ \frac{\partial^3 w}{\partial y^3} + (2-\nu)\frac{\partial^3 w}{\partial x^2 \partial y} = 0\,, &\qquad \text{on } \Gamma_{i,-} \text{ and } \Gamma_{i,+}\,, \end{aligned} \tag{106}$$

where $D = Eh^3/(12(1-\nu^2))$, and we denote the eigenvalue

$$\lambda = \gamma^2 = \frac{\ell^2}{\pi^2 D}(mV_0^2 - T_0)\,. \tag{107}$$

The traveling plate subjected to a constant tension experiences divergence instability at a critical velocity [6]:

$$(V_0^{\mathrm{cr}})^2 = \frac{T_0}{m} + \frac{\gamma_*^2}{m}\frac{\pi^2 D}{\ell^2}\,, \tag{108}$$

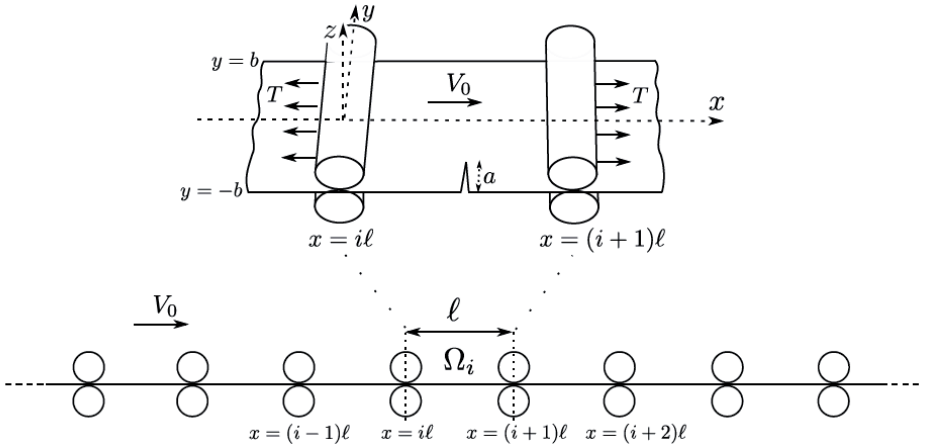

FIGURE 19 An axially moving plate having an initial crack and supported by a system of rollers delivering force balance for each web spans (from **PIV**).

where $\gamma_*^2 = \lambda_*$ is the minimal eigenvalue of problem (4.2).

Assume that the value of tension is constant $T = T_0$ and that the plate has small surface cracks that arise at the free boundaries of the plate and have length a with upper bound a^*, i.e.

$$a \leq a^* \ll 2\,b\,, \tag{109}$$

The stress intensity factor K can be expressed as (see [43], [94] or [120])

$$K = \beta\sigma\sqrt{\pi a} = \beta\frac{T}{h}\sqrt{\pi a}\,. \tag{110}$$

Here $\beta = 1.12$ is a geometric factor for a small edge crack ($a/2b$ is small) and $\sigma = \sigma_x$ is a component of a stress tensor. We express the brittle fracture condition as

$$K = K_{\mathrm{C}}\,, \tag{111}$$

where K_{C} is the fracture toughness of material. If we define the biggest admissible crack length as a critical crack length a^{cr}, based on (110) we can write the critical value for tension:

$$T_0^{\mathrm{cr}} \equiv (T_0)_{a=a^{\mathrm{cr}}} = \frac{K_C h}{\beta\sqrt{\pi a^{\mathrm{cr}}}}\,. \tag{112}$$

Consequently, we can now combine (108) and (112) to obtain a safe velocity limit where web divergence limit coincides at critical web tension T_{cr}:

$$0 < V_0 < V_0^* \equiv \sqrt{\gamma_*\frac{\pi^2 D}{m\ell^2} + \frac{K_{\mathrm{C}} h}{\beta m\sqrt{\pi a^{\mathrm{cr}}}}}\,. \tag{113}$$

Next we assume that the travelling plate is subjected to small cyclic tension variations during the process. For one cycle, the tension increases from $T = T_{min}$ up to $T = T_{max}$ (the loading process) and then decreases from $T = T_{max}$ down to $T = T_{min}$ (the unloading process) depending on some external contributor such as edge contraction of the web near the detachment rollers [37]. We suppose quasi-static processes meaning that the dynamic effects are excluded.

We define parameters T_0 (average tension) and ΔT (small tension variation) such that

$$T_{\min} = T_0 - \Delta T \quad \text{and} \quad T_{\max} = T_0 + \Delta T\,, T_{\min} \leq T \leq T_{\max}\,, \tag{114}$$

and

$$T_0 - \Delta T > 0 \quad \text{and} \quad \frac{\Delta T}{T_0} \ll 1\,. \tag{115}$$

Using these assumptions (112) can be rewritten:

$$a^{\mathrm{cr}} = \frac{1}{\pi}\left(\frac{K_{\mathrm{C}}h}{\beta T_{\max}}\right)^2 \approx \frac{1}{\pi}\left(\frac{K_{\mathrm{C}}h}{\beta T_0}\right)^2\,. \tag{116}$$

The process of fatigue crack growth under cyclic tension (loading) can be described by the Paris' law [81]. The describing equation and initial condition are

$$\frac{da}{dn} = C(\Delta K)^k\,, \qquad (a)_{n=0} = a_0\,, \tag{117}$$

where the variation ΔK of the stress intensity factor K can be expressed as

$$\Delta K = \frac{2\beta\sqrt{\pi a}}{h}\Delta T\,. \tag{118}$$

In equation (117), C and k are material constants and n is the number of cycles. The critical number of stress cycles n^{cr} can be found out by solving n from (117) and applying (116):

$$n^{\mathrm{cr}} = (n)_{a=a^{\mathrm{cr}}} = A\left[\frac{1}{a_0^{(k-2)/2}} - \left(\frac{\sqrt{\pi}\beta T_0}{K_{\mathrm{C}}h}\right)^{k-2}\right]\,. \tag{119}$$

The process optimization of the cracked, imperfect web can be done using above parameters by finding solution to the following multi-optimization problem:

$$J^* = J(T_0^*) = \max_{T_0}\ J(T_0)\,, \tag{120}$$

where:

$$J(T_0) = \left\{\begin{array}{c} J_{\mathrm{V}}(T_0) \\ J_{\mathrm{N}}(T_0) \\ J_{\mathrm{M}}(T_0) \end{array}\right\} \equiv \left\{\begin{array}{c} V_0^{\mathrm{cr}}(T_0) \\ n^{\mathrm{cr}}(T_0) \\ M^{\mathrm{cr}}(T_0) \end{array}\right\}\,, \tag{121}$$

where:

$$M^{cr} = m_0 V^{cr} t_{\mathrm{f}}\,, \qquad m_0 = 2bm\,. \tag{122}$$

Equations (120) – (122) state, that we are maximizing web stress (tension) T_0 finding a Pareto optimum using the critical velocity V_0^{cr}, longevity n^{cr} and process effectiveness M^{cr}.

To solve this multi-objective optimization problem, we apply the weighting method, which is one of the most relevant substitutes for vector optimization problems. The preference function is formulated as a sum of the single objective functions J_{V}, J_{N}, J_{M} associated with the weighting factors C_{V}, C_{N}, C_{M}:

$$J_{\mathrm{C}} = C_{\mathrm{V}} J_{\mathrm{V}} + C_{\mathrm{N}} J_{\mathrm{N}} + C_{\mathrm{M}} J_{\mathrm{M}}\,, \tag{123}$$

where we suppose that

$$\begin{gathered} C_{\mathrm{V}} \geq 0, C_{\mathrm{N}} \geq 0, C_{\mathrm{M}} \geq 0\,, \\ C_{\mathrm{V}} + C_{\mathrm{N}} + C_{\mathrm{M}} = 1\,. \end{gathered} \tag{124}$$

If we assume that the process engineering is "fixed", i.e. the number of the critical stress changes that the web must withstand is $n^{cr} = 100$, we can perform web tension maximization according velocity criteria $\tilde{J}_{\mathrm{V}}$ (critical velocity criterion) and $\tilde{J}_{\mathrm{M}}$ (process effectiveness criterion). Based on (123) the weighting method problem is

$$\begin{gathered} \tilde{J}_2 \equiv C_{\mathrm{V}} \tilde{J}_{\mathrm{V}} + C_{\mathrm{M}} \tilde{J}_{\mathrm{M}}\,, \\ C_{\mathrm{V}} + C_{\mathrm{M}} = 1\,, \end{gathered} \tag{125}$$

so that we study

$$\max_{0 \leq \tilde{T}_0 \leq 1} \; C_{\mathrm{V}} (\tilde{T}_0 + d)^{1/2} + C_{\mathrm{M}} (\tilde{T}_0 + d)^{1/2} (1 - \tilde{T}_0)\,. \tag{126}$$

where nondimensional values $\tilde{T}_0$ and d are:

$$\tilde{T}_0 = \frac{\beta \sqrt{\pi a_0}}{K_{\mathrm{C}} h} T_0\,, \qquad d = \frac{\gamma_*^2 \pi^2 D \beta \sqrt{\pi a_0}}{l^2 K_{\mathrm{C}} h}\,, \qquad 0 < \tilde{T}_0 < 1\,. \tag{127}$$

Using process parameter and paper property values $\nu = 0.3$, $E = 10^9$ Pa, $m = 0.08$ kg/m^2, $h = 10^{-4}$ m, $\ell = 0.1$ m, $2b = 10$ m, $\beta = 1.12$, and $K_{\mathrm{C}} = 2.8 \cdot 10^6$ Pa$\sqrt{\mathrm{m}}$ (see [94], and [121]) we can present a Pareto front according web tension T_0 in Figure 20.

Results show that weighting of the C_M results in very steep dependence between web tension and the initial crack length, i.e. all the cracks appearing at the web edges should be eliminated with high web tension (stress) levels if high production efficiency is sought. The weighting of the $C_V = 1 - C_M$ gives slightly more freedom to maximize the production speed according to the web tension if the web stability limit is not violated.

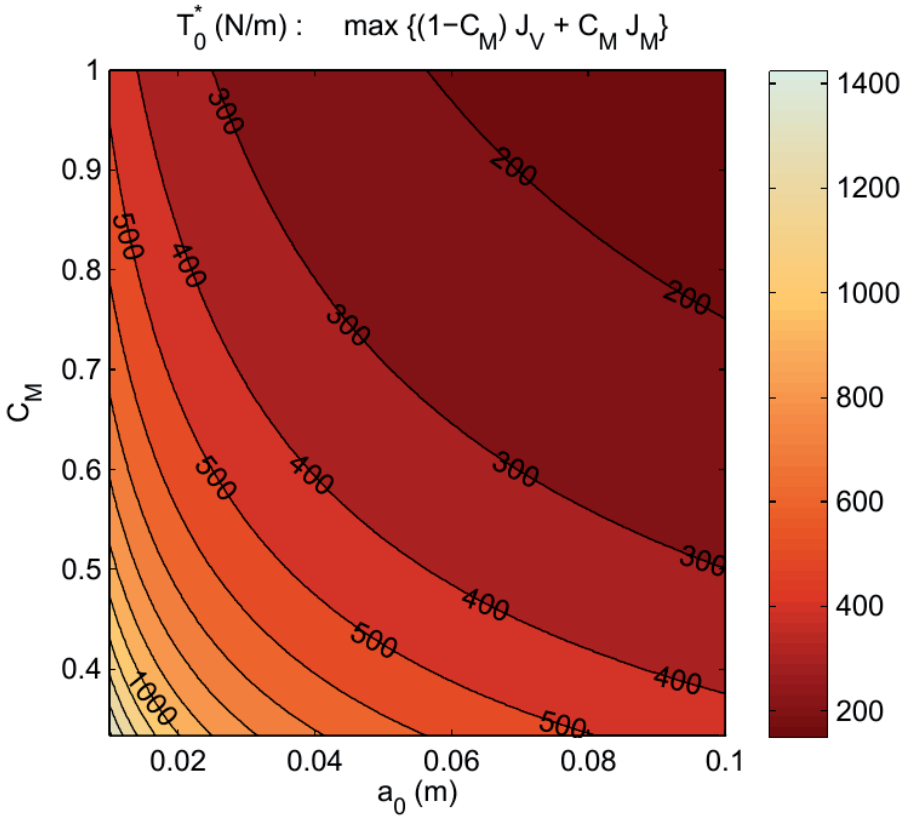

FIGURE 20 Dependence of the optimal tension T_0 on the initial crack length a_0 and the weight C_M, from **PIV**

5 VISCOELASTOPLASTICITY IN FIBROUS, TENSIONED WEB MATERIALS

Viscous properties of fibrous web materials have great significance in the creation of web stress. Production of the web material in paper and board industry is still water-oriented. Water removal in the process is realized at several different process stages, where the free, unbound water inside the fiber network is removed (in the forming and pressing sections) followed by paper drying, which removes the majority of the bound water inside the fiber walls.

The development of the web's strength on and along the production line must be taken into account in designing the runnability machinery for a specific paper or board making machine. It is notable that the strength of the web at the end of the free water removal stage (press section) is still only 10...15% of the final dry paper [68, 36, 56, 90]. However, as pointed out in **PV**, the production velocity is still essentially the same throughout the line. This means that both the viscoelastic and viscoelastoplastic properties of the wet paper web are in essential position in creating the web tension needed for ensured production efficiency.

The creation of the needed web stress (or web tension) is based on the creation a relative velocity difference between the starting and ending points of the web span to be stressed (see chapter 3.1). With the assumption of ideally elastic material assumption, the modulus of the elasticity is assumed to be constant, but with the fibrous materials, there is usually only small of elastic strain in the materials. At this elastic strain area, also the behavior of the fibrous webs is close to the viscoelastic behavior [55].

The straining of the wet, undried fibrous material presents different tensile results compared to dry paper. Elasticity of the wet paper is only 10% compared to dry paper and therefore the stress response with strain used is always significantly lower compared to dry paper. This is one of the greatest web handling challenges in paper and board making. Also, viscoelastic stress relaxation plays an increasingly important role because even a small decrease of stress loss can deteriorate the web stability in high velocity production environment [55, 53, 90].

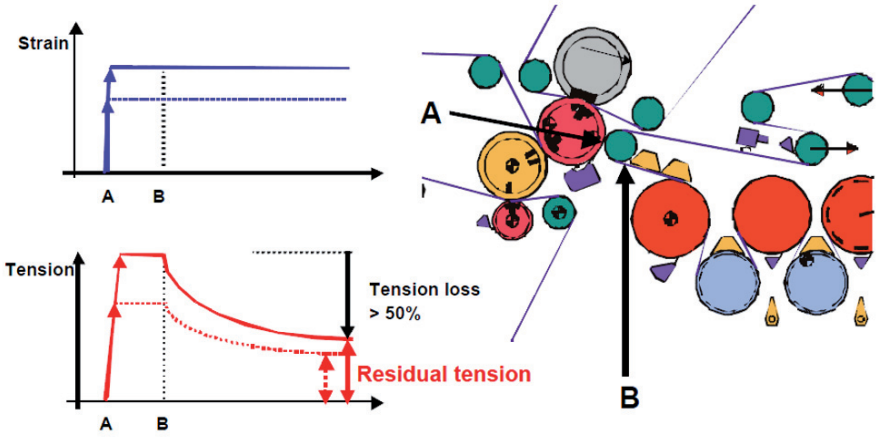

FIGURE 21 Tension relaxation appearing in paper machine press section, from **PV**.

Figure 21 illustrates the importance of the relaxation phenomena in the wet end of the papermaking. At this stage (the ending of wet pressing stage), the water content of the paper is still approximately 50%, and the straining between points A and B creates the tension to the web (see also Figure 9). At point B, the web enters to the lower surface of the drying fabric, where it is advancing, supported, to the dryer section. However, the strain (and velocity) does not change after the point B, and the fibrous web starts to lose its stress through relaxation [53].

Relaxation of the wet fibrous material generally is not measured from the pulp or paper samples. The measurement procedure, which is described in **PV**, is more demanding, when compared to standard tensile measurement, due to rapid drying tendency of the wet samples. A special measurement device and method were developed in order to study this rheological bottleneck of the paper production line.

In the laboratory measurement, a fibrous wet sample is attached between the jaws, and a desired strain is produced in the sample very rapidly in order to get realistic viscoelastoplastic response from the sample. The transform between the straining in moving web environment and static strain can be calculated by applying (48):

$$\frac{\mathrm{d}\varepsilon_{static}}{\mathrm{d}t} = \frac{\partial \varepsilon_{velocity\ difference}}{\partial x_{draw\ length}} U_{web}\ . \tag{128}$$

Since the wet tensile properties are usually exponentially dependent on the amount of water in the sample (i.e. dry solids content, see Figure 21 a), this measurement was always carried out at least with two dry solids content levels.

One important finding was that the raw material -based dependencies between wet and dry paper elasticity and strength are different. This was giving valuable information for the designing of a machine with different paper grades and production velocities [56, 90] .

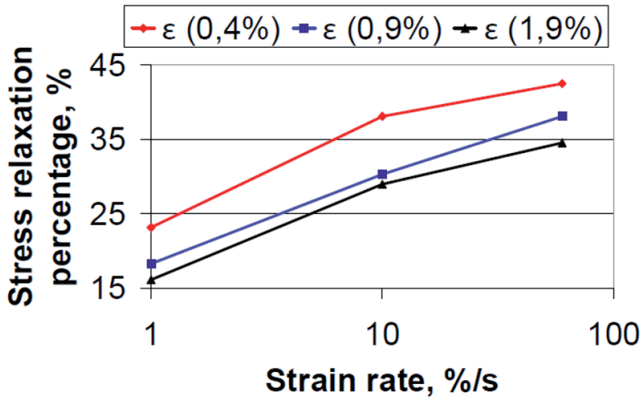

FIGURE 22 The development of stress relaxation in wet paper as a function of strain rate applied with different absolute strains from **PVI**.

Fibrous web travelling along a production line must be strained multiple times due to the mentioned tension relaxation phenomenon. Therefore, the web goes through several re-straining sequences, where the negative straining caused by drying shrinkage is possible [80].

One of the main findings in **PVI** was the significance of the tensile relaxation. Even though the phenomenon of the increased irrecoverable straining due to relaxation was known, wet fibrous material is mostly viscoelastoplastic, since both the amount of the relaxation and the straining velocity $d\varepsilon/dt$ increase the amount of the plasticity not only of the wet web but also the final dried paper [2, 55].

These findings further directed the development of the paper and board production lines to the direction where the stabilization of the web at the wet state becomes more benefical with external, supporting devices equipped with suitable underpressure which further stabilize the web against a supporting, permeable surface [47, 53].

6 ADAPTIVE WEB STABILIZATION

The basis of the adaptive web handling is the creation and optimization of physical, surface-dependent fluid drag effect on the roll surface. This is possible by utilizing the viscous properties of the air, which further are responsible for the boundary layer behavior in fluid flow [93].

Without roll grooving, boundary layers create the undesired overpressure effects especially to the closing pocket area. This is further emphasized by the rough surfaces of felts or fabrics [27, 61]. Due to this, the web will lose its contact with the roll if the web velocity is high enough. This can be avoided by grooving the roll surface in the optimized manner presented in **PVII**.

The fundamental principle in an adaptive, self-underpressurizing roll is to optimize roll geometry in a manner where the boundary layers attached to the groove walls are transporting exactly the right amount of the air forward, as the roll rotates. In the optimization, the groove volume is essential. On one hand, boundary layer air must have enough space to go to the grooves, but on the other, the groove walls must be close enough to each other to prevent air leakage from the wrap zone to become underpressurized.

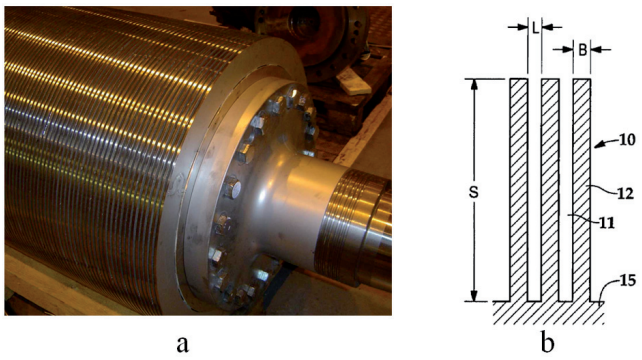

FIGURE 23 The adaptive, self-underpressurizing roll after manufacturing a) and drawing from the cross section of roll surface b) [60].

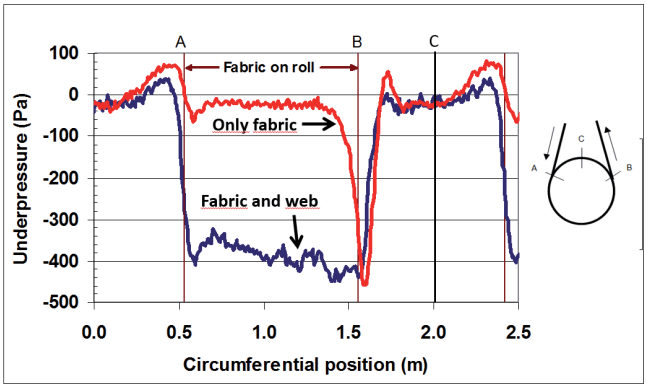

FIGURE 24 Rotational pressure curves measured from the bottom of the groove with and without the web [60].

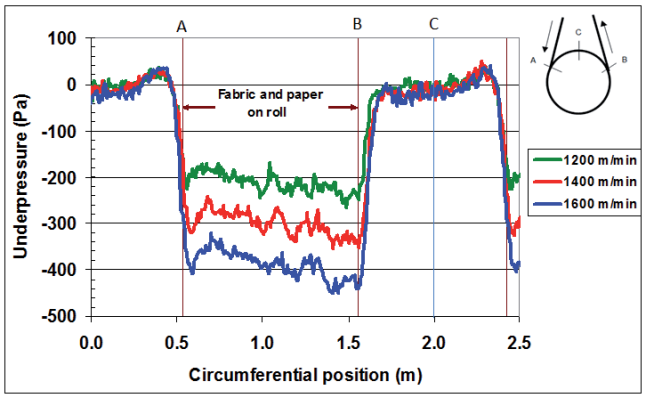

FIGURE 25 Measured rotational underpressure levels stabilizing the web during roll wrap area at three different web velocity levels [60].

During the wrap area stage, underpressure along the wrap slightly increases. When the point of rotation is approaching the opening pocket area (point B), air flow velocity increases as the opening pocket geometry is forming boundary layers starting from the detachment point which amplifies the underpressurization effect by removing the air from the grooves.

Optimal functioning of the roll demands that there exists a pocket geometry where a permeable fabric is in contact with the roll forming a wrap zone (see Figure 24, length A $\rightarrow$ B around the roll surface). When permeable, dryer section fabric is used, the boundary layers in the closing pocket area create a vortex, which improves sealing zone, partially preventing air from penetrating to the grooves. The air arriving to the grooves is accelerated by the boundary layers of the groove walls. This acceleration area is the starting point of the underpressurized area (see point A in Figure 24) [60]. If the rotational velocity (surface velocity) is increased, all these effects are amplified, causing increases in underpressure at the roll wrap zone. The effect of machine velocity (surface velocity) is shown in Figure 25.

With this roll configuration, it is possible to overcome the energy increase coming from external web stabilization arrangements. The adaptive roll application considered further helps to stabilize the web at areas where permeable fabrics are used. Also, with the adaptive technology makes it possible to minimize the stress needed in web and to optimize the raw materials used in improving the production economy.

7 CONCLUSION

Moving, viscous web continuum forms a physical entity, the research of which is typically divided into different subareas. Depending on the needs or ideas presented to the researchers, these subareas concern usually external surroundings of the web, i.e. the physical forces directed to the web and changing its visible behavior, or the contribution of different material components in the production of the web.

Suprisingly, modelling of the flow phenomenon of the in-plane solid continuum web has received limited interest. The traditional method to study the stress-strain behavior is the Lagrangian formulation, where material is stationary (no transport velocity) and the web model is completed using Dirichlet, Neumann or Robin boundary conditions. The Euler-Lagrangian formulation completes this modelling approach. Assuming the web to be a moving web continuum with material flow properties, it is possible to extend new features to the model.

The solution of a two-dimensional, viscoelastic third-order system of partial differential equations creates additional challenges. The nature of the third-order terms is convective, and therefore a numerical solution should be carefully designed. If a finite element method is applied, streamline upwinding methods should be used in order to avoid instabilities during numerical solution [25].

In modelling, special emphasis should be placed on the boundary conditions. The Dirichlet boundary condition is actually suitable in a stationary Lagrangian formulation, i.e. no information is going through the Dirichlet constraint. With the continuous moving web model, boundary conditions should be effective only at the surfaces, i.e. information flow should be allowed outside the area under observation. From the modelling point of view, the third-order partial differential equations developed give a new perspectives to this stress-strain formulation and solution of a continuum with convection created by transport velocity.

One of the more active research area concerns the effects of out-of-plane behavior of one- or two-dimensional moving web models. Especially challenging is the behavior of the thin webs with a large, unsupported surface area where the

thickness and density are low. In these cases, the modelling approach should be multiphysical, coupled fluid-structure model where tension is the main stabilizing contributor in the model. It should be noted that this same phenomenon is present in the vibration of stationary plate and should be paid careful attention to, in order to get reliable results based on the object's vibration characteristics [70, 92].

In a practical web handling environment, observable web handling items can be very different compared to the research. The first observable stability limits appearing in different positions in web handling processes are usually the formations of the out-of-plane deflections. This unwanted phenomenon occurs especially at the pocket areas near web-roll contact area and usually those are not accepted since those are prone to change their nature to time-dependent web vibration or unstable flutter. For this reason, both the modelling of the web divergence limits and effects of edge cracks on the fatigue strength of moving web are valuable.

Different models for fibrous-based materials are numerous. The primary motivation for the modelling is the finding the most economically benefical raw material components for the production of the web. Unfortunately, the connection between the dynamical, moving web behavior and material elasticity under study is often limited. The need of cheaper raw materials means in practise often lower web elasticity, tensile strength and decreased sustainability to strains applied during the production.

From this viewpoint, in design of the machinery for web handling, we always aim to the elimination of all steady-state or time-dependent deflections and out-of-plane disturbances. The reason for this is the need for efficiency and higher productivity. If the daily production of the machine including the moving web is high, then even very complex web handling techniques can be economically justified since few web breaks during one day can cause remarkable economical losses. It should be noted that this applies to the situation even when the web velocities are not at their highest level. One of the most important connection to be notified is between the web handling and raw material used. Essentially those two are the sides of the same coin: almost all engineered web handling improvements can utilized in raw material optimization for the production and vice versa. If possible, the physical environment itself should be utilized to ensure good web stability. In this sense, adaptive stability should be studied more carefully in order to minimize the external disturbances affecting the web.

Regardless of the subject under study, the tensile behavior of the moving web is always one of the essential items to be included. In this thesis, the stress-strain theme is considered from different viewpoints along the web handling continuation. Thus the mentioned different subareas of the web handling research are combined. By combining these areas further, possibilities arise to optimize the performance of the web handling line as a single multiphysical entity.

YHTEENVETO (FINNISH SUMMARY)

Suurella nopeudella liikkuvien, eri materiaaleista valmistettavien rainojen hallinta ja sen avulla saavutettava tuotantotehokkuus on yksi tärkeimmistä tekijöistä niitä valmistavassa teollisuudessa. Riippumatta käytetystä materiaalista (paperit, kartongit, muovit, kuljettimet, hihnat, kuitukankaat jne.), fysikaalinen mallinnusympäristö on kaikille sama. Muista vastaavista tutkimuksista poiketen tässä väitöskirjassa käsitellään sekä liikkuvan rainan fysikaalista ympäristöä että itse rainan materiaalia kokonaisuudessaan temaattisena jatkumona jossa uusia, poikkitieteellisesti teoreettisia ja käytännöllisiä rainan hallinnan tutkimustuloksia tuodaan esille.

Yhteisenä nimittäjänä esitetylle jatkumolle on rainaan vaikuttava jännitysvenymä käyttäytyminen, joka on keskeisessä asemassa kaikissa rainan hallinnan tilanteissa. Väitöskirjassa esitetään uusi, liikkuvan viskoelastisen kontinuumin teoria. Materiaalin viskoottisuudesta johtuen tuloksena saadaan kolmannen asteen osittaisdifferentiaaliyhtälöryhmä, jossa materiaaliderivaattaa hyödyntäen on mahdollista luoda Lagrange-Euler -tyypin liikkuva materiaalikontinuumi. Johdetut viskoottiseen Kelvin-Voigt materiaalimalliin pohjautuvat yhtälöt ratkaistaan ensin yhdessä ulottuvuudessa, jossa sekä analyyttinen että numeerinen elementtimenetelmän antama ratkaisu ovat yhtenevät lineaarisessa tapauksessa. Kaksiulotteinen ratkaisu on aina epälineaarinen koska sekä elastinen että viskoottinen kuroutuminen kytkeytyy rainan kulkutasossa esiintyviin x- ja y-suuntaisiin nopeuksiin.

Yleisenä teemana viskoelastisessa ratkaisussa on se, ettei liikkuvan rainan venymä ole vakio välin pituudella. Tällöin jännitystila syntyy elastisen venymän ja viskoottisen venymänopeuden yhdistelmästä. Esitetty kolmatta astetta oleva yhtälöryhmä sisältää myös ensimmäisen asteen Navier-Stokes -yhtälöiden kaltaiset konvektiotermit jotka ovat merkittäviä vain suurten siirtymien tapauksessa.

Esitetyssä temaattisessa jatkumossa rainan jännitystilalla on suuri merkitys rainan stabiiliudelle. Keskeisenä tekijänä on rainan divergoitumisen rajanopeus, jossa stabiilius menetetään. Suuressa osassa teollisesti valmistettuja rainoja materiaaliominaisuudet x- ja y-suunnissa poikkeavat toisistaan. Tällöin usein mallinnuksessa sovelletaan ortotrooppista materiaalioletusta, jolloin sen matemaattinen käsittely helpottuu. Tulosten mukaan ortotrooppisen materiaalin stabiilisuuden menetys poikkeaa isotrooppisesta materiaalista siten, että isotrooppisen materiaalin epästabiili muoto keskittyy enemmän radan reunaosiin.

Kytkettyä potentiaalivirtaus-rakennemallia hyödyntäen esitetään tässä työssä ratkaisu yksidimensionaalisen liikkuvan rainan rajanopeudelle. Kun oletetaan rainaa ympäröivän virtauksen olevan samansuuntainen rainan liikkeen kanssa, kytketty ongelma voidaan ratkaista numeerisesti Galerkinin menetelmällä. Mallin tulokset osoittavat mallin antavan tarkkoja tuloksia sovellettaessa niitä testeihin, joissa käytettiin tuulitunneliin asetettua, kiristettyä stationääristä rainaa.

Liikkuvien rainojen reunat muodostavat tärkeän, mutta harvoin mallinnuk-

sen avulla tutkitun rainan hallinnan osa-alueen. Murtumismekaniikkaa soveltaen esitetään Paris'n lakia hyödyntämällä liikkuvan rainan kestoiälle malli, jonka avulla rainassa esiintyvien reunasäröjen vaikutusta ratakatkoherkkyyteen voidaan tarkastella. Kehitettyä mallia on sovellettu monitavoiteoptimointiin, jossa rainan kireydelle on mahdollista muodostaa Pareto-optimaali tuotantotehokkuuden, rainan kestoiän ja sen nopeuden avulla.

Käytännön rainan hallinnassa materiaalin jännitys-venymä -ominaisuuksia voidaan hyödyntää vain rajallisesti johtuen materiaaliin syntyvistä palautumattomista, rainan laatua heikentävistä venymistä. Kuitenkin suurissa nopeuksissa rainaan kohdistuu toisaalta ulkoisia voimavaikutuksia, joista aiheutuva stabiiliuden menetys heikentää tuotantotehokkuutta. Lisäksi kaikissa viskoelastisissa materiaaleissa tapahtuu sisäistä jännityksen laskua, relaksaatiota, jota esiintyy myös liikkuvassa radassa aina kun se ei ole aktiivisen kiristyksen kohteena. Tätä silmälläpitäen on kehitetty mittausmenetelmä, jonka avulla materiaalien nopeaa relaksaatiota on mahdollista mitata myös käytännössä. Tulosten mukaan tilanteissa, joissa aktiivisen venymän avulla rainan jännitystilaa on kohotettu, alkaa erittäin nopea jännitystilan lasku sen saavuttua tuetulle rainanvientiosuudelle jossa rataa ei ole mahdollista kiristää. Relaksaation seurauksena materiaalin oma, palautumattoman venymän suhteellinen osuus myös kasvaa. Mikäli tuotantonopeuksia kasvatetaan, tämä johtaa rainaa kiristettäessä myöhemmän relaksaation aikana entistä suurempien palautumattomien venymien muodostumiseen, mikä voi vaikeuttaa rainan hallintaa myöhemmissä mahdollisissa rainan käsittelyissä lisäten täten ratakatkojen todennäköisyyttä.

Tilanteissa, joissa rainaa ei voida kiristää, se on stabiloitava liikkuvaa, tukevaa pintaa vasten ulkoisia voimavaikutuksia apuna käyttäen. Stabiloitava, alhaisen kireyden rata voidaan tukea läpäisevää kudosta vasten hyödyntämällä adaptiivista alipaineen muodostusta. Tässä työssä esitelty, omasta pyörimisliikkeestään alipaineen muodostava tela on mahdollista toteuttaa optimoimalla telan pinnan urarakenne niin, että urien muodostaman tilavuuden on mahdollista ottaa vastaan rajakerrosten mukaan tuoma ilma ja samalla kuljettaa se kudoksen muodostaman peittoalueen läpi siten, että kudoksen läpi tapahtuu virtausta telan pinnan urarakenteeseen. Alipaineen tuottoa vahvistaa edelleen kudoksen ja telan välinen avautuva taskutila, jossa syntyvä alipainevaikutus poistaa ilmaa uratilavuudesta. Yhdessä nämä tekijät saavat aikaan sen, että optimoidulla urarakenteella telan alipaine tehostuu nopeuden funktiona saaden aikaan adaptiivisen stabiloinnin.

REFERENCES

[1] M. Alava and K. Niskanen. The physics of paper. *Reports on Progress in Physics*, 69(3):669–723, 2006.

[2] O. Andersson and L. Sjöberg. Tensile studies of paper at different rates of elongation. *Svensk Papperstidining*, 56(13):615–624, 1953.

[3] F. R. Archibald and A. G. Emslie. The vibration of a string having a uniform motion along its length. *ASME Journal of Applied Mechanics*, 25:347–348, 1958.

[4] M. Bachene, R. Tiberkak, and S. Rechak. Vibration analysis of cracked plates using the extended finite element method. *Archive of Applied Mechanics*, 79(3):249–262, 2009.

[5] N. Banichuk, S. Ivonova, M. Kurki, T. Saksa, M. Tirronen, and T. Tuovinen. Safety analysis and optimization of travelling webs subjected to fracture and instability. In S. Repin, T. Tiihonen, and T. Tuovinen, editors, *Numerical methods for differential equations, optimization, and technological problems. Dedicated to Professor P. Neittaanmäki on his 60th Birthday*, volume 27 of *Computational Methods in Applied Sciences*, pages 379–392. Springer Netherlands, 2013. ISBN: 978-94-007-5287-0 (Print) 978-94-007-5288-7 (Online).

[6] N. Banichuk, J. Jeronen, M. Kurki, P. Neittaanmäki, T. Saksa, and T. Tuovinen. On the limit velocity and buckling phenomena of axially moving orthotropic membranes and plates. *International Journal of Solids and Structures*, 48(13):2015–2025, 2011.

[7] N. Banichuk, J. Jeronen, P. Neittaanmäki, and T. Tuovinen. On the instability of an axially moving elastic plate. *International Journal of Solids and Structures*, 47(1):91–99, 2010.

[8] N. Banichuk, J. Jeronen, P. Neittaanmäki, and T. Tuovinen. Static instability analysis for travelling membranes and plates interacting with axially moving ideal fluid. *Journal of Fluids and Structures*, 26(2):274–291, 2010.

[9] Roberto Brighenti. Numerical buckling analysis of compressed or tensioned cracked thin plates. *Engineering Structures*, 27(2):265–276, 2005.

[10] J. Castro and M. Ostoja-Starzewski. Elasto-plasticity of paper. *International Journal of Plasticity*, (19):2083–2098, 2003.

[11] J. L. Chance. Drying and runnability for high speed paper machines, 1982. United States Patent 4,483,083.

[12] Y. B. Chang and P. M. Moretti. Interaction of fluttering webs with surrounding air. *TAPPI Journal*, 74(3):231–236, 1991.

[13] Y. B. Chang and P. M. Moretti. Flow-induced vibration of free edges of thin films. *Journal of Fluids and Structures*, 16(7):989–1008, 2002.

[14] L.-Q. Chen. Principal parametric resonance of axially accelerating viscoelastic strings with an integral constitutive law. In *Proceedings of the Royal Society A: Mathematical, Physical and Engineering Sciences*, volume 461, pages 2701–2720. The Royal Society Publishing, 2005. DOI: 10.1098/rspa.2005.1471.

[15] L.-Q. Chen, H. Chen, and C.W. Lim. Asymptotic analysis of axially accelerating viscoelastic strings. *International Journal of Engineering Science*, 46(10):976 – 985, 2008. DOI: 10.1016/j.ijengsci.2008.03.009.

[16] L.-Q. Chen and H. Ding. Steady-state transverse response in coupled planar vibration of axially moving viscoelastic beams. *ASME Journal of Vibrations and Acoustics*, 132:011009–1–9, 2010. http://dx.doi.org/10.1115/1.4000468.

[17] L.-Q. Chen and B. Wang. Stability of axially accelerating viscoelastic beams: asymptotic perturbation analysis and differential quadrature validation. *European Journal of Mechanics - A/Solids*, 28(4):786 – 791, 2009. DOI: 10.1016/j.euromechsol.2008.12.002.

[18] L.-Q. Chen and X.-D. Yang. Vibration and stability of an axially moving viscoelastic beam with hybrid supports. *European Journal of Mechanics - A/Solids*, 25(6):996 – 1008, 2006. DOI: 10.1016/j.euromechsol.2005.11.010.

[19] L.-Q. Chen, N.-H. Zhang, and J. W. Zu. Bifurcation and chaos of an axially moving viscoelastic string. *Mechanics Research Communications*, 29(2–3):81 – 90, 2002. DOI: 10.1016/S0093-6413(02)00241-0.

[20] L.-Q. Chen and W.-J. Zhao. A numerical method for simulating transverse vibrations of an axially moving string. *Applied Mathematics and Computation*, 160(2):411 – 422, 2005. DOI: 10.1016/j.amc.2003.11.012.

[21] L.-Q. Chen, J. W. Zu, J. Wu, and X.-D. Yang. Transverse vibrations of an axially accelerating viscoelastic string with geometric nonlinearity. *Journal of Engineering Mathematics*, 48(2):171–182, 2004. DOI: 10.1023/B:ENGI.0000011929.17902.87.

[22] E. F. DeCrosta and S. L. N. Vennos. What happens in a dryer pocket. *TAPPI Journal*, 51(7):289–298, 1968.

[23] Andrew D. Dimarogonas. Vibration of cracked structures: A state of the art review. *Engineering Fracture Mechanics*, 55(5):831–857, 1996.

[24] C. T. J. Dodson. The nature of bonds in paper and the behaviour of paper under mechanical strain. *Reports on Progress in Physics*, 33(1):1–43, 1970.

[25] Jean Donea and Antonio Huerta. *Finite Element Methods for Flow Problems*. Wiley, 2003. ISBN: 0-471-49666-9.

[26] A. Erkkilä, Leppänen T., and J. Hämäläinen. Empirical plasticity models applied for paper sheets having different anisotropy and dry solids content levels. *International Journal of Solids and Structures*, 50:2151–2179, 2013.

[27] L. Fagerholm. Aerodynamical properties of dryer fabrics for high speed paper machines. In *TAPPI Engineering Conference Proceedings*, pages 165–170. TAPPI, 1990.

[28] Wilhelm Flügge. *Viscoelasticity*. Springer-Verlag, New York, 2nd edition, 1975.

[29] R.-F. Fung, J.-S. Huang, and Y.-C. Chen. The transient amplitude of the viscoelastic travelling string: An integral constitutive law. *Journal of Sound and Vibration*, 201(2):153 – 167, 1997. DOI: 10.1006/jsvi.1996.0776.

[30] R.-F. Fung, J.-S. Huang, Y.-C. Chen, and C.-M. Yao. Nonlinear dynamic analysis of the viscoelastic string with a harmonically varying transport speed. *Computers & Structures*, 66(6):777 – 784, 1998. DOI: 10.1016/S0045-7949(98)00001-7.

[31] A. A. Griffith. The phenomena of rupture and flow in solids. *Philosophical Transactions of the Royal Society of London*, A 221:163–198, 1921.

[32] X. Guan, M. S. High, and D. A. Tree. Viscoelastic effects in modeling web handling systems: Steady-state analysis. *ASME Journal of Applied Mechanics*, 62(4):908–914, 1995. DOI: 10.1115/1.2789031.

[33] X. Guan, M. S. High, and D. A. Tree. Viscoelastic effects in modeling web handling systems: Unsteady-state analysis. *ASME Journal of Applied Mechanics*, 65(1):234–241, 1998. DOI: 10.1115/1.2789031.

[34] W. Y. Hamad. On the mechanisms of cumulative damage and fracture in native cellulose fibres. *Journal of Materials Science Letters*, 17(5):433–436, 1998.

[35] Wadood Y. Hamad. Some microrheological aspects of wood-pulp fibres subjected to fatigue loading. *Cellulose*, 4(1):51–56, 1997.

[36] E. G. Hauptmann and K. A. Cutshall. Dynamic mechanical properties of wet paper webs. *Tappi Journal*, 60(10):106 – 108, 1977.

[37] L. Hauser. Analyse von laufproblemen in der papiermaschine und moderne konzeptionen der papiertrocknung. *Wochenblatt für Papierfabrikation*, (11–12):433–441, 1991.

[38] H. Hilton and S. Yi. The significance of anisotropic viscoelastic poisson ratio stress and time dependencies. *Journal of Solids Structures*, 35(23):3081–3095, 1998.

[39] H. Holik. Der schnellere lauf der papierbahn durch die papiermaschine – eine führungsaufgabe. *Wochenblatt für Papierfabrikation*, 37(3):90–102, 1985.

[40] D. T. Hristopulos and T. Uesaka. A model of machine-direction tension variations in paper webs with runnability applications. *Journal of Pulp and Paper Science*, 28(12):389–394, 2002.

[41] M. T. Huber. Die Theorie des kreuzweise bewehrten Eisenbetonplatten. *Der Bauingenieur*, 4:354–392, 1923.

[42] C. E. Inglis. Stresses in a plate due to the presence of cracks and sharp corners. *Trans. Institute of Naval Architecture*, 55:219–241, 1913.

[43] G. R. Irwin. Fracture. In S. Flugge, editor, *Handbuch der Physik*, volume VI, pages 551–590. Springer–Verlag, Berlin, 1958.

[44] C. Jentzen. *the Effect of Stress Applied During Drying on Some of The Properties of Individual Pulp Fibres*. PhD thesis, 1964. The Institute of Paper Chemistry.

[45] Juha Jeronen. *On the mechanical stability and out-of-plane dynamics of a travelling panel submerged in axially flowing ideal fluid: a study into paper production in mathematical terms*. PhD thesis, Department of Mathematical Information Technology, University of Jyväskylä, 2011. Jyväskylä studies in computing 148. ISBN 978-951-39-4595-4 (book), ISBN 978-951-39-4596-1 (PDF).

[46] M. Johnson and T. Urbanik. A nonlinear theory for elastic plates with application to characterizing paper properties. *Journal of Applied Mechanics*, 51(3):146–152, 1984.

[47] R. Jokinen, A. Komulainen, and K. Juppi. Method and apparatus in the drying section of a paper machine or the like, 2005. United States Patent, US 6 910 282.

[48] O. Joutsimo. *Effect of Mechanical Treatment on Softwood Kraft Fiber Properties*. PhD thesis, 2004. KCL, Keskuslaboratorio Oy.

[49] K. Juppi. *Experimental and Theoretical Study of the Effect of a New Dryer Construction of Paper Machine Runnability*. Doctoral dissertation, Helsinki University of Technology, 2001. Helsinki, Finland.

[50] M. Kankaanpää. Paper machine drying section and method fo operating same, 1980. United States Patent 4,202,113.

[51] J. Karlsson. *Teoretisk Undersökning av Torkvirans Inverkan pÃ¥ Arkfladder i en Pappermaskin*. Ms. thesis, Chalmers Tekniska HÃ¶gskola,Göteborg, 1989. Göteborg.

[52] M. Karlsson, editor. *Papermaking Science and Technology Vol. 9: Papermaking Part 2: Drying*. Fapet Oy, Helsinki, Finland, 2000. ISBN 952-5216-09-8.

[53] Markku Karlsson, editor. *Papermaking, Part 2 Drying*, volume 9 of *Papermaking Science and Technology*. Paperi ja Puu Oy, 2009. ISBN 978-952-5216-37-0 (book 9).

[54] H. Koivurova and E.-M. Salonen. Comments on non-linear formulations for travelling string and beam problems. *Journal of Sound and Vibration*, 225(5):845–856, 1999.

[55] J. Kouko, P. Kekko, and M. Kurki. Effect of strain rate on the strength properties of paper. In *Progress in Paper Physics Seminar, Oxford, Ohio 2006*. The Pulp & Paper Fundamental Research Society, 2006.

[56] J. Kouko, P. Kekko, H. Liimatainen, T. Saari, and M. Kurki. Wet runnability of fibre furnish for magazine papers. *Paperi ja Puu - Paper and Timber*, 88(3):1–6, 2006.

[57] M. Kurki. *Modeling of kinematical and rheological web line behavior in a papermaking environment*. Licentiate thesis, Lappeenranta University of Technology, Department of Mechanical Engineering, 2005. Lappeenranta, Finland.

[58] M. Kurki, J. Jeronen, T. Saksa, J. Tuovinen, and P. Neittaanmäki. Liikkuvan paperiradan kriittinen rajanopeus ja stabiiliusanalyysi paperi- ja kartonkikoneen eri osaprosesseissa (in finnish). *Paper and Timber (Paperi ja Puu)*, 93(1), 2011.

[59] M. Kurki and A. Lehtinen. In-plane strain field theory for 2-d moving viscoelastic webs. In *Papermaking Research Symposium 2009 (Kuopio, Finland)*. PRS, 2009.

[60] M. Kurki and P. Martikainen. Adaptive, self-underpressurizing suction roll for fast web handling concepts. In *8th Int. Conf. on Web Handling, IWEB2005, Conference Proceedings*. Web Handling Research Center, WHRC, 2005.

[61] K. Laakkonen. *Computational Flow-Field Modeling of Paper Machine Dryer Fabric*. Doctoral dissertation, Tampere University of Technology, 2003. Tampere, Finland.

[62] M. Lai, D. Rubin, and E. Krempl. *Introduction to Continuum Mechanics*. Butterworth & Heinemann, third edition edition, 1999.

[63] U. Lee and H. Oh. Dynamics of an axially moving viscoelastic beam subject to axial tension. *International Journal of Solids and Structures*, 42(8):2381 – 2398, 2005.

[64] K. M. Liew, K. C. Hung, and M. K. Lim. A solution method for analysis of cracked plates under vibration. *Engineering Fracture Mechanics*, 48(3):393–404, 1994.

[65] C. C. Lin. Stability and vibration characteristics of axially moving plates. *International Journal of Solids and Structures*, 34(24):3179–3190, 1997.

[66] C. C. Lin and C. D. Mote. Equilibrium displacement and stress distribution in a two-dimensional, axially moving web under transverse loading. *ASME Journal of Applied Mechanics*, 62:772–779, 1995.

[67] C. C. Lin and C. D. Mote. Eigenvalue solutions predicting the wrinkling of rectangular webs under non-linearly distributed edge loading. *Journal of Sound and Vibration*, 197(2):179–189, 1996.

[68] L. M. Lyne and W. Gallay. Studies in the fundamentals of wet web strength. *TAPPI Journal*, 37(12):698–704, 1954.

[69] R. W. Mann, G. A. Baum, and C. C. Habeger. Determination of all nine orthotropic elastic constants for machine-made paper. *TAPPI Journal*, 63(2):163–166, 1980.

[70] M. McIntyre and J. Woodhouse. On measuring the elastic and damping constants of orthotropic sheet materials. *Acta Metallurgica*, 36(6):1397–1416, 1988.

[71] W. L. Miranker. The wave equation in a medium in motion. *IBM Journal of Research and Development*, 4:36–42, 1960.

[72] E. M. Mockensturm and J. Guo. Nonlinear vibration of parametrically excited, viscoelastic, axially moving strings. *ASME Journal of Applied Mechanics*, 72(3):374–380, 2005. DOI: 10.1115/1.1827248.

[73] C. D. Mote. Divergence buckling of an edge-loaded axially moving band. *International Journal of Mechanical Sciences*, 10:281–195, 1968.

[74] C. D. Mote. Dynamic stability of an axially moving band. *Journal of the Franklin Institute*, 285(5):329–346, May 1968.

[75] A. S. Mujumdar and W. J. M. Douglas. Analytical modelling of sheet flutter. *Svensk Papperstidning*, 79:187–192, 1976.

[76] Kevin D. Murphy and Yin Zhang. Vibration and stability of a cracked translating beam. *Journal of Sound and Vibration*, 237(2):319–335, 2000.

[77] S. Nurmi. *Computational and Experimental Investigation of the Grooved Roll in Paper Machine Environment*. Doctoral dissertation, Lappeenranta University of Technology, 2009. ACTA Universitatis Lappeenrantaensis. ISBN 978-952-214-890-2 (book). ISBN 978-952-214-891-9 (PDF).

[78] H. Oh, J. Cho, and U. Lee. Spectral element analysis for an axially moving viscoelastic beam. *Journal of Mechanical Science and Technology*, 18(7):1159–1168, 2004. DOI: 10.1007/BF02983290.

[79] M. Ora. *The Effect of Web Structure on Wet Web Runnability*. PhD thesis, Aalto University, 2012. Aalto University 38/2012. ISBN 978-952-60-4568-9 (book). ISBN 978-952-60-4569-3 (PDF).

[80] A. Palokangas. Kuivatusviirojen kuluminen paperikoneen yksiviiravientiryhmissÃ€ (in finnish). *Paper and Timber*, 76(5):305–307, 1994.

[81] P. C. Paris and F. Erdogan. A critical analysis of crack propagation laws. *Journal of Basic Engineering, Transactions of the American Society of Mechanical Engineers*, D 85:528–534, 1963.

[82] M. Pecht and M. Johnson. The strain response of paper under various constant regain states. *TAPPI Journal*, 68(1):90–93, 1985.

[83] D. L. Prabhakara and P. K. Datta. Vibration and static stability characteristics of rectangular plates with a localized flaw. *Computers & Structures*, 49(5):825–836, 1993.

[84] D. L. Prabhakara and P. K. Datta. Vibration, buckling and parametric instability behaviour of plates with centrally located cutouts subjected to in-plane edge loading (tension or compression). *Thin-Walled Structures*, 27(4):287–310, 1997.

[85] A. Pramila. Sheet flutter and the interaction between sheet and air. *TAPPI Journal*, 69(7):70–74, 1986.

[86] A. A. Robertson. The physical properties of wet webs. *Svensk Papperstidning*, 66(1):477–497, 1963.

[87] P. Saarikivi and R. Virta. Roll for a paper machine, in particular for a paper drying device, and dryer group for a paper machine, 1982. Patent Cooperation Treaty (PCT) Patent WO/98/27274.

[88] R. A. Sack. Transverse oscillations in traveling strings. *British Journal of Applied Physics*, 5:224–226, 1954.

[89] E. Salikis, T. Urbanik, and B. Tokyay. Bilinear modelling of cellulosic orthotropic nonlinear materials. *Journal of Pulp and Paper Science*, 29(12):407–411, 2003.

[90] K. Salminen. *The Effects of Some Furnish and Paper Structure Related Factors on Wet Web Tensile and Relaxation Characteristics*. PhD thesis, University of Lappeenranta, 2010.

[91] I. B. Sanborn. A study of irreversible, stress-induced changes in the macrostructure of paper. *TAPPI Journal*, 45(6):465–474, 1962.

[92] J. Sato, I. Hutchings, and J. Woodhouse. Determination of the elastic properties of paper and paperboard from the low-frequency vibration modes of rectangular plate. *Appita Journal*, 61(4):291–296, 2008.

[93] Hermann Schlichting. *Boundary Layer Theory*. McGraw-Hill, 4th edition, 1960.

[94] R. S. Seth and D. H. Page. Fracture resistance of paper. *Journal of Materials Science*, 9(11):1745–1753, 1974.

[95] D. I. Sherman. On the stress distribution in partitions, an elastic heavy medium which is weakened by elliptic holes. *Izvestiya Akademii Nauk SSSR, Otdelenie Tekhnicheskikh Nauk (OTN)*, 7:992–1010, 1952.

[96] Changho Shin, Jintai Chung, and Wonsuk Kim. Dynamic characteristics of the out-of-plane vibration for an axially moving membrane. *Journal of Sound and Vibration*, 286(4-5):1019–1031, September 2005.

[97] Changho Shin, Wonsuk Kim, and Jintai Chung. Free in-plane vibration of an axially moving membrane. *Journal of Sound and Vibration*, 272(1–2):137–154, 2004.

[98] J. Skowronski and A. A. Robertson. A phenomenological study of the tensile deformation properties of paper. *Journal of Pulp and Paper Sciences*, 11(1):J21–J28, 1985.

[99] Rudolf Skutch. Uber die Bewegung eines gespannten Fadens, weicher gezwungen ist durch zwei feste Punkte, mit einer constanten Geschwindigkeit zu gehen, und zwischen denselben in Transversalschwingungen von gerlinger Amplitude versetzt wird. *Annalen der Physik und Chemie*, 61:190–195, 1897.

[100] S. Smith and Stolle D. A comparison of eulerian and updated lagrangian finite element algorithms for simulating film casting. *Finite Elements in Analysis and Design*, 38:401–415, 2002.

[101] J. Sorvari, J. Kouko, M. Malinen, M. Kurki, and J. Hämäläinen. Paper as a viscoelastic material: Comparison between different theories. In *Appita Conference and Exhibition (61th : 2007 : Gold Coast, Qld.)*, volume 2007, pages 389–396. Vic.: Appita Inc, 2007.

[102] B. Stahl and L. M. Keer. Vibration and stability of cracked rectangular plates. *International Journal of Solids and Structures*, 8(1):69–91, 1972.

[103] H. Struck. Ruby nozzles for improved edge trimming and for oscillating hp showers. In *PaperCon Conference Proceedings*, pages 2912–2919. TAPPI, 2011.

[104] L. Subramanian and L. Carlsson. Influence of voids on the engineering constants of paper, part 1: Continuum modeling. *TAPPI Journal*, 77(11):209–216, 1994.

[105] D. Swinehart and D. Broek. Tenacity and fracture toughness of paper and board. *Journal of pulp and paper science*, 21(11):J389–J397, 1995.

[106] R. D. Swope and W. F. Ames. Vibrations of a moving threadline. *Journal of the Franklin Institute*, 275:36–55, 1963.

[107] E. Tenfält and U. Molin. Sluten torkviraföring - ett enkelt, billigt och effektivt arrangemant. *Svensk Papperstidning*, 80(12):363–367, 1977.

[108] J. L. Thorpe. Paper as an orthotropic thin plate. *TAPPI Journal*, 64(3):119–121, 1981.

[109] A.L. Thurman and C.D. Mote, Jr. Free, periodic, nonlinear oscillation of an axially moving strip. *Journal of Applied Mechanics*, 36(1):83–91, March 1969.

[110] S. Timoshenko and J. Goodier. *Theory of Elasticity*. McGraw-Hill, second edition edition, 1951.

[111] S. P. Timoshenko and S. Woinowsky-Krieger. *Theory of plates and shells*. New York : Tokyo : McGraw-Hill, 2nd edition, 1959. ISBN 0-07-085820-9.

[112] Johan Tryding. *In-plane fracture of paper*. Report tvsm-1008, Lund University, Lund Institute of Technology, Division of Structural Mechanics, 1996. Sweden.

[113] T. Uesaka, K. Murakami, and R. Imamura. Two-dimensional linear viscoelasticity of paper. *Wood Science and Technology*, 14:131–142, 1980.

[114] A. G. Ulsoy and C. D. Mote. Vibration of wide band saw blades. *ASME Journal of Engineering for Industry*, 104:71–78, 1982.

[115] A. Vafai, M. Javidruzi, and H. E. Estekanchi. Parametric instability of edge cracked plates. *Thin-Walled Structures*, 40(1):29–44, 2002.

[116] A. Vainio. *Interfiber bonding and fibre segment activation in paper – observations on the phenomena and their influence on paper strength properties*. PhD thesis, 2007. Department of Forest Products Technology, Helsinki University of Technology.

[117] T. Wahlström and C. Fellers. Biaxial straining of paper during drying, relations between stresses, strains and properties. 1999. TAPPI Engineering Conference, Sept. 12-16, 1999, Anaheim, CA.

[118] R. Wathén. *Studies on fiber strength and its effect on paper properties*. PhD thesis, 2006. KCL, Keskuslaboratorio Oy.

[119] Rolf Wathén. *Characterizing the influence of paper structure on web breaks*. Licentiate thesis, Helsinki University of Technology, Department of Forest Products Technology, 2003. Espoo, Finland.

[120] H. M. Westergaard. Bearing pressures and cracks. *Journal of Applied Mechanics*, 6:A49–A53, 1939.

[121] T. Yokoyama and K. Nakai. Evaluation of in-plane orthotropic elastic constants of paper and paperboard. In *2007 SEM Annual Conference & Exposition on Experimental and Applied Mechanics*, 2007.

ORIGINAL PAPERS

PI

STRAIN FIELD THEORY FOR VISCOELASTIC CONTINUOUS HIGH-SPEED WEBS WITH PLANE STRESS BEHAVIOR

by

Matti Kurki, Juha Jeronen, Tytti Saksa and Tero Tuovinen 2012

European Congress on Computational Methods in Applied Sciences and Engineering, (ECCOMAS)

European Congress on Computational Methods
in Applied Sciences and Engineering (ECCOMAS 2012)
J. Eberhardsteiner et.al. (eds.)
Vienna, Austria, September 10-14, 2012

STRAIN FIELD THEORY FOR VISCOELASTIC CONTINUOUS HIGH-SPEED WEBS WITH PLANE STRESS BEHAVIOR

Matti J. Kurki[1], **Juha M. Jeronen**[2], **Tytti J. Saksa**[2], **and Tero T. Tuovinen**[2]

[1] JAMK University of Applied Sciences
P.O.B. 207, FIN-40101, FINLAND
e-mail: matti.kurki@jamk.fi

[2] University of Jyväskylä, Department of Mathematical InformationTechnology
P.O.B. 35, FIN-40014, Jyväskylä, FINLAND
e-mail: {juha.m.jeronen, tytti.j.saksa, tero.t.tuovinen}@jyu.fi

Keywords: Moving material, Viscoelasticity, In-plane stresses, Kelvin-Voigt model, Paper production

Abstract. *In this paper, we address to the problem of the origin of in-plane stresses in continuous, high-speed webs. In the case of thin, slender webs a typical modeling approach is the application of static in-plane stress approximation without considering the effects of in-plane velocity field. In the case of one-dimensional equations, we will study the effects of material viscoelasticity and Eulerian non-linearity of the transport velocity. Finite element solutions of the non-linear equation are presented with both elastic and viscoelastic material assumptions. Despite the limitations of the Kelvin-Voigt material assumption, fundamental coupling effects between viscoelasticity and velocity are visible. The strain behavior in the span under study is examined, and from both analytical and numerical results it is seen that the web strain is not constant during the span length. Results also indicate that the viscous properties of the material are closely connected to the overall tension level behavior in the stretched web span. Material time-dependency changes the web stress behavior: the span length, material viscosity and the web velocity cause significant effects, which are observed in the in-plane dynamics of the web.*

1 Introduction

In the handling of continuous, high-speed webs the origin of in-plane stresses creates a scientific problem, which is not yet completely understood. Especially, the type of the web material has a significant effect on both qualitative and quantitative characteristics of the in-plane stresses. Web tension in the moving continuous web systems can usually be controlled in the direction of the transport velocity, the tension being generated by a velocity difference between the starting and ending lines of the span. With high transport velocities, both web stress and web stability are under concern not only in this longitudinal direction but also in the direction perpendicular to the velocity in the plane of the web.

Since axially moving materials, such as strings, belts, beams, membranes and plates, have many applications in industry, e.g. in paper production, their mechanics have been studied widely. In processing of different kinds of thin, laterally moving solid webs, such challenges as efficiency of production and effects caused by high processing speed are met.

Research history of vibrations of travelling elastic materials goes back to the 1950's, when Sack [40] and Archibald and Emslie [1] studied transverse vibrations in a traveling string. In the 1960s and 70's, many researchers continued studies on moving strings and beams concentrating mainly on various aspects of free and forced transverse vibrations [31, 33, 34, 35, 43, 46]. Stability of small transverse vibrations of travelling two-dimensional rectangular membranes and plates have been studied by Ulsoy and Mote [51], and Lin [26]. When the web is advancing through processes without an external support, the inertial forces depending on the web speed are coupled with web tension. Also the transverse behavior of the web and the response in the flowing fluid (air) surrounding the web are coupled (see e.g. [7, 38]).

Lin and Mote studied an axially moving membrane in a 2D formulation, predicting the equilibrium displacement and stress distributions under transverse loading [27]. Later, the same authors studied the wrinkling of axially moving rectangular webs with a small flexural stiffness [28]. They predicted the critical value of the non-linear component of the edge loading after which the web wrinkles and the corresponding wrinkled shape of a web. It is also known, that lack of web tension will result in loss of stability in the moving web, which from the application viewpoint, disturbs required smooth advancing of the web (see e.g. [3, 4]). From the other hand, web tension too high may cause web breaks, which deteriorate production efficiency and the strength properties of the processeed material (see e.g. [2, 39, 41, 44]).

Considering wet paper material, the viscoelastic properties play an important role in the behavior of the web and, thus, are to be included in the model. The first study on transverse vibration of travelling viscoelastic material was carried out by Fung et. al. using a string model [15]. Extending their work, they studied the material damping effect in their later research [16].

Viscoelastic strings and beams have been studied recently exceedingly, see e.g. [30, 53]. Oh et al. studied critical speeds, eigenvalues and natural modes of the transverse displacement of axially moving viscoelastic beams using the spectral element model [25, 36]. Chen and Zhao [12] represented a modified finite difference method to simplify a non-linear model of an axially moving string. They studied numerically the free transverse vibrations of both elastic and viscoelastic strings. Chen and Yang studied free vibrations of viscoelastic beams travelling between simple supports with torsion strings [11]. They studied the viscoelastic effect by perturbing the similar elastic problem and using the method of multiple scales. Very recently, Yang et al. studied vibrations, bifurcation, and chaos of axially moving viscoelastic plates using finite differences and a non-linear model for transverse displacements [52].

Marynowski and Kapitaniak studied differences between the Kelvin-Voigt and Bürgers mod-

els in modeling of internal damping of axially viscoelastic moving beams. They found out that both models gave accurate results with small damping coefficients, but with a large damping coefficient, the Bürgers model was more accurate [29]. In 2007, they compared the models with the Zener model studying the dynamic behavior of an axially moving viscoelastic beam [30]. They found out that the Bürgers and Zener model gave similar results for the critical transport speed whereas the Kelvin-Voigt model gave a greater transport speed compared to the other two models.

The origin and structure of the tension distribution in a moving solid web seems to be an exceptionally unknown area. The often used models with the web materials are based on assumptions of isotropic or orthotropic material properties (see e.g. [5, 48]). Also, the web materials are often considered as viscoelastic or viscoplastic but there is no coupling between in-plane strain and web velocity effects (see e.g. [19, 37, 50]). Time-dependent, in-plane vibrations of a moving continuous membrane were studied by Shin et al. [42]. In their work, in-plane vibration modes of an isotropic web were studied between the traction lines. Also Guan et. al. have studied viscoelastic web behavior in both steady state and unsteady state cases [17, 18].

Usually, the partial time derivative has been used instead of the material derivative in the viscoelastic constitutive relations. Mockensturm and Guo suggested that the material derivative should be used [32]. They studied non-linear vibrations and dynamic response of axially moving viscoelastic strings. Kurki and Lehtinen suggested, independently, that the material derivative in the constitutive relations should be used in their study concerning the in-plane displacement field of a travelling viscoelastic plate [23]. In the study by Chen et al., the material derivative was used in the viscoelastic constitutive relations [8]. They studied parametric vibration of axially accelerating viscoelastic strings. Chen and Ding studied stability of axially accelerating viscoelastic beams using the method of multiple scales and the material derivative in the viscoelastic constitutive relations [13]. Chen and Wang studied stability of axially accelerating viscoelastic beams using asymptotic perturbation analysis and the material derivative in the viscoelastic relations [10]. In a recent research by Chen and Ding, the material derivative was also used to study dynamic response of vibrations of axially moving viscoelastic beams [9]. In their study, a non-linear model was used taking into account the coupling of the transverse displacement with the longitudinal (in-plane) displacement. However, the transverse behavior of the beam was their main focus.

In this paper, we will represent a study where the effects of material viscoelasticity and Eulerian non-linearity of the transport velocity U in are considered in the following one-dimensional equation:

$$\eta U \frac{\partial^3 u}{\partial x^3} + (E - \rho U^2) \frac{\partial^2 u}{\partial x^2} - \rho U \frac{\partial U}{\partial x} \frac{\partial u}{\partial x} = 0 \tag{1}$$

where η is viscosity, ρ is density of material, x is axial coordinate and u is the in-plane displacement. One fundamental observation of this study is the significance of strain-based boundary conditions; in the case on one-dimensional model, the strain (Dirichlet) boundary condition affects throughout the web thickness isolating the span under observation from other preceding or succeeding web spans.

2 Continuous web flow phenomenon

Continuous, moving web creates a flow continuum, which may be considered as a solid flow medium. Due to its solid nature, web continuum is always under the stress state, which is caused

by the strain state. Using the conservation of mass, we get the following equation:

$$\frac{\partial \rho}{\partial t} + \rho \nabla U = 0\,. \tag{2}$$

with web density ρ and longitudinal velocity U.

Assuming the density ρ to be constant, using Eq. (2) we may construct the mass conservation law for the situation described in Figure 1. Because there is a longitudinal strain component ε in the web span under observation, Eq. (2) can be represented as follows:

$$\rho A_1 U_1 - \rho A_2 U_2 = 0\,, \tag{3}$$

where

$$A_2 = \frac{A_1}{1 - \varepsilon_{\mathrm{T}}} \tag{4}$$

and ε_{T} is the strain at the end of the span, i.e at the area A_2 in Figure 1. From Eqs. (3) and (4), we obtain

$$\varepsilon_{\mathrm{T}} = \frac{U_2}{U_1} - 1\,. \tag{5}$$

Flowing solid continuum in the case above is assumed to be controlled only in the direction of the transport speed, i.e. in the longitudinal x-direction. Note that Eq. (3) can be applied only in the steady-state situation of the flow, i.e. the web is assumed to flow smoothly and without time-dependent disturbances [18]. Also, the traction lines at the cross-sectional areas A_1 and A_2 are assumed to affect only at the surfaces of the web, i.e. the stress and strain waves advancing inside the web thickness can cross the traction lines. Therefore the boundary conditions of the moving continuous webs in reality are consisting rather complicated friction-based force transmission phenomena at web-roll contact areas [22].

3 One-dimensional viscoelastic in-plane moving continuum equations

In this article, material assumption of the web continuum is based on viscoelasticity. With fibrous, composite-type materials, the elasticity properties are result of complicated material pre-processing, which further results in orthotropic anisotropy with material time-dependency (see e.g. [6, 20, 37, 50]). One can derive a vast number of different rheological models for the time-dependent material behavior but fundamental behavior of continuous flow of the solid viscoelastic web can be analyzed by using the simple Kelvin-Voigt model. The principle of the Kelvin-Voigt model is described in Figure 2.

Stress-strain behavior of one-dimensional Kelvin-Voigt material is (see e.g. [14])

$$\sigma = E\varepsilon + \eta \frac{\mathrm{d}\varepsilon}{\mathrm{d}t}\,, \tag{6}$$

where σ denotes the stress, ε the strain, E the Young's modulus, and η the viscosity coefficient.

In the following, we represent a description of the strains and deformations. A standard method to describe the structural deformations is to use *material* assumption with static medium according to the placement of observer. Longitudinal movement of material creates in-plane deformations, the modelling of which is a real challenge, since the actual deformation is to be handled using *spatial* or mixed Lagrange-Euler description[24, 45]. This description is standard

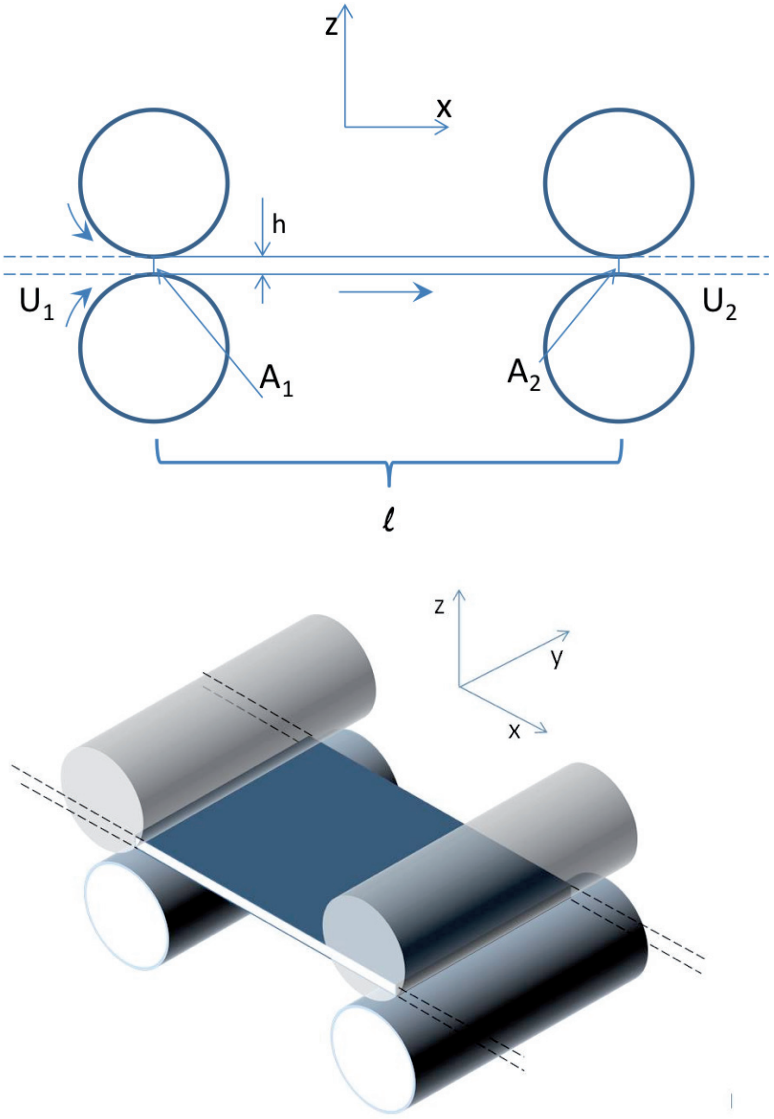

Figure 1: Solid web continuum flowing between the incoming and outgoing flow control areas A_1 and A_2 with longitudinal speeds U_1 and U_2 between the beginning and ending tractions lines, respectively.

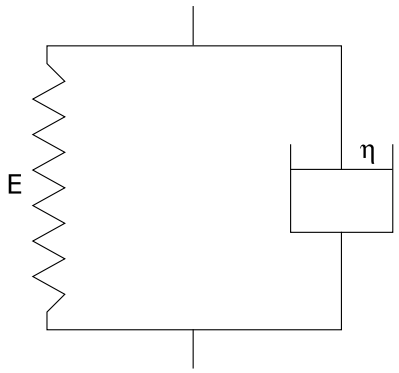

Figure 2: Kelvin-Voigt rheological model.

in fluid dynamics where the observer is *watching* a control volume where possible deformations will appear [21]. Using the same principle, we may construct a constitutive flow model for solid, anisotropic viscoelastic moving continuum. Therefore the strain ε is to be written in the Lagrange-Euler form:

$$\varepsilon = \varepsilon(x,t)\,. \tag{7}$$

The material derivative of strain ε is then

$$\frac{\mathrm{d}\varepsilon}{\mathrm{d}t} = \frac{\partial\varepsilon}{\partial x}\frac{\mathrm{d}x}{\mathrm{d}t} + \frac{\partial\varepsilon}{\partial t} = U\frac{\partial\varepsilon}{\partial x} + \frac{\partial\varepsilon}{\partial t}\,. \tag{8}$$

For time-dependent solid continuum flow, the following equation may be derived:

$$\rho\frac{\partial^2 u}{\partial t^2} + 2\rho U\frac{\partial^2 u}{\partial x\partial t} + \rho U^2\frac{\partial^2 u}{\partial x^2} + \rho\left(\frac{\partial U}{\partial t} + U\frac{\partial U}{\partial x}\right)\frac{\partial u}{\partial x} = E\frac{\partial^2 u}{\partial x^2} + \eta\left(\frac{\partial^3 u}{\partial x^2\partial t} + U\frac{\partial^3 u}{\partial x^3}\right)\,. \tag{9}$$

If we assume that there is no time-dependent fluctuation in x-directional displacement u, we can represent a steady-state equation for ideal, undisturbed axial narrow web flow in the following form:

$$\eta U\frac{\partial^3 u}{\partial x^3} + (E - \rho U^2)\frac{\partial^2 u}{\partial x^2} - \rho U\frac{\partial U}{\partial x}\frac{\partial u}{\partial x} = 0\,. \tag{10}$$

With the assumption of linear Cauchy strains states

$$\varepsilon = \partial u/\partial x \tag{11}$$

and based on the linearized form of Eq. (10) ,we will get the equation

$$\eta U\frac{\partial^2 \varepsilon}{\partial x^2} + (E - \rho U^2)\frac{\partial\varepsilon}{\partial x} = 0\,. \tag{12}$$

The similarity between Eq. (12) and the heat convection equation

$$k_{\mathrm{T}}\frac{\partial^2 T}{\partial x^2} - \rho c_{\mathrm{p}} U\frac{\partial T}{\partial x} = 0 \tag{13}$$

in one dimension is apparent. In Eq. (13), T is temperature, U the spatial motion of the media surrounding the object under heat transfer, c_{p} the specific heat of the object, and k_{T} the heat diffusion coefficient [47].

4 Algebraic solution of the linearized steady-state case

The solution of Eq. (12) can be achieved using algebraic methods. If only pure elasticity is present, solution is of the form:

$$(E - \rho U^2)\varepsilon = C\,, \tag{14}$$

where C is constant. Thus, the solution obeys Hookean behavior, i.e. the strain ε is constant regardless of the level of the transport velocity U.

However, with nonzero viscosity, Eq. (12) becomes

$$\frac{\partial^2 \varepsilon}{\partial x^2} + \left(\frac{E - \rho U^2}{\eta U}\right)\frac{\partial \varepsilon}{\partial x} = 0\,. \tag{15}$$

With the boundary conditions $\varepsilon(0) = 0$, $\varepsilon(\ell) = \varepsilon_{\mathrm{T}}$, the algebraic solution of Eq. (15) is [22]

$$\varepsilon(x) = \varepsilon_{\mathrm{T}}\frac{1 - e^{-kx}}{1 - e^{-k\ell}}, \tag{16}$$

where

$$k = \frac{E - \rho U^2}{\eta U} \tag{17}$$

and ℓ is the length of the span under observation.

Analytical solution of the strain can be obtained only for the linearized one-dimensional case. Based on Eq. (8), we define the spatial strain in the steady-state case:

$$\frac{\mathrm{d}\varepsilon}{\mathrm{d}t} = U\frac{\partial \varepsilon}{\partial x}\,. \tag{18}$$

Now the x-directional stress σ appearing in the moving viscoelastic span based on the strain in Eq. (16) is a superposition of the elastic and viscous stress components:

$$\sigma = E\varepsilon_{\mathrm{T}}\frac{1 - e^{-kx}}{1 - e^{-k\ell}} + \eta U\varepsilon_{\mathrm{T}}\frac{ke^{-kx}}{1 - e^{-k\ell}}\,. \tag{19}$$

Substitution of (17) into (19), one gets

$$\sigma = \frac{\varepsilon_{\mathrm{T}}}{1 - e^{-k\ell}}(E - \rho U^2 e^{-kx})\,. \tag{20}$$

5 Numerical results by FEM

Numerical solution of the viscoelastic moving continuum problem is realized using the finite element method (FEM). The derivation of the FEM matrices is performed using the principle of virtual work. Virtual work δW can be calculated using the virtual strain $\delta\varepsilon^T$ as follows [54]:

$$\delta W = \int_V \delta\varepsilon^T \bar{\sigma}\,\mathrm{d}V\,. \tag{21}$$

In the finite element method, the connection between the strain vector ε and displacements u_e in the element nodes are defined by using strain-displacement approximation in a matrix B

$$\varepsilon = \mathbf{B}u_e \qquad \text{where} \qquad \mathbf{B} = \frac{\partial}{\partial x}\mathbf{N}_e\,. \tag{22}$$

In Eq. (22), $\mathbf{N}_e$ is a shape function matrix defining the displacement approximations inside the element. If the element is undergoing a virtual displacement δu_e, we can write using Eq. (21) (see e.g. [54]):

$$\delta W = \delta u_e \int_V \mathbf{B}^T \bar{\sigma} \, \mathrm{d}V \, . \tag{23}$$

However, the stress $\bar{\sigma}$ inside the volume is calculated using the stress strain behaviour of the viscoelastic in-plane moving continuum model. One-dimensional non-linear equation (10) will be solved using the finite element method.

While the velocity U is a function of x, the terms in Eq. (10) may be regrouped as follows:

$$\frac{\partial}{\partial x}\left[\eta U \frac{\partial^2 u}{\partial x^2} + (E - \rho U^2)\frac{\partial u}{\partial x}\right] + \rho U \frac{\partial U}{\partial x}\frac{\partial u}{\partial x} - \eta \frac{\partial U}{\partial x}\frac{\partial^2 u}{\partial x^2} = 0 \, . \tag{24}$$

We denote

$$\bar{\sigma} = \eta U \frac{\partial^2 u}{\partial x^2} + (E - \rho U^2)\frac{\partial u}{\partial x} \, . \tag{25}$$

Using the finite element method approximation presented in Eq. (22), the displacement operators in Eq. (25) can be written as

$$\bar{\sigma} = \left[\eta U \mathbf{B}_2 + (E - \rho U^2)\mathbf{B}_1\right] u_e \, , \tag{26}$$

where

$$\mathbf{B}_1 = \frac{\partial}{\partial x}\mathbf{N} \qquad \text{and} \qquad \mathbf{B}_2 = \frac{\partial^2}{\partial x^2}\mathbf{N}. \tag{27}$$

On the other hand, $\bar{\sigma}$ can be expressed with the help of strains (see Eq. (11))

$$\bar{\sigma} = \left[\eta U \mathbf{B}_1 + (E - \rho U^2)\mathbf{N}\right] \varepsilon_e \, , \tag{28}$$

where ε_e are the strains in the element nodes.

The substitution of Eq. (28) to Eq. (23) will result in

$$\delta W = \delta u_e \left[\int_V \mathbf{B}^T \left[\eta U \mathbf{B}_1 + (E - \rho U^2)\mathbf{N}\right] \mathrm{d}V\right] \varepsilon_e \, . \tag{29}$$

However, inside the element area the virtual energy $\delta W = \delta u_e F_e$, where F_e is the force vector, affecting on the element. The forces affecting the element can be represented as

$$F_e = \mathbf{K}_e \varepsilon_e \, ,$$

where $\mathbf{K}_e$ is the following element stiffness matrix:

$$\mathbf{K}_e = A \int_0^{\ell_e} \left[\mathbf{B}^T \eta U \mathbf{B}_1 + \mathbf{B}^T (E - \rho U^2)\mathbf{N}\right] \mathrm{d}x \, . \tag{30}$$

The element used in the analysis is a 3-node quadratic rod element with three axial degrees of freedom. See Figure 3.

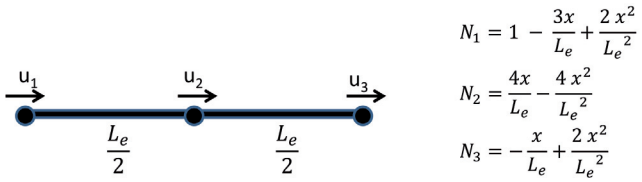

Figure 3: Quadratic 3-node rod element and its corresponding shape functions.

The final global finite element equation is

$$F = \mathbf{K}u\,. \tag{31}$$

Vector u includes the displacements based on the boundary conditions presented in the Section 4. Boundary conditions for the axial system of Figure 1 are

$$u_{x=0} = 0 \qquad \text{and} \qquad u_{x=\ell} = \varepsilon_{\mathrm{T}}\ell = \left(\frac{U_2}{U_1} - 1\right)\ell\,. \tag{32}$$

The solution of Eq. (31) is now realized by substituting the displacements of Eq. (32) to appropriate places in the displacement vector u. The corresponding forces are calculated to force vector F by using elimination. Finally, the rest unsolved displacements are computed using $u = \mathbf{K}^{-1}F$. The non-linear term in Eq. (24) is handled as a body force applied to the element nodes. By this, the effect of the non-linear term can be solved as a non-linear force

$$F_{Be} = \int_V \mathbf{N}^T F_{nl}\,\mathrm{d}V\,. \tag{33}$$

The force F_{nl} originating from the non-linear term, will be calculated for each element:

$$F_{nl} = \rho U\frac{\partial U}{\partial x}\varepsilon - \eta\frac{\partial U}{\partial x}\frac{\partial \varepsilon}{\partial x}\,. \tag{34}$$

The final nodal forces F_{Be} for each element are individual and take into account the current displacement, velocity and velocity gradient inside of each element. The problem with these body forces is solved via the Newton–Raphson method.

Using Eqs. (16), (18), and (19), the strain and stress states of the one-dimensional viscoelastic beam can be calculated.We have used parameter values $E = 2.5 \cdot 10^7$ N/m^2, $\eta = 4.0 \cdot 10^5$ Ns/m^2, $U = 10$ m/s, span length $\ell = 1.0$ m and strain $\varepsilon_{\mathrm{T}} = 0.03$. The cross-directional area, which is under draw, is $A = 2.0$ m^2, and the web density is 0.16 kg/m^3.

For the exemplary parameter values above, the results obtained are shown in the Figures 4 – 7. The analytical solution (with a constant velocity U) is obtained from Eq. (12), and the FEM solutions from the discretized form of Eq. (10) with velocity depending on x. For the first Newton–Raphson iteration, the U was set constant, but U was updated during the iteration with the help of nodal strains. The number of nodal points used in the FEM was 600.

The strain distribution during the draw differs from the constant-strain presented in theory of elasticity [49]. See Figure 4. In this figure, one may also notice a slight difference between the analytical solution with constant U and the numerical iterated solution where the velocity U depends on x. However, the FEM solution from the first iteration (having constant U) and the analytical solution coincided as desired.

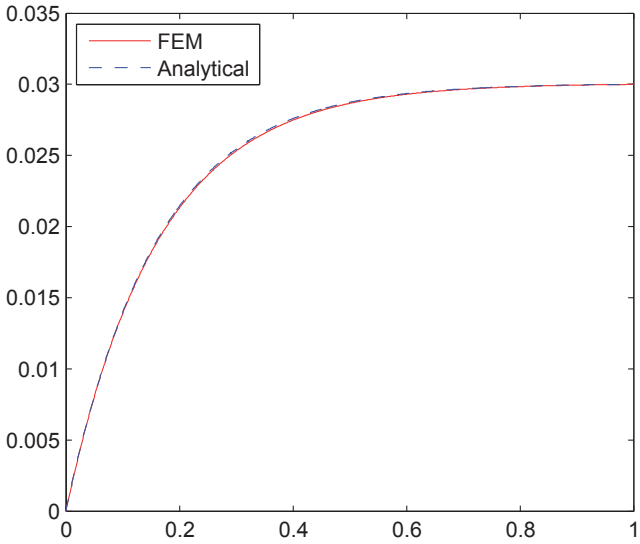

Figure 4: Analytical and numerical (FEM) solution of strain distribution during the length of the span.

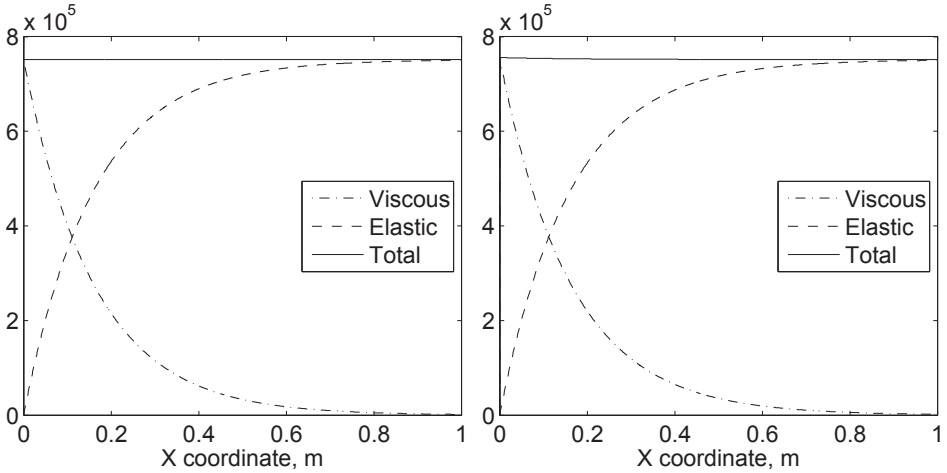

Figure 5: Analytical (left) and numerical (FEM) (right) solution of the stress distribution during the length of the span.

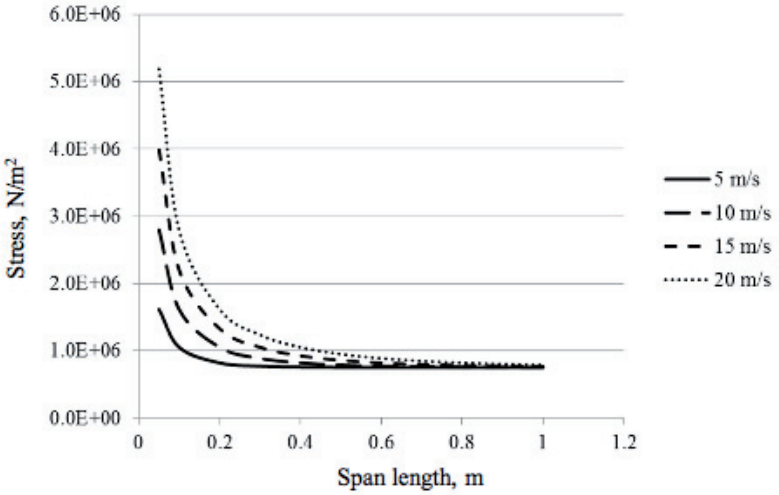

Figure 6: Effect of the span length to the web stress with different web speed levels.

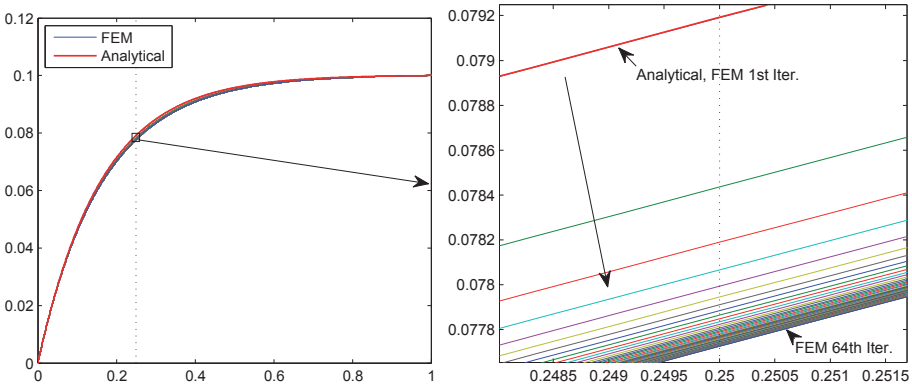

Figure 7: Strain distribution in the span and the effect of non-linearity. The strain at the end of the span is $\varepsilon_{\mathrm{T}} = 0.1$. On the right-hand side, the Newton–Raphson iteration is shown for some values of x.

Even though the strain distribution is not constant, the stress distribution is a combination of elastic and viscous forces based on Eq. (6) and it is *almost* constant. See Figure 5 and compare with the analytical solution in Eq. (20). The stress increases very slightly towards the traction line A_2.

The effect of the span length on the web stress state is visible in Figure 6. As seen, the shorter the processing time of the viscoelastic span, the higher the response of the time-dependent viscous force component. The effect of non-linearity is seen in Figure 7. However, the effect of non-linearity is relatively small.

In Table 1, numerical data in the case $\varepsilon_{\mathrm{T}} = 0.1$ is shown for some numbers of iterations. The value of the strain ε is collected for $x = 0.25$ m, 0.50 m, and 0.75 m (when the length of the span is $\ell = 1$ m). Also here, it is seen that the first iteration with constant velocity gives results that coincide with the analytical solution. This shows the accuracy of the FEM solution. When U is not constant, the strains seems to be slightly smaller than in the case when U is constant. See also Figure 7.

Table 1: Numerical data from the Newton–Raphson iteration. The value of the strain ε for some selected values of x and numbers of iterations (Iter.). At the first row, the analytical solution for the case of constant velocity is shown. The strain at the end of the span is $\varepsilon_{\mathrm{T}} = 0.1$. Compare with Figure 7.

Iter.	x (m)		
	0.25	0.50	0.75
Anal.	$7.9082{\cdot}10^{-2}$	$9.5768{\cdot}10^{-2}$	$9.9266{\cdot}10^{-2}$
1	$7.9081{\cdot}10^{-2}$	$9.5768{\cdot}10^{-2}$	$9.9266{\cdot}10^{-2}$
4	$7.7957{\cdot}10^{-2}$	$9.5119{\cdot}10^{-2}$	$9.9076{\cdot}10^{-2}$
16	$7.7683{\cdot}10^{-2}$	$9.4955{\cdot}10^{-2}$	$9.9026{\cdot}10^{-2}$
64	$7.7615{\cdot}10^{-2}$	$9.4914{\cdot}10^{-2}$	$9.9014{\cdot}10^{-2}$

6 Conclusions

In this paper, we presented models for handling of continuous, high-speed webs. We also took into consideration the type of the web material, which has a significant effect on both qualitative and quantitative characteristics of the in-plane stresses.

In this study, the effects of the material viscoelasticity and the Eulerian non-linearity were considered as a function of the transport velocity. Solutions of the one-dimensional non-linear equation were presented both with elastic and viscoelastic material assumptions. Finite element method (FEM) was used in the solution of the group of the second order PDEs.

Despite the limitations of the Kelvin-Voigt material assumption, fundamental coupling effects between viscoelasticity and the velocity field were visible. From the numerical solutions, the effect of the strain behavior in the span under study was seen: the web strain is not constant during the span length. In the case of pure elastic web material, the non-linear Euler term seemed to cause a qualitatively similar effect. The strain being non-constant originates from the velocity difference and the longitudinal strain wave velocity in the elastic material.

One fundamental observation on the significance of the strain-based boundary conditions was made. In the case of an one-dimensional model, the strain (Dirichlet) boundary condition affects throughout the web thickness isolating the span under observation from the (possibly) preceeding or succeeding web spans. Based on the Figure 1, this, however, is not the situation in reality. Even if the web was considered as slender, there would always be a possibility of the time-dependent strain waves advancing through the control areas A_1 and A_2. Therefore, one

of the future challenges in developing realistic in-plane moving web models are the boundary conditions applied.

REFERENCES

[1] F. R. Archibald and A. G. Emslie. The vibration of a string having a uniform motion along its length. *ASME Journal of Applied Mechanics*, 25:347–348, 1958.

[2] N. Banichuk, S. Ivonova, M. Kurki, T. Saksa, M. Tirronen, and T. Tuovinen. Safety analysis and optimization of travelling webs subjected to fracture and instability. In *Numerical methods for differential equations, optimization, and technological problems. Dedicated to Professor P. Neittaanmäki on his 60th Birthday*, Computational Methods in Applied Sciences. Springer, 2012. In press.

[3] N. Banichuk, J. Jeronen, M. Kurki, P. Neittaanmäki, T. Saksa, and T. Tuovinen. On the limit velocity and buckling phenomena of axially moving orthotropic membranes and plates. *International Journal of Solids and Structures*, 48(13):2015–2025, 2011.

[4] N. Banichuk, J. Jeronen, P. Neittaanmäki, and T. Tuovinen. On the instability of an axially moving elastic plate. *International Journal of Solids and Structures*, 47(1):91–99, 2010.

[5] G. A. Baum, D. C. Brennan, and C. C Habeger. Orthotropic elastic constants of paper. *Tappi Journal*, 64(8):97–101, 1981.

[6] J. Castro and M. Ostoja-Starzewski. Elasto-plasticity of paper. *International Journal of Plasticity*, (19):2083–2098, 2003.

[7] Y. B. Chang and P. M. Moretti. Interaction of fluttering webs with surrounding air. *TAPPI Journal*, 74(3):231–236, 1991.

[8] L.-Q. Chen, H. Chen, and C.W. Lim. Asymptotic analysis of axially accelerating viscoelastic strings. *International Journal of Engineering Science*, 46(10):976 – 985, 2008. DOI: 10.1016/j.ijengsci.2008.03.009.

[9] L.-Q. Chen and H. Ding. Steady-state transverse response in coupled planar vibration of axially moving viscoelastic beams. *ASME Journal of Vibrations and Acoustics*, 132:011009–1–9, 2010. http://dx.doi.org/10.1115/1.4000468.

[10] L.-Q. Chen and B. Wang. Stability of axially accelerating viscoelastic beams: asymptotic perturbation analysis and differential quadrature validation. *European Journal of Mechanics - A/Solids*, 28(4):786 – 791, 2009. DOI: 10.1016/j.euromechsol.2008.12.002.

[11] L.-Q. Chen and X.-D. Yang. Vibration and stability of an axially moving viscoelastic beam with hybrid supports. *European Journal of Mechanics - A/Solids*, 25(6):996 – 1008, 2006. DOI: 10.1016/j.euromechsol.2005.11.010.

[12] L.-Q. Chen and W.-J. Zhao. A numerical method for simulating transverse vibrations of an axially moving string. *Applied Mathematics and Computation*, 160(2):411 – 422, 2005. DOI: 10.1016/j.amc.2003.11.012.

[13] H. Ding and L.-Q. Chen. Stability of axially accelerating viscoelastic beams: multi-scale analysis with numerical confirmations. *European Journal of Mechanics - A/Solids*, 27(6):1108 – 1120, 2008. DOI: 10.1016/j.euromechsol.2007.11.014.

[14] Wilhelm Flügge. *Viscoelasticity*. Springer-Verlag, New York, 2nd edition, 1975.

[15] R.-F. Fung, J.-S. Huang, and Y.-C. Chen. The transient amplitude of the viscoelastic travelling string: An integral constitutive law. *Journal of Sound and Vibration*, 201(2):153 – 167, 1997. DOI: 10.1006/jsvi.1996.0776.

[16] R.-F. Fung, J.-S. Huang, Y.-C. Chen, and C.-M. Yao. Nonlinear dynamic analysis of the viscoelastic string with a harmonically varying transport speed. *Computers & Structures*, 66(6):777 – 784, 1998. DOI: 10.1016/S0045-7949(98)00001-7.

[17] X. Guan, M. S. High, and D. A. Tree. Viscoelastic effects in modeling web handling systems: Steady-state analysis. *ASME Journal of Applied Mechanics*, 62(4):908–914, 1995. DOI: 10.1115/1.2789031.

[18] X. Guan, M. S. High, and D. A. Tree. Viscoelastic effects in modeling web handling systems: Unsteady-state analysis. *ASME Journal of Applied Mechanics*, 65(1):234–241, 1998. DOI: 10.1115/1.2789031.

[19] E. G. Hauptmann and K. A. Cutshall. Dynamic mechanical properties of wet paper webs. *Tappi Journal*, 60(10):106 – 108, 1977.

[20] M. Johnson and T. Urbanik. A nonlinear theory for elastic plates with application to characterizing paper properties. *Journal of Applied Mechanics*, 51(3):146–152, 1984.

[21] H. Koivurova and E.-M. Salonen. Comments on non-linear formulations for travelling string and beam problems. *Journal of Sound and Vibration*, 225(5):845–856, 1999.

[22] M. Kurki. *Modeling of kinematical and rheological web line behavior in a papermaking environment*. Licentiate thesis, Lappeenranta University of Technology, Department of Mechanical Engineering, 2005. Lappeenranta, Finland.

[23] M. Kurki and A. Lehtinen. In-plane strain field theory for 2-d moving viscoelastic webs. In *Papermaking Research Symposium 2009 (Kuopio, Finland)*. PRS, 2009.

[24] M. Lai, D. Rubin, and E. Krempl. *Introduction to Continuum Mechanics*. Butterworth & Heinemann, third edition edition, 1999.

[25] U. Lee and H. Oh. Dynamics of an axially moving viscoelastic beam subject to axial tension. *International Journal of Solids and Structures*, 42(8):2381 – 2398, 2005.

[26] C. C. Lin. Stability and vibration characteristics of axially moving plates. *International Journal of Solids and Structures*, 34(24):3179–3190, 1997.

[27] C. C. Lin and C. D. Mote. Equilibrium displacement and stress distribution in a two-dimensional, axially moving web under transverse loading. *ASME Journal of Applied Mechanics*, 62:772–779, 1995.

[28] C. C. Lin and C. D. Mote. Eigenvalue solutions predicting the wrinkling of rectangular webs under non-linearly distributed edge loading. *Journal of Sound and Vibration*, 197(2):179–189, 1996.

[29] K. Marynowski and T. Kapitaniak. Kelvin-voigt versus bürgers internal damping in modeling of axially moving viscoelastic web. *International Journal of Non-Linear Mechanics*, 37(7):1147 – 1161, 2002. DOI: 10.1016/S0020-7462(01)00142-1.

[30] K. Marynowski and T. Kapitaniak. Zener internal damping in modelling of axially moving viscoelastic beam with time-dependent tension. *International Journal of Non-Linear Mechanics*, 42(1):118 – 131, 2007. DOI: 10.1016/j.ijnonlinmec.2006.09.006.

[31] W. L. Miranker. The wave equation in a medium in motion. *IBM Journal of Research and Development*, 4:36–42, 1960.

[32] E. M. Mockensturm and J. Guo. Nonlinear vibration of parametrically excited, viscoelastic, axially moving strings. *ASME Journal of Applied Mechanics*, 72(3):374–380, 2005. DOI: 10.1115/1.1827248.

[33] C. D. Mote. Divergence buckling of an edge-loaded axially moving band. *International Journal of Mechanical Sciences*, 10:281–195, 1968.

[34] C. D. Mote. Dynamic stability of axially moving materials. *Shock and Vibration Digest*, 4(4):2–11, 1972.

[35] C. D. Mote. Stability of systems transporting accelerating axially moving materials. *ASME Journal of Dynamic Systems, Measurement, and Control*, 97:96–98, 1975.

[36] H. Oh, J. Cho, and U. Lee. Spectral element analysis for an axially moving viscoelastic beam. *Journal of Mechanical Science and Technology*, 18(7):1159–1168, 2004. DOI: 10.1007/BF02983290.

[37] M. Pecht and M. Johnson. The strain response of paper under various constant regain states. *TAPPI Journal*, 68(1):90–93, 1985.

[38] A. Pramila. Sheet flutter and the interaction between sheet and air. *TAPPI Journal*, 69(7):70–74, 1986.

[39] Robertson. The physical properties of wet webs. *Svensk Papperstidning*, 66(1):477–497, 1963.

[40] R. A. Sack. Transverse oscillations in traveling strings. *British Journal of Applied Physics*, 5:224–226, 1954.

[41] I. B. Sanborn. A study of irreversible, stress-induced changes in the macrostructure of paper. *TAPPI Journal*, 45(6):465–474, 1962.

[42] Changho Shin, Wonsuk Kim, and Jintai Chung. Free in-plane vibration of an axially moving membrane. *Journal of Sound and Vibration*, 272(1–2):137–154, 2004.

[43] A. Simpson. Transverse modes and frequencies of beams translating between fixed end supports. *Journal of Mechanical Engineering Science*, 15:159–164, 1973.

[44] J. Skowronski and A. A. Robertson. A phenomenological study of the tensile deformation properties of paper. *Journal of Pulp and Paper Sciences*, 11(1):J21–J28, 1985.

[45] S. Smith and Stolle D. A comparison of eulerian and updated lagrangian finite element algorithms for simulating film casting. *Finite Elements in Analysis and Design*, 38:401–415, 2002.

[46] R. D. Swope and W. F. Ames. Vibrations of a moving threadline. *Journal of the Franklin Institute*, 275:36–55, 1963.

[47] J. C. Tannehill, D. A. Anderson, and R. H. Pletcher. *Computational Fluid Mechanics and Heat Transfer*. Series in Computational and Physical Processes in Mechanics and Thermal Sciences. Taylor & Francis, 2nd edition, 1997.

[48] J. L. Thorpe. Paper as an orthotropic thin plate. *TAPPI Journal*, 64(3):119–121, 1981.

[49] S. Timoshenko and J. Goodier. *Theory of Elasticity*. McGraw-Hill, second edition edition, 1951.

[50] T. Uesaka, K. Murakami, and R. Imamura. Two-dimensional linear viscoelasticity of paper. *Wood Science and Technology*, 14:131–142, 1980.

[51] A. G. Ulsoy and C. D. Mote. Vibration of wide band saw blades. *ASME Journal of Engineering for Industry*, 104:71–78, 1982.

[52] Xiao-Dong Yang, Wei Zhang, Li-Qun Chen, and Ming-Hui Yao. Dynamical analysis of axially moving plate by finite difference method. *Nonlinear Dynamics*, 67(2):997–1006, 2012.

[53] N.-H. Zhang and L.-Q. Chen. Nonlinear dynamical analysis of axially moving viscoelastic strings. *Chaos, Solitons & Fractals*, 24(4):1065 – 1074, 2005. DOI: 10.1016/j.chaos.2004.09.113.

[54] O. Zienkiewicz and R. Taylor. *The Finite Element Method Volume 1: The Basis*. Fifth edition edition, 2000.

PII

ON DISPLACEMENT-VELOCITY COUPLING AND THE ORIGIN OF IN-PLANE STRESSES IN ORTHOTROPIC MOVING CONTINUA

by

Matti Kurki, Juha Jeronen, Tytti Saksa and Tero Tuovinen 2014

Reports of the Department of Mathematical Information Technology Series B,
Scientific Computing, ISBN 978-951-39-5742-1, ISSN 1456-436X

Reports of the Department of Mathematical Information Technology
Series B. Scientific Computing
No. B 4/2014

On displacement-velocity coupling and the origin of in-plane stresses in orthotropic moving continua

Matti Kurki Juha Jeronen
Tytti Saksa Tero Tuovinen

University of Jyväskylä
Department of Mathematical Information Technology
P.O. Box 35 (Agora)
FI–40014 University of Jyväskylä
FINLAND
fax +358 14 260 2731
http://www.mit.jyu.fi/

ISBN 978-951-39-5742-1
ISSN 1456-436X

On displacement-velocity coupling and the origin of in-plane stresses in orthotropic moving continua*

Matti Kurki Juha Jeronen Tytti Saksa Tero Tuovinen

May 22, 2014

Abstract

In this paper, we address the problem of the origin of in-plane stresses in continuous, two-dimensional high-speed webs. In the case of thin, slender webs, a typical modeling approach is the application of a stationary in-plane model, without considering the effects of in-plane velocity field. However, for high-speed webs this approach is insufficient, because it neglects the coupling between the total material velocity and the deformation experienced by the material. By using a mixed Lagrange–Euler approach in model derivation, the solid continuum problem can be transformed to solid a continuum flow problem. Mass conservation in the flow problem, and the behaviour of free edges in the two-dimensional case, are both seen to influence the velocity field. We concentrate on the steady-state solutions of the model, and study briefly the coupled nature of material viscoelasticity and transport velocity in one dimension. Analytical solutions of the one-dimensional equation are presented with both elastic and viscoelastic material assumptions. Numerical solution of the two-dimensional elastic problem is also presented. Due to the nature of the velocity-dependent contraction, a nonlinear FEM solution procedure is used. The results indicate that inertial effects produce an additional contribution to elastic contraction in unsupported, free webs.

Keywords: axially moving, orthotropic, viscoelastic, elastic, one-dimensional, two-dimensional, free edges

1 Introduction

In the handling of continuous, high-speed webs the origin of in-plane stresses creates a scientific problem, which is not yet completely understood. Especially, the

*This research was supported by the Finnish Cultural Foundation.

type of the web material has a significant effect on both qualitative and quantitative characteristics of the in-plane stresses. Web tension in the moving continuous web systems can usually be controlled in the direction of the transport velocity, the tension being generated by a velocity difference between the starting and ending lines of the span. At high transport velocities, both web stress and web stability are of concern, not only in this longitudinal direction, but also in the direction perpendicular to the main transport velocity in the plane of the web.

Axially moving materials have many applications in industry, e.g. in paper production, and their mechanics have been studied widely. In the processing of different kinds of thin, laterally moving solid webs, challenges are met, such as the efficiency of production and effects caused by the high processing speed. The first studies of the vibrations of travelling elastic materials date back to the end of the 19th century (Skutch, 1897 [62]) and to the middle of the 20th century (Sack, 1954 [56]; Archibald and Emslie, 1958 [1]). A string model for the moving material was used in all of these studies. Later on, in the 1960s and 1970s, many researchers continued studies on moving strings and beams, concentrating mainly on various aspects of free and forced transverse vibrations (e.g. Miranker [45], Swope and Ames [65], Mote et. al. [47, 48, 49] and Simpson [60]).

The stability of small transverse vibrations of travelling two-dimensional rectangular membranes and plates have been studied by Ulsoy and Mote [70], and Lin [39]. When the web is advancing through a process without external support, the inertial forces depending on the web speed are coupled with web tension. Also the transverse behaviour of the web and the response of the fluid (air) surrounding the web are coupled (see e.g. [9, 53]). Studies modelling the moving web coupled with the surrounding air have been made by Pramila et al. [50, 54, 32]. In their studies, it was found that the surrounding air significantly reduces the eigenfrequencies and critical velocities of the web, when compared to the vacuum case. Chang and Moretti [9] studied membranes using potential flow theory, and Banichuk et al. [5, 6] used the flat panel model coupled with potential flow. This research was extended by Jeronen [30], where the eigenfrequency spectra were investigated for this model and for the moving string with damping. In Watanabe et al. [71], two different methods of analysis were developed for the phenomenon of paper flutter. One of these was a flutter simulation using a Navier–Stokes code, and the other method was based on a potential flow analysis of an oscillating thin airfoil.

Lin and Mote studied an axially moving membrane in a 2D formulation, predicting the equilibria of the displacement and the stress distribution under transverse loading [40]. Later, they continued studying the wrinkling of axially moving rectangular webs with a small flexural stiffness [41]. They predicted the critical value of the non-linear component of the edge loading after which the web wrinkles, and the corresponding wrinkled shape of the web. It is also known that the lack of web tension will result in a loss of stability of the moving web, which from the application viewpoint, disturbs the required smooth advancing of the web (see e.g. [4, 3]). On the other hand, high tension may cause web breaks, which deteriorates production efficiency (see e.g. [2, 55, 57, 61]).

Paper has often been modelled as an orthotropic elastic solid. Elastic constants have been measured for some paper-like materials by Mann, Baum and Habeger [42]; and Baum, Brennan and Habeger [7]. Recently, for anisotropic solids, Erkkilä et al. [17] have studied competent parameters based on modeled stress-strain curves for further construction of a material model. Out-of-plane Poisson ratios, specifically, have been recently studied by Stenberg and Fellers [64], who reported that paper is an auxetic material: stretching in the machine direction will cause the paper web to thicken in the out-of-plane direction. The relevant Poisson ratio, ν_{13}, is negative, and $|\nu_{13}|$ may be as large as 3.0. Incompressible and slightly compressible orthotropic and transversely isotropic materials have been investigated by Itskov and Aksel [29], who discovered nontrivial conditions that the elastic constants must satisfy in order to obtain incompressible or slightly compressible behaviour.

Considering wet paper material, the viscoelastic properties play an important role in the behaviour of the web, and thus, need to be included in the model. The first study on transverse vibration of travelling viscoelastic material was carried out by Fung et. al. using a string model [19]. Extending their work, they studied the viscous damping effect in their later research [20]. Viscoelastic strings and beams have recently been studied extensively, see e.g. [44, 73]. Oh et al. studied critical speeds, eigenvalues and natural modes of the transverse displacement of axially moving viscoelastic beams using the spectral element method [38, 51]. Chen and Zhao [14] presented a modified finite difference method to simplify a non-linear model of an axially moving string. They studied numerically the free transverse vibrations of both elastic and viscoelastic strings. Chen and Yang studied free vibrations of viscoelastic beams travelling between simple supports with torsion strings [13]. They studied the viscoelastic effect by perturbing the similar elastic problem and using the method of multiple scales. Very recently, Yang et al. studied vibrations, bifurcation, and chaos of axially moving viscoelastic plates using finite differences and a non-linear model for transverse displacements [72].

Marynowski and Kapitaniak studied differences between the Kelvin-Voigt and Burgers models in the modelling of the internal damping of axially moving viscoelastic beams. They found out that both models gave accurate results with small damping coefficients, but with a large damping coefficient, the Burgers model was more accurate [43]. In 2007, they compared the models with the Zener model studying the dynamic behaviour of an axially moving viscoelastic beam [44]. They found out that the Burgers and Zener models gave similar results for the critical transport speed whereas, the Kelvin-Voigt model gave a greater critical speed compared to the other two models.

The origin and structure of the in-plane stress and strain distribution in a moving solid web seems to be an exceptionally unknown area. The models used with web materials are often based on assumptions of isotropic or orthotropic material properties (see e.g. [7, 67]). The material is considered as viscoelastic or viscoplastic, but in the models, there is usually no coupling between the in-plane strain and the web velocity effects (see e.g. [23, 52, 69]).

Time-dependent, in-plane vibrations of a moving continuous membrane were

studied by Shin et al. [58]. In their work, in-plane vibration modes of an isotropic web were studied between the traction lines. Also Guan et. al. have studied viscoelastic web behaviour in both steady state and unsteady state cases [21, 22].

Traditionally, the partial time derivative has been used instead of the material derivative in the viscoelastic constitutive relations, but Mockensturm and Guo suggested that the material derivative should be used [46]. They studied non-linear vibrations and the dynamic response of axially moving viscoelastic strings. Kurki and Lehtinen also independently suggested that the material derivative should be used in the constitutive relations, in their study concerning the in-plane displacement field of a travelling viscoelastic plate [36, 34].

In a study by Chen et al., the material derivative was used in the viscoelastic constitutive relations [10]. They studied parametric vibration of axially accelerating viscoelastic strings. Chen and Ding studied the stability of axially accelerating viscoelastic beams using the method of multiple scales, and the material derivative was used in the viscoelastic constitutive relations [15]. Chen and Wang studied the stability of axially accelerating viscoelastic beams using asymptotic perturbation analysis and the material derivative in the viscoelastic relations [12]. The material derivative was also used in a recent paper by Chen and Ding, where the dynamic vibration response of axially moving viscoelastic beams was studied [11]. A non-linear model was used, taking into account the coupling of the transverse displacement with the longitudinal (in-plane) displacement. However, the transverse behaviour of the beam was their main focus.

In this paper, we propose to modify the classical two-dimensional model of a moving viscoelastic web by accounting for the coupling between the velocity field and the in-plane strain. A two-dimensional, thin open loop (non-conservative system) made of orthotropic membrane is stretched using a relative speed difference between the traction lines. The orthotropic viscoelastic material assumption is applied, using a viscoelastic model of the Kelvin–Voigt type. An originally Lagrange-based ”material” deformation formulation is used as the control volume, to which the mixed Lagrange-Euler-based ”spatial” formulation is then applied (see e.g. [66, 33]). With this method it is possible to handle solid, moving web behaviour using a control volume approach similar to the treatment of fluid flows. Preliminary one-dimensional studies have been reported in the paper [35]. In the present paper, the steady state of the two-dimensional moving continuum, in the pure elastic case, is solved using the nonlinear finite element method.

2 Strain generated by velocity difference of subsequent rollers

A continuous, moving web creates a flow continuum which is possible to consider as a solid medium experiencing flow. Due to its solid nature, the web continuum is always under a stress state, which is caused by a strain state, which further can be expressed in terms of the velocity difference between subsequent supporting rollers,

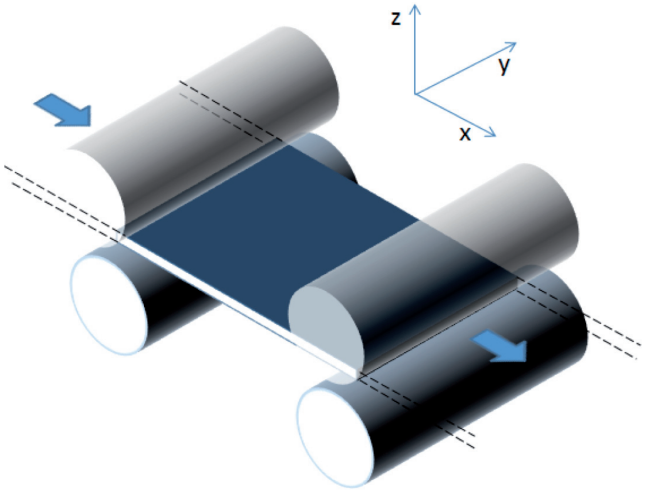

Figure 1: Schematic representation of the setup for modelling a moving viscoelastic web, stressed at the traction lines represented by the rollers. The arrows depict axial motion.

by the means of a mass conservation argument.

Consider an orthotropic material having initially (i.e. in the undeformed state) constant density ρ_0, undergoing steady-state longitudinal transport at velocity $\mathbf{U} = (U_x, 0, 0)$, depicted in Figure 1. Let us assume that the material axes 1, 2 and 3 are aligned with the global coordinate axes x, y and z, respectively. The continuity equation, as expressed in the Eulerian frame, is

$$\frac{\partial \rho}{\partial t} + \nabla \cdot (\rho \mathbf{U}) = 0 \,, \tag{1}$$

where ρ is density of the material, and $\partial/\partial t$ is the partial time derivative in the Eulerian frame. In a steady state, the equation reduces to

$$\nabla \cdot (\rho \mathbf{U}) = 0 \,. \tag{2}$$

Mass conservation requires that the flow rates at the incoming and outgoing flow control areas match; this requirement is readily obtained from equation (2). Let us consider a stationary control volume

$$\Omega = \{\, (x, y, z) : \, 0 < x < \ell \,, \; 0 < y < b \,, \; 0 < z < h \,\} \,,$$

where ℓ is the length of the span between the rollers, b is the width of the span, and h is the thickness of the sheet of material. Integrating equation (2) over the control volume Ω, applying the divergence theorem, and noting that ρ is a scalar, we have

$$\int_\Omega \nabla \cdot (\rho \mathbf{U}) \, \mathrm{d}\Omega = \int_{\partial\Omega} \rho \, (\mathbf{n} \cdot \mathbf{U}) \, \mathrm{d}\Gamma \,, \tag{3}$$

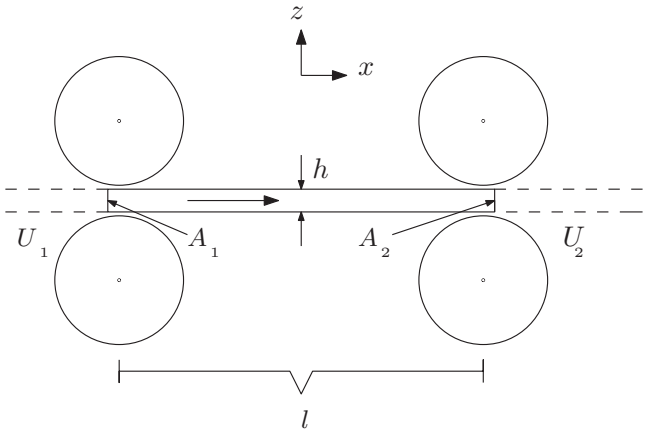

Figure 2: Solid web continuum flowing between the incoming and outgoing flow control areas (two-dimensional surfaces) A_1 and A_2, at longitudinal speeds U_1 and U_2 at the beginning and ending traction lines (respectively).

where $\partial\Omega$ is the closed surface delimiting the control volume Ω, and $\mathbf{n}$ represents outer unit normal vector. The differential $\mathrm{d}\Gamma$ refers to integration over a surface.

As is shown in Figure 2, flows in and out of the control volume occur only at the surfaces A_1 and A_2. Let us assume that ρ and $\mathbf{U}$ are constant across these in- and outflow surfaces, but that their values may change between these surfaces. In practice, there may exist small variations in the velocity at the outlet due to material straining, but for small strains and high velocity, constant velocity along these surfaces is a reasonable approximation.

Under these assumptions, the mass balance in the equation (3) becomes

$$-\rho_1 A_1 U_1 + \rho_2 A_2 U_2 = 0 \; . \tag{4}$$

The subscripts 1 and 2 for ρ and U refer to the (constant) values on the surfaces A_1 and A_2, respectively. Note the form of the velocity field, $\mathbf{U} = (U_x, 0, 0)$. Finally, it is convenient to rewrite (4) as

$$U_1 \, \frac{\rho_1 A_1}{\rho_2 A_2} - U_2 = 0 \; . \tag{5}$$

In order to manipulate equation (5) further, we must consider the ratios of the densities and the cross-sectional areas. When subjected to a small-displacement deformation $\mathbf{u} = (u, v, w)$, the volume V of a differential element initially (in the undeformed state) having volume V_0 becomes

$$V = V_0\big[1 + \nabla \cdot \mathbf{u}\big] \equiv V_0\big[1 + \varepsilon_x + \varepsilon_y + \varepsilon_z\big] \; , \tag{6}$$

as is known from the theory of elasticity. Here ε_x, ε_y and ε_z are the axial strains with respect to x, y and z -directions. Because the total mass M of the differential element

is conserved in the small deformation, it follows for the density ρ that

$$\rho \equiv \frac{M}{V} = \frac{1}{V_0}\,\frac{M}{V/V_0} = \frac{M}{V_0}\,\frac{1}{V/V_0} = \rho_0\big[1 + \varepsilon_x + \varepsilon_y + \varepsilon_z\big]^{-1} \,, \tag{7}$$

by (6) and the definition $\rho_0 \equiv M/V_0$.

Let us assume that the material is subjected to pure axial stress. This induces an axial strain ε_x, and via the Poisson effect, also the strains ε_y and ε_z in the two orthogonal directions:

$$\varepsilon_y = -\nu_{12}\varepsilon_x \,, \quad \varepsilon_z = -\nu_{13}\varepsilon_x \,, \tag{8}$$

where ν_{12} and ν_{13} are the (orthotropic) Poisson ratios for stretching in the direction of the material axis 1, describing the resulting contraction on material axes 2 and 3, respectively. This purely elastic approximation neglects all viscous effects, but since a steady state is being considered, this is reasonable. The cross-sectional area of the web is

$$A \;=\; (1+\varepsilon_z)h(1+\varepsilon_y)b \;\approx\; bh\,(\,1 + \varepsilon_y + \varepsilon_z\,) \,, \tag{9}$$

where second-order small terms have been neglected. Combining equations (8) and (9), we have

$$A = bh\,(\,1 - (\nu_{12} + \nu_{13})\varepsilon_x\,) \equiv bh\,(\,1 - \nu_{1A}\varepsilon_x\,) \,, \tag{10}$$

where the effective Poisson ratio for the change in cross-sectional area, when stretched along material axis 1, is defined as

$$\nu_{1A} \equiv \nu_{12} + \nu_{13} \,. \tag{11}$$

As was noted in the introduction, for paper materials, it is known (see e.g. the study by Stenberg and Fellers [64]) that $\nu_{13} < 0$, and that $|\nu_{13}|$ may be as large as 3.0. Typically, we will thus have $\nu_{1A} < 0$: the cross-sectional area may actually increase under tension, because the thickness increases. Even though the thickness itself is typically small, it may undergo a large relative change, and therefore must be considered when calculating the area of the cross-section.

It also follows from equations (6), (8) and (11) that

$$V = V_0\big[1 + (1 - \nu_{1A})\varepsilon_x\big] \,. \tag{12}$$

It should be pointed out that if for some particular material $\nu_{1A} = 1$, then $V = V_0$, and such a material behaves incompressibly when stretched along material axis 1. The effective Poisson ratio contains the directional Poisson ratios ν_{12} and ν_{13}. The only requirement for incompressibility under uniaxial stretching is that the sum of ν_{12} and ν_{13} is unity; unlike the isotropic case, neither of them needs to be 0.5.

Furthermore, the values of ν_{23}, ν_{21}, ν_{31} and ν_{32} still remain free. Elastic compatibility is required, but this brings in additional free parameters, because elastic compatibility involves not only the Poisson ratios, but also the Young moduli; e.g. $E_1\nu_{21} = E_2\nu_{12}$. Depending on the set of parameter values chosen, it is possible that an orthotropic material behaves incompressibly in axial stretching only when the deformation is applied along some particular axis.

It is thus evident that the conditions of incompressibility for anisotropic materials are more complicated than for isotropic materials, where the only requirement is $\nu = 0.5$. For a more thorough consideration of incompressibility in orthotropic and transversely isotropic materials, see the study by Itskov and Aksel [29].

By combining equations (7), (8) and (11), we obtain

$$\rho = \frac{\rho_0}{1 + (1 - \nu_{1A})\varepsilon_x} \, . \tag{13}$$

In the following, we shall assume that the material, subjected to constant axial tension at the rollers (traction lines), has zero strain at A_1, and experiences some nonzero axial strain ε_x at A_2, due to the applied axial stress. Preliminary one-dimensional results [35] indicate that such a strain state occurs at least for an axially travelling Kelvin–Voigt viscoelastic material; see also the treatment of the one-dimensional case further below, where we will show this briefly. By equation (10), the cross-sectional areas at the inflow and outflow surfaces A_1 and A_2 become

$$A_1 = bh \, , \qquad A_2 = bh(1 - \nu_{1A}\varepsilon_x) \, , \tag{14}$$

and by equation (13), the material densities on these surfaces are

$$\rho_1 = \rho_0 \, , \qquad \rho_2 = \frac{\rho_0}{1 + (1 - \nu_{1A})\varepsilon_x} \, . \tag{15}$$

By inserting equations (14) and (15) into the mass balance equation (5), simplifying, and solving for ε_x, we obtain the result

$$\varepsilon_x = \frac{\dfrac{U_2}{U_1} - 1}{1 + \left[\dfrac{U_2}{U_1} - 1\right] \nu_{1A}} \, . \tag{16}$$

Equation (16) gives the axial strain, at the traction line at $x = \ell$, for the problem of in-plane (visco-)elastic deformation, corresponding to given roller speeds U_1 and U_2. Obviously, in order for the model to remain valid, the given velocities must be such that the strain according to (16) remains in the small-deformation range.

The transport velocity of the flowing solid continuum in the above case is assumed to be controlled only in the x (longitudinal) direction; all in-plane deformations in the y (widthwise) direction are determined by the (visco-)elastic response. It should also be kept in mind that equation (16) only applies in a steady-state flow, i.e. when the web flows smoothly without time-dependent disturbances.

The traction lines at the cross-sectional areas A_1 and A_2 affect only the surfaces of the web, which implies that stress and strain waves advancing inside the web thickness can cross the traction lines. Therefore in the boundary conditions of moving continuous webs, in reality, one should consider rather complicated friction-based force transmission phenomena at web-roll contact areas [34].

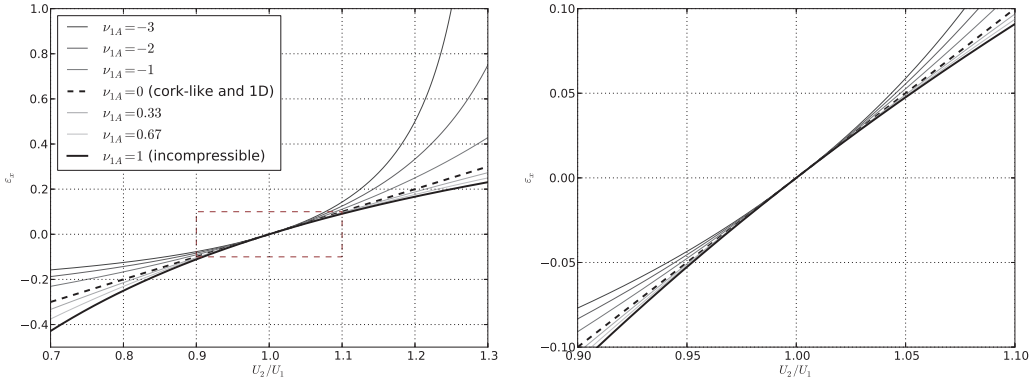

Figure 3: Roller-induced axial strain ε_x as a function of velocity ratio U_2/U_1, based on equations (16)–(18). *Left*: Overall behaviour of the functions, showing their curvature (only the line for $\nu_{1A} = 0$ is straight). *Right*: Zoomed-in view. Location of the zoomed area is shown by the dashed box in the left subfigure.

In the special case of a material which behaves incompressibly when stretched along axis 1, we have $\nu_{1A} = 1$. By inserting this into (16) and simplifying, we obtain

$$\varepsilon_x = 1 - \frac{U_1}{U_2} \,, \tag{17}$$

which holds only when $\nu_{1A} = 1$.

In the limit $\nu_{1A} \to 0$, equation (16) simplifies to

$$\varepsilon_x = \frac{U_2}{U_1} - 1 \,. \tag{18}$$

This corresponds to cork-like materials, which do not exhibit the Poisson effect. Note, however, that if the material is an auxetic orthotropic one, it is possible that $\nu_{13} = -\nu_{12}$, also leading to $\nu_{1A} = 0$.

The result (18) also arises in the case of a one-dimensional string model. Consider a compressible travelling string, undergoing steady-state flow through the span $0 < x < \ell$. Mass conservation now requires

$$R_1 U_1 - R_2 U_2 = 0 \,, \tag{19}$$

with similar definitions for the subscripts as above. Here R is the linear density, $[R] = \mathrm{kg/m}$, and the cross-sectional area of the string is assumed constant. As the string becomes stretched or compressed, the linear density changes as

$$R = \frac{R_0}{1 + \varepsilon_x} \,, \tag{20}$$

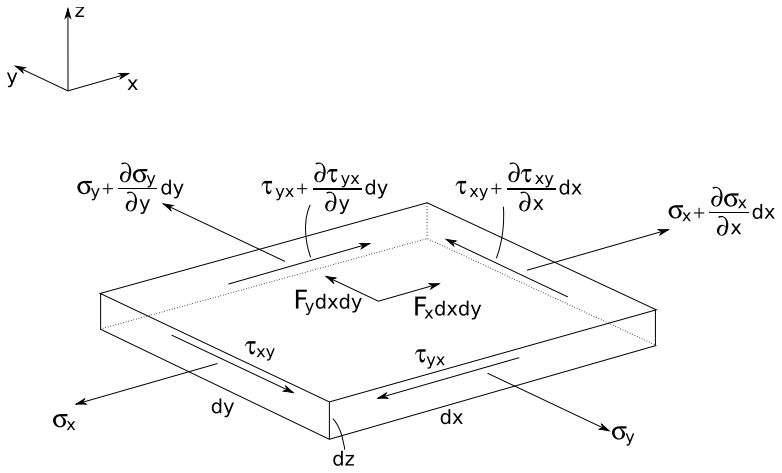

Figure 4: Differential parallelepiped and forces acting in the in-plane directions x and y.

where R_0 is the (constant) linear density in the initial (unstretched) state. Equation (20) follows directly from equation (7) and the assumption that the cross-sectional area is constant (whence $\varepsilon_y = \varepsilon_z = 0$).

As before, let as assume that at $x = 0$ the strain in the string is zero, and at $x = \ell$, the string experiences some nonzero strain ε_x due to axial tension applied at the ends of the span. As was noted above, this is consistent for a travelling Kelvin–Voigt viscoelastic string. Hence $R_1 = R_0$, and R_2 is given by equation (20). By combining equations (19) and (20), and solving for ε_x, the equation (18) is obtained.

The behaviour of equations (16)–(18) is illustrated in Figure 3.

3 The governing equations

In this section we will define the stresses and strains, deformations, material assumptions and velocity-dependent in-plane inertial forces for the moving web. This leads to both one- and two-dimensional models, and equations for the viscoelastic moving web continuum application.

The standard approach for describing structural deformations is the Lagrangean description. However, longitudinal in-plane deformations in axially moving materials are more challenging. One possibility is to actually move the medium at the desired speed, and update the boundary conditions at each timestep [63]. Another possibility is to use an 'Eulerian' flow description, and by this the actual deformation of the moving continuum can be handled using a mixed Lagrange–Euler description [33]. The Eulerian description is a standard approach in fluid dynamics where the observer is 'watching' a control volume, where possible deformations will appear [63, 37].

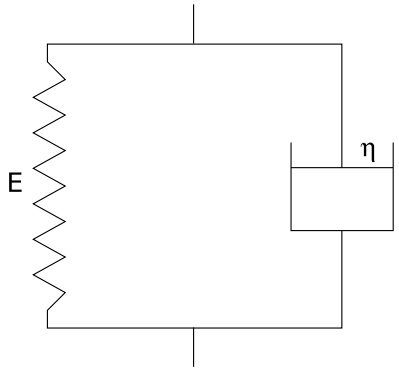

Figure 5: Schematic representation of the classical Kelvin-Voigt rheological model in one dimension. E is Young's modulus, η is the material viscosity.

In this paper, we consider two-dimensional in-plane membrane behaviour. Based on Figure 4, one can derive the following well-known force balance [68]:

$$\frac{\partial \sigma_x}{\partial x} + \frac{\partial \tau_{yx}}{\partial y} + F_x = 0 \,, \tag{21}$$

$$\frac{\partial \tau_{xy}}{\partial x} + \frac{\partial \sigma_y}{\partial y} + F_y = 0 \,, \tag{22}$$

where τ_{yx} and τ_{xy} are shear stresses and F_x and F_y are (external) body forces. The linear Cauchy strains are

$$\varepsilon_{xx} = \frac{\partial u}{\partial x} \,, \quad \varepsilon_{yy} = \frac{\partial v}{\partial y} \,, \quad \varepsilon_{xy} = \frac{\partial u}{\partial y} \,, \quad \varepsilon_{yx} = \frac{\partial v}{\partial x} \,, \quad \gamma_{xy} = \left(\frac{\partial u}{\partial y} + \frac{\partial v}{\partial x} \right) \,. \tag{23}$$

We will use the material assumption of orthotropic viscoelasticity. In the mixed Lagrange–Euler description, the strains

$$\varepsilon_{ij} = \varepsilon_{ij}\,(x, y, t) \tag{24}$$

lead to the time derivatives

$$\frac{\mathrm{d}\varepsilon_{ij}}{\mathrm{d}t} = \frac{\partial \varepsilon_{ij}}{\partial t} + \frac{\partial \varepsilon_{ij}}{\partial x}\frac{\mathrm{d}x}{\mathrm{d}t} + \frac{\partial \varepsilon_{ij}}{\partial y}\frac{\mathrm{d}y}{\mathrm{d}t} = \frac{\partial \varepsilon_{ij}}{\partial t} + \frac{\partial \varepsilon_{ij}}{\partial x}U_x + \frac{\partial \varepsilon_{ij}}{\partial y}U_y \,, \tag{25}$$

where (U_x, U_y) is the velocity field and $\mathrm{d}/\mathrm{d}t$ is the material derivative.

With fibrous, composite-type materials, the mechanical deformation response properties are the result of complicated material preprocessing, which results in orthotropic anisotropy and material time-dependence (see e.g. [69], [31], [52] and

[8]). It is possible to derive a vast number of different rheological models for time-dependent material behaviour, but the fundamental behaviour of continuous flow of a solid viscoelastic web can be analyzed using the simple Kelvin–Voigt model shown in Figure 5. The singular stress response to a step strain does not matter, because we are considering a steady state where no rapidly changing strains occur; hence the Kelvin–Voigt model is sufficient for the present application.

The stress-strain behaviour of one-dimensional Kelvin-Voigt material (see e.g. [18]) is simply

$$\sigma = \mathrm{E}\varepsilon + \eta\frac{\mathrm{d}\varepsilon}{\mathrm{dt}}\ , \tag{26}$$

where E is Young's modulus and η is the material viscosity. We will apply a two-dimensional, orthotropic plane stress extension of the above model, based on practical observations of fibrous web materials [67, 69]:

$$\sigma_x = \frac{E_x}{1-\nu_{12}\nu_{21}}\left(\varepsilon_{xx}+\nu_{21}\varepsilon_{yy}\right) + \frac{\eta_x}{1-\varphi_{12}\varphi_{21}}\left(\frac{\mathrm{d}\varepsilon_{xx}}{\mathrm{dt}}+\varphi_y\frac{\mathrm{d}\varepsilon_{yy}}{\mathrm{dt}}\right) \tag{27}$$

$$\sigma_y = \frac{E_y}{1-\nu_{12}\nu_{21}}\left(\varepsilon_{yy}+\nu_{12}\varepsilon_{xx}\right) + \frac{\eta_y}{1-\varphi_{12}\varphi_{21}}\left(\frac{\mathrm{d}\varepsilon_{yy}}{\mathrm{dt}}+\varphi_x\frac{\mathrm{d}\varepsilon_{xx}}{\mathrm{dt}}\right) \tag{28}$$

$$\tau_{yx} = \tau_{xy} = \mathrm{G}\gamma_{xy} + \Pi\frac{\mathrm{d}\gamma_{xy}}{\mathrm{dt}} \tag{29}$$

Here φ_{12} and φ_{21} are the viscous analogues of the orthotropic in-plane Poisson ratios ν_{12} and ν_{21}, G is a shear modulus, γ is a shear strain and Π is the viscous shear modulus.

Often, problems considering the in-plane behaviour of a continuous material are written using only an elastic model, involving the moduli of elasticity E_x and E_y, and the strain variables ε_{xx} and ε_{yy}. However, in practice all the elastic-related material properties are measured with some definite speed, and therefore apparent elasticity includes both elastic and viscous material properties [18]. Fundamentally, all materials exhibit some form of viscoelasticity, typically measured by normal and complex moduli E and E', respectively. It should also be pointed out that the viscoelastic Poisson ratios φ_{12} and φ_{21} cannot be calculated using compliances from the theory of elasticity [24].

The force balance equations (21) and (22) include also the body forces F_x and F_y, which are important especially with fibrous cellulose-based materials. Moisture-dependent dimension changes can be significant, which generates stresses in addition to those related to the strains based on external velocity differences (equation (16)).

Next, let us consider the dynamic equilibrium. According to Newton's second law, time-dependent dynamical behaviour always includes inertial forces. Two-dimensional inertial forces in in-plane membrane behaviour can be accounted for

using the following dynamic equilibrium equations (see e.g. [59]):

$$\frac{\partial \sigma_x}{\partial x} + \frac{\partial \tau_{xy}}{\partial y} + F_x = \rho \frac{\mathrm{d}^2 u}{\mathrm{d}t^2} \tag{30}$$

$$\frac{\partial \sigma_y}{\partial y} + \frac{\partial \tau_{yx}}{\partial x} + F_y = \rho \frac{\mathrm{d}^2 v}{\mathrm{d}t^2} \tag{31}$$

Note that the operator $\mathrm{d}^2/\mathrm{d}t^2$ describes the inertial behaviour in the Lagrangean reference frame. Thus the inertial terms depending on the displacements u and v, in the Eulerian frame, must be presented using the material derivative:

$$\frac{\mathrm{d}u}{\mathrm{d}t} = \frac{\partial u}{\partial t} + \sum_{i=1,2} \frac{\partial u}{\partial x_i} \frac{\mathrm{d}x_i}{\mathrm{d}t} \tag{32}$$

$$\frac{\mathrm{d}v}{\mathrm{d}t} = \frac{\partial v}{\partial t} + \sum_{i=1,2} \frac{\partial v}{\partial x_i} \frac{\mathrm{d}x_i}{\mathrm{d}t} \tag{33}$$

The second material derivatives of the displacements u and v are

$$\begin{aligned} \frac{\mathrm{d}^2 u}{\mathrm{d}t^2} = {} & \frac{\partial^2 u}{\partial t^2} + 2U_x \frac{\partial^2 u}{\partial x \partial t} + 2U_y \frac{\partial^2 u}{\partial y \partial t} + U_x^2 \frac{\partial^2 u}{\partial x^2} + 2U_x U_y \frac{\partial^2 u}{\partial x \partial y} + U_y^2 \frac{\partial^2 u}{\partial y^2} \\ & + \frac{\partial u}{\partial x} \left(\frac{\partial U_x}{\partial x} U_x + \frac{\partial U_x}{\partial y} U_y + \frac{\partial U_x}{\partial t} \right) + \frac{\partial u}{\partial y} \left(\frac{\partial U_y}{\partial x} U_x + \frac{\partial U_y}{\partial y} U_y + \frac{\partial U_y}{\partial t} \right) \end{aligned} \tag{34}$$

$$\begin{aligned} \frac{\mathrm{d}^2 v}{\mathrm{d}t^2} = {} & \frac{\partial^2 v}{\partial t^2} + 2U_x \frac{\partial^2 v}{\partial x \partial t} + 2U_y \frac{\partial^2 v}{\partial y \partial t} + U_x^2 \frac{\partial^2 v}{\partial x^2} + 2U_x U_y \frac{\partial^2 v}{\partial x \partial y} + U_y^2 \frac{\partial^2 v}{\partial y^2} \\ & + \frac{\partial v}{\partial x} \left(\frac{\partial U_x}{\partial x} U_x + \frac{\partial U_x}{\partial y} U_y + \frac{\partial U_x}{\partial t} \right) + \frac{\partial v}{\partial y} \left(\frac{\partial U_y}{\partial x} U_x + \frac{\partial U_y}{\partial y} U_y + \frac{\partial U_y}{\partial t} \right) \end{aligned} \tag{35}$$

By substituting the equations (34) – (35) and (27) – (29) into the equations (30) and (31), we obtain the following time-dependent two-dimensional equations for the in-plane, plane stress membrane behaviour of the moving viscoelastic web:

$$\begin{aligned} & \left(C_{11} - \rho U_x^2\right) \frac{\partial^2 u}{\partial x^2} + \left(C_{66} - \rho U_y^2\right) \frac{\partial^2 u}{\partial y^2} + C_{12} \frac{\partial^2 v}{\partial x \partial y} + C_{66} \frac{\partial^2 v}{\partial x \partial y} + K_{11} U_x \frac{\partial^3 u}{\partial x^3} \\ & + K_{11} U_y \frac{\partial^3 u}{\partial x^2 \partial y} + K_{11} \frac{\partial^3 u}{\partial x^2 \partial t} + \left(K_{12} + K_{66}\right) U_y \frac{\partial^3 v}{\partial x \partial y^2} + K_{66} U_y \frac{\partial^3 u}{\partial y^3} \\ & + \left(K_{12} + K_{66}\right) U_x \frac{\partial^3 v}{\partial x^2 \partial y} + \left(K_{12} + K_{66}\right) \frac{\partial^3 v}{\partial x \partial y \partial t} + K_{66} U_x \frac{\partial^3 u}{\partial x \partial y^2} + K_{66} \frac{\partial^3 u}{\partial y^2 \partial t} + F_x \\ = {} & \rho \frac{\partial^2 u}{\partial t^2} + 2\rho U_x U_y \frac{\partial^2 u}{\partial x \partial y} + 2\rho U_x \frac{\partial^2 u}{\partial x \partial t} + 2\rho U_y \frac{\partial^2 u}{\partial y \partial t} \\ & + \rho \frac{\partial u}{\partial y} \left(\frac{\partial U_x}{\partial x} U_x + \frac{\partial U_x}{\partial y} U_y + \frac{\partial U_x}{\partial t} \right) + \rho \frac{\partial u}{\partial y} \left(\frac{\partial U_y}{\partial x} U_x + \frac{\partial U_y}{\partial y} U_y + \frac{\partial U_y}{\partial t} \right) \end{aligned} \tag{36}$$

and

$$\begin{aligned}
&\left(C_{22}-\rho U_y^2\right)\frac{\partial^2 v}{\partial y^2}+\left(C_{66}-\rho U_x^2\right)\frac{\partial^2 v}{\partial x^2}+C_{21}\frac{\partial^2 u}{\partial x\partial y}+C_{66}\frac{\partial^2 v}{\partial x\partial y}+K_{22}U_y\frac{\partial^3 v}{\partial y^3}\\
&+K_{22}U_x\frac{\partial^3 v}{\partial x\partial y}^{\,2}+K_{22}\frac{\partial^3 v}{\partial x^2\partial t}+\left(K_{21}+K_{66}\right)U_x\frac{\partial^3 u}{\partial x^2\partial y}+K_{66}U_x\frac{\partial^3 v}{\partial x^3}\\
&+\left(K_{21}+K_{66}\right)U_y\frac{\partial^3 u}{\partial x\partial y^2}+\left(K_{21}+K_{66}\right)\frac{\partial^3 u}{\partial x\partial y\partial t}+K_{66}U_y\frac{\partial^3 v}{\partial x^2\partial y}+K_{66}\frac{\partial^3 v}{\partial y^2\partial t}+F_y\\
&=\quad \rho\frac{\partial^2 v}{\partial t^2}+2\rho U_xU_y\frac{\partial^2 v}{\partial x\partial y}+2\rho U_x\frac{\partial^2 v}{\partial x\partial t}+2\rho U_y\frac{\partial^2 v}{\partial y\partial t}\\
&+\rho\frac{\partial v}{\partial x}\left(\frac{\partial U_x}{\partial x}U_x+\frac{\partial U_x}{\partial y}U_y+\frac{\partial U_x}{\partial t}\right)+\rho\frac{\partial v}{\partial y}\left(\frac{\partial U_y}{\partial x}U_x+\frac{\partial U_y}{\partial y}U_y+\frac{\partial U_y}{\partial t}\right)\,,
\end{aligned}\tag{37}$$

where the coefficients are

$$C_{11}=\frac{E_x}{1-\nu_{12}\nu_{21}}\,,\qquad C_{22}=\frac{E_y}{1-\nu_{12}\nu_{21}}\,,\tag{38}$$

$$C_{12}=C_{11}\nu_{21}=C_{22}\nu_{12}=C_{21}\,,\qquad C_{66}=G\,,\tag{39}$$

$$K_{11}=\frac{\eta_x}{1-\varphi_{12}\varphi_{21}}\,,\qquad K_{22}=\frac{\eta_y}{1-\varphi_{12}\varphi_{21}}\,,\tag{40}$$

$$K_{12}=K_{11}\varphi_{21}=K_{22}\varphi_{12}=K_{21}\,,\quad K_{66}=\Pi\,.\tag{41}$$

The equations (36) and (37) are nonlinear. Nonlinearity appears in the velocities U_x and U_y, which are dependent on the deformation. There are also nonlinear Navier–Stokes type convection terms, the significance of which is small if the strains defined in the equation (23) can be considered small.

4 Steady state of one-dimensional viscoelastic moving continuum

One-dimensional application of the equations (36) and (37) will lead to the following time-dependent solid continuum flow equation [35]:

$$\begin{aligned}
&\rho\frac{\partial^2 u}{\partial t^2}+2\rho U_x\frac{\partial^2 u}{\partial x\partial t}+\rho U_x^2\frac{\partial^2 u}{\partial x^2}+\rho\frac{\partial u}{\partial x}\left(\frac{\partial U_x}{\partial x}U_x+\frac{\partial U_x}{\partial t}\right)\\
&\qquad=E_x\frac{\partial^2 u}{\partial x^2}+\eta_x\left(\frac{\partial^3 u}{\partial x^2\partial t}+U_x\frac{\partial^3 u}{\partial x^3}\right)
\end{aligned}\tag{42}$$

In a steady state, where there is no time-dependent fluctuation in the displacement, we can write the following equation for ideal, undisturbed axial narrow web flow:

$$\eta_x U_x \frac{\partial^3 u}{\partial x^3} + \left(E_x - \rho U_x^2\right) \frac{\partial^2 u}{\partial x^2} - \rho \frac{\partial u}{\partial x} \left(\frac{\partial U_x}{\partial x} U_x \right) = 0 \ . \tag{43}$$

In general, equation (43) is nonlinear due to the dependence of U_x on $\partial u/\partial x$. To see how this arises in the one-dimensional case, recall equation (16) and its one-dimensional specialization (18), which were obtained via a mass conservation argument. There are now two possibilities. The strain $\varepsilon_{xx} = \partial u/\partial x$ (equation (23)) either depends on x, or is constant along the span.

Let us first investigate the case where the strain depends on x. This was a starting assumption in the derivation of (18); if it holds, then also (18) holds. Let the velocity U_1 at the beginning of the span be fixed. By rearranging, (18) becomes

$$U_2 = U_1[1 + \varepsilon_{xx}] \ , \tag{44}$$

where we now use the notation ε_{xx} for the strain.

Because mass conservation must hold for any value of x, equation (44) is valid along the whole span, and we have $U_x(x) = U_2(x)$. However, because $\varepsilon_{xx} = \varepsilon_{xx}(x) = (\partial u/\partial x)(x)$ appears on the right-hand side of (44), actually $U_2 = U_2(\varepsilon_{xx})$. Thus, if the strain varies along the span, mass conservation implies that a linear relationship exists between the strain and velocity fields.

Because U_x is now a linear function of ε_{xx}, all terms of (43) involving factors of U_x and its derivatives become nonlinear with respect to the unknown u and its derivatives. Using U_2 from (44) as U_x in (43), we see that the nonlinearity is of a polynomial form; up to cubic terms are present. Numerical FEM solution of the nonlinear equation has been presented in [35].

The other possibility is that the strain is a constant along the whole span, in which case the starting assumption leading to (18) does not hold. On the other hand, a constant value for $\varepsilon_{xx} = \partial u/\partial x$ implies $\partial^2 u/\partial x^2 = \partial^3 u/\partial x^3 \equiv 0$. Let us investigate the nontrivial case where $\varepsilon_{xx} \neq 0$. The first and second terms in equation (43) vanish. Dividing by the nonzero constant strain $\partial u/\partial x$ and the material density $\rho \neq 0$, all that remains is

$$\frac{\partial U_x}{\partial x} U_x = 0 \ . \tag{45}$$

Equation (45) must hold pointwise at any x. Thus for each fixed x, either $\partial U_x/\partial x = 0$ or $U_x = 0$. More interesting of the two is $\partial U_x/\partial x = 0$, which leads to $U_x =$ constant.

We conclude that if a constant strain is observed, this implies that the velocity must also be constant. However, the reverse is not true, as we will see below. The value of the constant strain is determined by the boundary conditions, which were not analyzed here.

For the rest of this section, we again let ε_{xx} vary along the span, concentrating on the special case where U_x is approximately constant:

$$U_x(x) = U_0 + \phi(x) \ . \tag{46}$$

Here U_0 is a constant, and the arbitrary function $\phi(x)$ and its derivatives are considered small. If the strain variable and its derivatives are small, and the velocity field is of the form (44), this representation is applicable. Inserting (46) into (43) and dropping second-order small terms leads to a linear equation, namely

$$\eta_x U_0 \frac{\partial^2 \varepsilon_{xx}}{\partial x^2} + \left(E_x - \rho U_0^2\right) \frac{\partial \varepsilon_{xx}}{\partial x} = 0 \ . \tag{47}$$

To obtain this form, it is not sufficient that ϕ itself is small; also $\partial\phi/\partial x$ must be small to avoid an additional term $-\rho\varepsilon_{xx}[\partial\phi/\partial x]U_0$ on the left-hand side. Observe that equation (47) is exact in the case where U_x is (an exact) constant. Thus any conclusions will apply to cases with exactly constant as well as approximately constant transport velocities.

By comparing the equation (47) and the heat equation in presence of convection (see e.g. [66]):

$$k_T \frac{\partial^2 T}{\partial x^2} - \rho c_p U \frac{\partial T}{\partial x} = 0 \ , \tag{48}$$

where T is the temperature and U is the velocity of the medium, c_p is the specific heat of the object and k_T the heat diffusion coefficient, one can observe great similarity between the two.

The equation (47) can be solved using analytical methods. First, as a special case, if only pure elasticity is present ($\eta_x = 0$), the solution is of the form [35]

$$\left(E_x - \rho U_0^2\right) \varepsilon_{xx} = C \ . \tag{49}$$

In this case the solution describes Hookean behaviour, i.e., the strain ε_{xx} is constant along the whole span regardless of the magnitude of the constant transport velocity U_0. The corresponding stress field, from equation (26) with $\eta_x = 0$ and (49), is also constant:

$$\sigma_x = E_x \varepsilon_{xx} = \frac{E_x C}{(E_x - \rho U_0^2)} \equiv C' \ . \tag{50}$$

The values of the constants C and C' are determined by the boundary conditions. Because (49) is a first-order ordinary differential equation with respect to ε_{xx}, for this variable we may set only one boundary condition. Choosing this boundary condition as $\varepsilon_{xx}(\ell) = \varepsilon_T$, from (49) we have $C = (E_x - \rho U_0^2)\,\varepsilon_T$, which leads to $\varepsilon_{xx}(x) = \varepsilon_T$ (for all x), and for the stress $\sigma_x = E_x \varepsilon_T$. This may seem trivial, but it provides an important point of comparison for the following case.

Consider a material with viscosity $\eta_x \neq 0$. Equation (47) becomes, after division by $\eta_x U_0$,

$$\frac{\partial^2 \varepsilon_{xx}}{\partial x^2} + \left(\frac{E_x - \rho U_0^2}{\eta_x U_0}\right) \frac{\partial \varepsilon_{xx}}{\partial x} = 0 \ . \tag{51}$$

The differential equation is of the second order in ε_{xx}, hence two boundary conditions are required. With the choices $\varepsilon_{xx}(0) = 0$ and $\varepsilon_{xx}(\ell) = \varepsilon_T$, the analytical solution of the equation (51) is [34, 36]:

$$\varepsilon_{xx}(x) = \varepsilon_T \frac{1 - e^{-kx}}{1 - e^{-k\ell}} \ , \qquad \text{where} \quad k = \frac{E_x - \rho U_0^2}{\eta_x U_0} \ . \tag{52}$$

We have thus obtained the following result: for a Kelvin–Voigt viscoelastic material moving at a constant or an approximately constant transport velocity, loaded only by a prescribed strain at the ends of the span, the strain grows logarithmically along the span. This is unlike the case of purely elastic material, where the strain along the span is constant.

As $x \to \ell$, the strain approaches the same value it had in the elastic case, ε_T. Additionally, if ℓ is large, the exponential terms approximately vanish in most of the domain, and the strain approximately obtains its elastic value everywhere except in a short boundary layer at the start of the span. The larger k is, the shorter is the boundary layer. Especially, the boundary layer vanishes in the limits $\eta_x \to 0$ and $U_0 \to 0$, where $k \to \infty$ (see definition of k in equation (52)). This agrees with the elastic solution.

The physical conclusion is that the strain ε_{xx} depends on x only if both the viscosity η_x and the transport velocity U_0 are nonzero. In other words, in the context of this analysis, the effect appears only if the material is both viscoelastic and subjected to axial motion.

Finally, let us find the corresponding stress field. The stress, which is based on the strain in the equation (52), is a superposition of elastic and viscous stress components ([35]; see also equation (26)):

$$\sigma_x = E_x \varepsilon_{xx} + \eta_x \frac{\mathrm{d}\varepsilon_{xx}}{\mathrm{d}t} \, . \tag{53}$$

Straightforward analytical solution of the stress is easy to obtain only in the linearized, one-dimensional, steady-state case having constant transport velocity [35]. Using equations (24) and (25), the time derivative of the strain, in mixed Lagrange–Euler form, can be written for the steady-state solution as follows:

$$\frac{\mathrm{d}\varepsilon_{xx}}{\mathrm{d}t} = \frac{\partial \varepsilon_{xx}}{\partial x} U_x \, . \tag{54}$$

Inserting (54) into (53), using (46) for U_x, noting that both $\partial \varepsilon_{xx}/\partial x$ and $\phi(x)$ are small, and then using the analytical solution (52), we obtain the stress field as

$$\sigma_x = E_x \varepsilon_T \frac{1 - e^{-kx}}{1 - e^{-k\ell}} + \eta_x U_0 \varepsilon_T \frac{k e^{-kx}}{1 - e^{-k\ell}} \, . \tag{55}$$

where the elastic and viscous contributions are apparent. Both contributions follow a logarithmic curve. By expanding the multiplicative factor k in the second term of the equation (55) (using again (52)), the result simplifies to

$$\sigma_x = \frac{\varepsilon_T}{1 - e^{-k\ell}} \left(E_x - \rho U_0^2 e^{-kx} \right) , \tag{56}$$

which shows the total stress more clearly. Equation (56) is valid for $\eta_x \neq 0$, $U_0 \neq 0$. We observe that also the total stress follows a logarithmic curve.

Unlike the strain, the stress remains always slightly smaller than its elastic value $E_x \varepsilon_T$, even near the end of the span as $x \to \ell$. Physically, this observation can be interpreted as a viscous relaxation effect.

For large ℓ, the exponentials again approximately vanish in most of the domain, and the stress approximately obtains its elastic value, except in a short boundary layer at the start of the span. The previous observations regarding k apply also here.

We have thus seen that for a narrow strip of Kelvin–Voigt material moving at a constant or an approximately constant transport velocity, both the strain and stress fields follow a logarithmic shape along the span. This effect appears only if the material is both viscoelastic and subjected to axial motion.

5 The weak form and the natural boundary conditions

In the following, we will concentrate on the two-dimensional, steady-state, purely elastic case. This is obtained from the equations (36) – (37) by omitting time-dependent terms and setting the viscous coefficients to zero.

The aim in the rest of this paper is to numerically study the two-dimensional, orthotropic, elastic moving continuum plane stress problem using the finite element method (FEM). The above approach was extremely useful for the one-dimensional analysis that was performed, but it is difficult to correctly derive the weak form by starting from the equations (36) – (37).

The difficulty arises because the equations contain terms with mixed derivatives, $\partial^2 u/\partial x \partial y$ and $\partial^2 v/\partial x \partial y$. It is not immediately clear how these terms should be considered when applying integration by parts in the component-form equations. Each such mixed term can be integrated by parts in either the x or the y direction, and each such choice will produce different contributions to the natural boundary conditions of the weak problem. Most combinations of choices lead to boundary conditions which make no physical sense, and the correct combination of choices is not obvious.

Hence, we will derive the weak form in cartesian tensor notation. Although in the present study only a rectangular sheet will be studied, this approach provides the additional advantage of arbitrary domain shape. We start with the general dynamic equilibrium equations (30) – (31), rewritten in tensor notation, and then expand the second material derivative. The dynamic equilibrium reads

$$\rho \frac{\mathrm{d}^2 \mathbf{u}}{\mathrm{d}t^2} - \nabla \cdot \boldsymbol{\sigma}^{\mathrm{T}} = \mathbf{F} \,, \tag{57}$$

where $(\dots)^{\mathrm{T}}$ denotes the transpose of a rank-2 tensor. In the case where $\mathbf{U}$ is not time-dependent, the second material derivative expands as

$$\frac{\mathrm{d}^2 \mathbf{u}}{\mathrm{d}t^2} = \frac{\mathrm{d}}{\mathrm{d}t}\left(\frac{\partial \mathbf{u}}{\partial t} + \mathbf{U} \cdot \nabla \mathbf{u}\right) = \frac{\partial^2 \mathbf{u}}{\partial t^2} + 2\mathbf{U} \cdot \nabla \left(\frac{\partial \mathbf{u}}{\partial t}\right) + (\mathbf{U} \cdot \nabla)(\mathbf{U} \cdot \nabla \mathbf{u}) \,. \tag{58}$$

Applying (58), the steady-state form of equation (57) becomes

$$\rho \, (\mathbf{U} \cdot \nabla)(\mathbf{U} \cdot \nabla \mathbf{u}) - \nabla \cdot \boldsymbol{\sigma}^{\mathrm{T}} = \mathbf{F} \,. \tag{59}$$

Next, we will use the principle of virtual work. Let us take the dot product of the equation (59) with a vector-valued test function (virtual displacement) $\boldsymbol{\phi}$, and integrate the equation over the two-dimensional domain

$$\Omega \equiv \{\, (x, y) :\ 0 < x < \ell\,,\ 0 < y < b \,\}\ . \tag{60}$$

We assume that the material density ρ can be approximated as a constant and obtain

$$\rho \int_\Omega \boldsymbol{\phi} \cdot (\mathbf{U} \cdot \nabla)(\mathbf{U} \cdot \nabla \mathbf{u})\ \mathrm{d}\Omega - \int_\Omega \boldsymbol{\phi} \cdot [\nabla \cdot \boldsymbol{\sigma}^{\mathrm{T}}]\ \mathrm{d}\Omega = \int_\Omega \boldsymbol{\phi} \cdot \mathbf{F}\ \mathrm{d}\Omega\ . \tag{61}$$

In order to integrate by parts in the equation (61), we make use of the following two identities:

$$\int_\Omega \boldsymbol{\phi} \cdot [\nabla \cdot \boldsymbol{\sigma}^{\mathrm{T}}]\ \mathrm{d}\Omega = \int_{\partial\Omega} \boldsymbol{\phi} \cdot (\mathbf{n} \cdot \boldsymbol{\sigma}^{\mathrm{T}})\ \mathrm{d}\Gamma - \int_\Omega \nabla\boldsymbol{\phi} : \boldsymbol{\sigma}\ \mathrm{d}\Omega\ , \tag{62}$$

$$\begin{aligned} \int_\Omega \boldsymbol{\phi} \cdot (\mathbf{U} \cdot \nabla)(\mathbf{U} \cdot \nabla \mathbf{u}) &= \int_{\partial\Omega} \mathbf{n} \cdot [(\mathbf{U} \cdot \nabla \mathbf{u}) \cdot (\boldsymbol{\phi} \otimes \mathbf{U})]\ \mathrm{d}\Gamma \\ &\quad - \int_\Omega (\mathbf{U} \cdot \nabla \mathbf{u}) \cdot [\nabla \cdot (\mathbf{U} \otimes \boldsymbol{\phi})]\ \mathrm{d}\Omega\ . \end{aligned} \tag{63}$$

where $\mathbf{n}$ is the outer unit normal, and the notational conventions are

$$(\nabla \mathbf{a})_{ij} \equiv \partial_i a_j\ , \quad (\nabla \cdot \mathbf{A})_j \equiv \partial_i A_{ij} \quad (\mathbf{a} \otimes \mathbf{b})_{ij} = a_i b_j\ , \quad \mathbf{A} : \mathbf{B} \equiv A_{ij} B_{ji}\ . \tag{64}$$

Here $\mathbf{a}$ and $\mathbf{b}$ are vectors, and $\mathbf{A}$ and $\mathbf{B}$ are rank-2 tensors. The summation convention for repeated indices applies. Note the ordering of indices in the gradient.

The integration-by-parts formula (62) is standard in the theory of elasticity; only the formula (63) requires explanation. Observe that for any differentiable vector fields $\mathbf{a}$, $\mathbf{b}$ and $\mathbf{c}$,

$$\nabla \cdot (\mathbf{a} \cdot (\mathbf{b} \otimes \mathbf{c})) = \mathbf{b} \cdot (\mathbf{c} \cdot \nabla \mathbf{a}) + \mathbf{a} \cdot (\nabla \cdot (\mathbf{c} \otimes \mathbf{b}))\ . \tag{65}$$

By integrating the equation (65) over the domain Ω, applying the divergence theorem to the left-hand side, and choosing $\mathbf{a} = (\mathbf{U} \cdot \nabla \mathbf{u})$, $\mathbf{b} = \boldsymbol{\phi}$, and $\mathbf{c} = \mathbf{U}$, relation (63) follows.

Using equations (62) and (63) in (61), we obtain

$$\begin{aligned} &- \rho \int_\Omega (\mathbf{U} \cdot \nabla \mathbf{u}) \cdot [\nabla \cdot (\mathbf{U} \otimes \boldsymbol{\phi})]\ \mathrm{d}\Omega + \int_\Omega \nabla\boldsymbol{\phi} : \boldsymbol{\sigma}\ \mathrm{d}\Omega \\ &+ \rho \int_{\partial\Omega} \mathbf{n} \cdot [(\mathbf{U} \cdot \nabla \mathbf{u}) \cdot (\boldsymbol{\phi} \otimes \mathbf{U})]\ \mathrm{d}\Gamma - \int_{\partial\Omega} \boldsymbol{\phi} \cdot (\mathbf{n} \cdot \boldsymbol{\sigma}^{\mathrm{T}})\ \mathrm{d}\Gamma = \int_\Omega \boldsymbol{\phi} \cdot \mathbf{F}\ \mathrm{d}\Omega\ . \end{aligned} \tag{66}$$

By using the identity

$$\nabla \cdot (\mathbf{U} \otimes \boldsymbol{\phi}) = (\nabla \cdot \mathbf{U})\boldsymbol{\phi} + \mathbf{U} \cdot \nabla\boldsymbol{\phi} \tag{67}$$

and rearranging

$$\boldsymbol{\phi} \cdot (\mathbf{n} \cdot \boldsymbol{\sigma}^{\mathrm{T}}) = (\mathbf{n} \cdot \boldsymbol{\sigma}^{\mathrm{T}}) \cdot \boldsymbol{\phi} = \mathbf{n} \cdot (\boldsymbol{\sigma}^{\mathrm{T}} \cdot \boldsymbol{\phi})\ , \tag{68}$$

we have

$$
\begin{aligned}
&-\rho\int_\Omega(\mathbf{U}\cdot\nabla\mathbf{u})\cdot[(\nabla\cdot\mathbf{U})\boldsymbol{\phi}+\mathbf{U}\cdot\nabla\boldsymbol{\phi}]\,\mathrm{d}\Omega+\int_\Omega\nabla\boldsymbol{\phi}:\boldsymbol{\sigma}\,\mathrm{d}\Omega\\
&+\int_{\partial\Omega}\mathbf{n}\cdot\left[\rho\,(\mathbf{U}\cdot\nabla\mathbf{u})\cdot(\boldsymbol{\phi}\otimes\mathbf{U})-\boldsymbol{\sigma}^{\mathrm{T}}\cdot\boldsymbol{\phi}\right]\mathrm{d}\Gamma=\int_\Omega\boldsymbol{\phi}\cdot\mathbf{F}\,\mathrm{d}\Omega\,. \qquad (69)
\end{aligned}
$$

We may simplify (69) with

$$
(\mathbf{U}\cdot\nabla\boldsymbol{\phi})\cdot(\mathbf{U}\cdot\nabla\mathbf{u})=U_i(\partial_i\phi_j)U_k(\partial_k u_j)=(\partial_i\phi_j)(U_iU_k\partial_k u_j)=\nabla\boldsymbol{\phi}:\big(\mathbf{U}\otimes\mathbf{U}\cdot\nabla\mathbf{u}\big)^{\mathrm{T}}\,, \qquad (70)
$$

which allows us to combine some terms on the first line:

$$
\begin{aligned}
&-\rho\int_\Omega\boldsymbol{\phi}\cdot(\mathbf{U}\cdot\nabla\mathbf{u})(\nabla\cdot\mathbf{U})\,\mathrm{d}\Omega+\int_\Omega\nabla\boldsymbol{\phi}:\left[\boldsymbol{\sigma}-\rho\,\big(\mathbf{U}\otimes\mathbf{U}\cdot\nabla\mathbf{u}\big)^{\mathrm{T}}\right]\mathrm{d}\Omega\\
&+\int_{\partial\Omega}\mathbf{n}\cdot\left[\rho\,(\mathbf{U}\cdot\nabla\mathbf{u})\cdot(\boldsymbol{\phi}\otimes\mathbf{U})-\boldsymbol{\sigma}^{\mathrm{T}}\cdot\boldsymbol{\phi}\right]\mathrm{d}\Gamma=\int_\Omega\boldsymbol{\phi}\cdot\mathbf{F}\,\mathrm{d}\Omega\,. \qquad (71)
\end{aligned}
$$

Finally, observing that

$$
\begin{aligned}
&\mathbf{n}\cdot\big[\,(\mathbf{U}\cdot\nabla\mathbf{u})\cdot(\boldsymbol{\phi}\otimes\mathbf{U})\big]=(\mathbf{U}\cdot\nabla\mathbf{u})\cdot(\boldsymbol{\phi}\otimes\mathbf{U})\cdot\mathbf{n}=\big((\mathbf{U}\cdot\nabla\mathbf{u})\cdot\boldsymbol{\phi}\big)(\mathbf{U}\cdot\mathbf{n})\\
&=(\mathbf{n}\cdot\mathbf{U})\big((\mathbf{U}\cdot\nabla\mathbf{u})\cdot\boldsymbol{\phi}\big)\quad=(n_iU_i)\big((U_j\partial_j u_k)\phi_k\big)\quad=n_i\big(U_iU_j\partial_j u_k\big)\phi_k\\
&=\mathbf{n}\cdot\big(\mathbf{U}\otimes\mathbf{U}\cdot\nabla\mathbf{u}\big)\cdot\boldsymbol{\phi}\quad=\boldsymbol{\phi}\cdot\big(\mathbf{U}\otimes\mathbf{U}\cdot\nabla\mathbf{u}\big)^{\mathrm{T}}\cdot\mathbf{n} \qquad (72)
\end{aligned}
$$

we obtain the result

$$
\begin{aligned}
&-\rho\int_\Omega\boldsymbol{\phi}\cdot(\mathbf{U}\cdot\nabla\mathbf{u})(\nabla\cdot\mathbf{U})\,\mathrm{d}\Omega+\int_\Omega\nabla\boldsymbol{\phi}:\left[\boldsymbol{\sigma}-\rho\,\big(\mathbf{U}\otimes\mathbf{U}\cdot\nabla\mathbf{u}\big)^{\mathrm{T}}\right]\mathrm{d}\Omega\\
&+\int_{\partial\Omega}\boldsymbol{\phi}\cdot\left[-\boldsymbol{\sigma}+\rho\,(\mathbf{U}\otimes\mathbf{U}\cdot\nabla\mathbf{u})^{\mathrm{T}}\right]\cdot\mathbf{n}\,\mathrm{d}\Gamma=\int_\Omega\boldsymbol{\phi}\cdot\mathbf{F}\,\mathrm{d}\Omega\,. \qquad (73)
\end{aligned}
$$

Equation (73) holds for the steady-state in-plane equilibrium of any sheet of travelling material, as long as ρ is approximately constant. We will apply the material model later.

We see from the equation (73) that if $\nabla\cdot\mathbf{U}=0$, then the first term vanishes. In such a case, the equations have the same form as those of a stationary membrane, but now the stresses obtain contributions (both inside the domain and on the traction boundaries) from the additional term involving velocity. However, if the velocity field has nonzero divergence, then no such analogy can be drawn.

The boundary term of the equation (73) gives the natural boundary conditions for this problem. The natural quantity to be prescribed is the normal component of the following rank-2 tensor:

$$
\boldsymbol{\sigma}_{\text{eff}}\equiv\boldsymbol{\sigma}-\rho\,(\mathbf{U}\otimes\mathbf{U}\cdot\nabla\mathbf{u})^{\mathrm{T}}\,. \qquad (74)
$$

This can be interpreted as an effective stress tensor, where the apparent stress (in laboratory coordinates) is modified by the centrifugal inertial effect.

6 Component form of the weak form

For convenience of software implementation, let us split equation (73) into component form. Let us denote the components of the virtual displacement as $\boldsymbol{\phi} \equiv (\phi, \psi)$. In the two-dimensional case being investigated in the present study, equation (73) gives the two equations

$$\begin{aligned}
&\int_\Omega \left[-\sigma_x + \rho U_x^2 \frac{\partial u}{\partial x} + \rho U_y U_x \frac{\partial u}{\partial y} \right] \frac{\partial \phi}{\partial x} \, \mathrm{d}\Omega \\
&+ \int_\Omega \left[-\tau_{xy} + \rho U_x U_y \frac{\partial u}{\partial x} + \rho U_y^2 \frac{\partial u}{\partial y} \right] \frac{\partial \phi}{\partial y} \, \mathrm{d}\Omega \\
&+ \rho \int_\Omega \left\{ \left[U_x \frac{\partial u}{\partial x} + U_y \frac{\partial u}{\partial y} \right] \left[\frac{\partial U_x}{\partial x} + \frac{\partial U_y}{\partial y} \right] \right\} \phi \, \mathrm{d}\Omega \\
&+ \int_{\partial\Omega} n_x \left[\sigma_x - \rho U_x^2 \frac{\partial u}{\partial x} - \rho U_y U_x \frac{\partial u}{\partial y} \right] \phi \, \mathrm{d}\Gamma \\
&+ \int_{\partial\Omega} n_y \left[\tau_{xy} - \rho U_x U_y \frac{\partial u}{\partial x} - \rho U_y^2 \frac{\partial u}{\partial y} \right] \phi \, \mathrm{d}\Gamma \\
&+ \int_\Omega F_x \phi = 0 \, .
\end{aligned} \tag{75}$$

and

$$\begin{aligned}
&\int_\Omega \left[-\tau_{yx} + \rho U_x^2 \frac{\partial v}{\partial x} + \rho U_y U_x \frac{\partial v}{\partial y} \right] \frac{\partial \psi}{\partial x} \, \mathrm{d}\Omega \\
&+ \int_\Omega \left[-\sigma_y + \rho U_x U_y \frac{\partial v}{\partial x} + \rho U_y^2 \frac{\partial v}{\partial y} \right] \frac{\partial \psi}{\partial y} \, \mathrm{d}\Omega \\
&+ \rho \int_\Omega \left\{ \left[U_x \frac{\partial v}{\partial x} + U_y \frac{\partial v}{\partial y} \right] \left[\frac{\partial U_x}{\partial x} + \frac{\partial U_y}{\partial y} \right] \right\} \psi \, \mathrm{d}\Omega \\
&+ \int_{\partial\Omega} n_x \left[\tau_{yx} - \rho U_x^2 \frac{\partial v}{\partial x} - \rho U_y U_x \frac{\partial v}{\partial y} \right] \psi \, \mathrm{d}\Gamma \\
&+ \int_{\partial\Omega} n_y \left[\sigma_y - \rho U_x U_y \frac{\partial v}{\partial x} - \rho U_y^2 \frac{\partial v}{\partial y} \right] \psi \, \mathrm{d}\Gamma \\
&+ \int_\Omega F_y \psi = 0 \, ,
\end{aligned} \tag{76}$$

where the outer unit normal $\mathbf{n}$ has components $\mathbf{n} = (n_x \, , n_y \,)$. We have moved all terms to the left-hand side and multiplied each equation by -1.

Equations (75) – (76) represent the steady state in-plane equilibrium for any sheet of moving material. We obtain the equations for the orthotropic Kelvin–Voigt material by inserting the viscoelastic stress-strain relations (27) – (29). Then, we insert the mixed Lagrange–Euler representations (25) for the material derivative in the viscous

terms, and restrict the inserted terms to the steady state ($\partial/\partial t \to 0$). The result is

$$\begin{aligned}
\int_\Omega \Bigg[&- \left[C_{11}\varepsilon_{xx} + K_{11}(U_x\frac{\partial \varepsilon_{xx}}{\partial x} + U_y\frac{\partial \varepsilon_{xx}}{\partial y}) + C_{12}\varepsilon_{yy} + K_{12}(U_x\frac{\partial \varepsilon_{yy}}{\partial x} + U_y\frac{\partial \varepsilon_{yy}}{\partial y}) \right] \\
&\qquad + \rho U_x^2\frac{\partial u}{\partial x} + \rho U_y U_x\frac{\partial u}{\partial y} \Bigg] \frac{\partial \phi}{\partial x}\, \mathrm{d}\Omega \\
+ \int_\Omega \Bigg[&- \left[C_{66}\gamma_{xy} + K_{66}(U_x\frac{\partial \gamma_{xy}}{\partial x} + U_y\frac{\partial \gamma_{xy}}{\partial y}) \right] + \rho U_x U_y\frac{\partial u}{\partial x} + \rho U_y^2\frac{\partial u}{\partial y} \Bigg] \frac{\partial \phi}{\partial y}\, \mathrm{d}\Omega \\
&\qquad + \rho \int_\Omega \left\{ \left[U_x\frac{\partial u}{\partial x} + U_y\frac{\partial u}{\partial y} \right] \left[\frac{\partial U_x}{\partial x} + \frac{\partial U_y}{\partial y} \right] \right\} \phi\, \mathrm{d}\Omega \\
+ \int_{\partial\Omega} n_x \Bigg[&\left[C_{11}\varepsilon_{xx} + K_{11}(U_x\frac{\partial \varepsilon_{xx}}{\partial x} + U_y\frac{\partial \varepsilon_{xx}}{\partial y}) + C_{12}\varepsilon_{yy} + K_{12}(U_x\frac{\partial \varepsilon_{yy}}{\partial x} + U_y\frac{\partial \varepsilon_{yy}}{\partial y}) \right] \\
&\qquad - \rho U_x^2\frac{\partial u}{\partial x} - \rho U_y U_x\frac{\partial u}{\partial y} \Bigg] \phi\, \mathrm{d}\Gamma \\
+ \int_{\partial\Omega} n_y \Bigg[&\left[C_{66}\gamma_{xy} + K_{66}(U_x\frac{\partial \gamma_{xy}}{\partial x} + U_y\frac{\partial \gamma_{xy}}{\partial y}) \right] - \rho U_x U_y\frac{\partial u}{\partial x} - \rho U_y^2\frac{\partial u}{\partial y} \Bigg] \phi\, \mathrm{d}\Gamma \\
&\qquad + \int_\Omega F_x \phi\, \mathrm{d}\Omega = 0
\end{aligned} \tag{77}$$

and

$$\begin{aligned}
\int_\Omega \Bigg[&- \left[C_{66}\gamma_{xy} + K_{66}(U_x\frac{\partial \gamma_{xy}}{\partial x} + U_y\frac{\partial \gamma_{xy}}{\partial y}) \right] + \rho U_x^2\frac{\partial v}{\partial x} + \rho U_y U_x\frac{\partial v}{\partial y} \Bigg] \frac{\partial \psi}{\partial x}\, \mathrm{d}\Omega \\
+ \int_\Omega \Bigg[&- \left[C_{21}\varepsilon_{xx} + K_{21}(U_x\frac{\partial \varepsilon_{xx}}{\partial x} + U_y\frac{\partial \varepsilon_{xx}}{\partial y}) + C_{22}\varepsilon_{yy} + K_{22}(U_x\frac{\partial \varepsilon_{yy}}{\partial x} + U_y\frac{\partial \varepsilon_{yy}}{\partial y}) \right] \\
&\qquad + \rho U_x U_y\frac{\partial v}{\partial x} + \rho U_y^2\frac{\partial v}{\partial y} \Bigg] \frac{\partial \psi}{\partial y}\, \mathrm{d}\Omega \\
&\qquad + \rho \int_\Omega \left\{ \left[U_x\frac{\partial v}{\partial x} + U_y\frac{\partial v}{\partial y} \right] \left[\frac{\partial U_x}{\partial x} + \frac{\partial U_y}{\partial y} \right] \right\} \psi\, \mathrm{d}\Omega \\
+ \int_{\partial\Omega} n_x \Bigg[&\left[C_{66}\gamma_{xy} + K_{66}(U_x\frac{\partial \gamma_{xy}}{\partial x} + U_y\frac{\partial \gamma_{xy}}{\partial y}) \right] - \rho U_x^2\frac{\partial v}{\partial x} - \rho U_y U_x\frac{\partial v}{\partial y} \Bigg] \psi\, \mathrm{d}\Gamma \\
+ \int_{\partial\Omega} n_y \Bigg[&\left[C_{21}\varepsilon_{xx} + K_{21}(U_x\frac{\partial \varepsilon_{xx}}{\partial x} + U_y\frac{\partial \varepsilon_{xx}}{\partial y}) + C_{22}\varepsilon_{yy} + K_{22}(U_x\frac{\partial \varepsilon_{yy}}{\partial x} + U_y\frac{\partial \varepsilon_{yy}}{\partial y}) \right] \\
&\qquad - \rho U_x U_y\frac{\partial v}{\partial x} - \rho U_y^2\frac{\partial v}{\partial y} \Bigg] \psi\, \mathrm{d}\Gamma \\
&\qquad + \int_\Omega F_y \psi\, \mathrm{d}\Omega = 0\,.
\end{aligned} \tag{78}$$

Finally, by inserting into (77) and (78) the definitions of the Cauchy strains from (23), the weak form component equations for FEM implementation are obtained.

The final result is

$$\begin{aligned}
\int_\Omega \Bigg[&- \left[C_{11}\frac{\partial u}{\partial x} + K_{11}(U_x\frac{\partial^2 u}{\partial x^2} + U_y\frac{\partial^2 u}{\partial x \partial y}) + C_{12}\frac{\partial v}{\partial y} + K_{12}(U_x\frac{\partial^2 v}{\partial x \partial y} + U_y\frac{\partial^2 v}{\partial y^2}) \right] \\
&\qquad + \rho U_x^2 \frac{\partial u}{\partial x} + \rho U_y U_x \frac{\partial u}{\partial y} \Bigg] \frac{\partial \phi}{\partial x} \, \mathrm{d}\Omega \\
+ \int_\Omega \Bigg[&- \left[C_{66}(\frac{\partial u}{\partial y} + \frac{\partial v}{\partial x}) + K_{66}(U_x(\frac{\partial^2 u}{\partial x \partial y} + \frac{\partial^2 v}{\partial x^2}) + U_y(\frac{\partial^2 u}{\partial y^2} + \frac{\partial^2 v}{\partial x \partial y})) \right] \\
&\qquad + \rho U_x U_y \frac{\partial u}{\partial x} + \rho U_y^2 \frac{\partial u}{\partial y} \Bigg] \frac{\partial \phi}{\partial y} \, \mathrm{d}\Omega \\
&\qquad + \rho \int_\Omega \left\{ \left[U_x \frac{\partial u}{\partial x} + U_y \frac{\partial u}{\partial y} \right] \left[\frac{\partial U_x}{\partial x} + \frac{\partial U_y}{\partial y} \right] \right\} \phi \, \mathrm{d}\Omega \\
+ \int_{\partial\Omega} n_x \Bigg[&\left[C_{11}\frac{\partial u}{\partial x} + K_{11}(U_x\frac{\partial^2 u}{\partial x^2} + U_y\frac{\partial^2 u}{\partial x \partial y}) + C_{12}\frac{\partial v}{\partial y} + K_{12}(U_x\frac{\partial^2 v}{\partial x \partial y} + U_y\frac{\partial^2 v}{\partial y^2}) \right] \\
&\qquad - \rho U_x^2 \frac{\partial u}{\partial x} - \rho U_y U_x \frac{\partial u}{\partial y} \Bigg] \phi \, \mathrm{d}\Gamma \\
+ \int_{\partial\Omega} n_y \Bigg[&\left[C_{66}(\frac{\partial u}{\partial y} + \frac{\partial v}{\partial x}) + K_{66}(U_x(\frac{\partial^2 u}{\partial x \partial y} + \frac{\partial^2 v}{\partial x^2}) + U_y(\frac{\partial^2 u}{\partial y^2} + \frac{\partial^2 v}{\partial x \partial y})) \right] \\
&\qquad - \rho U_x U_y \frac{\partial u}{\partial x} - \rho U_y^2 \frac{\partial u}{\partial y} \Bigg] \phi \, \mathrm{d}\Gamma + \int_\Omega F_x \phi \, \mathrm{d}\Omega = 0
\end{aligned} \tag{79}$$

and

$$\begin{aligned}
\int_\Omega \Bigg[&- \left[C_{66}(\frac{\partial u}{\partial y} + \frac{\partial v}{\partial x}) + K_{66}(U_x(\frac{\partial^2 u}{\partial x \partial y} + \frac{\partial^2 v}{\partial x^2}) + U_y(\frac{\partial^2 u}{\partial y^2} + \frac{\partial^2 v}{\partial x \partial y})) \right] \\
&\qquad + \rho U_x^2 \frac{\partial v}{\partial x} + \rho U_y U_x \frac{\partial v}{\partial y} \Bigg] \frac{\partial \psi}{\partial x} \, \mathrm{d}\Omega \\
+ \int_\Omega \Bigg[&- \left[C_{21}\frac{\partial u}{\partial x} + K_{21}(U_x\frac{\partial^2 u}{\partial x^2} + U_y\frac{\partial^2 u}{\partial x \partial y}) + C_{22}\varepsilon_{yy} + K_{22}(U_x\frac{\partial^2 v}{\partial x \partial y} + U_y\frac{\partial^2 v}{\partial y^2}) \right] \\
&\qquad + \rho U_x U_y \frac{\partial v}{\partial x} + \rho U_y^2 \frac{\partial v}{\partial y} \Bigg] \frac{\partial \psi}{\partial y} \, \mathrm{d}\Omega \\
&\qquad + \rho \int_\Omega \left\{ \left[U_x \frac{\partial v}{\partial x} + U_y \frac{\partial v}{\partial y} \right] \left[\frac{\partial U_x}{\partial x} + \frac{\partial U_y}{\partial y} \right] \right\} \psi \, \mathrm{d}\Omega \\
+ \int_{\partial\Omega} n_x \Bigg[&\left[C_{66}(\frac{\partial u}{\partial y} + \frac{\partial v}{\partial x}) + K_{66}(U_x(\frac{\partial^2 u}{\partial x \partial y} + \frac{\partial^2 v}{\partial x^2}) + U_y(\frac{\partial^2 u}{\partial y^2} + \frac{\partial^2 v}{\partial x \partial y})) \right] \\
&\qquad - \rho U_x^2 \frac{\partial v}{\partial x} - \rho U_y U_x \frac{\partial v}{\partial y} \Bigg] \psi \, \mathrm{d}\Gamma \\
+ \int_{\partial\Omega} n_y \Bigg[&\left[C_{21}\frac{\partial u}{\partial x} + K_{21}(U_x\frac{\partial^2 u}{\partial x^2} + U_y\frac{\partial^2 u}{\partial x \partial y}) + C_{22}\frac{\partial v}{\partial y} + K_{22}(U_x\frac{\partial^2 v}{\partial x \partial y} + U_y\frac{\partial^2 v}{\partial y^2}) \right] \\
&\qquad - \rho U_x U_y \frac{\partial v}{\partial x} - \rho U_y^2 \frac{\partial v}{\partial y} \Bigg] \psi \, \mathrm{d}\Gamma + \int_\Omega F_y \psi \, \mathrm{d}\Omega = 0 \, .
\end{aligned} \tag{80}$$

Equations (79) – (80) represent the weak form of the classical strong form equations (36) – (37), when consideration is restricted to the steady state.

We see that the weak form contains second derivatives in the viscous terms. Thus, to enforce integrability (see e.g. [28]), C1 continuity of basis functions across element boundaries is required in the viscoelastic case.

The corresponding pure elastic equations are obtained by setting $K_{11} = K_{12} = K_{21} = K_{22} = K_{66} = 0$. Explicitly, we have

$$\begin{aligned}
&\int_\Omega \left[-\left[C_{11}\frac{\partial u}{\partial x} + C_{12}\frac{\partial v}{\partial y}\right] + \rho U_x^2 \frac{\partial u}{\partial x} + \rho U_y U_x \frac{\partial u}{\partial y}\right]\frac{\partial \phi}{\partial x}\,\mathrm{d}\Omega \\
&+\int_\Omega \left[-\left[C_{66}(\frac{\partial u}{\partial y} + \frac{\partial v}{\partial x})\right] + \rho U_x U_y \frac{\partial u}{\partial x} + \rho U_y^2 \frac{\partial u}{\partial y}\right]\frac{\partial \phi}{\partial y}\,\mathrm{d}\Omega \\
&+\rho \int_\Omega \left\{ \left[U_x \frac{\partial u}{\partial x} + U_y \frac{\partial u}{\partial y}\right]\left[\frac{\partial U_x}{\partial x} + \frac{\partial U_y}{\partial y}\right]\right\}\phi\,\mathrm{d}\Omega \\
&+\int_{\partial\Omega} n_x \left[\left[C_{11}\frac{\partial u}{\partial x} + C_{12}\frac{\partial v}{\partial y}\right] - \rho U_x^2 \frac{\partial u}{\partial x} - \rho U_y U_x \frac{\partial u}{\partial y}\right]\phi\,\mathrm{d}\Gamma \\
&+\int_{\partial\Omega} n_y \left[\left[C_{66}(\frac{\partial u}{\partial y} + \frac{\partial v}{\partial x})\right] - \rho U_x U_y \frac{\partial u}{\partial x} - \rho U_y^2 \frac{\partial u}{\partial y}\right]\phi\,\mathrm{d}\Gamma \\
&+\int_\Omega F_x \phi\,\mathrm{d}\Omega = 0
\end{aligned} \tag{81}$$

and

$$\begin{aligned}
&\int_\Omega \left[-\left[C_{66}(\frac{\partial u}{\partial y} + \frac{\partial v}{\partial x})\right] + \rho U_x^2 \frac{\partial v}{\partial x} + \rho U_y U_x \frac{\partial v}{\partial y}\right]\frac{\partial \psi}{\partial x}\,\mathrm{d}\Omega \\
&+\int_\Omega \left[-\left[C_{21}\frac{\partial u}{\partial x} + C_{22}\frac{\partial v}{\partial y}\right] + \rho U_x U_y \frac{\partial v}{\partial x} + \rho U_y^2 \frac{\partial v}{\partial y}\right]\frac{\partial \psi}{\partial y}\,\mathrm{d}\Omega \\
&+\rho \int_\Omega \left\{ \left[U_x \frac{\partial v}{\partial x} + U_y \frac{\partial v}{\partial y}\right]\left[\frac{\partial U_x}{\partial x} + \frac{\partial U_y}{\partial y}\right]\right\}\psi\,\mathrm{d}\Omega \\
&+\int_{\partial\Omega} n_x \left[\left[C_{66}(\frac{\partial u}{\partial y} + \frac{\partial v}{\partial x})\right] - \rho U_x^2 \frac{\partial v}{\partial x} - \rho U_y U_x \frac{\partial v}{\partial y}\right]\psi\,\mathrm{d}\Gamma \\
&+\int_{\partial\Omega} n_y \left[\left[C_{21}\frac{\partial u}{\partial x} + C_{22}\frac{\partial v}{\partial y}\right] - \rho U_x U_y \frac{\partial v}{\partial x} - \rho U_y^2 \frac{\partial v}{\partial y}\right]\psi\,\mathrm{d}\Gamma \\
&+\int_\Omega F_y \psi\,\mathrm{d}\Omega = 0\ .
\end{aligned} \tag{82}$$

Equations (81) and (82) are the basis of the two-dimensional solutions presented in this article. Only first derivatives of the displacements are needed. Hence, C0 finite elements are sufficient.

Once a basis is chosen for u and v, it is straightforward to insert the Galerkin representation of both displacement variables into (81) and (82). Then, considering that the virtual displacement $\boldsymbol{\phi}$ is arbitrary, we use the basis functions of u as the test functions ϕ and the basis functions of v as the test functions ψ, obtaining the discrete equation system for the classical Galerkin method. Essential and natural boundary conditions are then applied as usual.

If the velocity field is divergence-free, we may omit the third line in both equations, and the velocity can be allowed to have finite discontinuities across element boundaries. In all other cases, the velocity field must have C0 continuity across element boundaries, in order to enforce integrability of (81) – (82). This is because the terms on the third line of both equations follow directly from the weak form of the problem, and thus cannot be applied only in element interiors (as is done e.g. when second derivatives appear in certain numerical stabilization schemes for flow problems; see e.g. [16]).

7 Coupling between drive velocity and in-plane displacement

If some edges of the domain are free, the velocity field driving the material may cause them to move. Each free edge will move until the velocity field becomes tangential to it. For small deformations, it is possible to avoid deforming the mesh, and still account for the slightly changed direction of the free edges by using approximate methods.

When free edges are present, the effective velocity field in the material is a priori unknown. In a sense, the driving velocity field modifies itself when the free edge deformations are taken into account. Thus, instead of taking $\mathbf{U}$ as a prescribed external velocity, this quantity may be redefined to fulfill two tasks. First, it will still be based on the driving velocity field, but secondly, the modified $\mathbf{U}$ will also take into account the small deformations in the free edges, including the effect that the free edge deformations have on the effective velocity field inside the domain.

We will use a deformation-based approach. Consider the differential plane element in the small-displacement regime. See Figure 6. The original, undeformed edges are given by the vectors $\mathbf{x} = (\mathrm{d}x, 0)$ and $\mathbf{y} = (0, \mathrm{d}y)$. After deformation by a displacement field $\mathbf{u} = (u, v)$, these edges become (with the help of a first-order

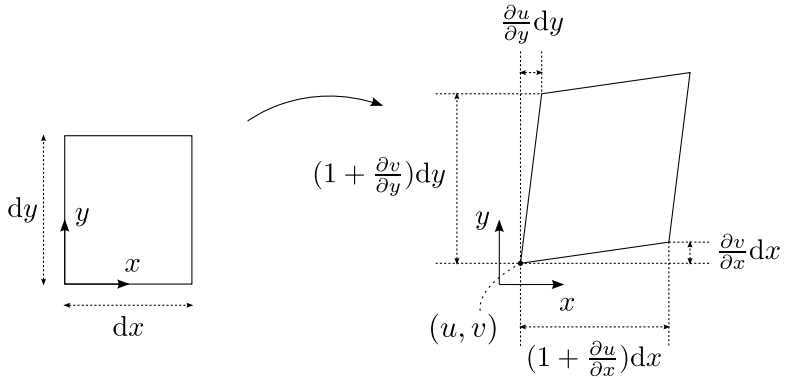

Figure 6: Small deformation of a differential plane element.

two-dimensional Taylor expansion of each of the fields u and v)

$$\tilde{\mathbf{x}} = \left((1 + \frac{\partial u}{\partial x})\mathrm{d}x,\ \frac{\partial v}{\partial x}\mathrm{d}x \right) , \quad \tilde{\mathbf{y}} = \left(\frac{\partial u}{\partial y}\mathrm{d}y,\ (1 + \frac{\partial v}{\partial y})\mathrm{d}y \right) . \tag{83}$$

The projection

$$\mathbf{u}_{\mathbf{X}} = \mathbf{M} \cdot \mathbf{u}_{\mathbf{x}} , \tag{84}$$

that is,

$$\begin{bmatrix} u_X \\ u_Y \end{bmatrix} = \begin{bmatrix} \hat{\mathbf{x}} \cdot \hat{\mathbf{X}} & \hat{\mathbf{y}} \cdot \hat{\mathbf{X}} \\ \hat{\mathbf{x}} \cdot \hat{\mathbf{Y}} & \hat{\mathbf{y}} \cdot \hat{\mathbf{Y}} \end{bmatrix} \begin{bmatrix} u_x \\ u_y \end{bmatrix} , \tag{85}$$

transforms any vector field $\mathbf{u}$ given in $\mathbf{x} = (x, y)$ components into $\mathbf{X} = (X, Y)$ components. Here $\hat{\mathbf{x}}$ and $\hat{\mathbf{y}}$ (respectively $\hat{\mathbf{X}}$ and $\hat{\mathbf{Y}}$) are the unit vectors giving the directions of the axes of the (x, y) (respectively (X, Y)) coordinate systems. The boldface subscript denotes which coordinate system the quantity is given in, and the plain subscripts denote components.

We choose

$$\hat{\mathbf{X}} := (1, 0) , \quad \hat{\mathbf{Y}} := (0, 1) , \tag{86}$$

and take $\hat{\mathbf{x}}$ and $\hat{\mathbf{y}}$ as the unit vectors corresponding to the edges of the deformed differential element:

$$\hat{\mathbf{x}} := \tilde{\mathbf{x}} / \left\| \tilde{\mathbf{x}} \right\| , \quad \hat{\mathbf{y}} := \tilde{\mathbf{y}} / \left\| \tilde{\mathbf{y}} \right\| . \tag{87}$$

Here $\| \dots \|$ denotes the euclidean norm.

Now, instead of prescribing the velocity field $\mathbf{U}_{\mathbf{X}}$, we prescribe $\mathbf{U}_{\mathbf{x}}$ (along the deformed coordinate directions), and then project it to the capital-$\mathbf{X}$ axes using (85). Then we set $\mathbf{U} = \mathbf{U}_{\mathbf{X}}$ in equations (81) – (82).

Using (85) – (87), we obtain the corrected velocity components as

$$\begin{aligned} U_X &= (\hat{\mathbf{x}} \cdot \hat{\mathbf{X}})\, U_x + (\hat{\mathbf{y}} \cdot \hat{\mathbf{X}})\, U_y = \hat{x}_1 U_x + \hat{y}_1 U_y , \\ U_Y &= (\hat{\mathbf{x}} \cdot \hat{\mathbf{Y}})\, U_x + (\hat{\mathbf{y}} \cdot \hat{\mathbf{Y}})\, U_y = \hat{x}_2 U_x + \hat{y}_2 U_y . \end{aligned} \tag{88}$$

Here $\hat{x}_j$ denotes the jth component of the vector $\hat{\mathbf{x}}$, and we have used (86).

If consider not only direction changes, but also length changes, of the reference vectors (that were originally unit vectors), it is possible to use

$$\hat{\mathbf{x}} := \tilde{\mathbf{x}} / \mathrm{d}x , \quad \hat{\mathbf{y}} := \tilde{\mathbf{y}} / \mathrm{d}y . \tag{89}$$

instead of (87), using the fact that the original lengths of the sides of the differential element were $\mathrm{d}x$ and $\mathrm{d}y$. In this case, we obtain

$$\begin{aligned} U_X &= \hat{x}_1 U_x + \hat{y}_1 U_y = (1 + \frac{\partial u}{\partial x}) U_x + \frac{\partial u}{\partial y} U_y , \\ U_Y &= \hat{x}_2 U_x + \hat{y}_2 U_y = \frac{\partial v}{\partial x} U_x + (1 + \frac{\partial v}{\partial y}) U_y . \end{aligned} \tag{90}$$

Then, up to first order, the deformed reference vector lengths (squared) are

$$\begin{aligned} \|\hat{\mathbf{x}}\|^2 &= (1+\frac{\partial u}{\partial x})^2 + (\frac{\partial v}{\partial x})^2 \approx 1 + 2\frac{\partial u}{\partial x} \,, \\ \|\hat{\mathbf{y}}\|^2 &= (\frac{\partial u}{\partial y})^2 + (1+\frac{\partial v}{\partial y})^2 \approx 1 + 2\frac{\partial v}{\partial y} \,. \end{aligned} \tag{91}$$

In case of pure axial input flow, $U_x = U_{\text{in}}$ and $U_y = 0$, we have

$$\begin{aligned} U_X &= (1+\frac{\partial u}{\partial x})U_{\text{in}} \,, \\ U_Y &= \frac{\partial v}{\partial x}U_{\text{in}} \,. \end{aligned} \tag{92}$$

In the present study, equations (92) have been used for computing the velocity field $\mathbf{U_X}$.

Note that the corrections (88) and (90) make the effective velocity field $\mathbf{U_X}$ space-dependent, even if the original input $\mathbf{U_x}$ is not, due to the space dependence of $\mathbf{u}$. Hence, we cannot assume $\mathbf{U}$ to be constant; terms involving its derivatives must thus be retained in the equations.

Regardless of whether one uses (88) or (90), the corrected velocity field will violate mass conservation, because the calculation is based on geometric considerations only. Thus, a correction is required to preserve mass. We will need two different approaches depending on whether the material is compressible.

For a compressible material, we may use the mass conservation equation (1) to compute the velocity field inside the domain, using in boundary conditions the edge data for the normal component (in (X, Y) coordinates) of the proposed velocity given by (88) or (90).

To do this, one can view the mass conservation equation as diffusion of velocity potential. Assume that the velocity field is irrotational ($\nabla \times \mathbf{v} = 0$); this is reasonable for steady state flow of a solid. In a steady state, $\partial\rho/\partial t = 0$. We have

$$\nabla \cdot (\rho \mathbf{v}) = 0 \,. \tag{93}$$

After multiplication by a test function χ, integrating over the domain Ω, and applying the divergence theorem, we have the weak form

$$\int_{\partial\Omega} (\mathbf{n}\cdot\mathbf{v})\,\rho\,\chi \,\mathrm{d}\Gamma - \int_{\Omega} \rho\,\nabla\chi\cdot\mathbf{v} \,\mathrm{d}\Omega = 0 \,. \tag{94}$$

Note that here ρ does not need to be constant. Next, let us use the fact that an irrotational vector field has a scalar potential:

$$\mathbf{v} = \nabla V \,, \tag{95}$$

where V is a scalar-valued function. Inserting (95) into (94) obtains

$$\int_{\partial\Omega} (\mathbf{n}\cdot\nabla V)\,\rho\,\chi \,\mathrm{d}\Gamma - \int_{\Omega} \rho\,\nabla\chi\cdot\nabla V \,\mathrm{d}\Omega = 0 \,. \tag{96}$$

which is a steady-state diffusion equation (Poisson equation) for the velocity potential V. The natural boundary condition is

$$(\mathbf{n} \cdot \nabla V)\rho = q \ , \tag{97}$$

i.e. one can prescribe the normal component of mass flow as a known function q. Hence, if the density at the edge is known, it is possible to prescribe the normal component of velocity there, via use of the natural boundary condition.

Recall equation (7), which gives density in terms of the axial strains, which in turn are easily obtained from the displacements via equations (23). Thus the density field can be computed once the displacements are known. Any C0 elements can be used for representing V.

By computation of the scalar potential V, the tangential velocity component at the edges will adjust itself such that mass balance is satisfied. Furthermore, the computed velocity field ∇V inside the domain will also satisfy mass balance.

Because we have a Poisson problem with purely natural boundary conditions, the solution V is unique only up to an arbitrary additive constant. This can be remedied by standard techniques. One that is easy to implement is to add a small reaction term $\int_\Omega \epsilon \, \chi \, V \ \mathrm{d}\Omega$ to the left-hand side of (96), where ϵ is a small constant (e.g. $\epsilon = 10^{-8}$).

In the case of an incompressible material, in the steady state the mass conservation equation (1) becomes simply $\nabla \cdot \mathbf{v} = 0$, i.e., the velocity field of an incompressible material must be divergence-free.

Therefore, in this case we simply compute the divergence-free projection of the proposed velocity field (88) or (90). The projection can be obtained using the standard trick based on Helmholtz decomposition. For completeness, let us review this briefly. Let $\mathbf{U}_e$ be the expected velocity field before the correction for mass conservation. Define a scalar potential p such that

$$\Delta p = \nabla \cdot \mathbf{U}_e \ . \tag{98}$$

Since the laplacian $\Delta(\dots) \equiv \nabla \cdot \nabla(\dots)$, equation (98) is equivalent with

$$\nabla \cdot \nabla p = \nabla \cdot \mathbf{U}_e \ . \tag{99}$$

By rearranging terms, we have

$$\nabla \cdot (\mathbf{U}_e - \nabla p) = 0 \ , \tag{100}$$

i.e. the difference $\mathbf{U}_e - \nabla p$ is divergence-free. Define the final velocity field as

$$\mathbf{U} = \mathbf{U}_e - \nabla p \ . \tag{101}$$

Then $\mathbf{U}$ is the divergence-free projection of $\mathbf{U}_e$. As the boundary conditions, one may require

$$\mathbf{n} \cdot \nabla p = 0 \tag{102}$$

on all boundaries. This ensures that the normal component of the correction ∇p vanishes at the boundaries. The solution will then adjust the tangential component at the boundaries to enforce the divergence-free property there; in the interior of the domain, both components are allowed to change.

Again, we have a Poisson problem with purely natural boundary conditions, and thus the solution p is unique only up to an arbitrary additive constant. This can be worked around as above. Let ϵ be a small constant, e.g. $\epsilon = 10^{-8}$. The final weak form of the projection problem is

$$-\int_\Omega \nabla p \cdot \nabla \chi \, \mathrm{d}\Omega + \epsilon \int_\Omega p\,\chi \, \mathrm{d}\Omega + \int_{\partial\Omega} (\mathbf{n} \cdot \nabla p)\chi \, \mathrm{d}\Gamma = \int_\Omega (\nabla \cdot \mathbf{U}_e)\chi \, \mathrm{d}\Omega \,, \qquad (103)$$

where χ is a test function. Any C0 elements can be used for representing p.

Strictly speaking, if $\mathbf{u}$ is represented by C0 elements, the divergence of $\mathbf{U}_e$ (which depends on the second derivatives of $\mathbf{u}$) is not integrable due to singularities at the element boundaries. However, the right-hand side of (99) is basically arbitrary, as is also the velocity field $\mathbf{U}$ when viewed as input to (81) – (82). The only requirement is that either $\nabla \cdot \mathbf{U} \equiv 0$, or alternatively, that $\nabla \cdot \mathbf{U}$ is integrable. Thus, we may choose to omit the singularities when defining the auxiliary quantity p by (99); any practical solver code will then see $\mathbf{U} = \mathbf{U}_e - \nabla p$ as a divergence-free velocity field.

This also has implications for the compressible case treated further above. There, nonzero divergence was allowed for the velocity field (via local variations in density). Now, however, the divergence of the velocity field is present in the original equations (81) – (82) themselves, and we cannot ignore singularities if we are to represent the problem correctly. If the presented free-edge approximation is used, then u and v must be represented using elements having C1 continuity across the element edges. In the present study, we have chosen to ignore this issue by using a divergence-free velocity field, allowing us to omit the problematic terms in (81) – (82).

There is one final issue that must be accounted for. The presented free-edge approximation will make the equations (81) – (82) nonlinear, since the effective velocity field $\mathbf{U}$ depends on the displacement $\mathbf{u}$. Thus an iterative process must be introduced to find the solution.

8 Numerical results

In this section, we will present numerical results from both the one- and two dimensional models. In the one-dimensional case, the full viscoelastic model is used. The two-dimensional study is focused on the inertial contribution in the pure elastic case.

In the one-dimensional model, the strain and stress states can be calculated analytically using the equations (52) and (56). Using the parameter values $E_x = 2.5 \cdot 10^7$ N/m^2, $\eta_x = 4.0 \cdot 10^5$ Ns/m^2, $U_x = 10$ m/s, span length $L = 1.0$ m and strain $\varepsilon_T = 0.03$, the results shown in Figures 7 – 9 are obtained. The numerical solutions, also shown in Figures 7 and 8, are reproduced from the previous study [35].

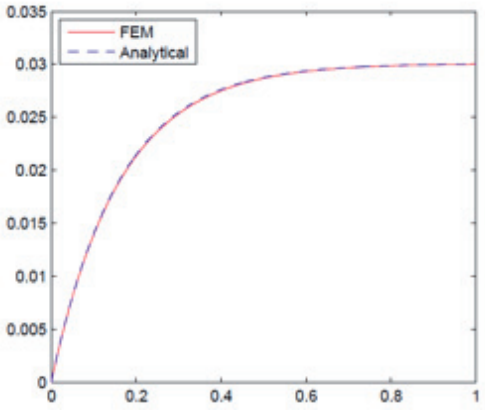

Figure 7: Analytical and numerical finite element solution of strain distribution along the length of the web span [35].

As was pointed out in the analysis, the strain distribution along the travelling viscoelastic span differs from the traditional constant strain that is observed for purely elastic materials [68]. However, even though the strain distribution is not constant, the stress distribution is a combination of elastic and viscous forces based on the equation (21), and it is almost constant. The stress increases very slightly towards the traction line A2; this is a consequence of the acceleration of the web due to higher outlet velocity, $U_2 > U_1$ [35]. The effect of the span length on the web stress state is visible. Basically, the shorter the processing time of the viscoelastic span is, the higher is the response of time-dependent viscous force component.

In case of the two-dimensional model, a purely elastic travelling two-dimensional sheet was investigated numerically using finite elements. See Figure 10. The unknowns were the displacements u and v. The element type used was Q2 (quadratic and quadrangular). Isoparametric mapping (i.e. also Q2) was used for the coordinates. The auxiliary potential p for divergence-free velocity projection was represented using Q1 (bilinear quadrangular) elements. The classical Galerkin method was used; for each unknown quantity, its own basis functions were used as the test functions.

The mesh was set up as a uniform cartesian grid with 16×16 elements for each of the unknowns. Discretizations were produced automatically from equations (81) – (82) and (103). Dirichlet boundary conditions, prescribing displacements, were enforced by the elimination technique. Homogeneous natural (i.e. zero Neumann) boundary conditions required no action on part of the implementation. The discretization lead to 32895 global degrees of freedom in the linear problem (u and v only), and 37120 in the nonlinear problem (u, v and auxiliary potential p).

The solution of the corresponding linear problem for the stationary elastic sheet ($\mathbf{U} = 0$) was used as the initial guess for $\mathbf{u}$, and fixed-point iteration was used to refine the solution of the nonlinear problem of the moving sheet. At each fixed-

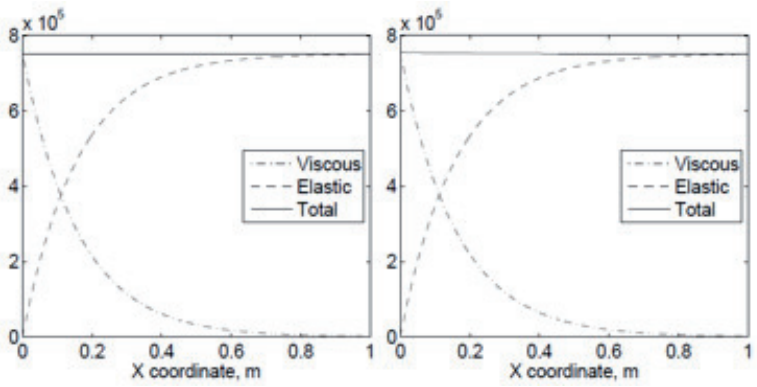

Figure 8: Analytical (left) and numerical (right) finite element solution of stress distribution along the length of the span [35].

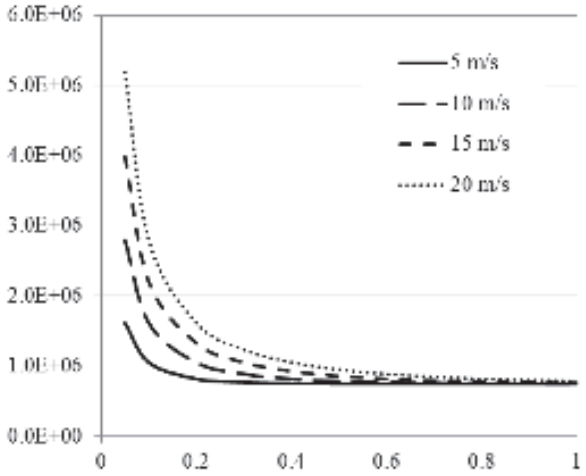

Figure 9: Effect of web span length on the web stress [35].

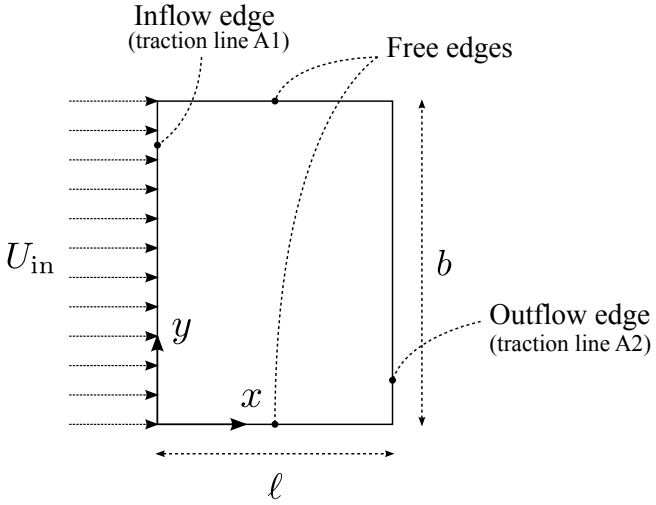

Figure 10: Setup for the two-dimensional numerical investigation. Elastic material enters from the left at velocity U_{in}, and flows through the domain at a velocity determined by the interaction of U_{in} and the approximated behaviour of the free edges.

point iteration, the linear equation system was solved by a direct solver. The velocity field $\mathbf{U}$ was computed starting from a purely axial inflow, as described above. See equations (92), (101) and (103).

A common desktop computer with 4 CPU cores was used for the finite element computations. With MPI-parallelized matrix assembly, each nonlinear problem took about one minute of wall time. The implementation was based on the scientific Python software stack.

Problem parameter values used in the study are listed in Table 1. The shear modulus based on the geometric average,

$$G = \frac{\sqrt{E_1 E_2}}{2(1+\sqrt{\nu_{12}\nu_{21}})} \,, \tag{104}$$

was used for both the isotropic and orthotropic materials. Equation (104) is sometimes known as the Huber value for the shear modulus, after M. T. Huber who proposed this relation for orthotropic materials [25, 26, 27].

The boundary conditions for the displacements u and v were

$$u(y) = v(y) = 0 \quad \text{at} \quad x = 0, \quad 0 < y < b \,, \tag{105}$$

$$u(y) = u_{\mathrm{f}} \quad \text{at} \quad x = \ell, \quad 0 < y < b \,, \tag{106}$$

and zero Neumann for v at $x = \ell$, $0 < y < b$. In (106), u_{f} is a prescribed constant value for the displacement. Note that at the outflow edge, only u is fixed; v is determined by the zero Neumann condition.

Table 1: Parameter values used in the two-dimensional numerical study. All 24 combinations resulting from the choices of U_{in} (4 values), b (3 values) and the two materials were investigated. The shear modulus based on the geometric average (equation (104)) was used for both the isotropic and orthotropic materials. Note elastic compatibility $E_1\nu_{21} = E_2\nu_{12}$ (see e.g. [37]).

U_{in} [m/s]	ℓ [m]	b [m]	ρ [kg/m^3]	u_{f} [m]
0	0.5	0.1	800	$0.03 \cdot \ell$
15		0.5		
25		2.5		
50				

	E_1 [10^7 Pa]	E_2 [10^7 Pa]	ν_{12}	ν_{21}
Isotropic	2.5	2.5	0.3	0.3
Orthotropic	5.0	1.25	0.6	0.15

On the free edges, $0 < x < \ell$, $y = 0$ and $0 < x < \ell$, $y = b$, the zero Neumann condition was used for both u and v. The zero Neumann condition (weakly) prescribes zero normal component for the effective stress tensor (74), i.e.

$$\boldsymbol{\sigma}_{\text{eff}} \cdot \mathbf{n} \equiv \left[\boldsymbol{\sigma} - \rho(\mathbf{U} \otimes \mathbf{U} \cdot \nabla \mathbf{u})^{\text{T}}\right] \cdot \mathbf{n} = 0 \,. \tag{107}$$

Explicitly, accounting for our geometry and spelling out the component form, from equation (82) we can read the following condition corresponding to v at the outflow boundary:

$$C_{66}(\frac{\partial u}{\partial y} + \frac{\partial v}{\partial x}) - \rho U_x^2 \frac{\partial v}{\partial x} - \rho U_y U_x \frac{\partial v}{\partial y} = 0 \quad \text{at} \quad x = \ell, \quad 0 < y < b \,, \tag{108}$$

and from equations (81) and (82), the following conditions corresponding to u and v (respectively) on the free boundaries:

$$C_{66}(\frac{\partial u}{\partial y} + \frac{\partial v}{\partial x}) - \rho U_x U_y \frac{\partial u}{\partial x} - \rho U_y^2 \frac{\partial u}{\partial y} = 0 \quad \text{at} \quad 0 < x < \ell, \quad y = \{0, b\} \,, \tag{109}$$

$$C_{21}\frac{\partial u}{\partial x} + C_{22}\frac{\partial v}{\partial y} - \rho U_x U_y \frac{\partial v}{\partial x} - \rho U_y^2 \frac{\partial v}{\partial y} = 0 \quad \text{at} \quad 0 < x < \ell, \quad y = \{0, b\} \,. \tag{110}$$

The boundary conditions for the auxiliary potential p were (102) on all boundaries. As was mentioned, this requires that the normal component of the velocity correction vanishes at the boundaries.

The problem was solved numerically for all 24 input value combinations resulting from the choices of U_{in} (4 values), b (3 values) and the two materials, as listed in Table 1. The quantities studied were u, v, ε_{xx}, ε_{yy}, γ_{xy}, σ_{xx}, σ_{yy} and τ_{xy}. In addition, when $U_{\text{in}} > 0$, the relative velocity field defined as

$$\mathbf{U}_{\text{rel}} \equiv (\, U_x - U_{\text{in}} \,,\, U_y \,) \tag{111}$$

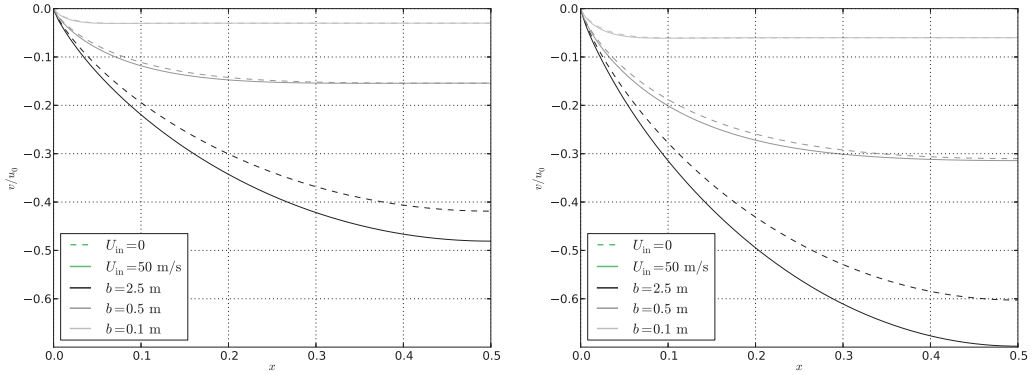

Figure 11: Displacement v, normalized to $u_{\rm f}$, along the free edge $0 < x < \ell$, $y = b$. *Left*: isotropic. *Right*: orthotropic. Line style indicates inflow velocity $U_{\rm in}$, darkness indicates span width b.

was also studied.

Figure 11 shows the y-directional displacement profile (displacement v) along the free edge $0 < x < \ell$, $y = b$ for representative isotropic and orthotropic cases for both stationary and moving materials.

Figures 12–28 display contour plots of all studied quantities for a stationary material (linear reference case), and material moving at $U_{\rm in} = 50$ m/s (representative example of nonlinear case).

For all investigated cases, it was observed that for each quantity studied, the difference between the nonlinear and linear solutions is small, when compared to the maximum value of the linear solution. While varying the magnitude of $U_{\rm in}$ changed the magnitude of this difference, the shape of the difference field (nonlinear minus linear) for each quantity studied remained the same. See Figures 29 – 36 for representative examples of the difference fields.

All effects were observed to become more pronounced for small aspect ratios ℓ/b, i.e. spans that are wide and short. The span length ℓ was kept constant, and the width b was varied; hence in the figures, large values of b correspond to small aspect ratios.

In all investigated cases, inertial effects caused additional elastic contraction of the travelling span, on top of the contraction already observed for a stationary material. This effect can be seen especially clearly in the y-directional displacement profile, Figure 11, and the shape of the relative velocity field $\mathbf{U}_{\rm rel}$, Figure 12.

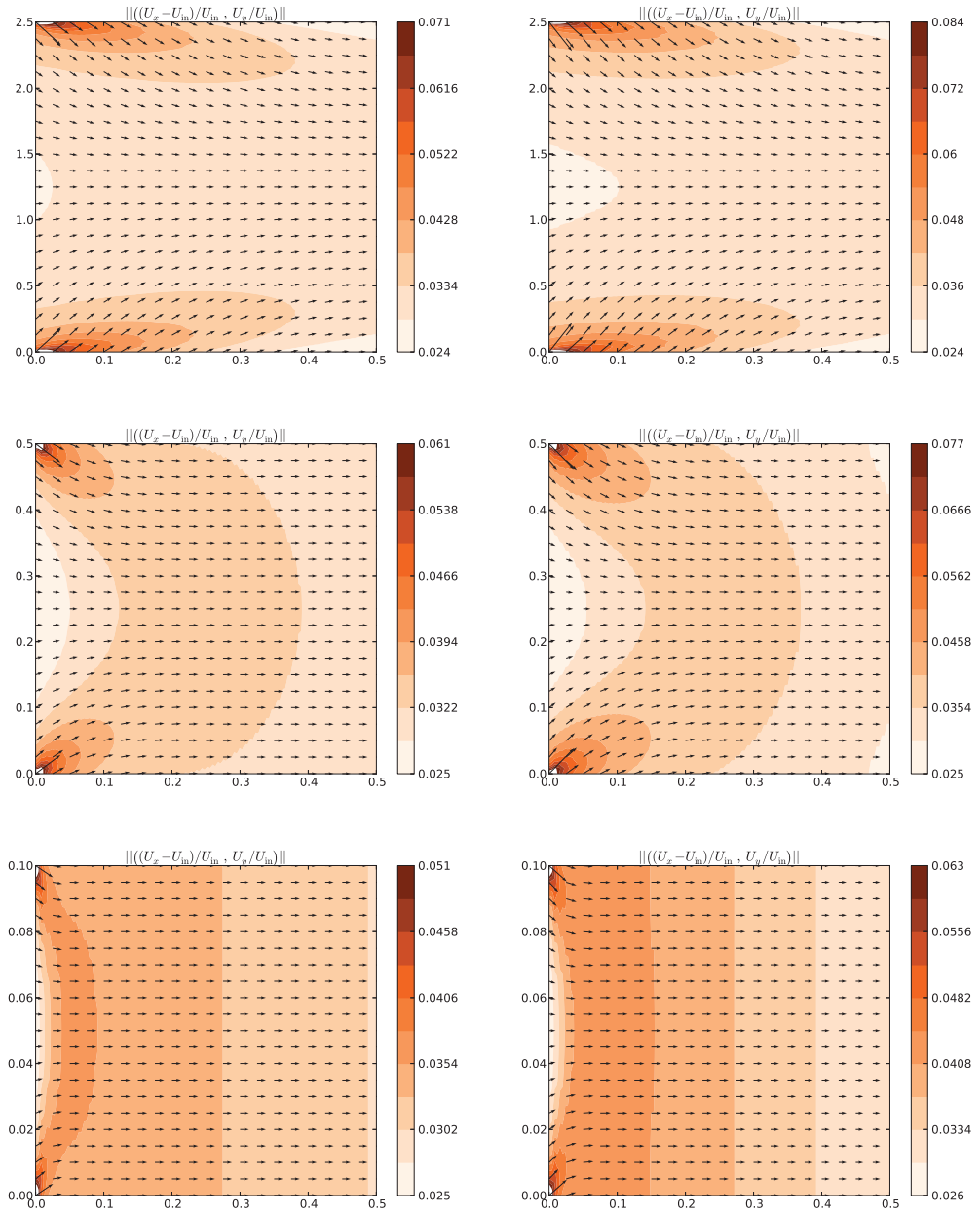

Figure 12: Relative velocity field $\mathbf{U}_{\mathrm{rel}}$, normalized to $U_{\mathrm{in}} = 50$ m/s (representative). *Left*: isotropic. *Right*: orthotropic. *Top to bottom*: $b = 2.5,\ 0.5,\ 0.1$ m ($\ell/b = 1/5,\ 1,\ 5$).

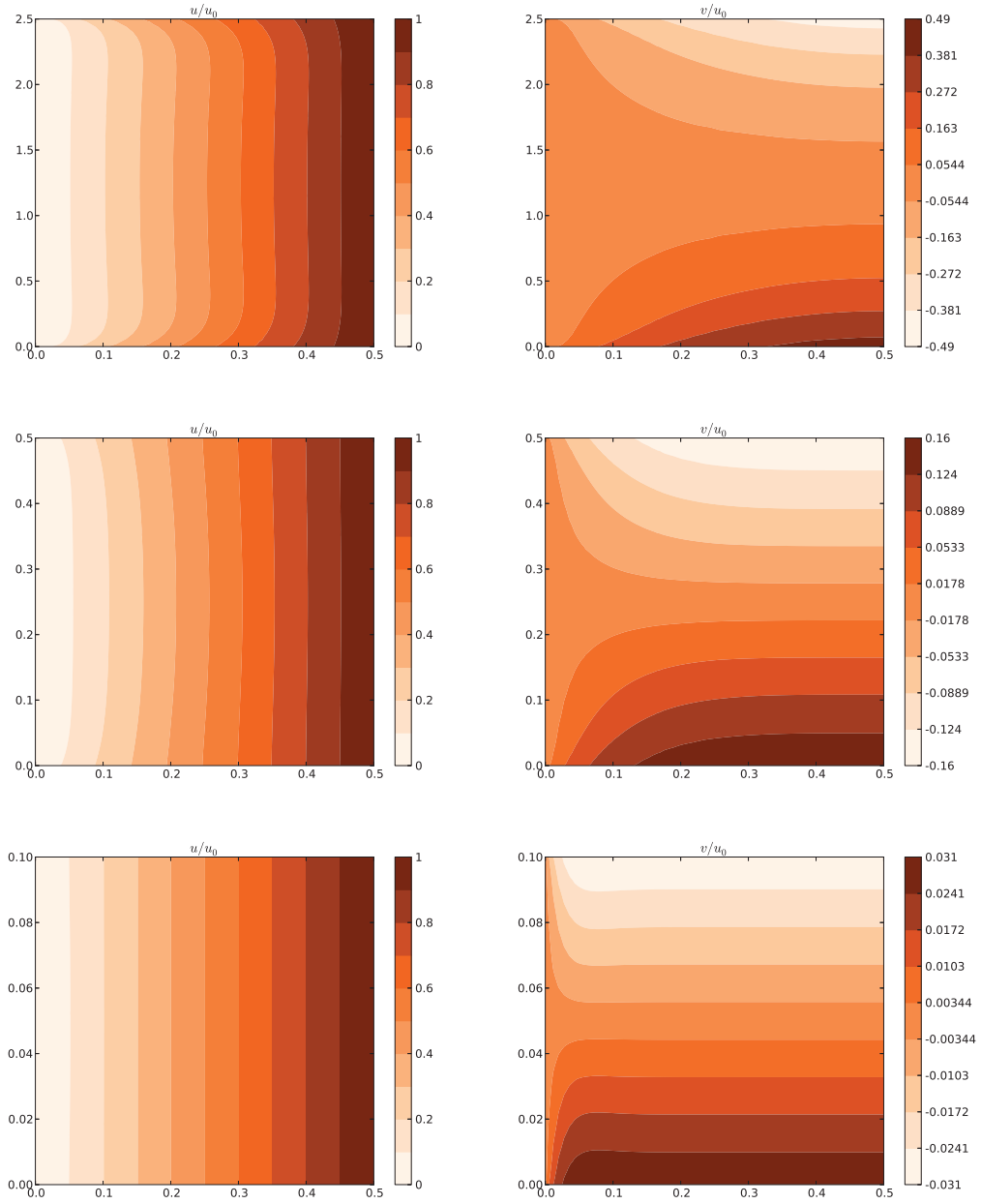

Figure 13: Displacements u and v, normalized to u_f. Isotropic, $U_\mathrm{in} = 0$ (linear reference). *Top to bottom:* $b = 2.5,\ 0.5,\ 0.1\,m$ ($\ell/b = 1/5,\ 1,\ 5$).

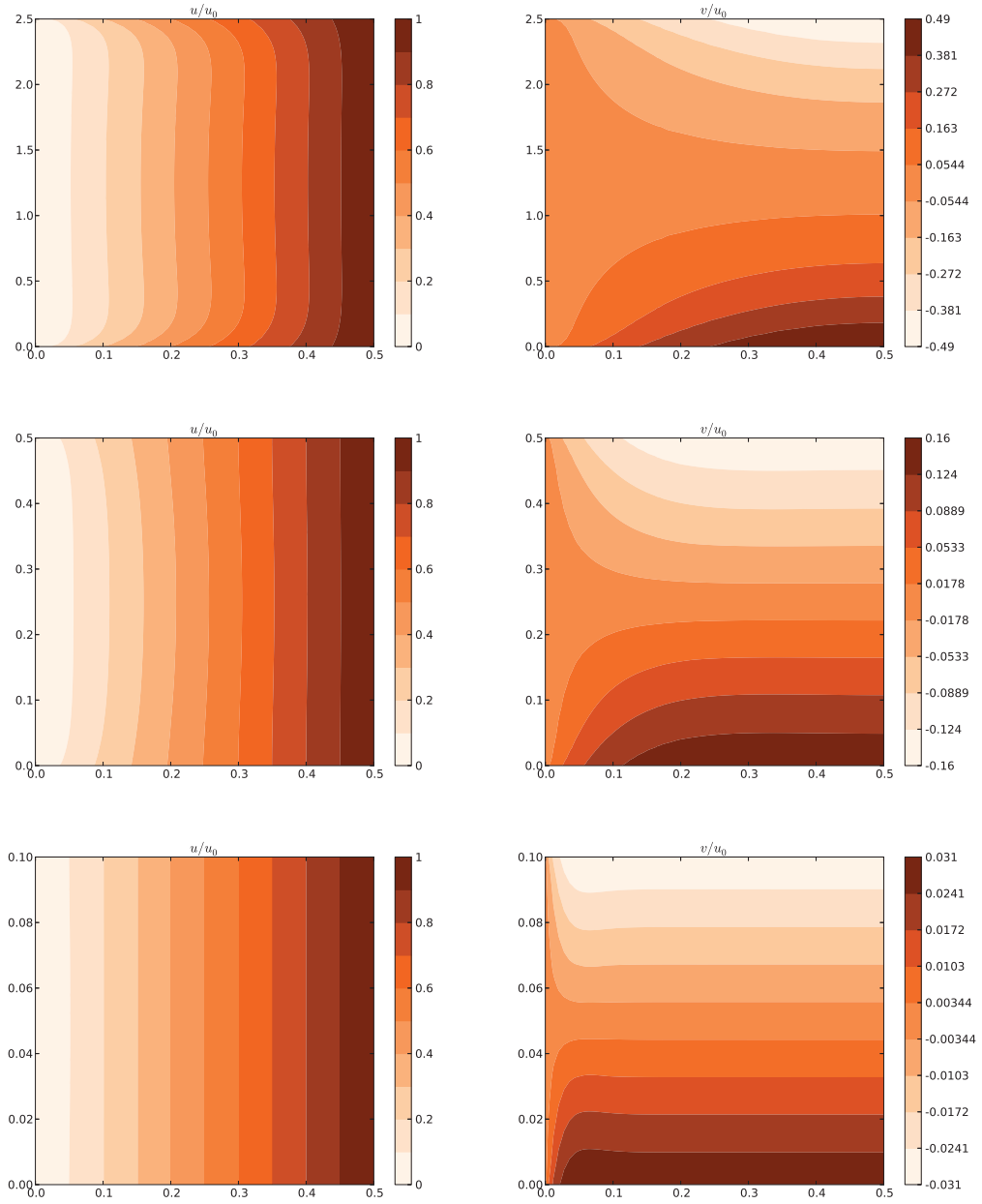

Figure 14: Displacements u and v, normalized to u_f. Isotropic, $U_\mathrm{in} = 50$ m/s (representative). *Top to bottom:* $b = 2.5,\ 0.5,\ 0.1\,m$ ($\ell/b = 1/5,\ 1,\ 5$).

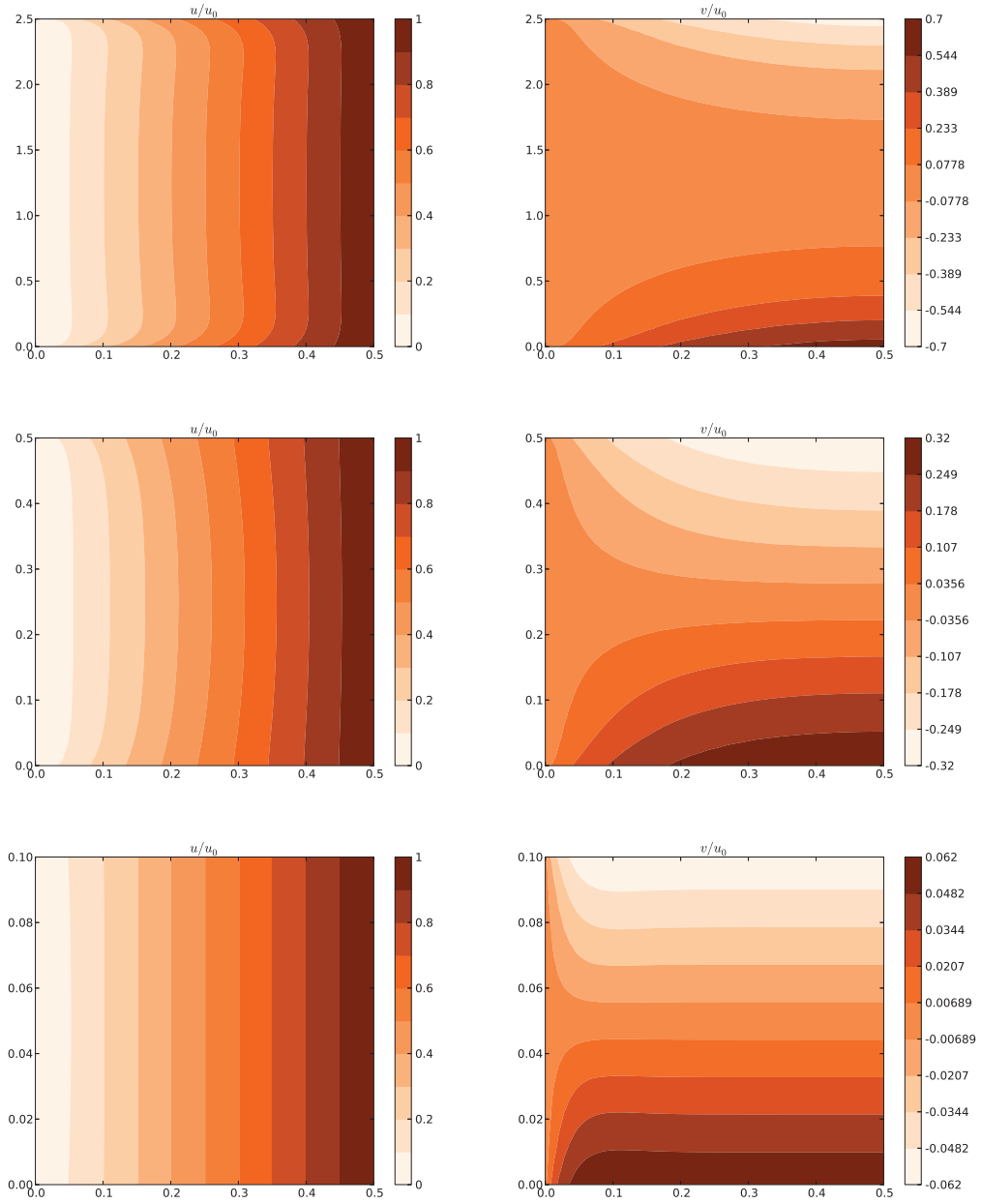

Figure 15: Displacements u and v, normalized to u_{f}. Orthotropic, $U_{\mathrm{in}} = 0$ (linear reference). *Top to bottom:* $b = 2.5,\ 0.5,\ 0.1\,m$ ($\ell/b = 1/5,\ 1,\ 5$).

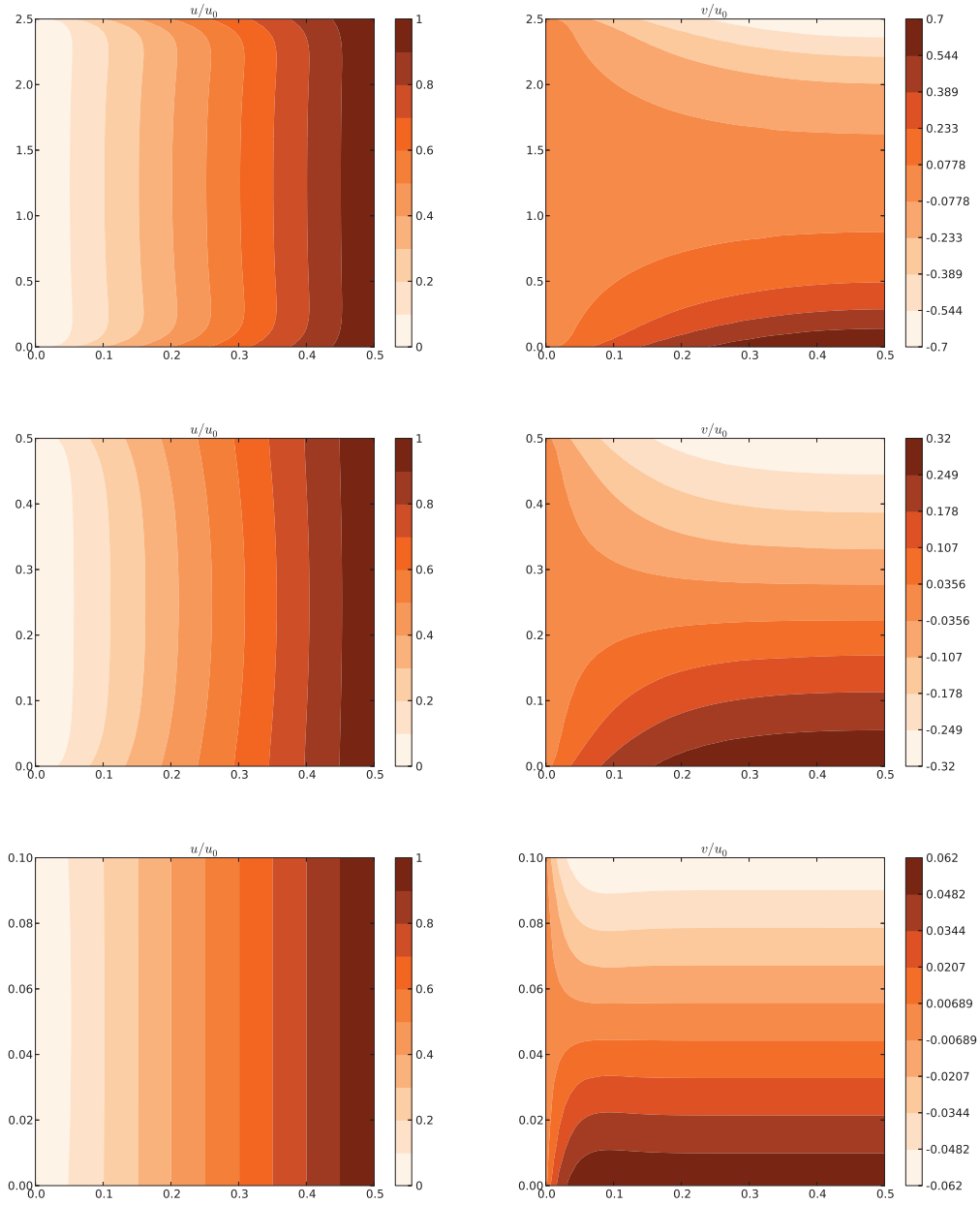

Figure 16: Displacements u and v, normalized to u_f. Orthotropic, $U_\mathrm{in} = 50$ m/s (representative). *Top to bottom:* $b = 2.5,\ 0.5,\ 0.1\,m$ ($\ell/b = 1/5,\ 1,\ 5$).

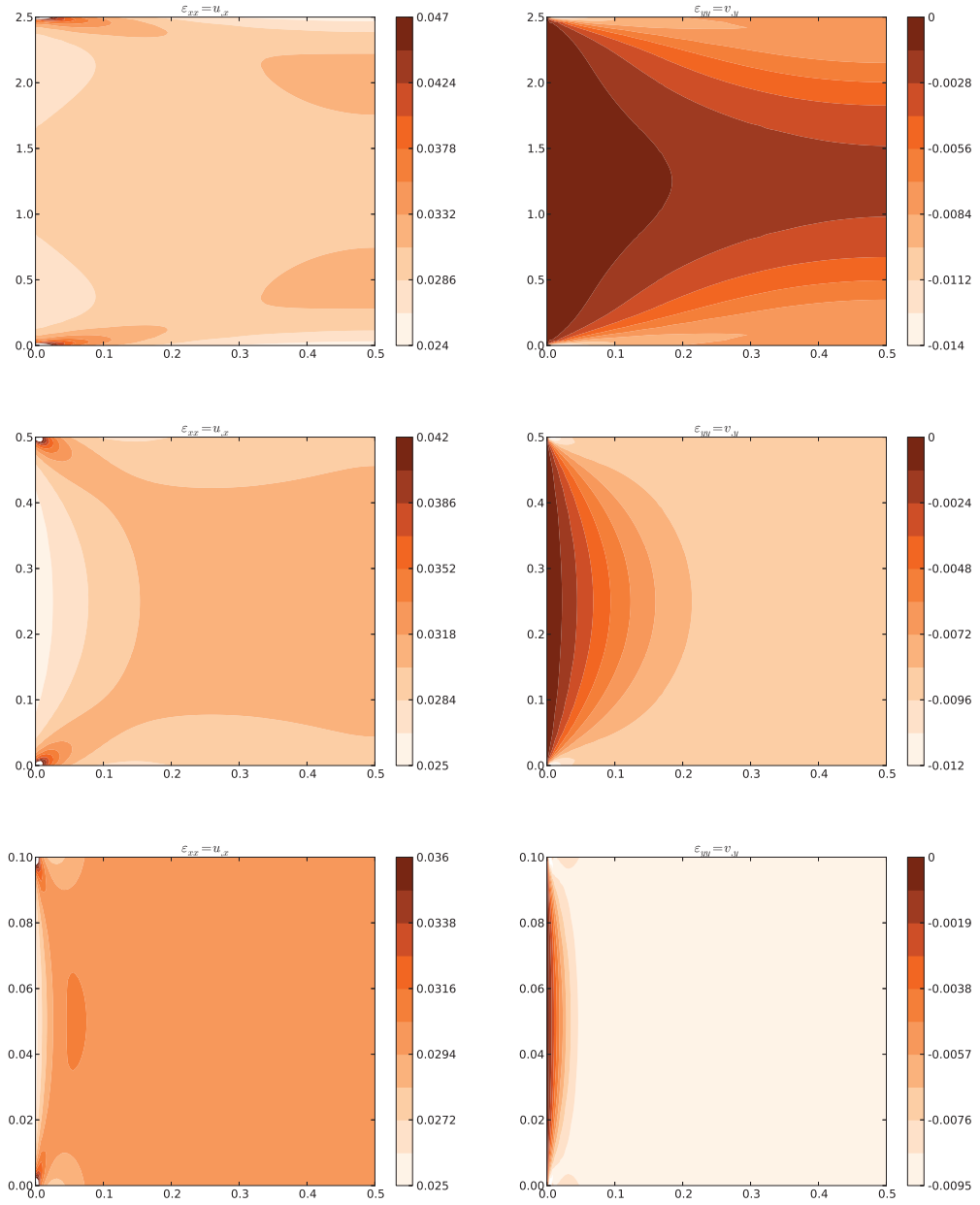

Figure 17: Axial strains ε_{xx} and ε_{yy}. Isotropic, $U_{\text{in}} = 0$ (linear reference). *Top to bottom:* $b = 2.5,\ 0.5,\ 0.1\,m$ ($\ell/b = 1/5,\ 1,\ 5$).

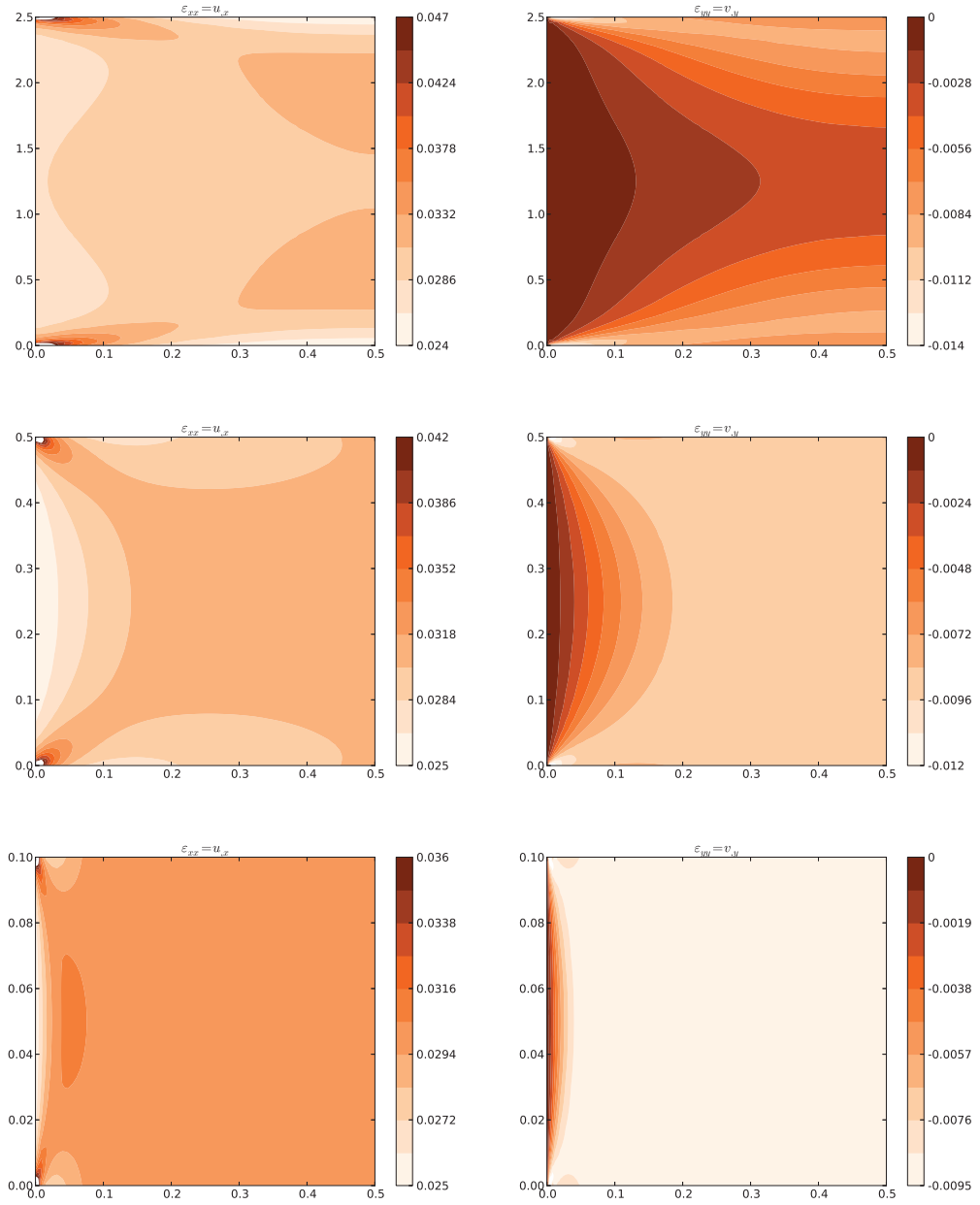

Figure 18: Axial strains ε_{xx} and ε_{yy}. Isotropic, $U_{\text{in}} = 50$ m/s (representative). *Top to bottom:* $b = 2.5,\ 0.5,\ 0.1\,m$ ($\ell/b = 1/5,\ 1,\ 5$).

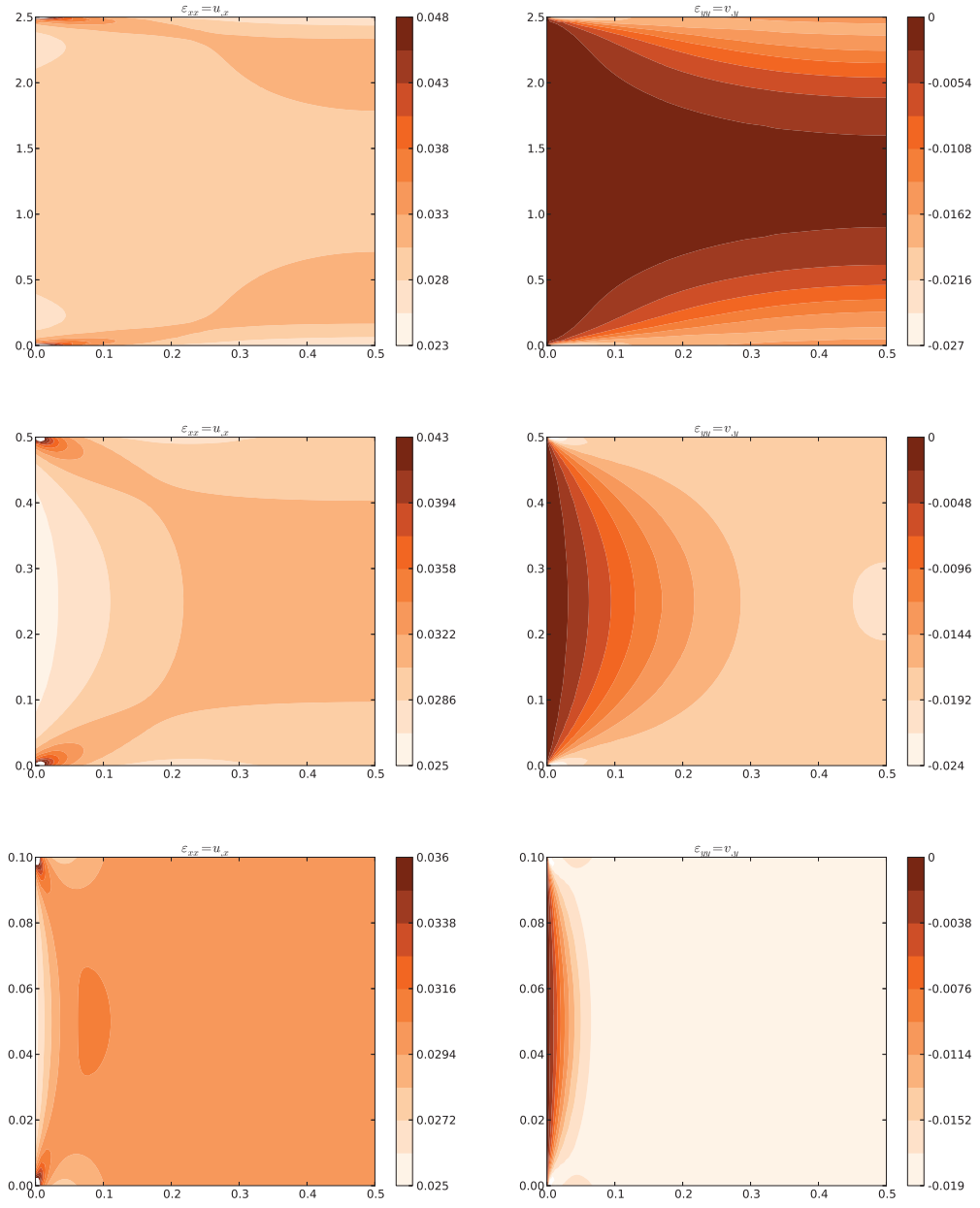

Figure 19: Axial strains ε_{xx} and ε_{yy}. Orthotropic, $U_{\text{in}} = 0$ (linear reference). *Top to bottom:* $b = 2.5,\ 0.5,\ 0.1\,m$ ($\ell/b = 1/5,\ 1,\ 5$).

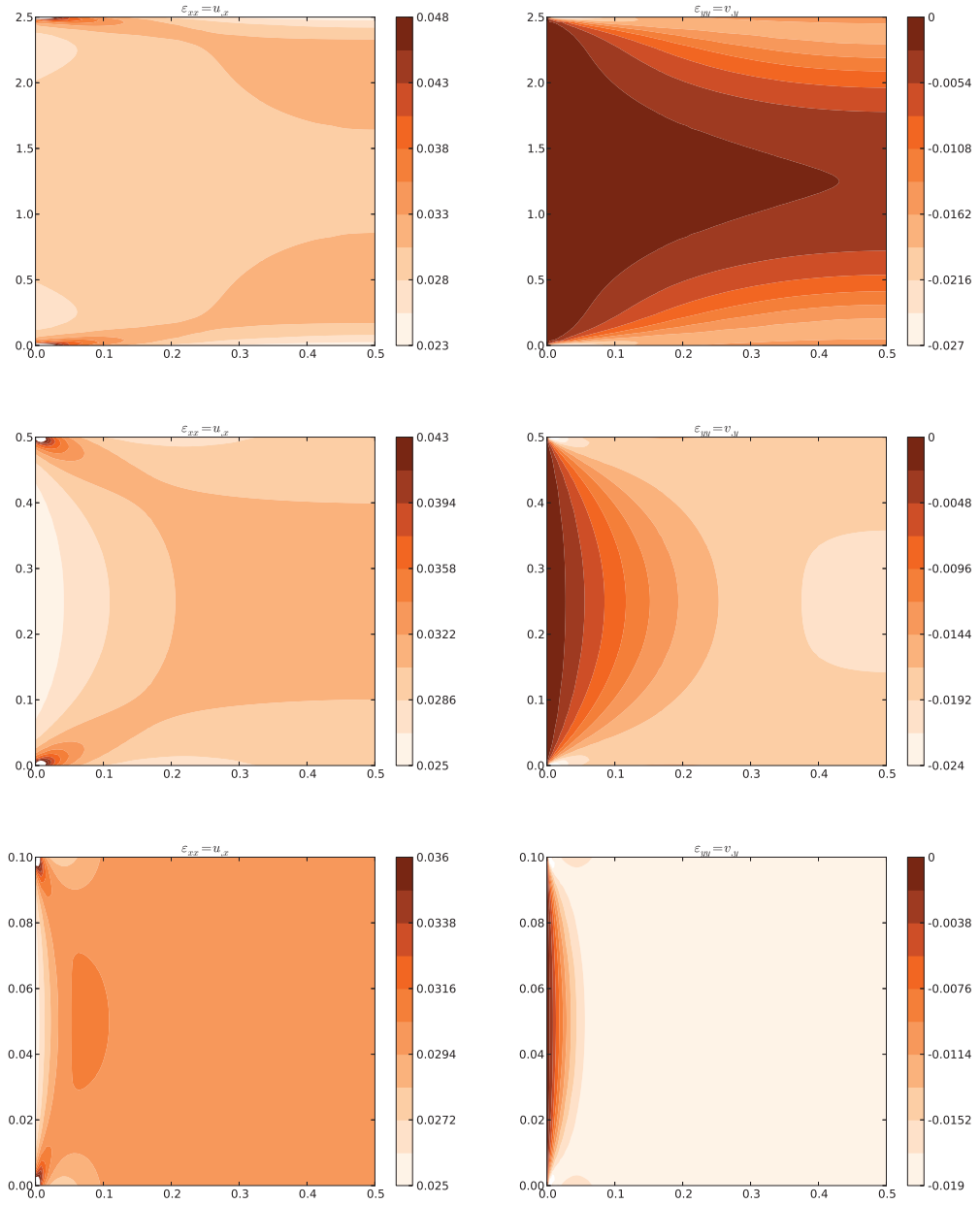

Figure 20: Axial strains ε_{xx} and ε_{yy}. Orthotropic, $U_{\text{in}} = 50$ m/s (representative). *Top to bottom:* $b = 2.5,\ 0.5,\ 0.1\,m$ ($\ell/b = 1/5,\ 1,\ 5$).

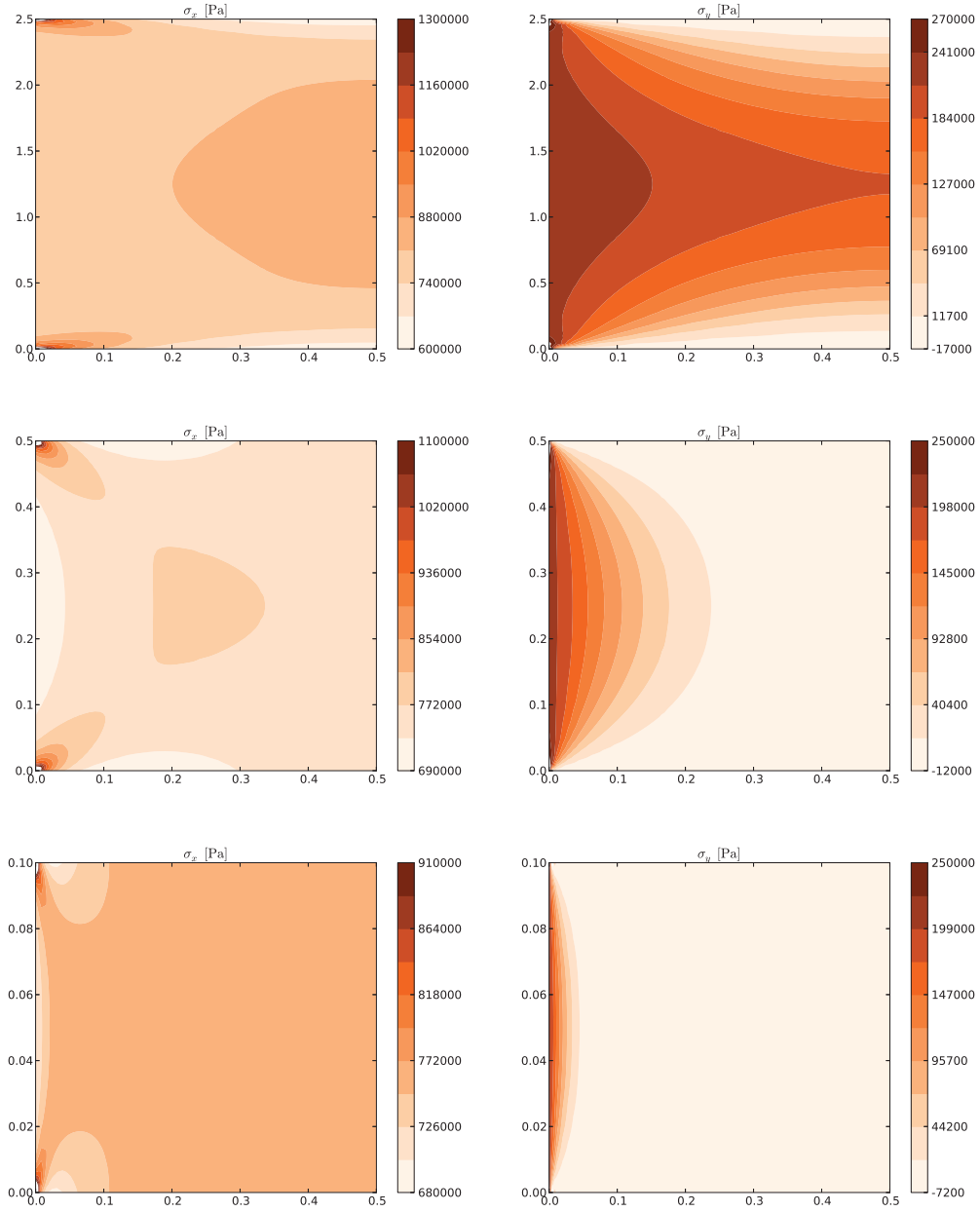

Figure 21: Axial stresses σ_{xx} and σ_{yy}. Isotropic, $U_{\text{in}} = 0$ (linear reference). *Top to bottom:* $b = 2.5,\ 0.5,\ 0.1\,m$ ($\ell/b = 1/5,\ 1,\ 5$).

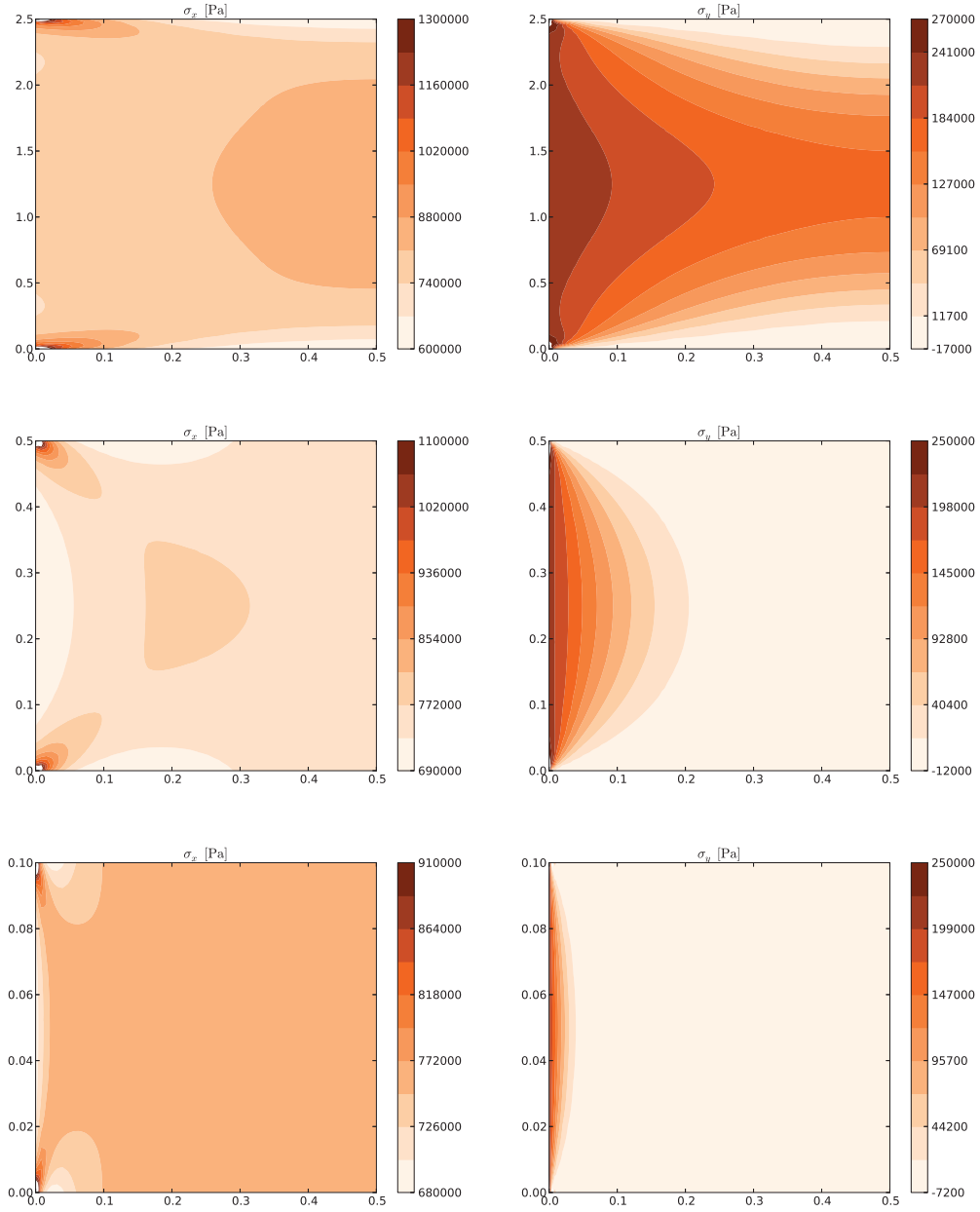

Figure 22: Axial stresses σ_{xx} and σ_{yy}. Isotropic, $U_{\text{in}} = 50$ m/s (representative). *Top to bottom:* $b = 2.5,\ 0.5,\ 0.1\,m$ ($\ell/b = 1/5,\ 1,\ 5$).

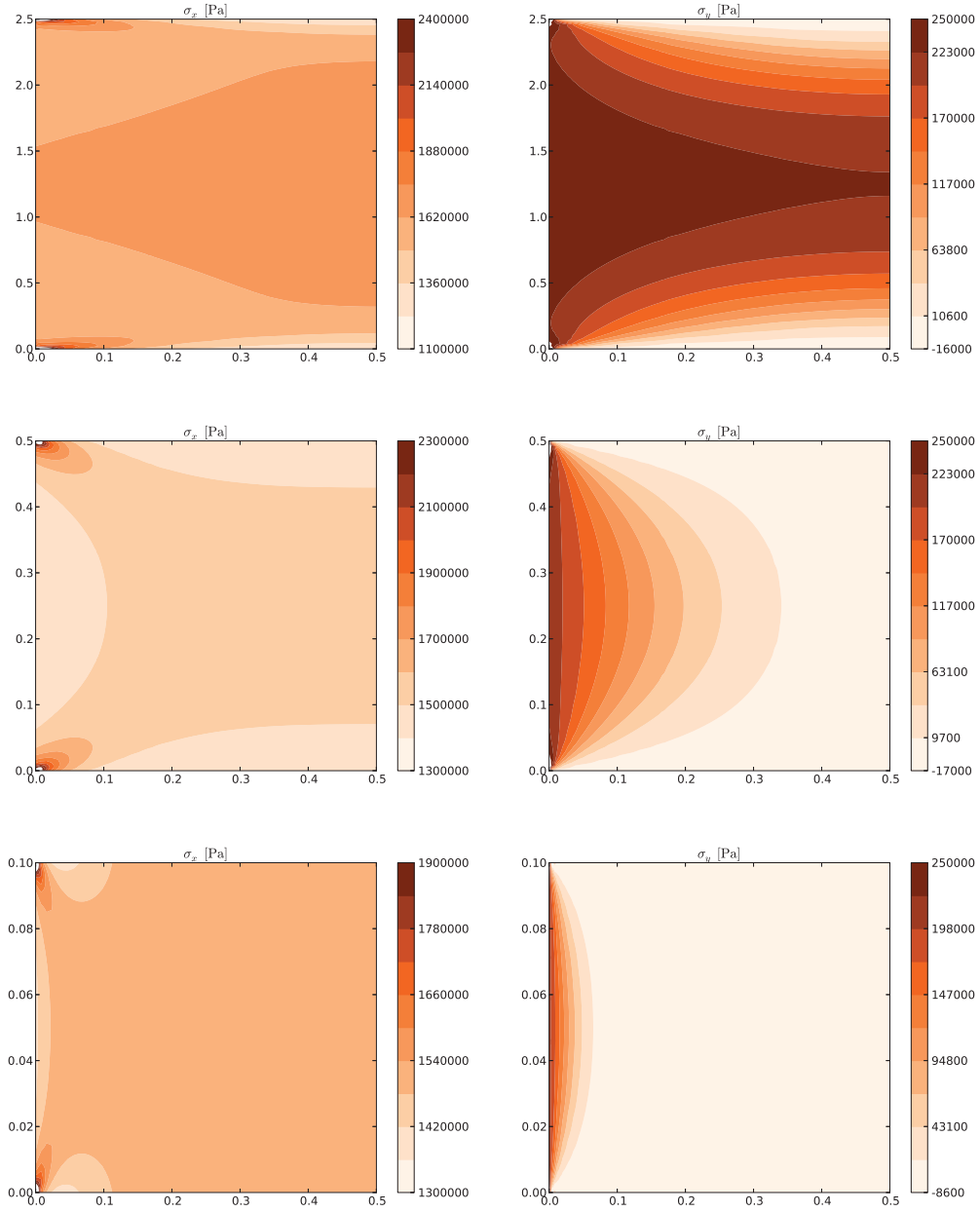

Figure 23: Axial stresses σ_{xx} and σ_{yy}. Orthotropic, $U_{\text{in}} = 0$ (linear reference). *Top to bottom:* $b = 2.5,\ 0.5,\ 0.1\,m$ ($\ell/b = 1/5,\ 1,\ 5$).

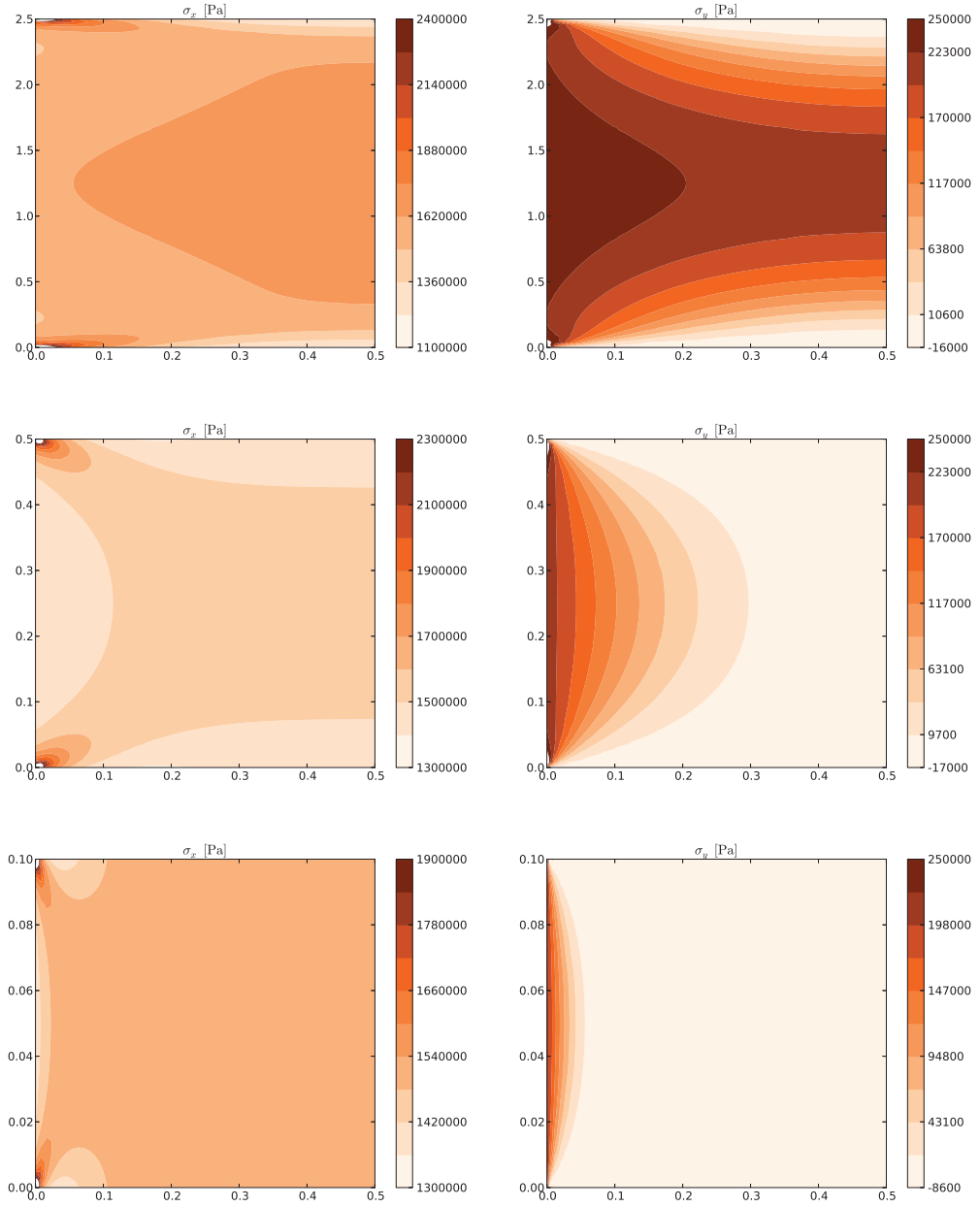

Figure 24: Axial stresses σ_{xx} and σ_{yy}. Orthotropic, $U_{\text{in}} = 50$ m/s (representative). *Top to bottom:* $b = 2.5,\ 0.5,\ 0.1\,m$ ($\ell/b = 1/5,\ 1,\ 5$).

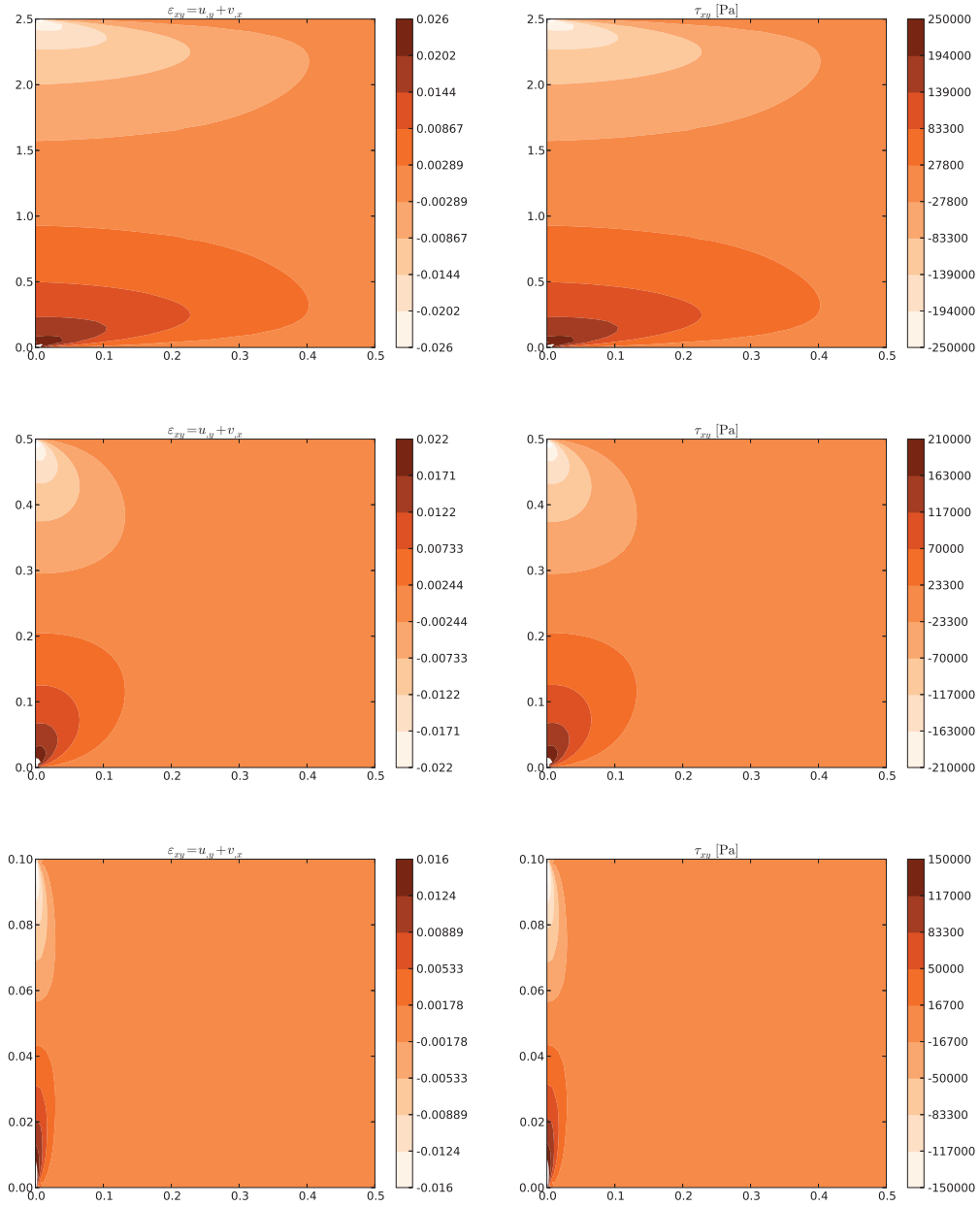

Figure 25: Shear strain γ_{xy} and shear stress τ_{xy}. Isotropic, $U_{\text{in}} = 0$ (linear reference). *Top to bottom:* $b = 2.5,\ 0.5,\ 0.1\,m$ ($\ell/b = 1/5,\ 1,\ 5$).

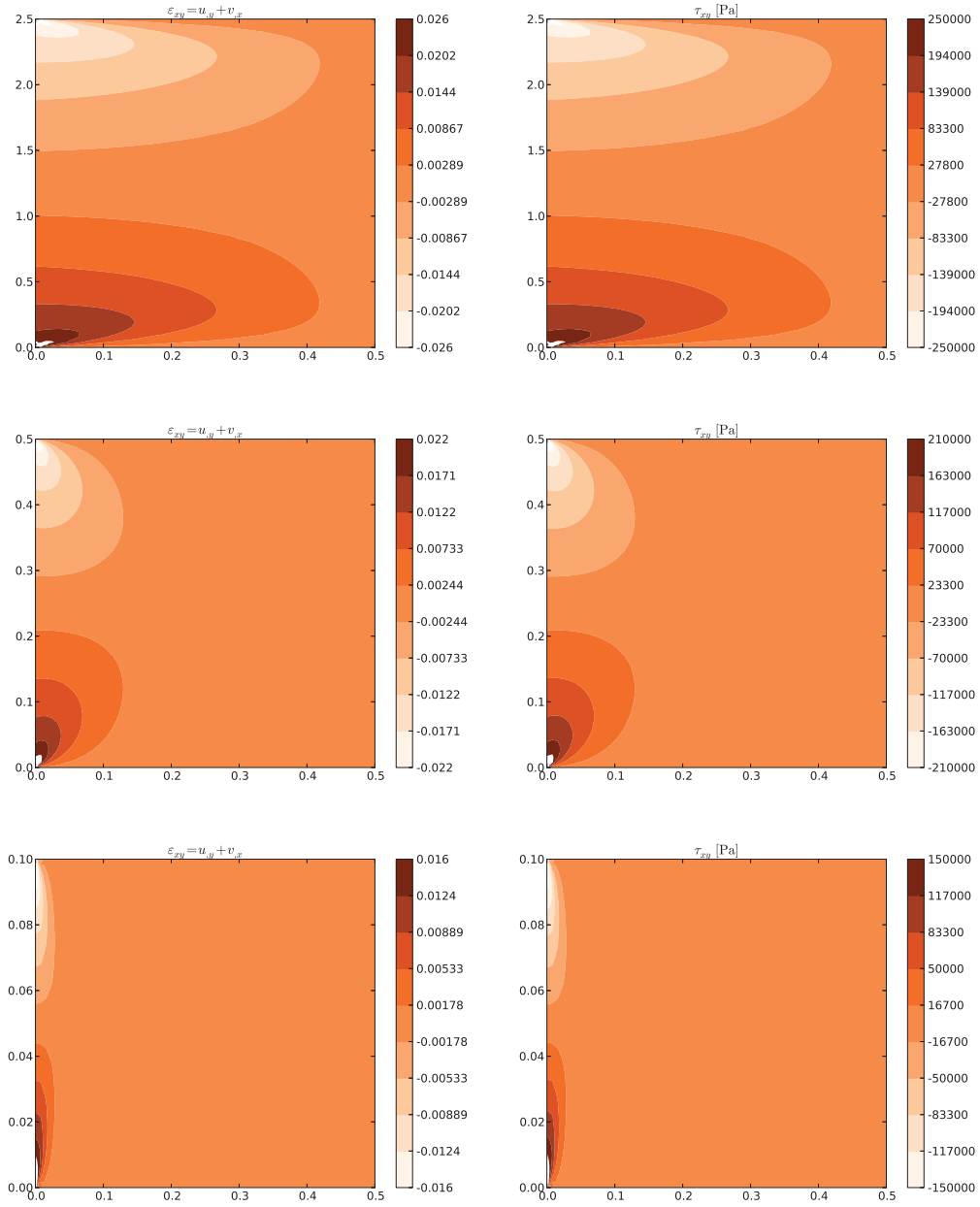

Figure 26: Shear strain γ_{xy} and shear stress τ_{xy}. Isotropic, $U_{\text{in}} = 50$ m/s (representative). *Top to bottom:* $b = 2.5,\ 0.5,\ 0.1\,m$ ($\ell/b = 1/5,\ 1,\ 5$).

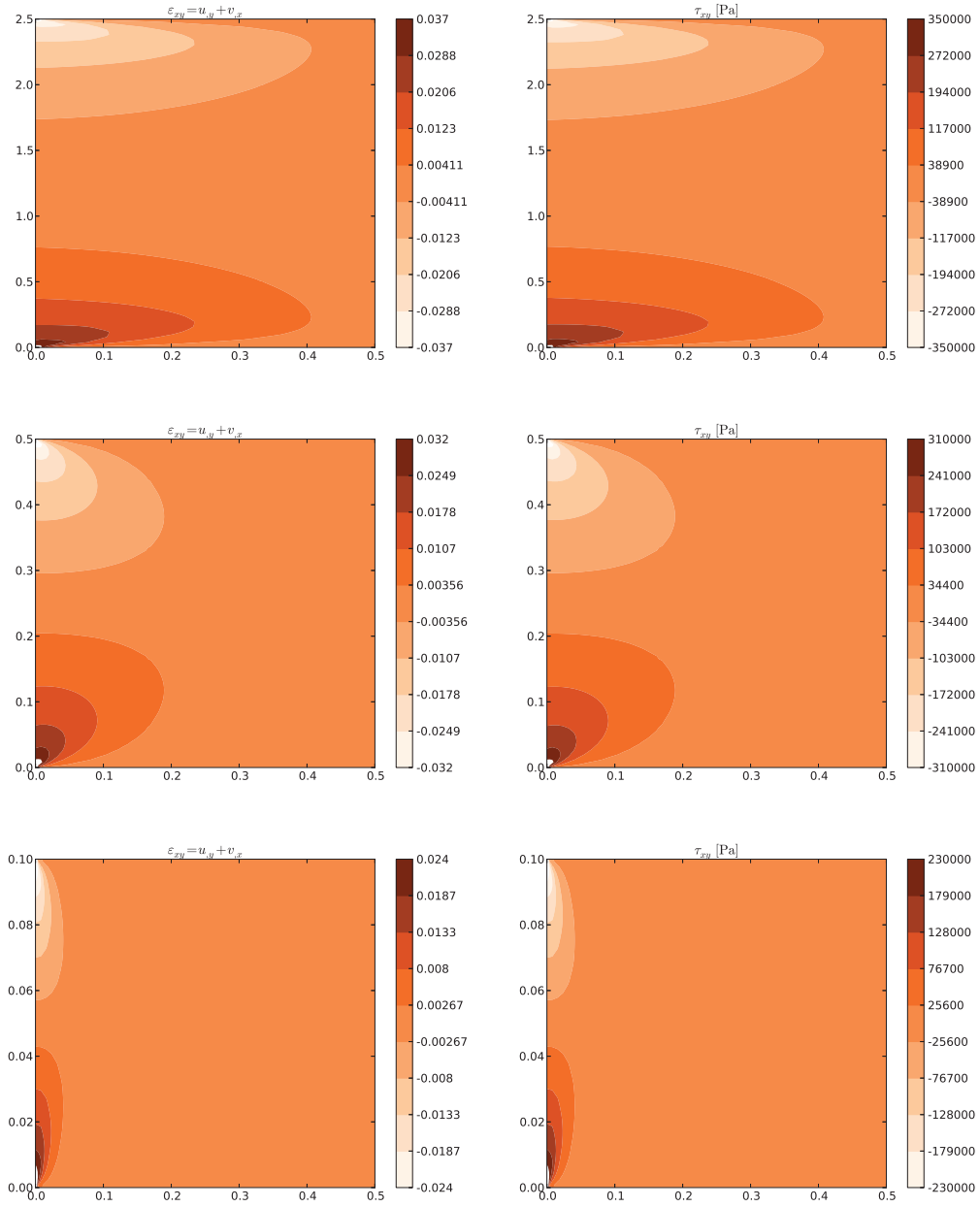

Figure 27: Shear strain γ_{xy} and shear stress τ_{xy}. Orthotropic, $U_{\text{in}} = 0$ (linear reference). *Top to bottom:* $b = 2.5,\ 0.5,\ 0.1\,m$ ($\ell/b = 1/5,\ 1,\ 5$).

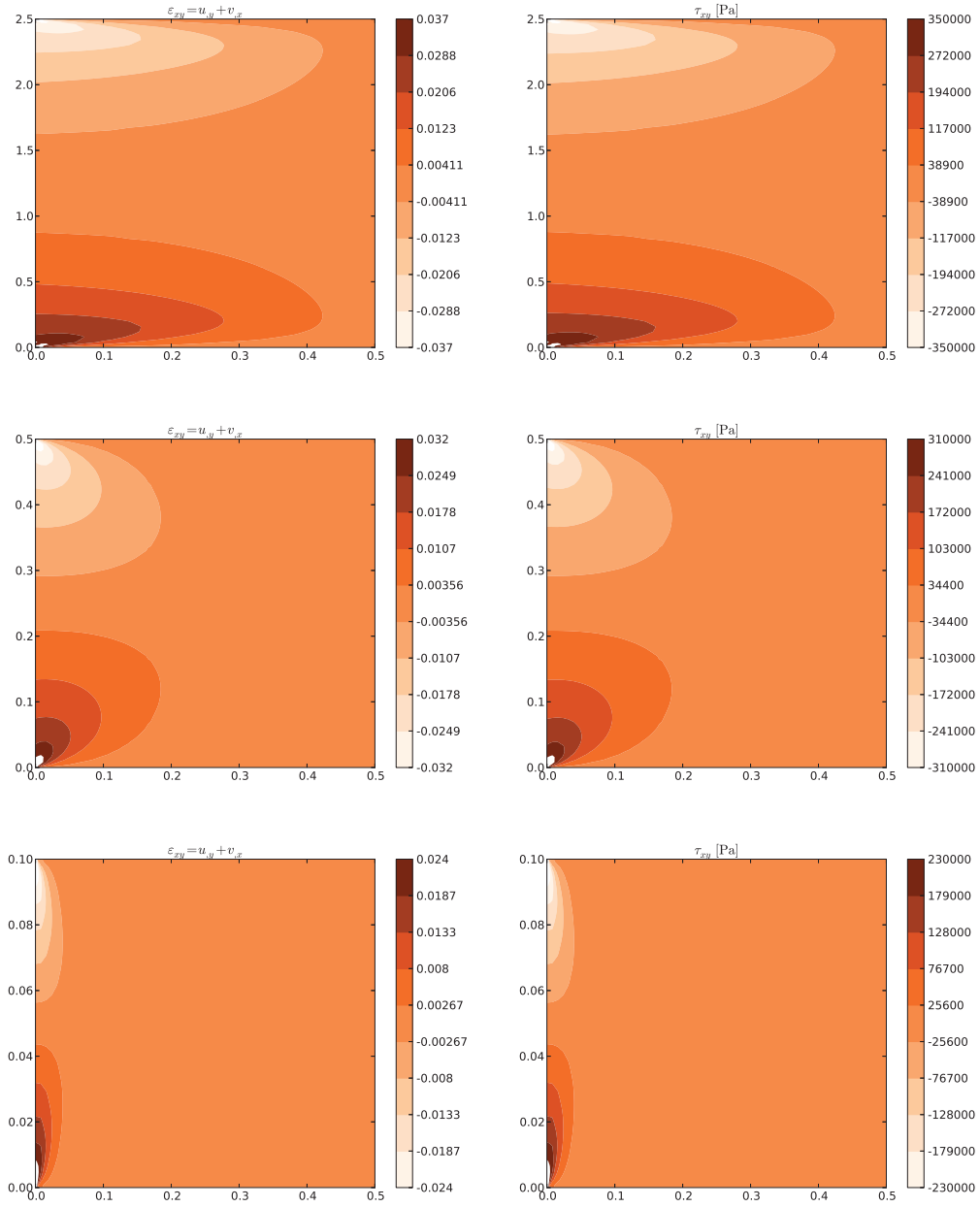

Figure 28: Shear strain γ_{xy} and shear stress τ_{xy}. Orthotropic, $U_{\text{in}} = 50$ m/s (representative). *Top to bottom:* $b = 2.5,\ 0.5,\ 0.1\,m$ ($\ell/b = 1/5,\ 1,\ 5$).

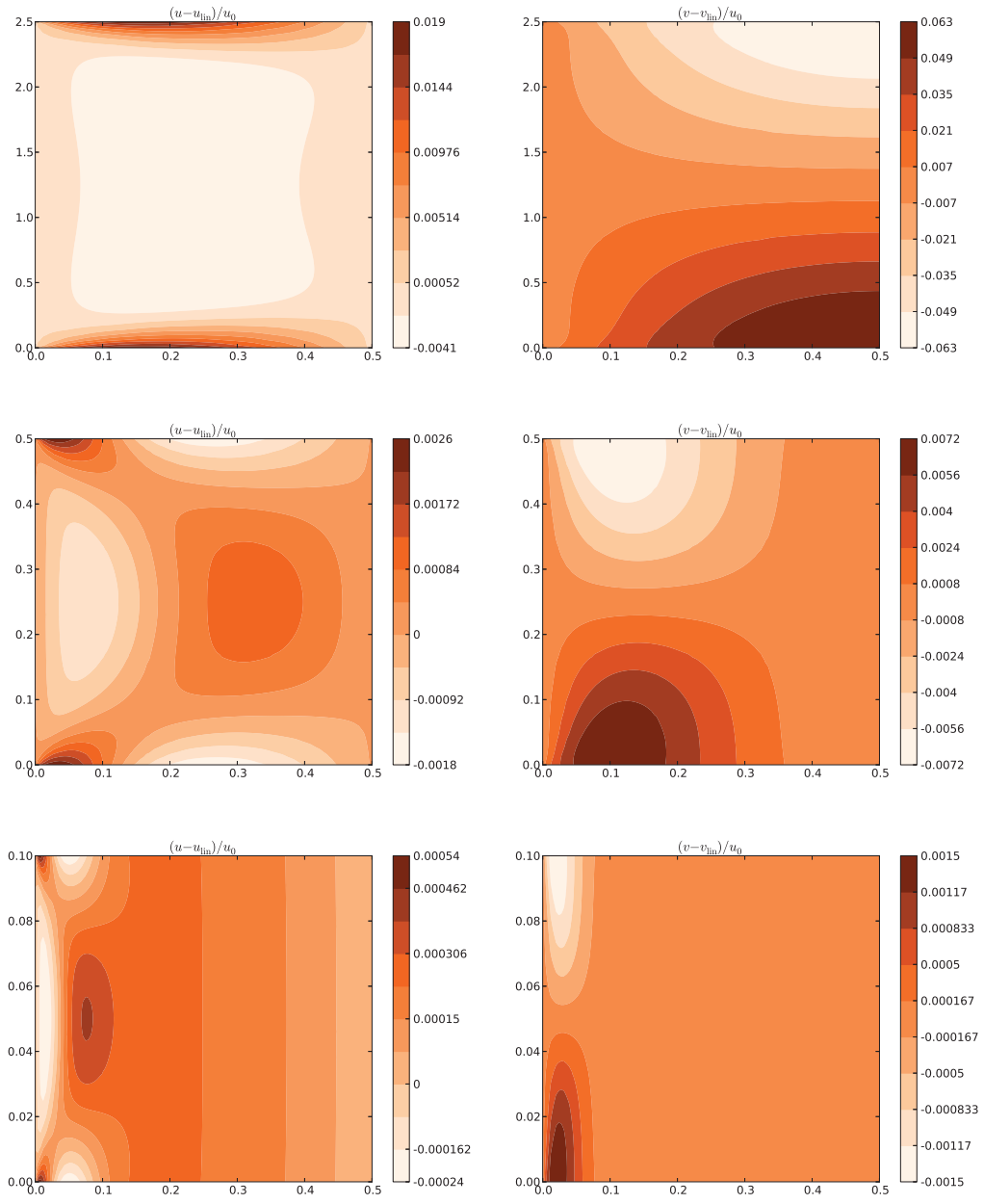

Figure 29: Nonlinear contribution to displacements, normalized to u_{f}. Isotropic, $U_{\mathrm{in}} = 50$ m/s (representative). *Top to bottom:* $b = 2.5,\ 0.5,\ 0.1\,m$ ($\ell/b = 1/5,\ 1,\ 5$).

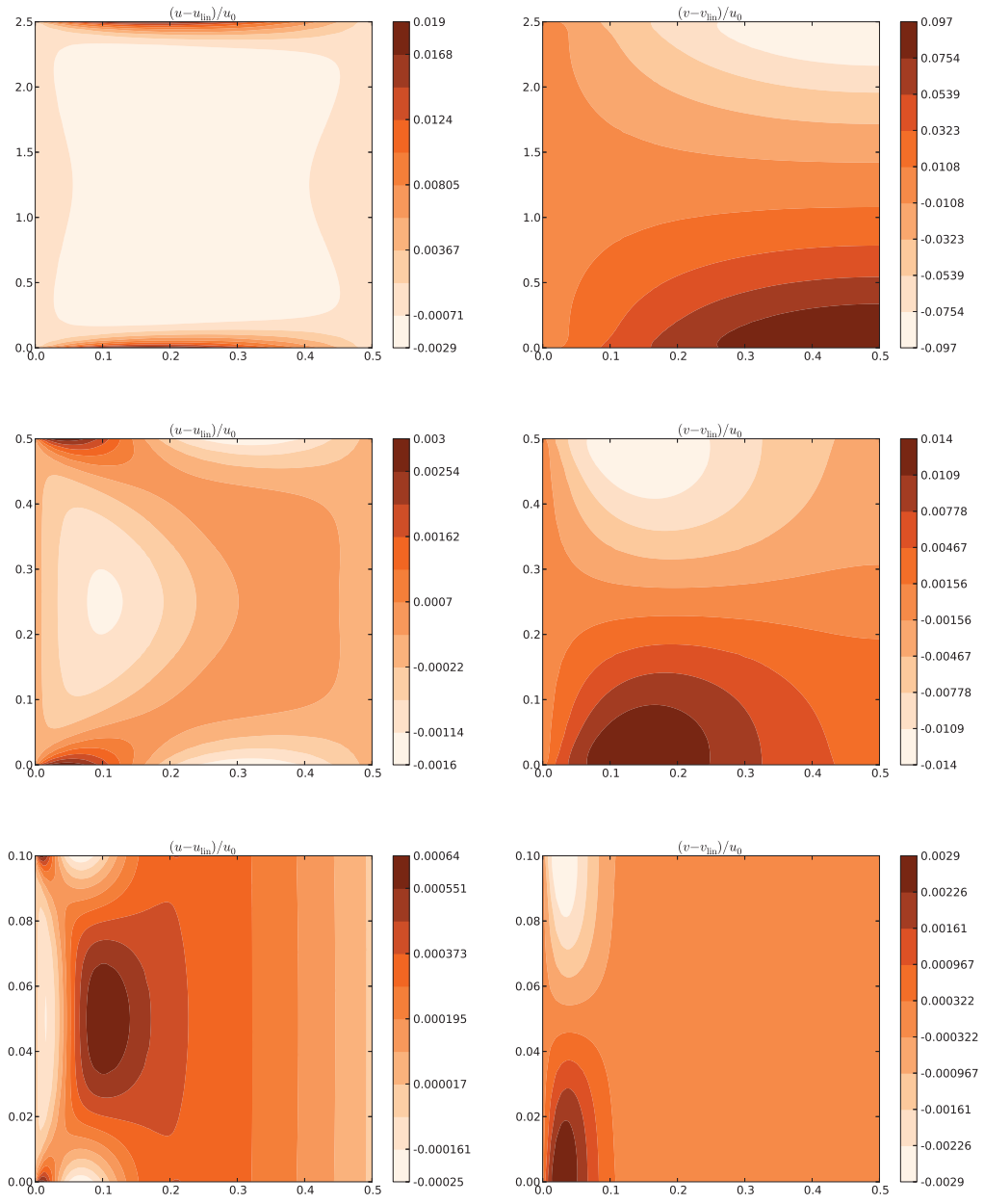

Figure 30: Nonlinear contribution to displacements, normalized to u_{f}. Orthotropic, $U_{\mathrm{in}} = 50$ m/s (representative). *Top to bottom:* $b = 2.5,\ 0.5,\ 0.1\,m$ ($\ell/b = 1/5,\ 1,\ 5$).

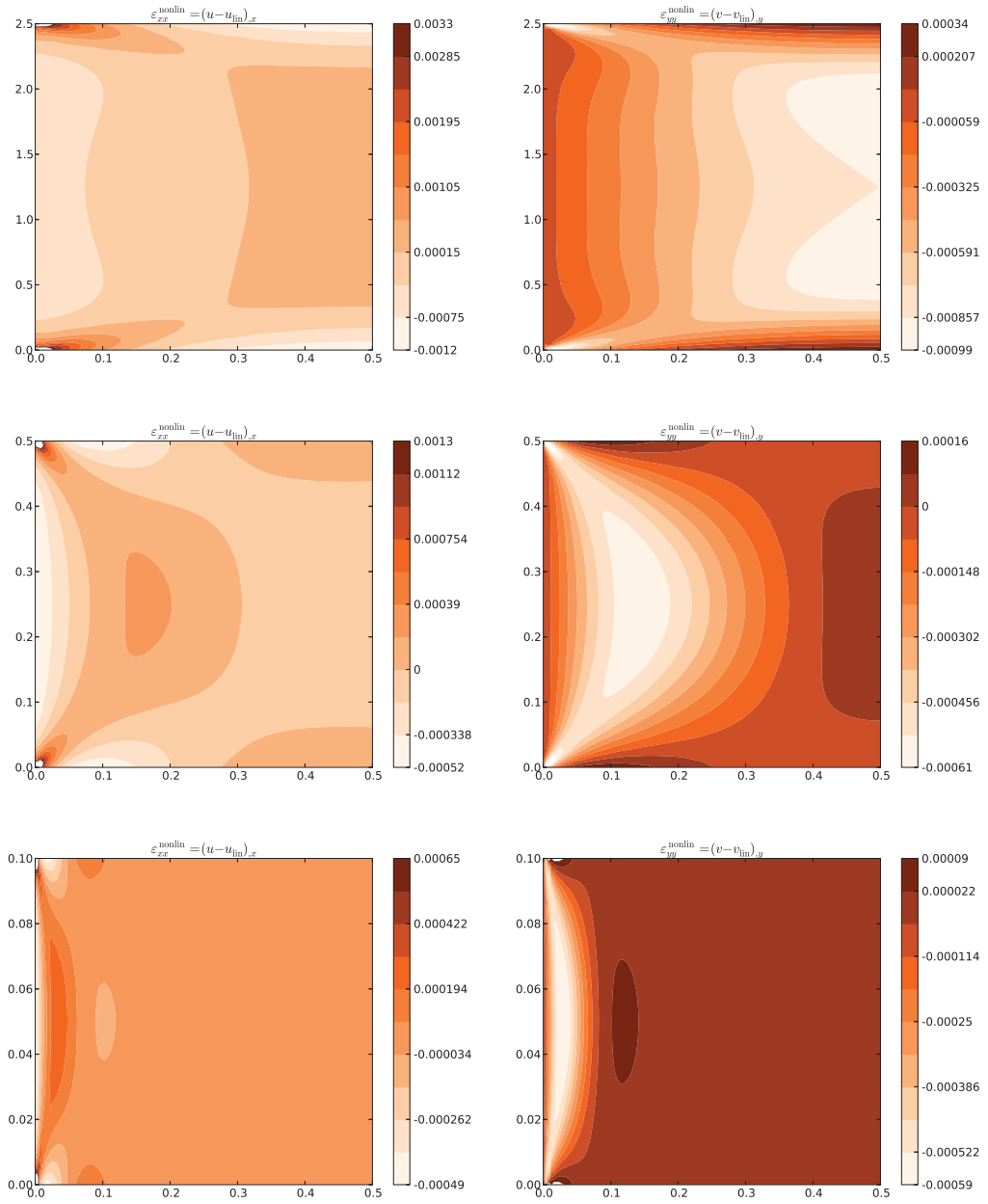

Figure 31: Nonlinear contribution to axial strains. Isotropic, $U_{\text{in}} = 50$ m/s (representative). *Top to bottom:* $b = 2.5,\ 0.5,\ 0.1\,m$ ($\ell/b = 1/5,\ 1,\ 5$).

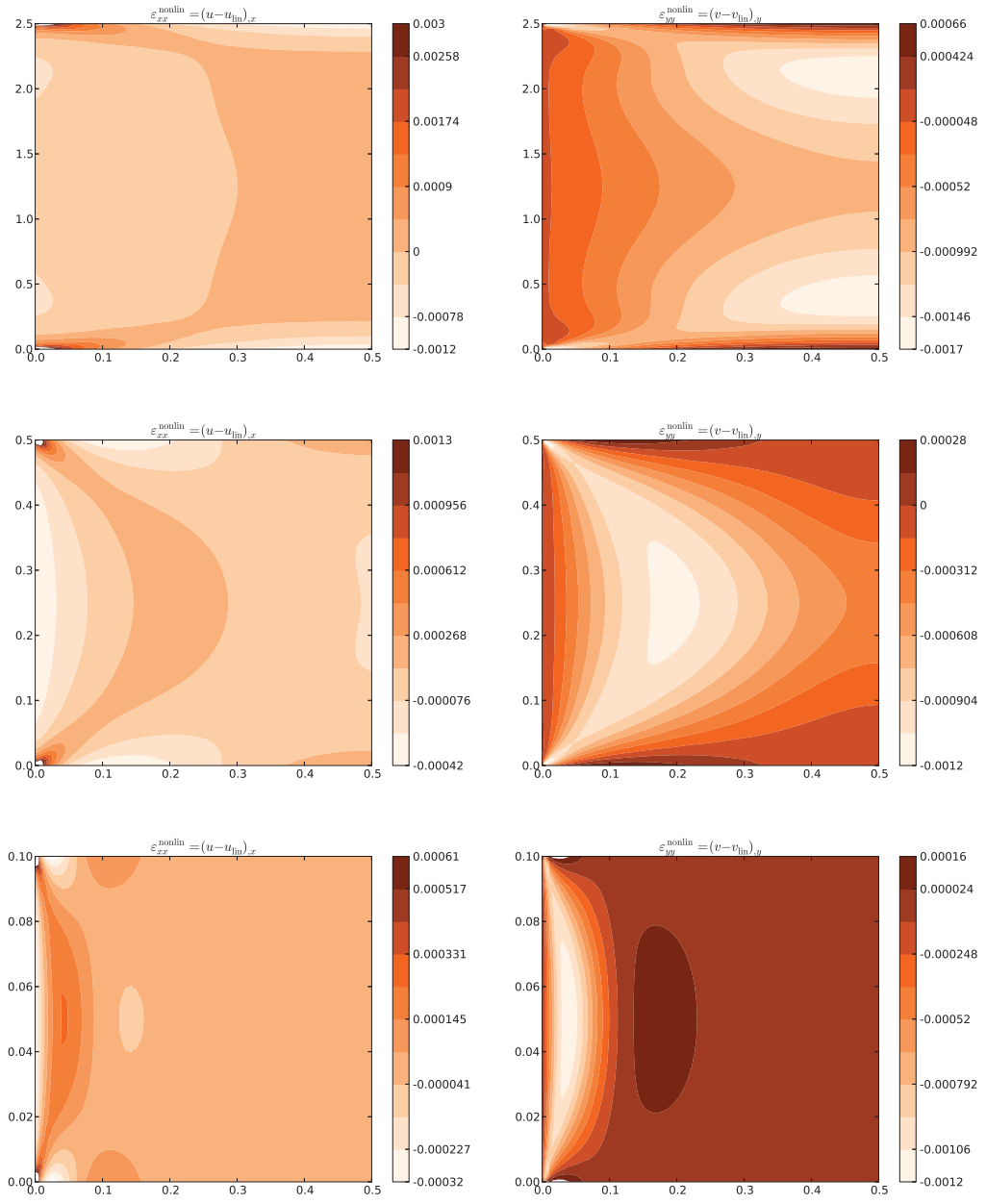

Figure 32: Nonlinear contribution to axial strains. Orthotropic, $U_{\text{in}} = 50$ m/s (representative). *Top to bottom:* $b = 2.5,\ 0.5,\ 0.1\,m$ ($\ell/b = 1/5,\ 1,\ 5$).

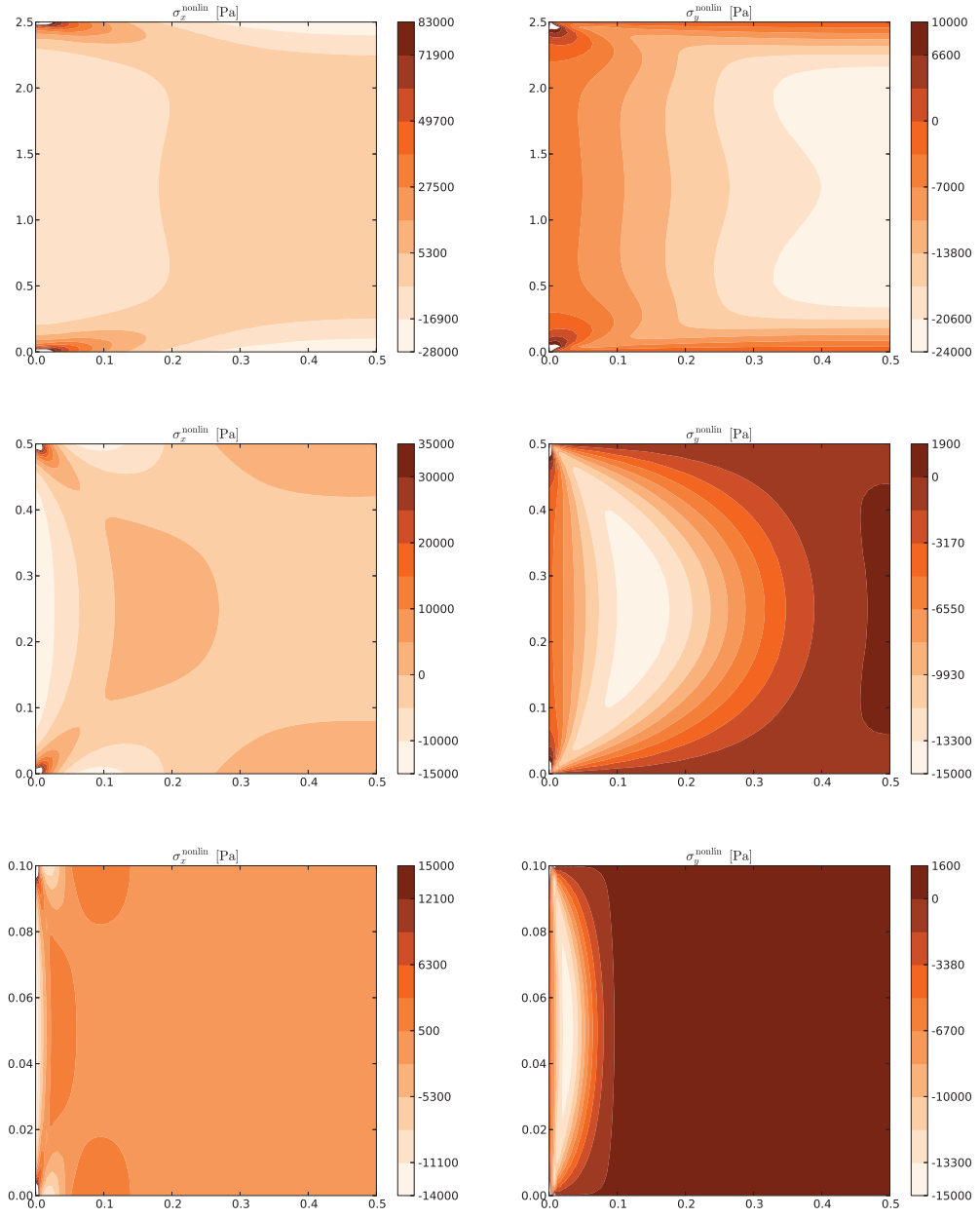

Figure 33: Nonlinear contribution to axial stresses. Isotropic, $U_{\text{in}} = 50$ m/s (representative). *Top to bottom:* $b = 2.5,\ 0.5,\ 0.1\,m$ ($\ell/b = 1/5,\ 1,\ 5$).

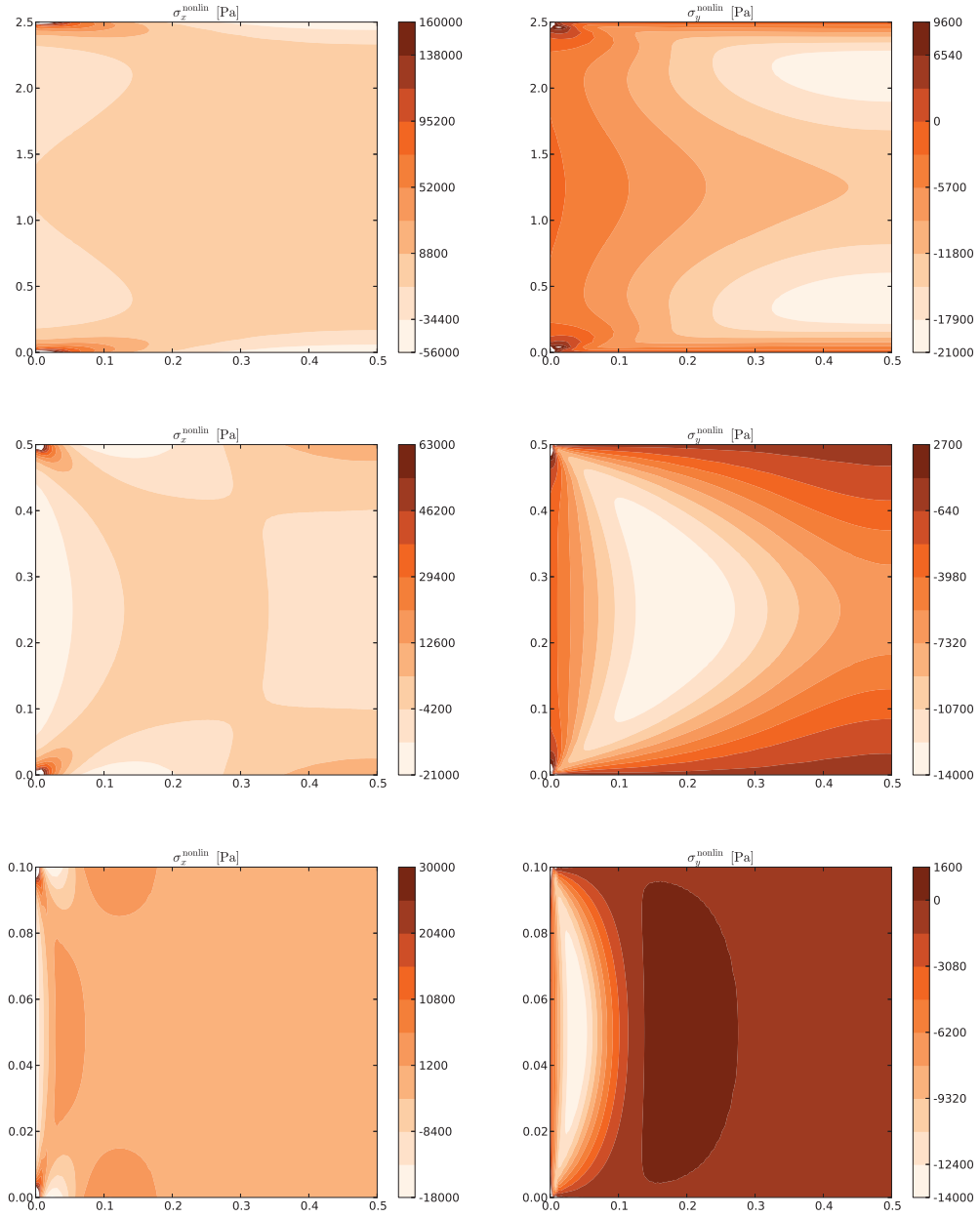

Figure 34: Nonlinear contribution to axial stresses. Orthotropic, $U_{\text{in}} = 50$ m/s (representative). *Top to bottom:* $b = 2.5,\ 0.5,\ 0.1\,m$ ($\ell/b = 1/5,\ 1,\ 5$).

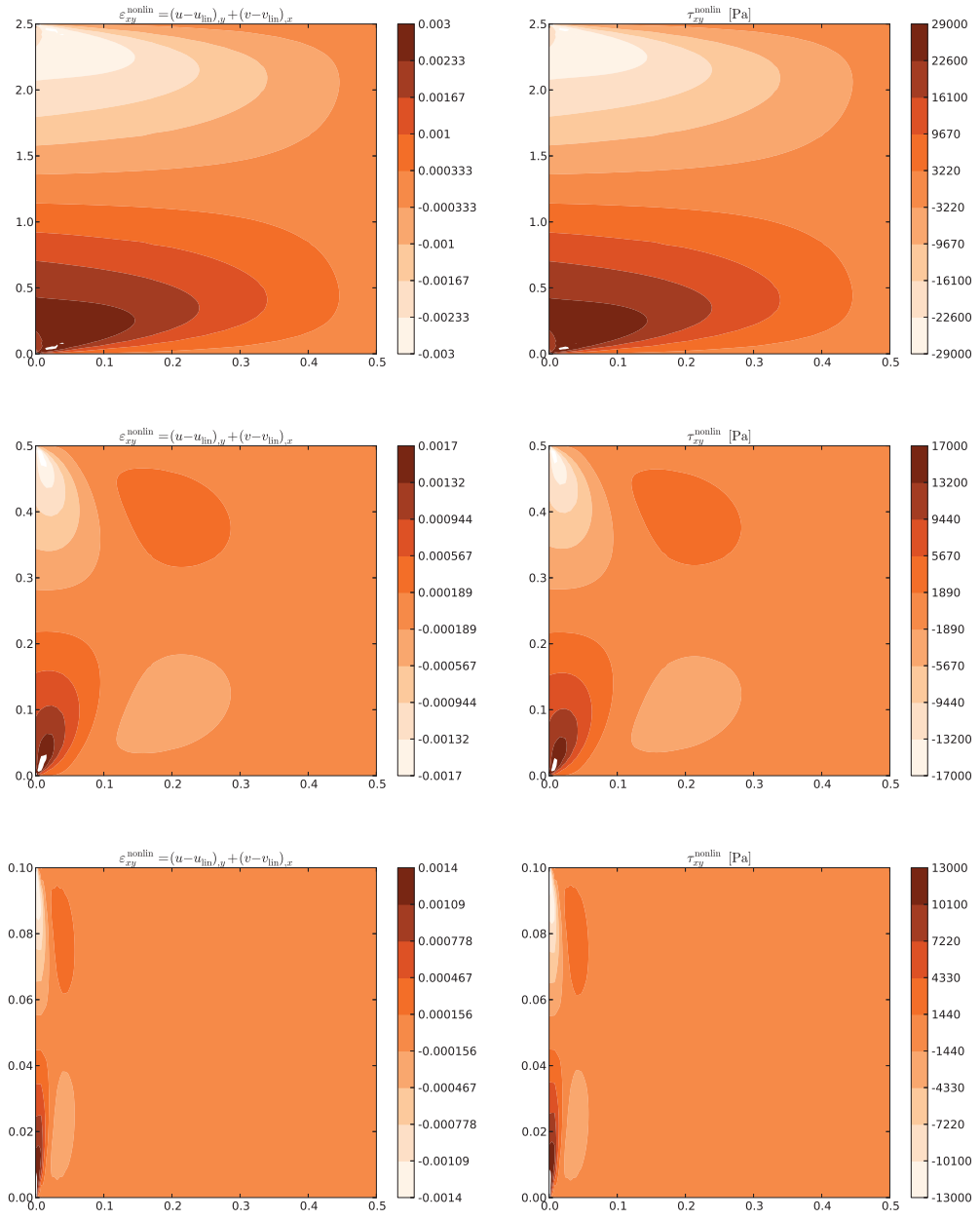

Figure 35: Nonlinear contribution to shear strain and shear stress. Isotropic, $U_{\text{in}} = 50$ m/s (representative). *Top to bottom:* $b = 2.5,\ 0.5,\ 0.1\,m$ ($\ell/b = 1/5,\ 1,\ 5$).

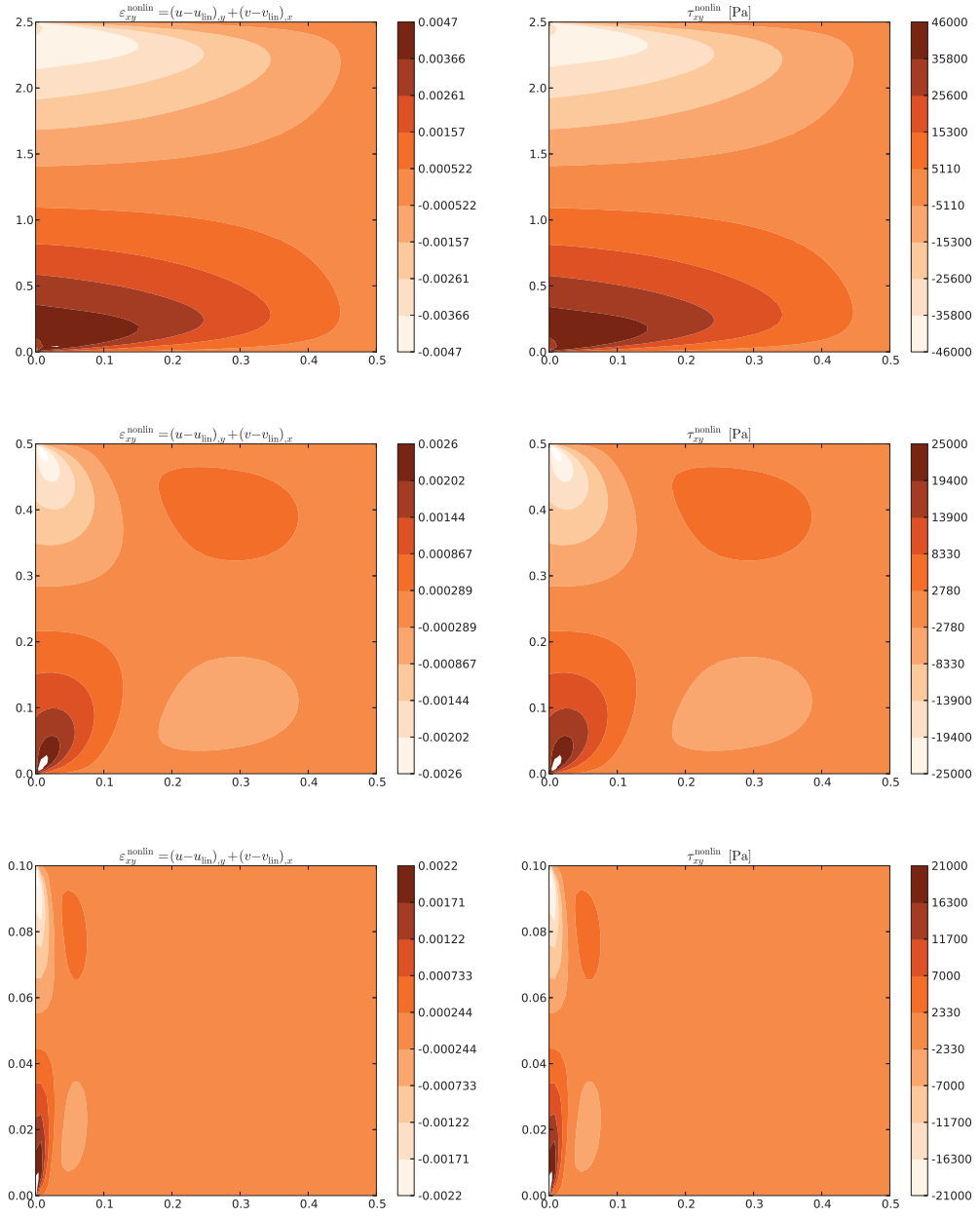

Figure 36: Nonlinear contribution to shear strain and shear stress. Orthotropic, $U_{\text{in}} = 50$ m/s (representative). *Top to bottom:* $b = 2.5,\ 0.5,\ 0.1\,m$ ($\ell/b = 1/5,\ 1,\ 5$).

9 Conclusion

The analysis performed gives new insights to the modelling of axially moving continuous materials. Fundamentally, the model used is comparable to fluid flow models (Navier–Stokes), where the velocity is the main variable to be calculated. Similarly, the fundamental variable here, displacement, can be understood as a steady-state "Eulerian snapshot" from the moving continuum. It must be noted that the velocity levels used in the model are assumed to affect the in-plane flow of the material "as such", without the loss of stability or deflections in the out-of-plane direction [4, 9, 53]. The full time-dependent model also includes terms comparable with Newtonian viscosity. Standard viscosity of Newtonian fluids is defined using viscosity and velocity gradient (in the x-direction):

$$\tau = \mu \frac{\partial U_x}{\partial y}, \tag{112}$$

where μ is fluid viscosity. Studying the equations (36) and (37), there are terms dependent only on the web material viscosity Π. It is possible to write following for partial shear stresses τ_1 and τ_2:

$$\frac{\partial \tau_1}{\partial y} = \Pi \frac{\partial^3 u}{\partial y^2 \partial t} \qquad \text{and} \qquad \frac{\partial \tau_2}{\partial x} = \Pi \frac{\partial^3 v}{\partial x^2 \partial t} \tag{113}$$

Equation (113) can be rewritten as an 'Eulerian' viscosity law for shear stress dependent on the web viscosity, displacement gradient and time:

$$\tau_1 = \Pi \frac{\partial}{\partial t} \frac{\partial u}{\partial y} \qquad \text{and} \qquad \tau_2 = \Pi \frac{\partial}{\partial t} \frac{\partial v}{\partial x} \tag{114}$$

It is noticeable that equation (113) does not include the transport velocity itself and must be defined separately in both in-plane directions.

The presented two-dimensional model makes possible to study elastic two-dimensional strain distribution of moving continua. One key finding is that inertial effects cause additional contraction on top of the contraction already observed for a stationary material.

The model presented is always nonlinear. The reason for this is that due to mass conservation and the behaviour of free edges, the total material velocity $\mathbf{U}$ is dependent on the displacement $\mathbf{u}$, which further is dependent on the same in-plane velocity.

If the material is assumed ideal linear-elastic, the one-dimensional moving web model will produce constant strain, similarly to linear elastic stationary models. However, in reality, there is always some degree of viscous properties in all materials, and therefore with moving webs, the constant strain approach is not possible.

The limitations of the present study are also apparent. The model was studied in a steady state, which does not allow for temporal variations in the flowing medium preceding the observation span under study. To include such effects, a time-dependent formulation must be used.

Also, from a physical viewpoint, the use of Dirichlet boundary conditions in two-dimensional web handling models is problematic. In a two-dimensional model, there is no dimension in the thickness direction. Thus, the Dirichlet boundary conditions affect the whole thickness of the web, even though in reality all web handling systems are based on surface traction. In the interior of the web, the actual axial displacement will differ from the value set by the Dirichlet boundary condition, which in physical terms represents a prescribed displacement at the surface. Therefore, more realistic two-dimensional web continuum models should be based on Neumann or Robin boundary conditions with finite thickness modelling.

A logical future step to continue along the present line of study would be to consider the effects viscoelasticity also in the two-dimensional case, since the web velocity and viscous properties are closely connected with each other [35].

Acknowledgments

This research was supported by the Finnish Cultural Foundation. The authors would like to thank prof. Reijo Kouhia for pointing out the identity (65).

References

[1] F. R. Archibald and A. G. Emslie. The vibration of a string having a uniform motion along its length. *ASME Journal of Applied Mechanics*, 25:347–348, 1958.

[2] N. Banichuk, S. Ivonova, M. Kurki, T. Saksa, M. Tirronen, and T. Tuovinen. Safety analysis and optimization of travelling webs subjected to fracture and instability. In S. Repin, T. Tiihonen, and T. Tuovinen, editors, *Numerical methods for differential equations, optimization, and technological problems. Dedicated to Professor P. Neittaanmäki on his 60th Birthday*, volume 27 of *Computational Methods in Applied Sciences*, pages 379–392. Springer Netherlands, 2013. ISBN: 978-94-007-5287-0 (Print) 978-94-007-5288-7 (Online).

[3] N. Banichuk, J. Jeronen, M. Kurki, P. Neittaanmäki, T. Saksa, and T. Tuovinen. On the limit velocity and buckling phenomena of axially moving orthotropic membranes and plates. *International Journal of Solids and Structures*, 48(13):2015–2025, 2011.

[4] N. Banichuk, J. Jeronen, P. Neittaanmäki, and T. Tuovinen. On the instability of an axially moving elastic plate. *International Journal of Solids and Structures*, 47(1):91–99, 2010.

[5] N. Banichuk, J. Jeronen, P. Neittaanmäki, and T. Tuovinen. Static instability analysis for travelling membranes and plates interacting with axially moving ideal fluid. *Journal of Fluids and Structures*, 26(2):274–291, 2010.

[6] N. Banichuk, J. Jeronen, P. Neittaanmäki, and T. Tuovinen. Dynamic behaviour of an axially moving plate undergoing small cylindrical deformation submerged in axially flowing ideal fluid. *Journal of Fluids and Structures*, 27(7):986–1005, 2011.

[7] G. A. Baum, D. C. Brennan, and C. C Habeger. Orthotropic elastic constants of paper. *Tappi Journal*, 64(8):97–101, 1981.

[8] J. Castro and M. Ostoja-Starzewski. Elasto-plasticity of paper. *International Journal of Plasticity*, (19):2083–2098, 2003.

[9] Y. B. Chang and P. M. Moretti. Interaction of fluttering webs with surrounding air. *TAPPI Journal*, 74(3):231–236, 1991.

[10] L.-Q. Chen, H. Chen, and C.W. Lim. Asymptotic analysis of axially accelerating viscoelastic strings. *International Journal of Engineering Science*, 46(10):976 – 985, 2008. DOI: 10.1016/j.ijengsci.2008.03.009.

[11] L.-Q. Chen and H. Ding. Steady-state transverse response in coupled planar vibration of axially moving viscoelastic beams. *ASME Journal of Vibrations and Acoustics*, 132:011009–1–9, 2010. http://dx.doi.org/10.1115/1.4000468.

[12] L.-Q. Chen and B. Wang. Stability of axially accelerating viscoelastic beams: asymptotic perturbation analysis and differential quadrature validation. *European Journal of Mechanics - A/Solids*, 28(4):786 – 791, 2009. DOI: 10.1016/j.euromechsol.2008.12.002.

[13] L.-Q. Chen and X.-D. Yang. Vibration and stability of an axially moving viscoelastic beam with hybrid supports. *European Journal of Mechanics - A/Solids*, 25(6):996 – 1008, 2006. DOI: 10.1016/j.euromechsol.2005.11.010.

[14] L.-Q. Chen and W.-J. Zhao. A numerical method for simulating transverse vibrations of an axially moving string. *Applied Mathematics and Computation*, 160(2):411 – 422, 2005. DOI: 10.1016/j.amc.2003.11.012.

[15] H. Ding and L.-Q. Chen. Stability of axially accelerating viscoelastic beams: multi-scale analysis with numerical confirmations. *European Journal of Mechanics - A/Solids*, 27(6):1108 – 1120, 2008. DOI: 10.1016/j.euromechsol.2007.11.014.

[16] Jean Donea and Antonio Huerta. *Finite Element Methods for Flow Problems*. Wiley, 2003. ISBN: 0-471-49666-9.

[17] Anna-Leena Erkkilä, Teemu Leppänen, and Jari Hämäläinen. Empirical plasticity models applied for paper sheets having different anisotropy and dry solids content levels. *Int. J. Solids Struct.*, in press, 2013.

[18] Wilhelm Flügge. *Viscoelasticity*. Springer-Verlag, New York, 2nd edition, 1975.

[19] R.-F. Fung, J.-S. Huang, and Y.-C. Chen. The transient amplitude of the viscoelastic travelling string: An integral constitutive law. *Journal of Sound and Vibration*, 201(2):153 – 167, 1997. DOI: 10.1006/jsvi.1996.0776.

[20] R.-F. Fung, J.-S. Huang, Y.-C. Chen, and C.-M. Yao. Nonlinear dynamic analysis of the viscoelastic string with a harmonically varying transport speed. *Computers & Structures*, 66(6):777 – 784, 1998. DOI: 10.1016/S0045-7949(98)00001-7.

[21] X. Guan, M. S. High, and D. A. Tree. Viscoelastic effects in modeling web handling systems: Steady-state analysis. *ASME Journal of Applied Mechanics*, 62(4):908–914, 1995. DOI: 10.1115/1.2789031.

[22] X. Guan, M. S. High, and D. A. Tree. Viscoelastic effects in modeling web handling systems: Unsteady-state analysis. *ASME Journal of Applied Mechanics*, 65(1):234–241, 1998. DOI: 10.1115/1.2789031.

[23] E. G. Hauptmann and K. A. Cutshall. Dynamic mechanical properties of wet paper webs. *Tappi Journal*, 60(10):106 – 108, 1977.

[24] H. Hilton and S. Yi. The significance of anisotropic viscoelastic poisson ratio stress and time dependencies. *Journal of Solids Structures*, 35(23):3081–3095, 1998.

[25] M. T. Huber. Die Grundlagen einer rationellen Berechnung der kreuzweise bewehrten Eisenbetonplatten. *Zeitschrift der Österreichische Ingeniur- und Architekten-Vereines*, 30:557–564, 1914.

[26] M. T. Huber. Die Theorie des kreuzweise bewehrten Eisenbetonplatten. *Der Bauingenieur*, 4:354–392, 1923.

[27] M. T. Huber. Einige Andwendungen fer Biegungstheorie orthotroper Platten. *Zeitschrift für angewandte Mathematik und Mechanik*, 6(3):228–232, June 1926.

[28] T. J. R. Hughes. *The Finite Element Method. Linear Static and Dynamic Finite Element Analysis.* Dover Publications, Inc., Mineola, N.Y., USA, 2000. ISBN 0-486-41181-8.

[29] M. Itskov and N. Aksel. Elastic constants and their admissible values for incompressible and slightly compressible anisotropic materials. *Acta Mechanica*, 157:81–96, 2002.

[30] Juha Jeronen. *On the mechanical stability and out-of-plane dynamics of a travelling panel submerged in axially flowing ideal fluid: a study into paper production in mathematical terms*. PhD thesis, Department of Mathematical Information Technology, University of Jyväskylä, 2011. Jyväskylä studies in computing 148. ISBN 978-951-39-4595-4 (book), ISBN 978-951-39-4596-1 (PDF).

[31] M. Johnson and T. Urbanik. A nonlinear theory for elastic plates with application to characterizing paper properties. *Journal of Applied Mechanics*, 51(3):146–152, 1984.

[32] H. Koivurova and A. Pramila. Nonlinear vibrations of axially moving membrane by finite element method. *Computational Mechanics*, 20:573–581, 1997.

[33] H. Koivurova and E.-M. Salonen. Comments on non-linear formulations for travelling string and beam problems. *Journal of Sound and Vibration*, 225(5):845–856, 1999.

[34] M. Kurki. *Modeling of kinematical and rheological web line behavior in a papermaking environment*. Licentiate thesis, Lappeenranta University of Technology, Department of Mechanical Engineering, 2005. Lappeenranta, Finland.

[35] M. Kurki, J. Jeronen, T. Saksa, and T. Tuovinen. Strain field theory for viscoelastic continuous high-speed webs with plane stress behavior. In J. Eberhardsteiner, H. J. Böhm, and F. G. Rammerstorfer, editors, *CD-ROM Proceedings of the 6th European Congress on Computational Methods in Applied Sciences and Engineering (ECCOMAS 2012)*, Vienna, Austria, 2012. Vienna University of Technology. ISBN 978-3-9502481-9-7.

[36] M. Kurki and A. Lehtinen. In-plane strain field theory for 2-d moving viscoelastic webs. In *Papermaking Research Symposium 2009 (Kuopio, Finland)*. PRS, 2009.

[37] M. Lai, D. Rubin, and E. Krempl. *Introduction to Continuum Mechanics*. Butterworth & Heinemann, third edition edition, 1999.

[38] U. Lee and H. Oh. Dynamics of an axially moving viscoelastic beam subject to axial tension. *International Journal of Solids and Structures*, 42(8):2381 – 2398, 2005.

[39] C. C. Lin. Stability and vibration characteristics of axially moving plates. *International Journal of Solids and Structures*, 34(24):3179–3190, 1997.

[40] C. C. Lin and C. D. Mote. Equilibrium displacement and stress distribution in a two-dimensional, axially moving web under transverse loading. *ASME Journal of Applied Mechanics*, 62:772–779, 1995.

[41] C. C. Lin and C. D. Mote. Eigenvalue solutions predicting the wrinkling of rectangular webs under non-linearly distributed edge loading. *Journal of Sound and Vibration*, 197(2):179–189, 1996.

[42] R. W. Mann, G. A. Baum, and C. C. Habeger. Determination of all nine orthotropic elastic constants for machine-made paper. *TAPPI Journal*, 63(2):163–166, 1980.

[43] K. Marynowski and T. Kapitaniak. Kelvin-Voigt versus Bürgers internal damping in modeling of axially moving viscoelastic web. *International Journal of Non-Linear Mechanics*, 37(7):1147 – 1161, 2002. DOI: 10.1016/S0020-7462(01)00142-1.

[44] K. Marynowski and T. Kapitaniak. Zener internal damping in modelling of axially moving viscoelastic beam with time-dependent tension. *International Journal of Non-Linear Mechanics*, 42(1):118 – 131, 2007. DOI: 10.1016/j.ijnonlinmec.2006.09.006.

[45] W. L. Miranker. The wave equation in a medium in motion. *IBM Journal of Research and Development*, 4:36–42, 1960.

[46] E. M. Mockensturm and J. Guo. Nonlinear vibration of parametrically excited, viscoelastic, axially moving strings. *ASME Journal of Applied Mechanics*, 72(3):374–380, 2005. DOI: 10.1115/1.1827248.

[47] C. D. Mote. Divergence buckling of an edge-loaded axially moving band. *International Journal of Mechanical Sciences*, 10:281–195, 1968.

[48] C. D. Mote. Dynamic stability of axially moving materials. *Shock and Vibration Digest*, 4(4):2–11, 1972.

[49] C. D. Mote. Stability of systems transporting accelerating axially moving materials. *ASME Journal of Dynamic Systems, Measurement, and Control*, 97:96–98, 1975.

[50] J. Niemi and A. Pramila. Vibration analysis of an axially moving membrane immersed into ideal fluid by FEM. Technical report, Tampereen teknillinen korkeakoulu (Tampere University of Technology), Tampere, 1986.

[51] H. Oh, J. Cho, and U. Lee. Spectral element analysis for an axially moving viscoelastic beam. *Journal of Mechanical Science and Technology*, 18(7):1159–1168, 2004. DOI: 10.1007/BF02983290.

[52] M. Pecht and M. Johnson. The strain response of paper under various constant regain states. *TAPPI Journal*, 68(1):90–93, 1985.

[53] A. Pramila. Sheet flutter and the interaction between sheet and air. *TAPPI Journal*, 69(7):70–74, 1986.

[54] A. Pramila. Natural frequencies of a submerged axially moving band. *Journal of Sound and Vibration*, 113(1):198–203, 1987.

[55] A. A. Robertson. The physical properties of wet webs. *Svensk Papperstidning*, 66(1):477–497, 1963.

[56] R. A. Sack. Transverse oscillations in traveling strings. *British Journal of Applied Physics*, 5:224–226, 1954.

[57] I. B. Sanborn. A study of irreversible, stress-induced changes in the macrostructure of paper. *TAPPI Journal*, 45(6):465–474, 1962.

[58] Changho Shin, Jintai Chung, and Wonsuk Kim. Dynamic characteristics of the out-of-plane vibration for an axially moving membrane. *Journal of Sound and Vibration*, 286(4-5):1019–1031, September 2005.

[59] Changho Shin, Wonsuk Kim, and Jintai Chung. Free in-plane vibration of an axially moving membrane. *Journal of Sound and Vibration*, 272(1–2):137–154, 2004.

[60] A. Simpson. Transverse modes and frequencies of beams translating between fixed end supports. *Journal of Mechanical Engineering Science*, 15:159–164, 1973.

[61] J. Skowronski and A. A. Robertson. A phenomenological study of the tensile deformation properties of paper. *Journal of Pulp and Paper Sciences*, 11(1):J21–J28, 1985.

[62] Rudolf Skutch. Uber die Bewegung eines gespannten Fadens, weicher gezwungen ist durch zwei feste Punkte, mit einer constanten Geschwindigkeit zu gehen, und zwischen denselben in Transversal-schwingungen von gerlinger Amplitude versetzt wird. *Annalen der Physik und Chemie*, 61:190–195, 1897.

[63] S. Smith and Stolle D. A comparison of eulerian and updated lagrangian finite element algorithms for simulating film casting. *Finite Elements in Analysis and Design*, 38:401–415, 2002.

[64] Niclas Stenberg and Christer Fellers. Out-of-plane Poisson's ratios of paper and paperboard. *Nordic Pulp and Paper Research Journal*, 17(4):387–394, 2002.

[65] R. D. Swope and W. F. Ames. Vibrations of a moving threadline. *Journal of the Franklin Institute*, 275:36–55, 1963.

[66] J. C. Tannehill, D. A. Anderson, and R. H. Pletcher. *Computational Fluid Mechanics and Heat Transfer*. Series in Computational and Physical Processes in Mechanics and Thermal Sciences. Taylor & Francis, 2nd edition, 1997.

[67] J. L. Thorpe. Paper as an orthotropic thin plate. *TAPPI Journal*, 64(3):119–121, 1981.

[68] S. Timoshenko and J. Goodier. *Theory of Elasticity*. McGraw-Hill, second edition edition, 1951.

[69] T. Uesaka, K. Murakami, and R. Imamura. Two-dimensional linear viscoelasticity of paper. *Wood Science and Technology*, 14:131–142, 1980.

[70] A. G. Ulsoy and C. D. Mote. Vibration of wide band saw blades. *ASME Journal of Engineering for Industry*, 104:71–78, 1982.

[71] Y. Watanabe, K. Isogai, S. Suzuki, and M. Sugihara. A theoretical study of paper flutter. *Journal of Fluids and Structures*, 16(4):543–560, 2002.

[72] Xiao-Dong Yang, Wei Zhang, Li-Qun Chen, and Ming-Hui Yao. Dynamical analysis of axially moving plate by finite difference method. *Nonlinear Dynamics*, 67(2):997–1006, 2012.

[73] N.-H. Zhang and L.-Q. Chen. Nonlinear dynamical analysis of axially moving viscoelastic strings. *Chaos, Solitons & Fractals*, 24(4):1065 – 1074, 2005. DOI: 10.1016/j.chaos.2004.09.113.

PIII

ON THE LIMIT VELOCITY AND BUCKLING PHENOMENA OF AXIALLY MOVING ORTHOTROPIC MEMBRANES AND PLATES

by

Nikolay Banichuk, Juha Jeronen, Matti Kurki, Pekka Neittaanmäki, Tytti Saksa and Tero Tuovinen 2011

International Journal of Solids and Structures, Vol. 48, pp. 2015-2025

PIV

OPTIMIZATION AND ANALYSIS OF PROCESSES WITH MOVING MATERIALS SUBJECTED TO FATIGUE FRACTURE AND INSTABILITY

by

Nikolay Banichuk, Matti Kurki, Pekka Neittaanmãki, Tytti Saksa, Maria Tirronen And Tero Tuovinen 2013

Mechanics Based Design of Structures and Machines, Vol. 41, Issue 2, pp. 146-167, DOI:10.1080/15397734.2012.708630

PV

LABORATORY SCALE MEASUREMENT PROCEDURE OF PAPER MACHINE WET WEB RUNNABILITY: PART 1

by

Matti Kurki, Pasi Kekko and Jarmo Kouko 2004

Paper and Timber (Paperi ja Puu), Vol. 86, No. 4

Matti Kurki and Pasi Kekko, Metso Paper
Jarmo Kouko, VTT Processes

Laboratory scale measurement procedure of paper machine wet web runnability. Part 1.

ABSTRACT

The fast tensile test rig Impact has been built and developed for paper tensile strength and relaxation studies. By the method it is possible to study the tensile and relaxation properties of wet pressed and dry papers. The elognation velocity of a paper sample is 1.0 m/s, which corresponds to the speed differences in the web transport of a paper machine. Wet paper samples are measured with two different dry solids contents. The analyses of wet dynamic tensile and relaxation results are carried out as a function of dry solids content.

This new method gives excellent opportunity to estimate furnishes compositions and the effects of refining and/or furnish preparation on optimizing paper machine runnability. Also new raw materials, new fiber properties and existing fiber properties can be developed in order to find the economically best paper making environment for paper and board making lines. With the help of this method, furnish properties can be measured straightforwardly without the effects caused by the wet end of paper machines.

This method will also speed up the product development procedure & process simplification since the effects of fiber processing can preliminarily be estimated without pilot trials.

From the viewpoint of paper physics, relaxation phenomenon will raise questions as to the tensile behavior of paper. Especially interesting is the reason for the difference between wet strength and relaxation responses with applied strain.

Wet web runnability must be examined on the basis of wet paper test results. Still, there is no dry paper test procedure that can reliably describe wet paper web runnability.

TIIVISTELMÄ

Laboratoriomittakaavan mittausmenetelmä puristinkuivan paperiradan ajettavuuden arvioimiseksi. Osa 1.

Paperin vetolujuus- ja relaksaatiomittauksia varten on rakennettu nopean vedon mittalaite Impact. Tämä mahdollistaa vetolujuus- ja relaksaatio-ominaisuuksien mittaamisen puristinkuivista ja kuivista paperinäytteistä. Venytysnopeus 1 m/s vastaa paperikoneella radan siirrossa tapahtuvaa muodonmuutos nopeutta. Puristinkuivat paperinäytteet mitataan kahdessa kuiva-ainepitoisuudessa. Vetolujuus- ja relaksaatiokokeiden tulosten analysointi tapahtuu kuiva-ainepitoisuuden funktiona.

Tämä uusi menetelmä antaa erinomaiset mahdollisuudet arvioida uusia massaseoksia ja jauhatuksen sekä massan käsittelyn vaikutuksia paperikoneen ajettavuutta optimoitaessa. Uusia raaka-aineita sekä uusia ja olemassa olevia kuitu-ominaisuuksia voidaan kehittää, jotta löydetään taloudellisesti paras ympäristö paperin ja kartongin valmistuslinjoille. Tämän menetelmän avulla, massan ominaisuudet voidaan mitata suoraviivaisesti ilman paperikoneen märän pään prosessivaikutuksia.

Tämä menetelmä nopeuttaa tuotekehitystä, koska kuidun käsittelyn vaikutukset voidaan testata ensivaiheessa ilman koeajoja. Tutkittaessa lopullisia vaikutuksia paperikonemittakaavassa koeajot ovat tarpeellisia vahvistamaan laboratoriomittauksen tulokset.

Paperifysiikan kannalta relaksaatioilmiö herättää kysymyksiä paperin jännitys-venymäkäyttäytymisen suhteen. Erityisen kiinnostava on ero märkälujuuden ja relaksaation välillä vakiovenymässä.

Märän paperiradan ajettavuutta pitää tutkia märästä paperinäytteestä tehdyn mittaustuloksen perusteella. Edelleenkään ei ole olemassa kuivalle paperille kehitettyä testimenetelmää, joka kuvaisi luotettavasti märän paperiradan ajettavuutta.

Introduction

During recent years paper machine production capability and efficiency has been emphasized. Generally speaking, the most profitable paper making companies are producing paper with the highest production rates. In studying paper machine runnability one of the most important factors is paper machine speed, the development of which can be seen in Fig. 1.

At this moment the highest top 24-hour speed is more than 1900 m/min (> 114 km/h). It is obvious that water removal, wet pressing and web handling are challenging at that speed range. External forces affecting the wet paper web at the beginning of the dryer section create demands which can be handled not only with runnability components but also with the development of fiber properties /1; 7/.

The wet strength and measuring procedures of wet paper have been of interest to papermakers for a long time. Results have been applied to paper machine process control with quantity changes or changes to pulp blends. Correlation between measured results and process control typically varies case by case. However, the time-dependent stress-strain behavior, i.e. the viscoelasticity, creates an important area which has to be taken into account when studying the connection between fiber properties and runnability. The properties of pulp and fiber (for example fiber dimensions, polymer structure, fibrils, water removal and single fiber stiffness) are essential factors in developing the wet strength of the paper web.

In the beginning of the drying section good stabilization of the wet web depends mainly on web tension, which is typically created by the speed difference in the web transfer between the press and drying section. During that time the dry solids content of the paper web is typically 45–55%. In the transfer, the wet paper web undergoes a fast speed increase. Absolute straining speeds can be even 1 m/s. The amount of wet straining depends particularly on wet web viscoelasticity. Typically, relative

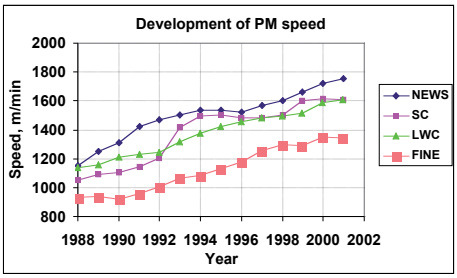

Fig. 1. Speed development of printing paper machines during the 1990's. Each dot marks the average yearly production speed of the best machine.

speed differences after the press section vary between 2–5%.

Many runnability studies made on a laboratory scale have been done using wet hand sheets. The procedure of making hand sheets and handling wet samples has been varied /2–4; 8–15; 20/. Wet paper mechanical testing has typically been done with a slow strain rate. The results of time-dependent relaxation tests have rarely been published.

We will present in this article a new method and advanced test rig to analyze wet paper tensile and time-dependent properties. The procedure includes the making of hand sheets, wet sample handling, storage and measurements. As a result, it is possible to do repeatable tensile and relaxation tests in two different press drynesses – typically between 30–65% – and in a dried state. Fast tensile testing will be done using the novel Impact test rig with an absolute straining speed of 1 m/s.

The measurement procedure and test rig have been developed to study the fast tensile properties of paper /16/. Additionally they give us a new opportunity to analyze the runnability and wet web handling of paper machines on a laboratory scale. This procedure also enables the development of furnish mixes, fiber refining, fiber handling, filler properties etc. The method has been successfully used to optimize furnish runnability at the beginning of the dryer section. We have noticed that there is a correlation between the measured laboratory results and paper machine dryer section runnability /6; 21/.

Known studies

There are a wide range of different procedures and instruments to measure paper strength. However, there is no standard procedure for relaxation or creep tests, which are both time-dependent tensile properties. When performing a relaxation test, the tension of the paper is measured as a function of time at a constant strain. When performing a creep test, the strain of the paper is measured as a function of time at a constant tension. The time frame of a relaxation or creep test can vary from fragments of a second to hours /8/. Instruments used for paper relaxation measurements have typically been general material testing instruments.

When using standard test procedures, tensile tests must be performed with certain absolute strain rates, which are 12, 22 or 100 mm/min. However, the relation between the tensile properties of paper and the strain rate has been noted in many earlier studies /9; 10/. Paper material parameters are dependent on strain rate, which should always be taken into account when tensile results are applied for example to the paper making process.

Wet paper

Many different measuring procedures and instruments for wet paper studies have been introduced /8; 11–16/. The properties of wet paper have been studied even at 8% dry solids content /11/. Wet paper's dry solids content increases rapidly under laboratory temperature and humidity. This leads to uncontrolled variation in dry solids content and the shrinkage of samples. These deteriorate the accuracy of measurement results. When repeating tensile tests with different dry solids contents, controlling the shrinkage of the paper has an effect on tensile results /17/.

Laboratory results have been used to estimate the runnability of the paper machine dryer section. Typical variables in the studies along with dry solids content have been the content and refining of kraft pulp /14; 15/. Measured parameters of wet paper have typically been tensile strength, elastic modulus, strain at break and T.E.A.. The typical parameter of relaxation measurement is tension at the beginning of strain step. The relaxation test can be performed at desired strain levels, which gives more information on the time-dependent properties of paper. Laboratory scale analyses for paper machine runnability have been presented /14/.

Additionally, models for wet paper strength have been developed. These depend on fiber dimensions, coarseness, relative bonded area etc. /18/. However, the connection to actual fiber properties and fiber network structure is found to be complicated.

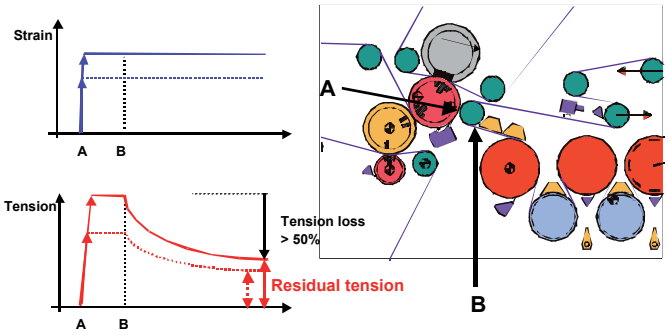

Fig. 2. Schematic presentation of web tension drop in the wet paper web during press-to-dryer section transfer (two draw levels).

Present studies

Comparing the above-mentioned different procedures and instruments with each other is usually very difficult. This is due to:

- Dry solids content,
- Handling time of wet paper sample (laboratory environment),
- Control of shrinkage in specific dry solids content area,
- Controlled change of dry solids content,
- Controlled drying of both ends of wet sample,
- Control and accuracy of jaw motion (strain),
- Control and accuracy of strain rate,

- Dimensions of samples.

In general the repeatability of tests is challenging, but with exact control of the factors listed above it is possible to create a reliable test environment for wet paper samples.

The absolute necessity for successful wet sample testing is a standard laboratory environment (controlled moisture and temperature) and equally timed sample handling and measuring procedures.

Description of THE papermaking process

Generally, successful runnability and web handling is achieved when the following inequality is valid:
Forces applied to moving web = Web tension < Wet tensile strength

When speeds are increasing, greater external force components (centrifugal etc.) force us to use bigger web tensions. This leads closer to the upper limiting tension, which is obviously the wet tensile strength. The above statement also means that the greater the web tension in the draw, the better the stability of the web both during the draw *and after the draw*.

The fundamental idea in this hypothesis is to take into account the fact that paper is a viscoelastic-plastic material, which means that elastic properties are time-dependent during and after web straining. Fig. 2 shows a schematic presentation of web tension behavior in press-to-dryer section transfer.

It is notable that web tension does not remain constant after the straining in the open draw and thus can be substantially lower in the beginning of the dryer section. The level of this tension drop is typically between 20–60% of the tension during stretching. Most of the relaxation occurs during the 0.5 sec relaxation time. The relaxation phenomenon is closely related to the elasticity of the fiber network. Therefore fiber properties and water amount are the main contributors to this effect /3/.

Since web transfer from the center roll (Fig. 2) is a very sensitive operation due to the low web strength and web elasticity, the tensioning of the web via stretching is the normal way to control web stabilization. On the other hand, due to increasing machine speeds, increasing external force components coerce the paper maker to increase this open draw tension and strain /19; 20/.

The increase of wet straining, however, has many negative effects on the overall quality of the paper. The increase of porosity is one of the main results, but also the loss of web plasticity, i.e. the strain potential of the paper is important since paper should have the capability of T.E.A. on later finishing and printing processes /1; 2; 4/.

Stretching in the paper machine between paper making subprocesses is much more rapid compared to normal strain speed in the laboratory made with tensile testing equipment. The biggest relative speed differences in papermaking are appr. 4%. This means that with the fastest machine the absolute straining speed is over 1.0 m/s.

For this reason, the straining speed in relaxation testing also has to be fast, since it has an effect on tensile values and also on the strain potential of the stretched paper /5, p. 264–265/.

Procedure of PULP Runnability potential measurement

Measuring procedure

The fast tensile test rig Impact has been built and developed in co-operation with VTT Processes and Metso Paper. The average strain rate of the Impact test rig is 1 m/s. The test rig is applied for paper tensile strength and relaxation tests. In relaxation test exceeding of target value is typically about 5% in motion of 1 mm. Due to the high strain rate, tests are named as dynamic tensile tests /16/.

In addition to the tensile test instrument, an essential instrument in test procedure is a moisture analyzer, with which the dry solids content of paper samples are measured after a tensile test. The principle of the test procedure is presented in Fig. 3.

Laboratory hand sheets for the fast tensile strength and relaxation tests are always made at VTT Processes. Standard dry hand sheets of 60 g/m^2 are formed according to SCAN-C27:76. The white water circulation of hand sheet former is used every time mechanical pulp or filler is blended. Usually only cold disintegration is performed for mechanical pulps.

Preparing and handling wet hand sheets is different from preparing and handling dry hand sheets. Wet hand sheets of 60 g/m^2 (dry weight) are also formed according to SCAN-C27:76. The dry solids content of wet hand sheets is controlled by wet pressing with two different pressure levels. After this the wet pressing hand sheets are piled between drying plates and stored. The width of tensile test strips is 15 mm and 20 mm for dry and wet test strips respectively. The span of both dry and wet test strips is always 100 mm.

The dry solids content of paper samples is measured with a moisture analyzer immediately after the relaxation or tensile test. During the test the wet paper sample dries and it is therefore difficult to determine the true dry solids content during testing. However, by standardizing work procedure, the delay between the tensile strength or relaxation test to the start of the moisture analysis is the same every time.

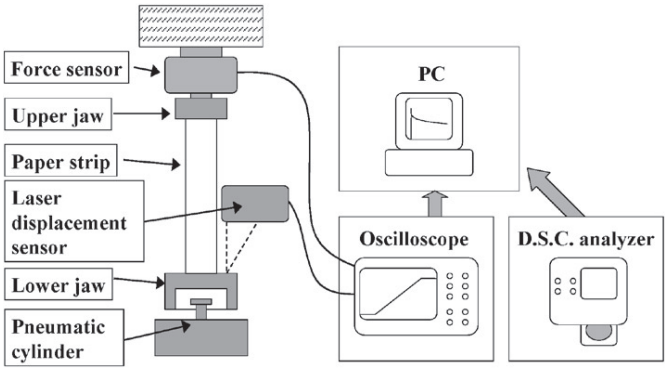

Fig. 3. Principle of test procedure with Impact.

Dynamic tensile and relaxation properties

Fig. 4 shows the tension-strain-figure of wet paper in a dynamic tensile strength test. Typical quantities determined in a dynamic tensile strength test are:

- Tensile strength = maximum tension in tension-strain-figure,
- Strain at break = strain corresponding to maximum tension in tension-strain-figure,
- Elastic modulus = maximum value of slope of secant in tension-strain-figure, when secant fixed in origin,
- Dynamic modulus = value of slope of secant in tension-strain-figure, when secant fixed between origin and maximum tension value.

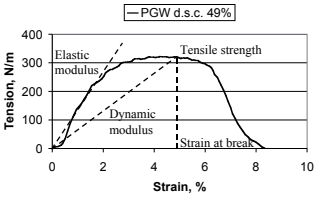

Fig. 4. Tension-strain-figure of dynamic tensile strength test.

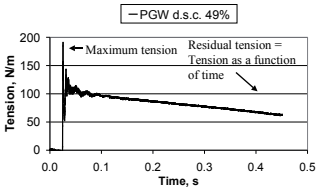

Fig. 5. Tension-time-figure of relaxation test.

Fig. 5 shows the tension-time-figure of wet paper in a dynamic relaxation test. Typical quantities determined in a dynamic relaxation test are:

- Maximum tension = maximum tension in tension-time-figure,
- Residual (relaxation) tension = tension at a constant strain at a certain time after straining is stopped. Wet paper residual tension is examined after 0.475 s and dry paper residual tension is examined after 9.5 s.

The above relaxation times are chosen from the viewpoint of web transfer delays between paper machine subprocesses.

The dynamic tensile strength describes paper tension at breaking point. When the paper web runs through the paper machine, there is no intention to break the paper web by straining. If paper machine runnability is studied with dry paper, tensile strength, drying shrinkage, straining during drying, etc. can not be taken into account in the final results.

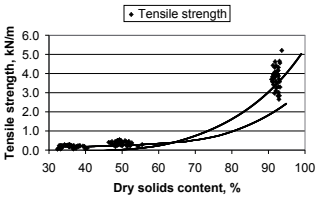

Fig. 6. Dynamic tensile strength values of different LWC blend hand sheets by Impact as a function of dry solids content.

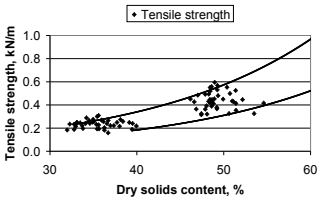

Fig. 7. Dynamic tensile strength values of different LWC blend hand sheets by Impact test rig as a function of dry solids content (enlarged from Figure 6).

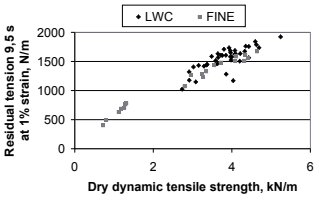

Fig. 8. Residual tension 9.5 s at 1% strain of dry LWC and Fine blends as a function of dry dynamic tensile strength.

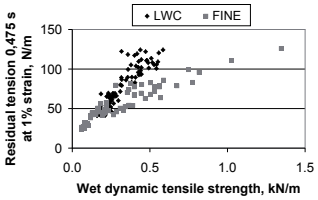

Fig. 9. Residual tension 0.475 s at 1% strain of wet LWC and Fine blends as a function of wet dynamic tensile strength.

Residual tension is the most important parameter in Figs. 4 and 5. Elastic modulus is important when tension growth is estimated. Strain at break is important when the potential of strain or tensile energy absorption is estimated.

Analyzing procedure

Wet paper samples are measured with two different dry solids contents. The analyzing of wet dynamic tensile and relaxation results is carried out as a function of dry solids content. Typically a linear interpolation is made between the two measured wet points. Then wet dynamic tensile and relaxation properties are studied usually with a 50% dry solids content, which is a typical dry solids content after the paper machine press section.

After a pulp runnability study of a couple of hundred different pulps, it has become clear that not only tensile strength but also elastic modulus, residual tension and maximum tension develop exponentially as a function of dry solids content. In Figs. 6 and 7 the exponential growth of dynamic tensile strength as a function of dry solids content is shown. These two figures show a large selection of different pulps, which have a large variation in wet tensile strength.

Studied samples

Different LWC and Fine pulp blends were studied. In LWC blends the softwood chemical pulp content varied between 0–40 % and the filler content between 0–20%. In the fine pulps studied the softwood chemical pulp content varied between 0–40% and the filler content between 0–30%.

Results

Differences between wet and dry paper strength properties

In earlier sections the differences between wet and dry paper elasticity have been discussed. In this section we shall look more closely at those differences from the viewpoint of wet web runnability and tension preservation capability (residual tension).

Residual tension typically correlates with dynamic tensile strength when dry paper is studied. Correlation is usually independent of pulp type.

Fig. 9 shows the correlation between residual tension 0.475 s at 1% strain of wet LWC and Fine blends as a function of wet dynamic tensile strength. In Fig. 9 wet Fine pulps have the same kind of correlation as dry Fine pulps in Fig. 8. Fine pulps have a lower slope compared to LWC blends.

Figs. 8 and 9 show the difference between the nature of dry and wet paper relaxation. Dry paper relaxation test results have a higher slope of correlation with dry paper tensile strength, as in Fig. 8.

Wet paper relaxation test results have a lower correlation with wet or dry paper tensile strength, as shown in Fig. 10. However, the correlation between wet paper and dry paper tensile strength presented in Fig. 11 is clearly different to that in Fig. 10. In other words, it is difficult to obtain reliable wet paper relaxation test results by means of dry tensile testing.

Presenting exact correlations over a large scale can be misleading. On a smaller scale it is possible to find different dependencies compared to the larger scale correlation, as presented in Fig. 12. These phenomena are especially emphasized with modern paper machines, where operational process parameter windows are optimized for production efficiency.

Fig. 13 reveals that the correlation between dry tensile strength and wet elastic modulus is very unclear and artificially em-

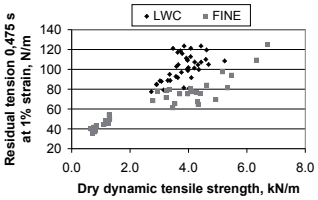

Fig. 10. Residual tension 0.475 s at 1% strain of wet LWC and Fine hand sheets as a function of dry dynamic tensile strength.

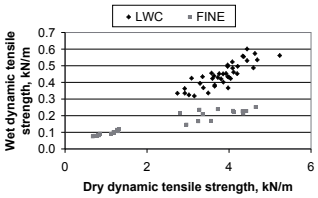

Fig. 11. Dynamic tensile strength of wet LWC and Fine hand sheets as a function of dry dynamic tensile strength.

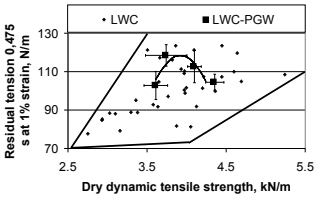

Fig. 12. Residual tension 0.475 s at 1% strain of wet LWC hand sheets as a function of dry dynamic tensile strength. Chemical pulp content has been varied in bold trial points (enlarged from Figure 10).

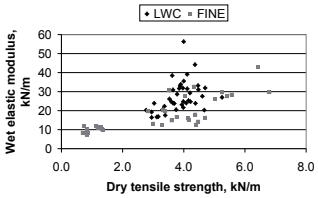

Fig. 13. Elastic modulus of wet LWC and Fine hand sheets as a function of dry dynamic tensile strength.

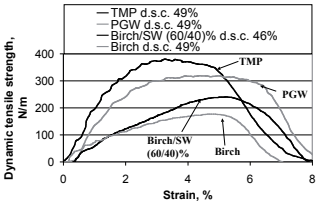

Fig. 14. Dynamic tensile-strain-curves of TMP, PGW and birch at 49% dry solids content and Birch/SW (60/40)% at 46% dry solids content.

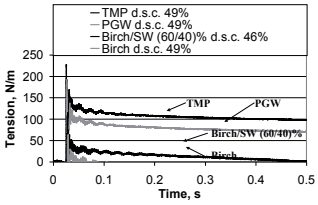

Fig. 15. Tension-time-figures of TMP, PGW and birch at 49% dry solids content and Birch/SW (60/40)% at 46% dry solids content at 1% strain.

phasized due to the higher filler content trial points in the lower left corner.

Fig. 14 presents an example of the tension-strain behavior of 100% mechanical pulp (TMP) and 100% chemical pulp (birch) hand sheets. The tensile strength of mechanical pulp is twice the tensile strength of chemical pulp when the paper sample is wet and never dried.

Fig. 15 presents an example of the tension-strain behavior of a relaxation test at 1% with 100% mechanical pulp and 100% chemical pulp hand sheets. Residual tension 0.475 s at 1% strain of mechanical pulp is more than twice the corresponding residual tension of chemical pulp.

Dry paper standard strength properties (tensile strength, strain at break, tear index, etc.) have been studied extensively for decades and the typical values are widely known. For wet paper there are no practical or functional standards for strength measurements and therefore published wet paper tensile strength studies differ significantly from each other. Wet paper strength properties and differences, for example between LWC and Fine grades, are therefore mostly unknown.

Discussion / Conclusion

This new method presented gives excellent opportunities to estimate new furnish compositions and the effects of refining and/or furnish preparing on optimizing paper machine runnability. With the help of this method, furnish properties can be measured straightforwardly without the effects caused by the wet end of paper machines.

It will also speed up the product development procedure & process simplification since the effects of fiber processing can preliminarily be estimated without trials. However, it is clear that when studying the final effects in the paper machine real-scale trials are necessary in order to confirm the laboratory results. The application of this method is presented in /21/, where it was possible to optimize the material composition of LWC base paper using BSK reduction.

From the viewpoint of paper physics, relaxation phenomenon will raise questions as to the tensile behavior of paper. Especially interesting is the reason for the difference between wet strength and relaxation responses with applied strain. As shown above, wet fibers create a stiffness response, but its nature is more dependent on water inside the fiber and the type of inter-fiber bonding. In addition, the nature of mechanical pulp and its fiber material is interesting. Even though the mechanical pulp includes nonbonding lignin, it seems that fines create additional bonding which improves the elastic performance of wet mechanical fiber.

Using standardized 60 gsm hand sheets, the large scale correlation in the dry tensile strength of Fine and LWC samples is similar. However, wet residual tensions are clearly at a lower level with Fine samples made from bleached chemical pulp. Interestingly enough, this same situation does not occur between wet and dry tensile strength.

An important feature is the elastic response difference between TMP and birch. With low strain levels the created tension is on the same level which means that both pulps are equally good for runnability, if it is possible to keep press-to-dryer draw at a very low level. With higher draw levels TMP performs clearly better, giving a 100% better tension level compared to Fine's 3% strain level. From the runnability point of view, a 3% strain level seems to be the saturation level for studied mechanical pulp. The tension no longer increases but other paper properties rapidly deteriorate with high strain levels, due to the rupture of the fiber network.

The disadvantage of this method is its length and complicated procedure. Wet laboratory hand sheets have to be made and treated in an accurately controlled laboratory environment. In addition, sample preparation and measurement procedure standardization are mandatory.

Wet web runnability must be examined on the basis of wet paper test results. Still, there is no dry paper test procedure that

can reliably describe wet paper web runnability.

Typically, the runnability of a paper machine press section and dryer section are optimized in order to achieve the greatest possible machine speed with the optimized number of web breaks. The linkage, knowledge flow and knowledge utilization between furnish mills, stock preparation and paper making is inadequate. With this method new raw materials, new fiber properties and existing fiber properties can be developed in order to find the economically best paper making environment for paper and board making lines.

References

1. *Kurki, M., Saarikivi, P., Kekko, P.*: New Web Handling Techniques and Paper Property Development in Single Tier Dryer Section, PIRA Paper Machine Runnability Conference, Jan. 2001, Gothenburg.
2. *Baum, G. A. Pers, K. Shepard, D. R. Ave'Lallemant, T. A.*: Wet Straining of Paper. Tappi Journal, 1984. Vol. 67, No. 5, p. 100–104.
3. *Sanborn, I. B.*: A Study of Irreversible, Stress-Induced Changes in the Macrostructure of Paper. TAPPI Journal, 1962. Vol. 45, No. 6, p. 465–474.
4. *Brecht, W., Erfurt, H.*: Wet-Web Strength of Mechanical and Chemical Pulps of Different Form Composition. TAPPI Journal, 1959. Vol. 42, No. 12, p. 959–968.
5. *Niskanen, K.*: Rheology and Moisture Effects. In: Paper Making Science and Technology, Part 16, Paper Physics, 1998. 324 p.
6. *Kouko, J. Kekko, P. Liimatainen, H. Saari, T. Kurki, M.*: Wet Runnability of Fibre Furnish for Magazine Papers, to be published 2004.
7. *Pakarinen, P. Kurki, M.*: Development of High-Speed Paper Machines. In: Kinnunen, L. et. al. High Technology in Finland 1995. Espoo: Academies of Technology, Espoo, 1996. p. 90.
8. *Johansson, F. Kubat, J.*: Measurements of stress relaxation in paper. Svensk papperstidning, 1964. No. 20, p. 822–832.
9. *Andersson, O., Sjöberg, L.*: Tensile studies of paper at different rates of elongation. Svensk papperstidning, 1953. No. 16, p. 615–624.
10. *Göttsching, L.*: Das Festigkeitsverhalten von Papier unter ststischer und dynamischer beanspruchung, 1971. Dissertation.
11. *Lyne, L. M. Gallay, W.*: Measurement of wet web strength. Tappi, 1954. Vol. 37, No. 12, p. 694–697.
12. *Craven, B. D.*: Stress relaxation and work hardening in paper. Appita 16(2):57…70, 1962.
13. *Robertson, A. A.:* The physical properties of wet webs. Tappi Journal, 1959. Vol. 42, No. 12, p. 969–978 ,
14. *Mardon, J. Cutshall, K. A. Laurila, P. S.*: The Load Stretch (Wet Web Strength) Behaviour of Selected Paper Pulps and Furnishes. Pulp and Paper Magazine of Canada, 1973. Vol. 74, No. 11, p. 99–108.
15. *Jantunen, J.*: Visco-Elastic Properties of Wet Webs Under Dynamic Conditions. Transactions of the eighth fundamental research symposium held at Cambridge, Vol. 1, September 1985. London: Mechanical Engineering Publications Ltd., 1985. p. 133–162.
16. *Kurki, M. Kekko, P. Martikainen, P.*: Fast elasticity properties of paper web. Proceedings of Tappi Papermakers Conference 1999, 2, s. 411–426.
17. *Nanko, H. Ohsawa, J.*: Mechanisms of fibre bond formation. Transactions of the ninth fundamental research symposium held at Cambridge. Vol. 2, September 1989. London: Mechanical Engineering Publications Ltd., 1990. p. 783–829.
18. *Page, D. H.*: A Quantitative Theory of the Strength of Wet Webs. Journal of Pulp & Paper Science, 1993. Vol. 19, No. 4, p. J175–176.
19. *Hauser, L.*: Analyse von Laufprobleme in der Papiermaschine und Moderne Konzeptionen der Papiertrocknung. Wochenblatt für Papierfabrikation, 1991. No. 11/12, p. 433–441.
20. *Schwartz, M., Bechtel, K.*: Initiale Gefügefestigkeit bei der Blattbildung. Wochenblatt für Papierfabrikation, 2003. No. 16, p. 950–957.
21. *Liimatainen, H., Tuominen, R., Heimonen, J., Jonsson, S.*: Furnish Concepts. Metso Paper Technology Days, Lahti, Finland, 2003.

Addresses of the authors:

Matti Kurki and Pasi Kekko, Metso Paper, P.O.Box 587, FI-40101 Jyväskylä, Finland

Jarmo Kouko, VTT Processes, P.O.Box 1603, FI-40101 Jyväskylä, Finland

184x133

PVI

LABORATORY SCALE MEASUREMENT PROCEDURE OF PAPER MACHINE WET WEB RUNNABILITY: PART 2

by

Jarmo Kouko, Kristian Salminen and Matti Kurki 2007

Paper and Timber (Paperi ja Puu), Vol. 89, No. 7–8

PEER-REVIEWED

Jarmo Kouko[1], Kristian Salminen[1], Matti Kurki[2]

Laboratory scale measurement procedure for the runnability of a wet web on a paper machine, Part 2

Keywords:
Runnability, relaxation, tensile strength, residual tension, elasticity, wet web, chemical pulp, mechanical pulp, orientation.

Abstract

In the second part of the series we further link wet paper results of fast tensile test rig IMPACT with paper machine runnability. This paper presents the effects of filler and Kraft content, refining level, jet/wire ratio, and strain rate on the tensile and relaxation properties of a wet web. Since relaxation occurs in all papers subjected to a constant strain increase, the key item is the tension holding capacity of paper. It depends naturally on draw levels, but also greatly on properties of furnish, including its numerous modification possibilities at different raw material handling and stock preparation stages.

The effect of the filler content on handsheets in-plane tensile and relaxation properties were shown to be strongly dependent on dry solids content. Filler content level was shown to affect more wet web tensile than relaxation properties. The relationship between density and tensile strength of dry paper was shown to be linear. Wet paper tensile strength and residual tension were not developed linearly by increasing density. In order to evaluate wet web runnability, both residual tension and dry solids content of paper should be observed.

The effect of the jet/wire ratio was similar on both wet and dry MD/CD tensile strength ratios, whereas at constant jet/wire ratio the MD/CD ratio of residual tension was significantly higher. This was mainly due to low elasticity of wet web in CD. Strain rate were shown to have significant effect on stress relaxation percentage as well as the maximum tension of wet paper.

Tiivistelmä

Kirjoittajat! Tähän suomenkielinen otsikko!

IMPACT nopean vedon mittalaitetta esittelevän julkaisusarjan toisessa osassa jatkamme märän paperin mittaustulosten ja paperikoneen ajettavuuden välisen yhteyden tarkastelua. Tässä julkaisussa esitetään täyteaine- ja pitkäkuitusellun osuuden, massan jauhatuksen, suihkuviirasuhteen ja vetonopeuden vaikutuksia märän rainan vetolujuus- ja relaksaatio-käyttäytymiseen. Relaksaatiota tapahtuu kaikissa papereissa venytyksen jälkeen, joten olennaista on paperin kireydenpitokyky (kireyden relaksaation nopeus). Kireydenpitokyky riippuu vedon määrästä, mutta myös massaseoksen koostumuksesta mukaan lukien lukemattomat muutosmahdollisuudet raaka-aineen ja massan valmistuksen eri vaiheissa.

Täyteainepitoisuuden vaikutus tasonsuuntaisiin vetolujuus- ja relaksaatio-ominaisuuksiin havaittiin laboratorioarkeilla riippuvan voimakkaasti kuiva-ainepitoisuudesta. Täyteainepitoisuus vaikuttaa märän rainan vetolujuusominaisuuksiin voimakkaammin kuin relaksaatio-ominaisuuksiin. Kuivan paperin ja tiheyden välillä havaittiin lineaarinen riippuvuus, kun taas märän paperin vetolujuus ja jäännöskireys kehittyivät epälineaarisesti tiheyden funktiona. Märän rainan ajettavuutta arvioitaessa tulisi tarkastella sekä märän rainan jäännöskireyttä että kuiva-ainepitoisuutta.

Kuivan ja märän paperin vetolujuussuhteet kehittyivät samalla tavalla suihku/viirasuhteen muuttuessa. Sen sijaan vakioidulla suihku/viira-suhteella märän rainan jäännöskireyssuhde oli selvästi suurempi kuin vetolujuussuhde. Tämä oli seurausta märän rainan alhaisesta poikkisuuntaisesta elastisuudesta. Vetonopeudella osoitettiin olevan suuri merkitys märän rainan maksimikireyteen vedossa, sekä kireyden relaksaatioon.

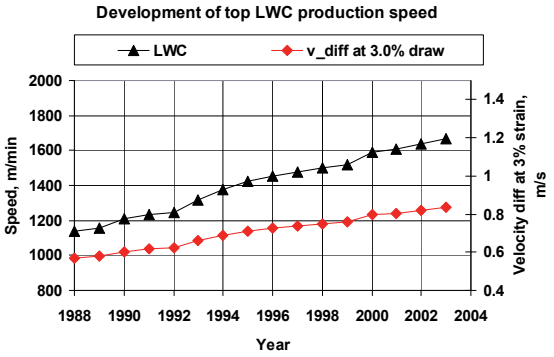

Fig. 1. **Average annual production speed of the best LWC machine, and absolute open draw speed difference at 3.0% strain level.**

Introduction

In this article we address further the natural rheological behavior of paper from the viewpoint of paper machine runnability /1/. The nature of the moving web and its tensioning on the paper machine with the help of speed differences constitute a very different environment compared to normal paper applications and functional demands in the end-user environment. The main difference in papermaking is *processing speed*. Papermaking line processes are usually very fast, and processing time decreases as production speed increases. For this reason, viscoelastoplastic paper properties will be increasingly important as time-dependent features are emphasized. This article will provide deeper insight into the implications

1. *Jarmo Kouko, Kristian Salminen*, VTT Technical Research Centre of Finland, PO Box 1603, FI-40101 Jyväskylä, Finland.

2. *Matti Kurki*, Metso Paper, PO Box 587, FI-40101, Jyväskylä, Finland. Present address: Oy Metsä Botnia Ab, Äänekoski Mill, FI-44100 Äänekoski, Finland.

of strain rate based rapid paper testing responses and some other key paper machine process variables.

Paper machine speeds have continued to increase at the rate noted in Fig. 1 /1/. For the most part, this development is based on more stable and better-controlled process parameters and raw material utilization, but runnability component technology has also improved web stability. It is clear that this area will gain added emphasis as external forces continue to increase faster than speed.

Paper rheology

According to Perkins, the most common form of elasticity to be assumed is linear elasticity. The linear elastic model of paper behavior is commonly used in many applications. It is considered to be an accurate model when environmental conditions are constant, when the duration of loading or strain is relatively short, and when the stresses and strains are maintained at a low level. /2/

The elastic strain level of paper is not easy to determine, and it may be as low as 0.15%–0.30%. Linear elastic behavior, as determined in Hooke's law, requires that the relationship between stress and strain is linear, and that strain is zero when stress is removed /2/. These requirements and the behavior of paper are inconsistent, and paper is therefore not linearly elastic.

Linear viscoelasticity (time-dependent) is a proper assumption if the environmental conditions of temperature and relative humidity are constant over time and their values are moderate, and if the levels of applied stress or imposed strain are small /2, 3/. However, these stresses and strains are unfortunately not on a practical scale, which means that this theory is not accurate enough to describe the behavior of paper even in relatively simple situations. According to Craven, stress relaxation and the superposition behavior of paper are hard to explain by any linear viscoelastic theory /4/.

Relaxation phenomenon is known to exist for paper and other materials, but because time-dependent stress and strain analysis methods have not been standardized for paper, relaxation properties are not commonly used for major control parameter in papermaking. The absence of a valid general theory of short time scale paper web stress-strain behavior increases lack of knowledge, and the importance of stress relaxation is not properly understood.

The phase lengths of runnability-related paper machine disturbances are typically 100–500 ms, which reflect, for example, the rotating speed of rolls. The paper web dwell time in a press-nip is 1–30 ms, and its dwell time in open draws is 5–20 ms. The time scales used in the mechanical testing of paper should theoretically match those found on the paper machine /5/. Many different analytical models of disturbances on and in the web have been published /6–9/.

Because web handling is based on a stepwise increase of consecutive strains, stress relaxation provides a more sophisticated indicator than tensile testing. Because creep is stress-generated, it is not as useful as relaxation. Velocity differences generate draw, which is suddenly applied to the paper web on the paper machine. Draw first generates strain in the web, and this strain is followed by an increase in stress. A number of equations have been presented for the calculation of relative speed differences on a paper machine /10–12/.

Due to the nature of the relaxation phenomenon, especially the straining time should be shorter than the time constants of paper relaxation /5/. At large time scale, stress relaxation is linear in proportion to the common logarithm of time according to Craven /4/. Craven was aware of the limitations of his model and the difficulty of setting parameters for short and long-term relaxation. Similar models have also been introduced before and after Craven /4, 13, 14/.

$$\sigma(t) = const - F\log(t + t_0) \qquad (1)$$

Craven's formula introduces the constant t_0 = 2 s. This constant, t_0, fixed nonlinearity at short relaxation times. Relaxation times that matter for paper machine runnability are typically less than 0.5 s. Because the shortest relaxation time in Craven's study was 0.5 s, stress behavior related to shorter than 0.5 s relaxation times was left unclear.

We have made our stress relaxation measuring method as similar to the real papermaking process as possible in terms of strain. The strain rate of the IMPACT tester is 1,000%/s and paper samples are tested at their initial dry solids content, typically 30%–70%. For simplification of the method, laboratory sheets are tested in order to exclude the effects of orientation on results /1/.

Standardized in-plane strength properties (tensile strength, tear strength, etc…) are typically poor predictors of paper machine runnability. The majority of runnability problems on a paper machine occurs at low web dry solids contents (30%–70%) at the press section and dryer section. The lack of a general relationship between the time-dependence of stress, strain and the dry solids content of paper forces one to conduct experimental studies, especially when pulp properties are studied in order to improve paper machine runnability.

The strain rate of in-plane tensile tests has been standardized since the 1960s. Some standards have fixed the rate of loading, but fixing the strain rate has been more typical. This means that the ratio of strip length and strain speed is fixed. In recent standards the strain speed is typically 100 mm/min, but the strip length in not necessarily fixed.

Tensile testing methods are static and the paper sample is stationary, whereas the real process is dynamic and the paper web is moving. On a paper machine the strain rate is considerably higher 100–10,000%/s. The strain rate used in the test methods of the 1960s was low due to data recording limitations /15/. By 1953, Andersson and Sjöberg had already tested paper samples and recorded data at strain speeds over 100 mm/s /3/. Now, in the 21st century, there are no technical limitations for increasing the strain rate to 100%/s, for example.

The strain rate has been noted to have an affect on tensile strength, work-at-rupture and elasticity /3, 13–19/. The strain rate has not been proven to affect strain at break. Göttshing found that the strain rate had no effect on strain-to-rupture /17/. Davidson, on the other hand, noticed that the strain rate had an effect on strain-to-rupture /18/. The results of Andersson and Sjöberg showed slight variation in strain-to-rupture values /15/. Stress-strain models give no proper explanation of strain rate or strain-to-rupture. Meanwhile, even the simplest dash-pot and spring models typically explain the effect of strain rates on tensile strength /13/.

Stress relaxation increases with increased strain rate /3, 13/. Stress relaxation is not explained by linear viscoelastic theory because stress curves generated at different strains will not coincide even after a long time. According to Jantunen, the viscoelastic component of stress relaxation, which depends on strain rate, will disappear at a given stress level. The plastic component of stress relaxation has no equilibrium, and it therefore continues to relax slowly /5/. The viscoelastic component rules when fast relaxation is studied and the plastic component of stress relaxation is negligible.

The moisture content of paper increases stress relaxation rapidly /5/. Few studies have been published on the stress relaxation of wet paper at high strain rates.

Wet paper rheology

Experimental

Detailed description of experimental method is published earlier /1, 20/. Main target is to measure rheological properties of wet furnishes. Both tensile strength and relaxation properties of wet and dry paper were investigated. The term 'dynamic tensile property' is used here because the average strain rate in the tensile and relaxation tests was 1000%/s (1 m/s) with IMPACT /1/. This article includes results also from advanced tensile tester C-IMPACT /20/.

Furnish mixture of fine pilot samples were approximately hardwood 70% softwood 30%, but filler content was varied. Fine paper type handsheets were studied with varied filler content and pulp combinations.

Furnish components of LWC-type handsheets were Nordic thermomechanical pulp (TMP) and two Nordic pressure groundwood pulps (PGW) of the LWC and SC type. These mechanical pulps were blended with chemical softwood (Kraft) reinforcement pulp. The mechanical pulps examined were decker pulps from Nordic paper mills made out of Norway spruce. Combinations of the pulps are presented in /21/.

Wet handsheets

The increase of filler content is known to decrease the tensile properties of dry paper due to lowered density and RBA /22, 23/. Flocs of filler, fines and fibers cover fiber-fiber crossings in the web structure, and these flocs prevent the development of hydrogen bonds between fibers. Due to intensive flocculation, poor formation may enhance the development of stress peaks in the web during strain and therefore decrease tensile strength. The tensile strength of dry and wet handsheets as a function of filler content is presented in Figs. 2 and 3. Handsheets were formed in accordance with the SCAN standard, except that the wet sheets were pressed at two different pressure levels (50 kPa and 350 kPa) in order to reach two different dry solids content levels.

Filler content had a bigger effect on dry paper tensile strength than on wet paper. The mechanical properties of dry paper are determined mainly by fiber-to-fiber bonds, which are blocked by filler particles. In wet paper, the main parameters determining the mechanical properties of the web are the average distance between fibers, the amount of free water, and the surface tension of the water. The effect of filler content on residual tension after 0.475 s at 1% strain is presented in Figs. 4 and 5.

The residual tensions of dry and wet handsheets decreased rapidly when the amount of filler was increased. The higher the filler content, the smaller the effect of filler increase. The increase of filler content from 25% to 30% had only a minor effect on residual tension. Even though increased filler content lowered residual tension significantly, relative differences between furnishes remained the same. These results indicate that the effects of filler content variations are crucial in controlling web behavior on a paper machine, especially with magazine paper grades based on recycled pulps.

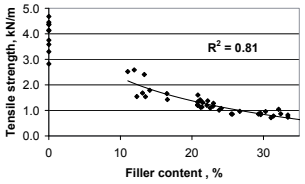

Fig. 2. Tensile strength of dry fine paper handsheets (several different combinations) as a function of filler content (strain rate 1,000%/s).

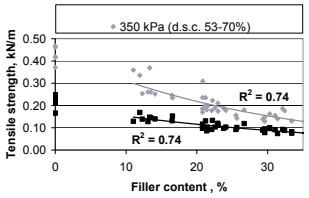

Fig. 3. Tensile strength of press-dry fine paper handsheets (several different combinations) as a function of filler content (strain rate 1,000%/s).

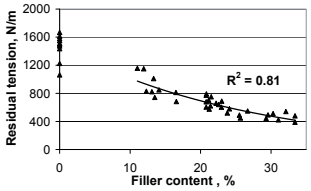

Fig. 4. Residual tension after 0.475 s at 1% strain in dry fine paper handsheets (several different combinations) as a function of filler content (strain rate 1,000%/s).

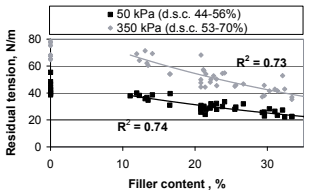

Fig. 5. Residual tension after 0.475 s at 1% strain in press-dry fine paper handsheets (several different combinations) as a function of filler content (strain rate 1,000%/s).

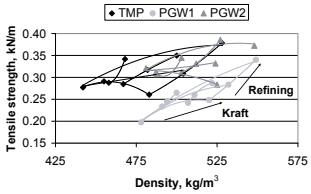

Fig. 6. LWC handsheet tensile strength vs. dry paper density at dry solids content of 40% (strain rate 1,000 %/s).

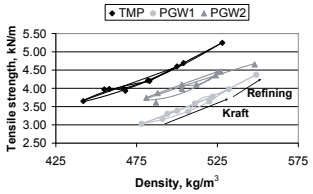

Fig. 7. Dry LWC handsheet tensile strength vs. dry paper density (strain rate 1,000%/s).

Differences between wet and dry paper strength properties

Kouko et al. presented various properties of LWC pulps at 40% dry solids content and at dry state. Detailed handsheet combinations and properties are tabulated in the reference /21/. Density had a different effect on wet and dry paper tensile strength in Figs. 6 and 7. Dry paper tensile strength depended linearly on density, which was affected by mechanical pulp type and BSK content (bleached softwood kraft). A linear relationship between density and tensile strength seemed to be a typical property of dry paper. Wet paper tensile strength depended on mechanical pulp type, BSK content and also on the degree of BSK refining, but the relationship with density was not linear.

In Fig. 6 the arrow labeled "Kraft" stands for the direction in which tensile strength changes as a function of density when the proportion of BSK is increased. The arrow labeled "Refining" stands for the direction in which tensile strength changes as a function of density when the refining of BSK is increased. Density thus reflects the changing proportion of BSK and the degree to which it is refined. The density of blended pulp

is increased by an increase in BSK refining and an increase in the relative proportion of BSK.

Apparent density increases clearly in mechanical pulp-based handsheets as the proportion of BSK in the blend is increased. *Fig. 6* shows that the degree of refining increases apparent density the more the greater the proportion of BSK in the blend. Both PGW blends have similar apparent densities, which are higher than the apparent densities of the TMP blends.

Density had a different effect on residual tension and tensile strength in Figs. 8 and 9. Dry paper residual tension depended on the degree of BSK refining, as well as mechanical pulp type and BSK content. Increased refining gave bigger differences in wet paper residual tension than in tensile strength. Residual tension in wet handsheets decreased with increased BSK content.

The residual tension of paper can be determined through some other variable, depending on whether the paper is wet or dry (see Figs. 10 and 11). Dry paper residual tension typically had a stronger linear relationship with tensile strength than wet paper residual tension.

Dry paper tensile strength had linear relationships with dry paper maximum and residual tensions in Fig. 10. However, the same is not true for wet paper /1/. Wet paper residual tension after 0.475 s at 1% strain had a nearly linear relationship with wet paper maximum tension at 1% strain in Fig. 11. However, apparent correlation depends strongly on pulp type and strain rate and therefore relative amount of apparent elasticity and plasticity changes.

In Figs. 12 and 13, different levels of dry solids content were applied at 50 kPa and 350 kPa wet pressing pressures. Wet paper residual tension after 0.475 s at 1% strain correlated with dry paper maximum or residual tension after 0.475 s at 1% strain. However, the slopes and R^2 correlations are low in Fig. 12 and 13 and therefore high dry maximum tension or residual tension after 9.5 s at 1% strain does not necessarily lead to high wet residual tension after 0.475 s. There is typically weak relationship between dry maximum tension or residual tension and paper machine wet runnability.

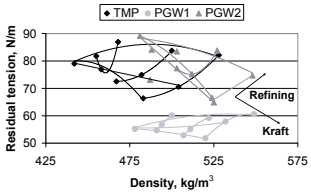

Fig. 8. LWC handsheet residual tension at 1% strain after 0.475 s relaxation vs. dry paper density at dry solids content of 40% (strain rate 1,000 %/s).

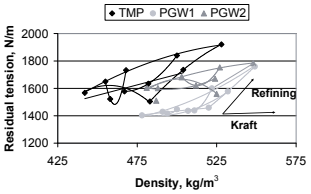

Fig. 9. Dry LWC handsheet residual tension at 1% strain after 9.5 s relaxation vs. dry paper density (strain rate 1,000%/s).

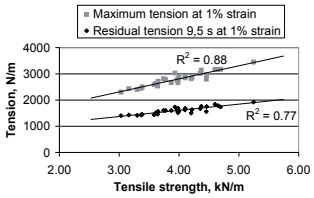

Fig. 10. Maximum and residual tension in dry handsheets after 9.5 s at 1% strain as a function of dry paper tensile strength.

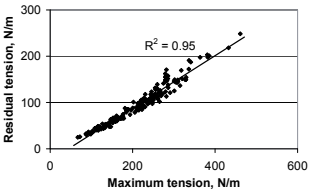

Fig. 11. Wet handsheet (d.s.c. 33...55%) residual tension in LWC handsheets after 0.475 s at 1% strain as a function of wet handsheet maximum tension at 1% strain.

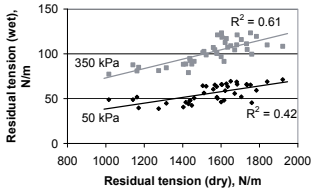

Fig. 12. Residual tension after 0.475 s at 1% strain (wet handsheets d.s.c. 33...55%) as a function of residual tension 9.5 s at 1% strain (dry handsheets).

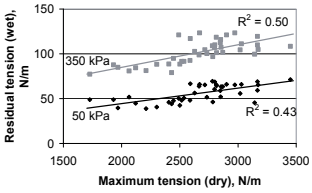

Fig. 13. Residual tension after 0.475 s at 1% strain (wet handsheets d.s.c. 33...55%) as a function of maximum tension at 1% strain (dry handsheets).

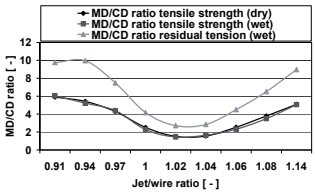

Fig. 14. Tensile strength of dry and wet fine paper and residual tension after 0.475 s at 1% strain of wet fine paper as a function of the jet/wire ratio.

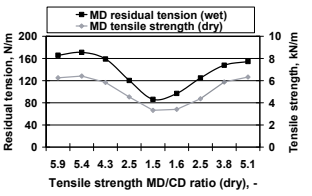

Fig. 15. Dry fine paper tensile strength and wet fine paper residual tension after 0.475 s at 1% strain as a function of the dry paper MD/CD ratio.

Oriented wet web results for fine paper

The maximum production speed of fine paper grades is limited by high bulk and the quality demands of the market. In order to prevent moisture-induced cockling and curl, high bending stiffness and uniform structure are usually required /24/. Because of these requirements, fine paper is often produced using a low jet/wire ratio and reduced nip loads on the press section. The tensile strength of dry and wet paper, and residual tension as a function of the jet/wire ratio, are presented in Figs. 14 and 15.

The MD/CD ratio of tensile strength is similar for dry and wet samples as a function of the jet/wire ratio. If the MD/CD ratio is increased from 2.5 (typical for fine paper) to 3.8 (typical for LWC), MD residual tension is increased only by 15%. The production speeds of paper grades do not determine their respective MD/CD ratios. In prior studies mechanical pulps gave 100% high-

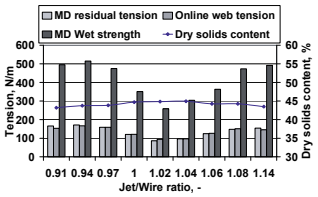

Fig. 16. Residual tension of press dry fine paper (grammage 70 g/m², hardwood 70% softwood 30%, filler content 10%) after 0.475 s at 1% strain (1,000%/s), online measured tension and tensile strength as a function of the jet/wire ratio.

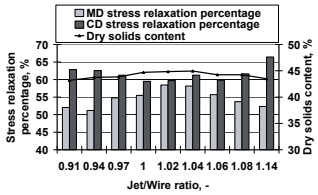

Fig. 17. Stress relaxation percentage of press dry fine papers (grammage 70 g/m², hardwood 70% softwood 30%, filler content 10%) after 0.475 s at 1% strain as a function of the jet/wire ratio.

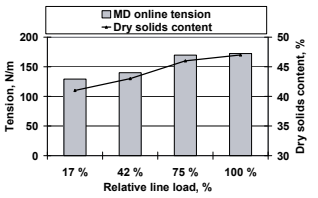

Fig. 18. Online web tension of wet fine paper (grammage 70 g/m², hardwood 70% softwood 30%, filler content 10%) as a function of relative wet pressing line load.

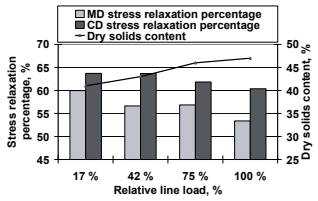

Fig. 19. Stress relaxation percentage of wet fine paper (grammage 70 g/m², hardwood 70% softwood 30%, filler content 10%) after 0.475 s at 1% strain as a function of relative wet pressing line load.

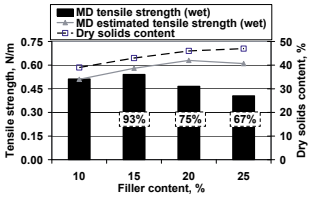

Fig. 20. Measured and estimated tensile strength of press-dry fine papers (grammage 70 g/m², hardwood 70% softwood 30%, filler content was varied).

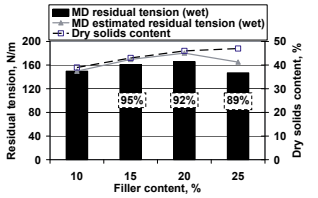

Fig. 21. Measured and estimated residual tension after 0.475 s at 1% strain for press-dry fine papers (grammage 70 g/m², hardwood 70% softwood 30%, filler content was varied).

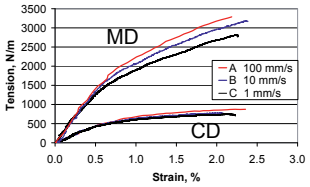

Fig. 22. Dry LWC paper stress-strain curves at different strain rates.

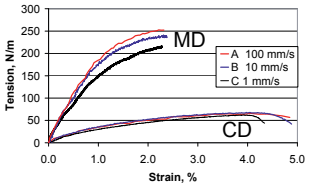

Fig. 23. Wet (d.s.c. 45%) LWC paper stress-strain curves at different strain rates.

er residual tension in wet handsheets than chemical pulps /1, 21/.

Fig. 16 shows the effect of the jet/wire ratio on residual tension, online web tension and the tensile strength of wet web. Online web tension in open press-to-dryer transfer and residual tension were affected in the same manner by the jet/wire ratio. However, it was a pure coincidence that online web tension and residual tension were at same level in Fig. 16.

Web tension was only 30%–35% of the tensile strength of a wet web in Fig. 16, and runnability problems are therefore not typically related to the tensile strength of the wet web. Defects in wet paper web increases rapidly the probability of web breaks. Problems occur in an open draw, but also after the draw due to the relaxation.

The effects of the jet/wire ratio on the stress relaxation percentages of wet samples (MD and CD) at 1% strain are presented in Fig. 17. A higher degree of fiber orientation in the loading direction decreased the stress relaxation percentage. MD/CD ratio for fine was 2.5 with jet/wire ratio 1.06. At this orientation level, 55% of the web tension was lost in 0.475 seconds. By increasing the jet/wire ratio to 1.08, MD/CD ratio was 3.8, and the stress relaxation percentage was lowered to 53%. The CD relaxation percentage was also significantly higher than the MD percentage. This can be explained by the fact that the CD stiffness of the web is actually generated during the web shrinkage on the dryer section.

The effects of relative wet pressing line loads on online web tension and stress relaxation percentages are presented in Figs. 18 and 19. Stress relaxation percentage is the lost component of stress during the relaxation. Web tension increased by 30% when the dry solids content was increased through wet pressing from 41% to 47%. Adhesion between the wet web and center roll is known to increase with increased line load. Both adhesion and dry solids content have a strong effect on wet web behavior.

Increased filler content with constant wet pressing gave higher apparent wet web dry solids contents (Fig. 18). Higher dry solids content will not always improve wet web tensile properties. Fibers absorb water whereas filler particles do not, and therefore dry solids content is increased (the dry solids content of filler particles is close to 100%). In fact, the consolidation of the wet web may be reduced by increased filler content because the removal of free water residing between fibers is reduced.

The change of filler content changed both dry solids content and mechanical properties of samples. The effect of filler content on mechanical properties is shown in Figs. 20 and 21. The dashed lines in Figs. 20 and 21 represent the estimated values, if only dry solids content would have changed (estimated from Fig. 18).

The maximum tensile strength was achieved with 15% filler content, and the maximum residual tension with 20% filler content (see Figs. 20 and 21). Residual tension values are closer to calculated values than tensile strength values.

Strain rate

The MD and CD effect of strain was studied with dry and wet LWC base paper (initial dry solids contents 45%, TMP 60%, kraft 40%, filler content 14%) /21/. Samples were dried with shrinkage control. MD tension was 5 to 6-fold compared to CD tension. The strain rates in Figs. 22 and 23 were (A) 100 mm/s, (B) 10 mm/s and (C) 1 mm/s. The higher the strain rate, the higher the tension in Figs. 22 and 23.

Tensile strength of wet paper at 45% dry solids content was about 10% of the tensile strength of dry paper (Figs. 22 and 23). A wet web runs on the paper machine at the same speed as a dry web even though the strength of the wet web is significantly lower.

Maximum tension after draw increased linearly in relation to the common logarithm of the strain rate (Fig. 24, arrow A). On the other hand, the stress relaxation percentage also increased linearly against the logged strain rate (Fig. 24, arrow B). The strained paper both gained more tension at a higher strain rate and also lost more tension over the same relaxation period. The ultimate level of residual tension that ensures runnability depends strongly on the relaxation time. After a very short relaxation time (<< 0.5 s), residual tension was higher at higher strain rates, but the difference was smaller with longer relaxation times.

The stress relaxation percentage was decreased by increased strain at any given strain rate (Fig. 24, arrow B). This means that at smaller strains a bigger percentage of tension was lost during stress relaxation. The absolute value of stress relaxation was, of course, increased by increased strains (and tension) and higher maximum tension. The higher values of stress relaxation at low strains (tension levels) may be the result of fiber activation.

Essential in Fig. 24 are the paper grade and fiber orientation. Wet fine paper typically has lower maximum tension at the same amount and rate of strain than wet wood containing paper. At higher fiber orientation, the stress relaxation percentage is lower (see Fig. 17).

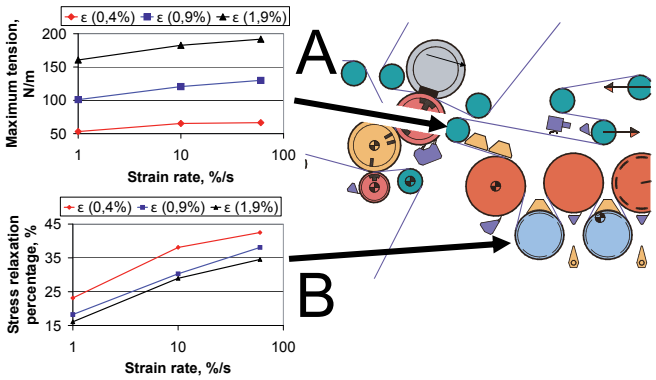

Fig. 24. Wet (d.s.c. 56%) fine paper (hardwood 70%, softwood 30%) handsheet maximum tension (A) and stress relaxation percentage after 0.475 s relaxation (B) at three elongations (0.4%, 0.9%, 1.9%) and three strain rates (1%/s, 10%/s, 60%/s). Maximum tension (A) describes web tension in a paper machine open draw and stress relaxation percentage (B) describes the amount of lost tension component on the first drying cylinders of paper machine.

Conclusion

This paper machine runnability study examined the effects of filler and Kraft content, refining level, the jet/wire ratio, and strain rate on the tensile and relaxation properties of a wet web.

The effect of the filler content of handsheets on in-plane tensile and relaxation properties was shown to be strongly dependent on dry solids content. Dry paper was affected more by filler content than wet paper. The distance between particles and the amount of free water determines the mechanical properties of wet paper /25/. Despite this, increased filler content radically lowers the residual tension of wet paper and general wet web runnability properties.

It was also shown that filler content affects more wet web tensile than relaxation properties. Maximal tensile strength and residual tension were gained at a filler content level of 10%–20% with constant press section parameters. These maximum values were probably reached with the minimum amount of free water in the wet web. The optimal amount of filler depends on filler and pulp type, as well as fiber orientation, and on paper machine running parameters at the forming and press sections.

Reinforcement pulp content is typically increased when wet web runnability problems occur on a paper machine. Reinforcement pulp is increased because dry paper strength is known to increase with higher reinforcement pulp content, and also because appropriate running parameter adjustments to address the problem are not known. We have shown here that the wet and dry tensile strength of paper and residual tension of wet paper were affected differently by apparent paper density and pulp composition (reinforcement pulp content).

The proper way to evaluate runnability would be to observe both residual tension and dry solids content. Wet web runnability can sometimes be improved by adding reinforcement pulp. However, improved runnability is brought about by increased press solids content, not by the properties of the reinforcement fiber.

The residual tension of pure reinforcement pulp at a 40%–60% dry solids content is typically low compared to pure mechanical pulps. The increased refining of reinforcement pulp improved the tensile strength and residual tension of dry and wet paper (mechanical and chemical pulp mix). Reinforcement pulp refining is limited by increased energy consumption and worse optical properties.

The effect of the jet/wire ratio was similar on both wet and dry MD/CD tensile strength ratios, whereas the MD/CD ratio of residual tension was significantly higher. This result further indicates the significance of drying and drying shrinkage control for the development of the CD elasticity properties of paper.

The increase of relative line load increased web tension and decreased the stress relaxation percentage after draw. However, this is also known to increase the adhesion force between the center roll and the web, which may neutralize the effect of a higher dry solids content /26/.

The indicated effects of strain rate on stress relaxation are not valid for all paper grades. Stress relaxation over short relaxation times may depend on fiber properties. The indicated effects of strain rate on tensile properties do apply to all paper grades, dry solids contents (30%...90%), and fiber orientations.

Wet end runnability and dry end runnability generally represent two different con-

siderations that cannot be addressed in the same manner. The probability of web breaks relates to the runnability of dry paper, where different types of flaws appearing in the web pretty much dictate break sensitivity. This is easy to understand, as the tensile strength of dry paper is typically 2.0–6.0 kN/m but web tensions on the paper machine are typically 150–400 N/m. In other words, only 10%–20% of web's total strength potential is used at the dry end of a paper machine.

In the case of the wet end, web tensions in open draw areas are on the order of 70–180 N/m, which is actually the same as the wet tensile strength of oriented paper! Based on this, it is clear that flaws appearing on the web are very important, but that web tension itself and its dynamic behavior are also relevant.

Given this, it is important to understand the nature of the relative speed differences (draws) that create web tension. The basic system employed in a modern paper machine is to create enough tension with wet strain for stable web travel while still limiting wet strain to a level where final dry paper properties are at an acceptable level. The wet web is attached to a supporting fabric surface after draws without any slippage, typically using external negative pressure. Since relaxation occurs in all papers subjected to a constant strain increase, the key item is the paper's tension preservation capability. This depends on draw levels, but most importantly on furnish and final pulp composition, including its numerous modification possibilities at different raw material handling and stock preparation stages.

References

1. *Kurki, M., Kouko, J., Kekko, P., Saari, T.*: Laboratory scale measurement procedure of paper machine wet web runnability. Part 1, Paperi ja Puu, 86(4):2004, 256–262.
2. *Perkins, R.W.*: Models for describing the elastic, viscoelastic, and inelastic mechanical behavior of paper and board, Mark, R.E., Handbook of Physical and Mechanical Testing of Paper and Paperboeard, Volume 1, p. 23–75.
3. *Johansson F., Kubát J.*: Measurements of Stress Relaxation in Paper, Svensk papperstidning, 67(20):1964, 822–832.
4. *Craven, B.D.*: Stress Relaxation And Work Hardening In Paper, Appita 16(2):1962, 57–70.
5. *Jantunen J.*: Visco-elastic properties of wet webs under dynamic conditions, 8th Fundamental Research Symposium, Oxford, 1985, 133–162.
6. *Mujumdar, A.S., Douglas, W.J.M*: Analytical modelling of sheet flutter, svensk papperstidning, nr. 6:1976, 187–192.
7. *Pramila A.*: Sheet flutter and the interaction between sheet and air, Tappi Journal, 69(7):1986, 70–74
8. *Chang, Y.B., Moretti, P.M.*: Interaction of fluttering webs with surrounding air, Tappi Journal, 74(3):1991, 231–236.
9. *Olsen, J.E.*: Lateral Mechanics of an Imperfect Web, Journal of Pulp And Paper Science, 28(9):2002, 310–314.
10. *Kurki, M., Vestola, J., Martikainen, P.*, at al.: The Effect of Web Rheology and Peeling on Web Transfer in Open Draw, 1997 Proceedings of the Fourth International Conference of Web Handling, Web Handling Research Center, Stillwater, p. 443.
11. *Hristopulos, D.T, Uesaka, T.*: A Model of Machine-Direction Tension Variations in Paper Webs with Runnability Applications, Journal of Pulp And Paper Science, 28(12):2002, 389–394.
12. *Kurki, M.*: Modeling of Kinematical and Rheological Web Line Behavior in a Papermaking Environment, Licentiate Thesis, University of Lappeenranta, 2005.
13. *Andersson O., Sjöberg, L.*: Tensile Studies of Paper at Different Rates of Elongation, Svensk papperstidning, 56(16):1953, 615–624.
14. *Rance, H.F.*: The Formulation of Methods and Objectives Appropriate to the Rheological Study of Paper, Tappi, 39(2):1956, 104–115.
15. *Malmberg, B.*: Remslängd och töjningshastighet vid spänningstöjningsmätningar på papper, Svensk Papperstidning, 67(17):1964, 690–692.
16. *Göttsching, L.*: Das Festigkeitsverhalten von Papier unter staischer und dynamischer Beanspruchung. Teil II., Paperi ja Puu 52(9):1970, 535–554.
17. *Göttsching, L.*: Das Festigkeitsverhalten von Papier unter staischer und dynamischer Beanspruchung. Teil III., Paperi ja Puu 52(10):1970, 655–669.
18. *Davidson R.W.*: The Weak Link in Paper Dry Strength, Tappi 55(4):1972, 567–573.
19. *Paetow, R.*: Über sad Spannungs- Verformungs-Verhalten von Papier, Doctoral Thesis, 1991.
20. *Kouko, J., Kekko, P., Kurki, M.*: Effect of strain rate on strength properties of paper, Proceedings of the 2006 Progress in Paper Physics – A Seminar, Miami University, Oxford, Ohio.
21. *Kouko, J., Kekko, P., Liimatainen, H., Saari, T., Kurki, M.*: Wet runnability of fibre furnish of magazine papers, Paperi ja Puu 88(3):2006, 169–174.
22. *Gill, R.A.*: Performance of precipuitated calcium carbonate fillers on fine quality printing and writing papers, Materials Interactions Relevant to Pulp, Paper and Woos industries Symposiumm San Francisco, April 18–20, 1990, 325–431
23. *Gill, R.A.*: The behaviour of on-site synthesized precipitated calsium carbonates and other calcium carbonate fillers on paper properties, Nordic Pulp and Paper research Journal, 4(1989), 120–127
24. *Kajanto. I.*: Structural mechanism of paper and board, paper physics chapter 6, Niskanen, K., Papermaking science and technology, book 16, Gullichsen, J., paulapuro, H., Fapet Oy Jyväskylä 1999, 192–202.
25. *Corson, S.R.*: Influence of fibre and fines fractions on thermomechanical pulp properties, Doctoral Thesis, Trondheim Norway, 1979.
26. *Shallhorn, P.M., Karnis, A.*: The mechanism of picking at the presses of a paper machine, CPPA Transactions of the Technical Section, 1(1975)4, 102–106.

Received June 22, 2006

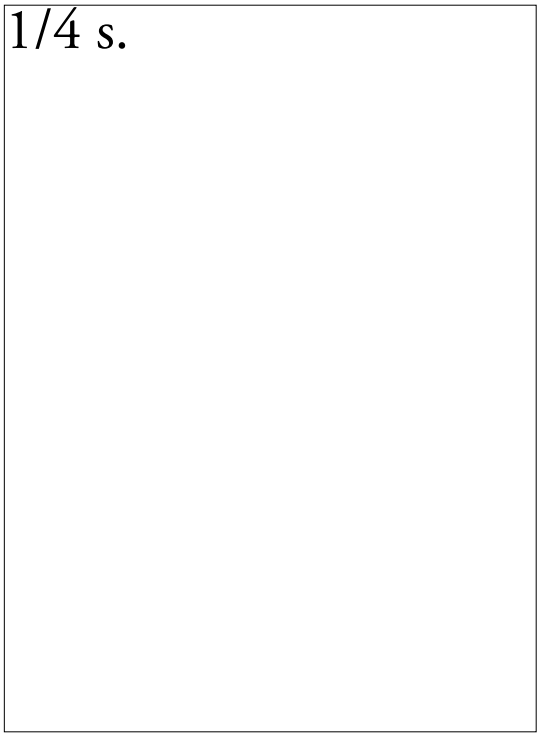

PVII

ROLL IN A PAPER OR BOARD MACHINE AND A DRYER GROUP IN A PAPER OR BOARD MACHINE

by

Matti Kurki and Pekka Martikainen 2008

United States Patent US20050075229

US007351309B2

(12) **United States Patent**
Kurki et al.

(10) **Patent No.: US 7,351,309 B2**
(45) **Date of Patent: Apr. 1, 2008**

(54) **ROLL IN A PAPER OR BOARD MACHINE AND A DRYER GROUP IN A PAPER OR BOARD MACHINE**

(75) Inventors: **Matti Kurki**, Jyväskylä (FI); **Pekka Martikainen**, Vaajakoski (FI)

(73) Assignee: **Metso Paper, Inc.**, Helsinki (FI)

(*) Notice: Subject to any disclaimer, the term of this patent is extended or adjusted under 35 U.S.C. 154(b) by 534 days.

(21) Appl. No.: **10/959,456**

(22) Filed: **Oct. 6, 2004**

(65) **Prior Publication Data**

US 2005/0075229 A1 Apr. 7, 2005

(30) **Foreign Application Priority Data**

Oct. 7, 2003 (FI) 20031461

(51) **Int. Cl.**
D21F 5/04 (2006.01)

(52) **U.S. Cl.** **162/207**; 162/363; 162/367; 162/368; 162/372; 34/116; 492/20; 492/30

(58) **Field of Classification Search** 162/363, 162/364, 367, 370, 371, 374, 206, 207; 34/109, 34/111, 116, 117, 120; 492/20, 30, 38
See application file for complete search history.

(56) **References Cited**

U.S. PATENT DOCUMENTS

3,259,961 A 7/1966 Bryand
3,283,415 A 11/1966 Schnyder
3,550,286 A 12/1970 Konttinen
3,773,613 A 11/1973 Lee et al.
4,202,113 A * 5/1980 Kankaanpaa 34/456
4,359,828 A * 11/1982 Thomas 34/114
4,441,263 A 4/1984 Vedenpää
4,516,330 A 5/1985 Eskelinen et al.
4,677,762 A * 7/1987 Futcher 34/114
4,882,854 A * 11/1989 Wedel et al. 34/115
4,888,883 A * 12/1989 Kerttula 34/116
4,905,380 A 3/1990 Eskelinen et al.
5,022,163 A 6/1991 Ilvespää et al.
5,172,491 A 12/1992 Ilvespää et al.
5,241,760 A * 9/1993 Wedel 34/115
5,347,728 A 9/1994 Pinter et al.
5,495,679 A 3/1996 Deshpande et al.
5,522,151 A * 6/1996 Deshpande et al. 34/114
5,542,192 A 8/1996 Deshpande et al.
5,996,244 A 12/1999 Saarikivi et al.

* cited by examiner

Primary Examiner—Eric Hug
(74) *Attorney, Agent, or Firm*—Stiennon & Stiennon

(57) **ABSTRACT**

A roll in a paper or board machine has a roll frame or center shaft (**15**) with bearings mounted at its ends and a groove-like surface structure (**10**). There is a contact between the surface structure and the center shaft so that an essentially closed structure is formed. The roll produces a vacuum that keeps the web attached to the outer surface of a fabric in the fabric wrap area of the roll circle by utilizing the boundary layer airflows of the surface structure flow and/or of the web. A dryer group has at least one contact dryer cylinder and at least one turning roll with a single fabric run arrangement.

12 Claims, 8 Drawing Sheets

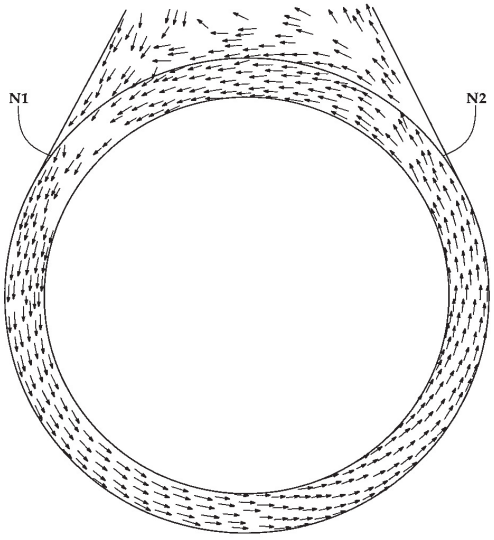

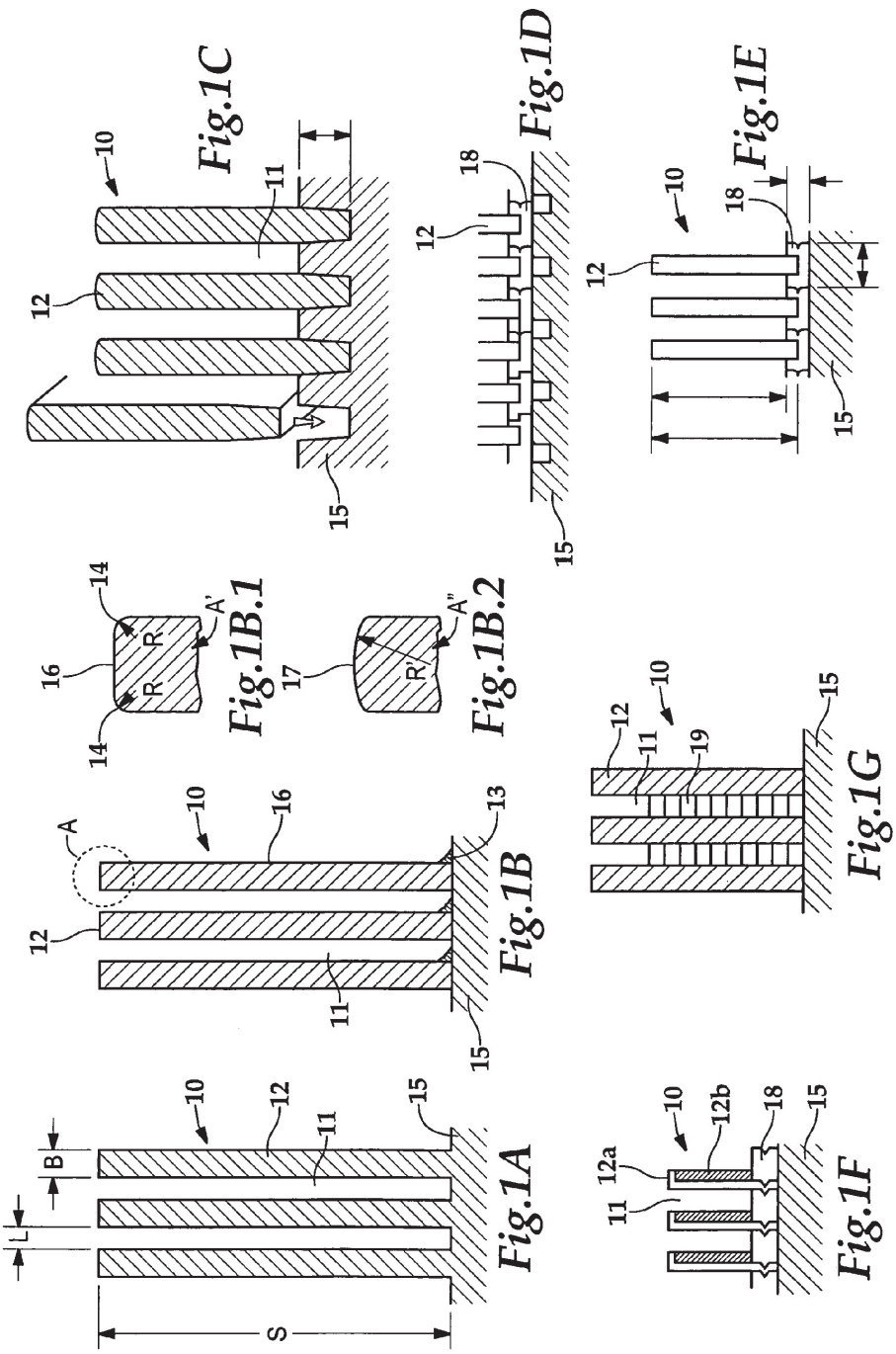
10
11
12
15
Fig.1C
18
Fig.1D
Fig.1E
14
16
17
R
R'
A'
A"
Fig.1B.1
Fig.1B.2
A
13
Fig.1B
19
Fig.1G
12a
12b
Fig.1F
B
L
S
Fig.1A

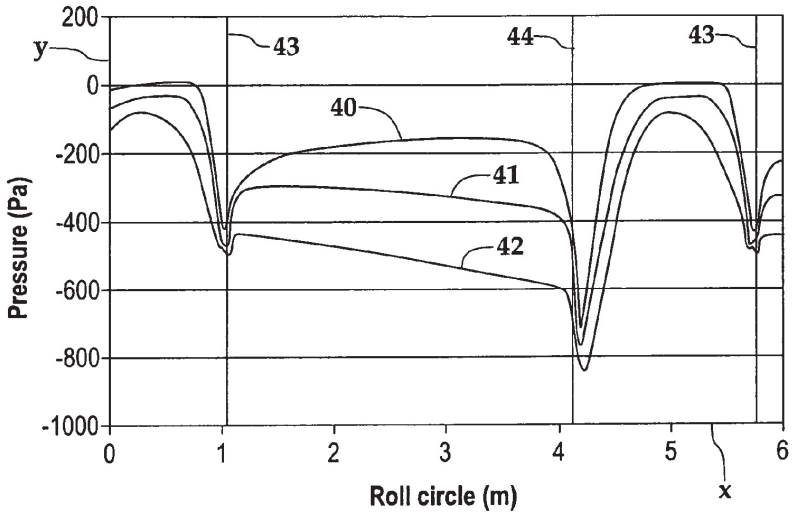
200
y
0
-200
-400
-600
-800
-1000
Pressure (Pa)
43
44
43
40
41
42
0
1
2
3
4
5
6
Roll circle (m)
x

Fig.2A

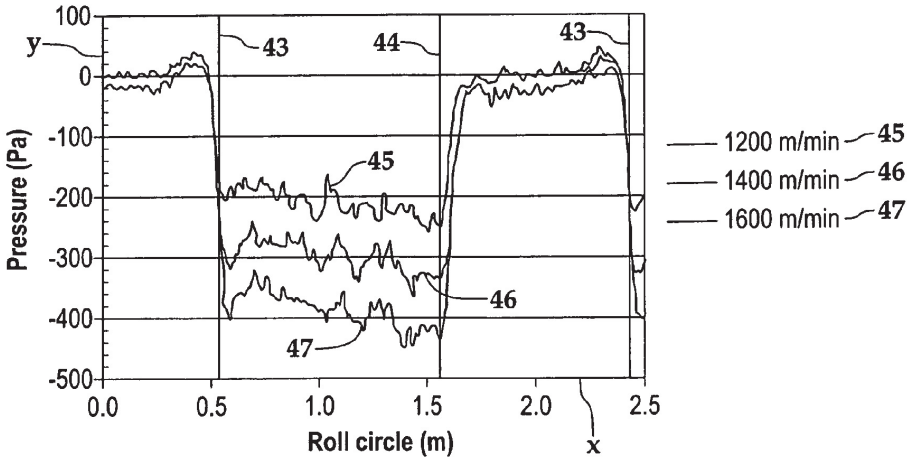
100
y
0
-100
-200
-300
-400
-500
Pressure (Pa)
43
44
43
45
46
47
0.0
0.5
1.0
1.5
2.0
2.5
Roll circle (m)
x
1200 m/min 45
1400 m/min 46
1600 m/min 47

Fig.2B

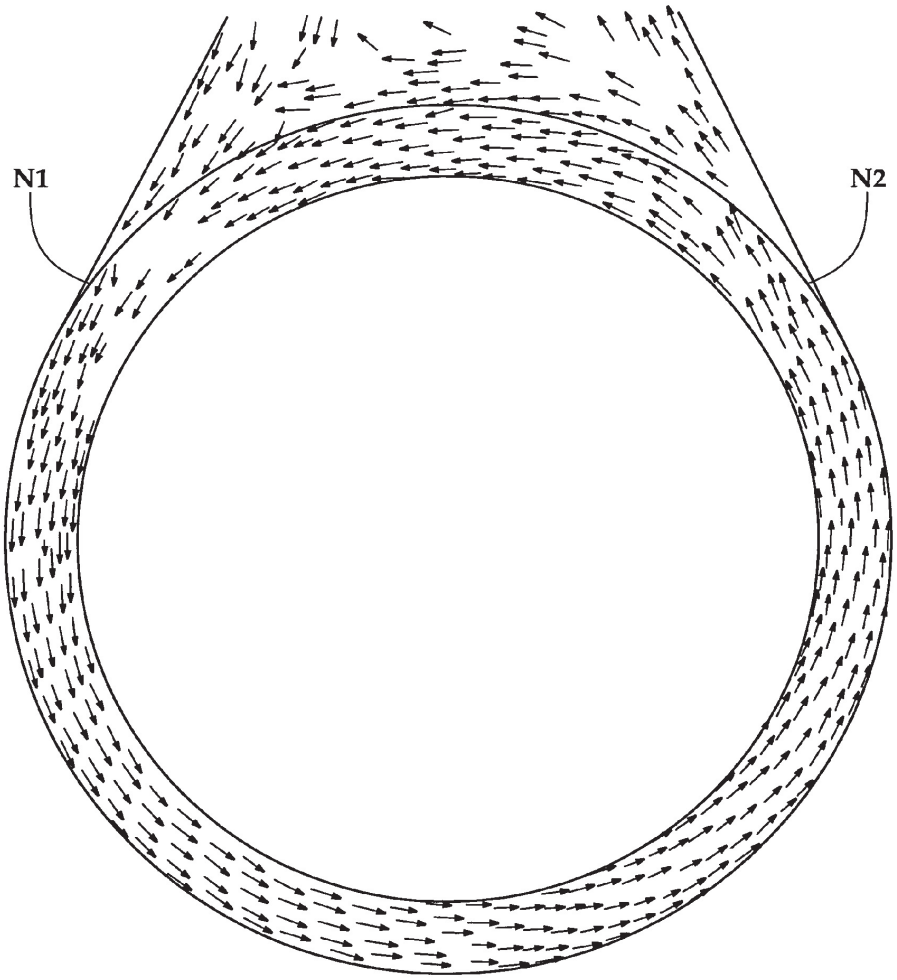

Fig.3

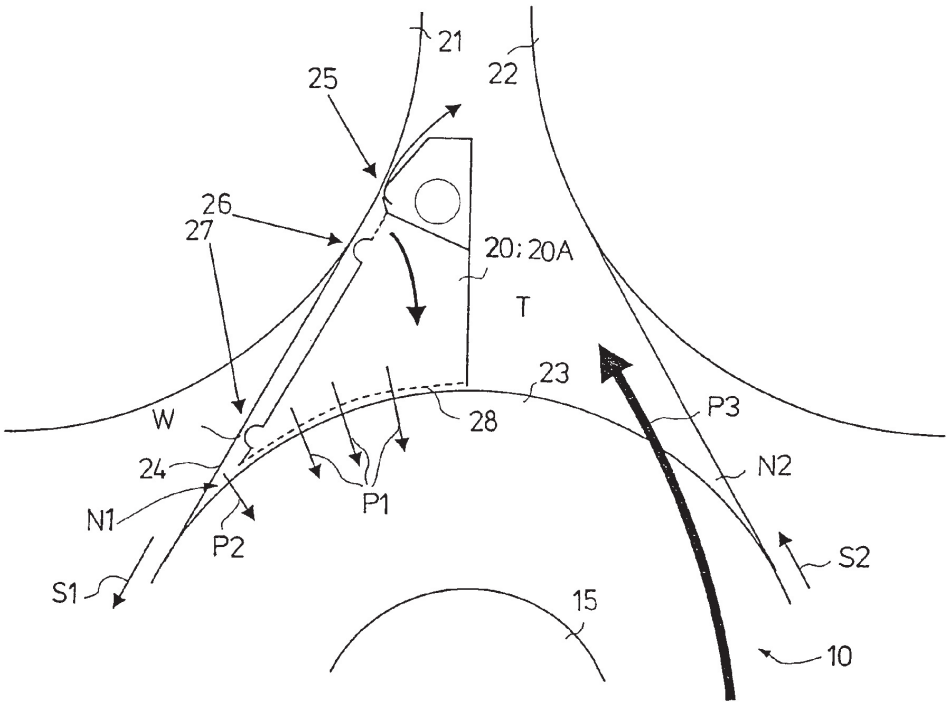

FIG. 4

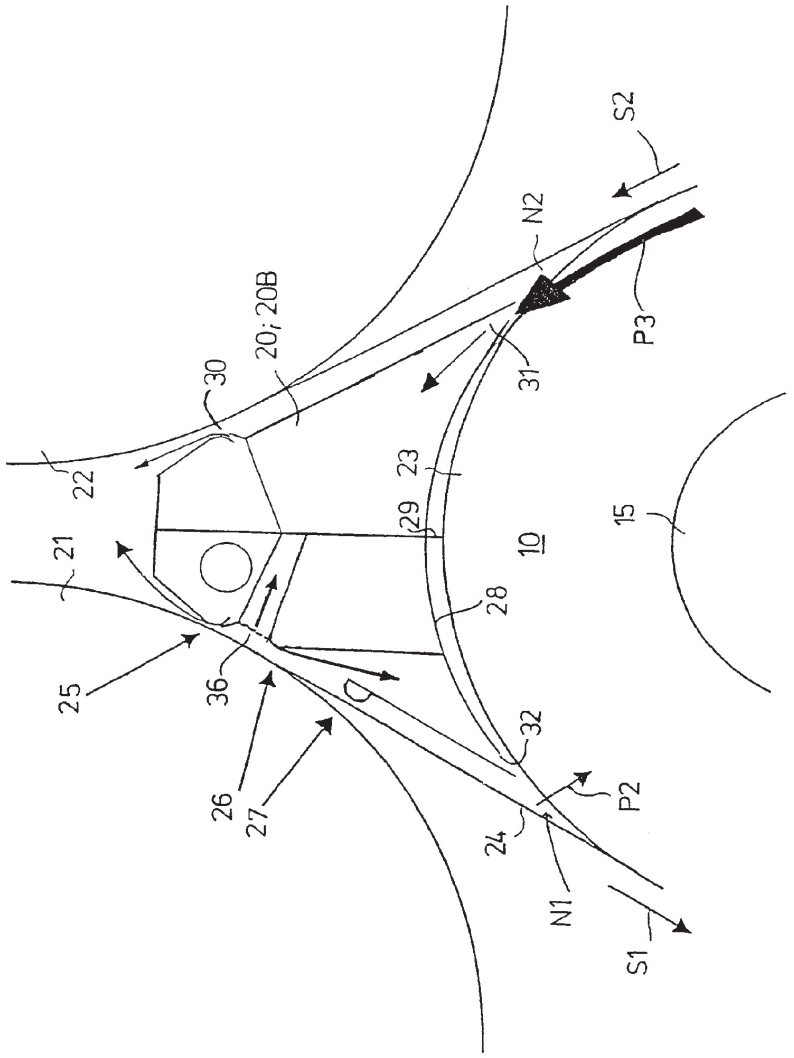

FIG. 5

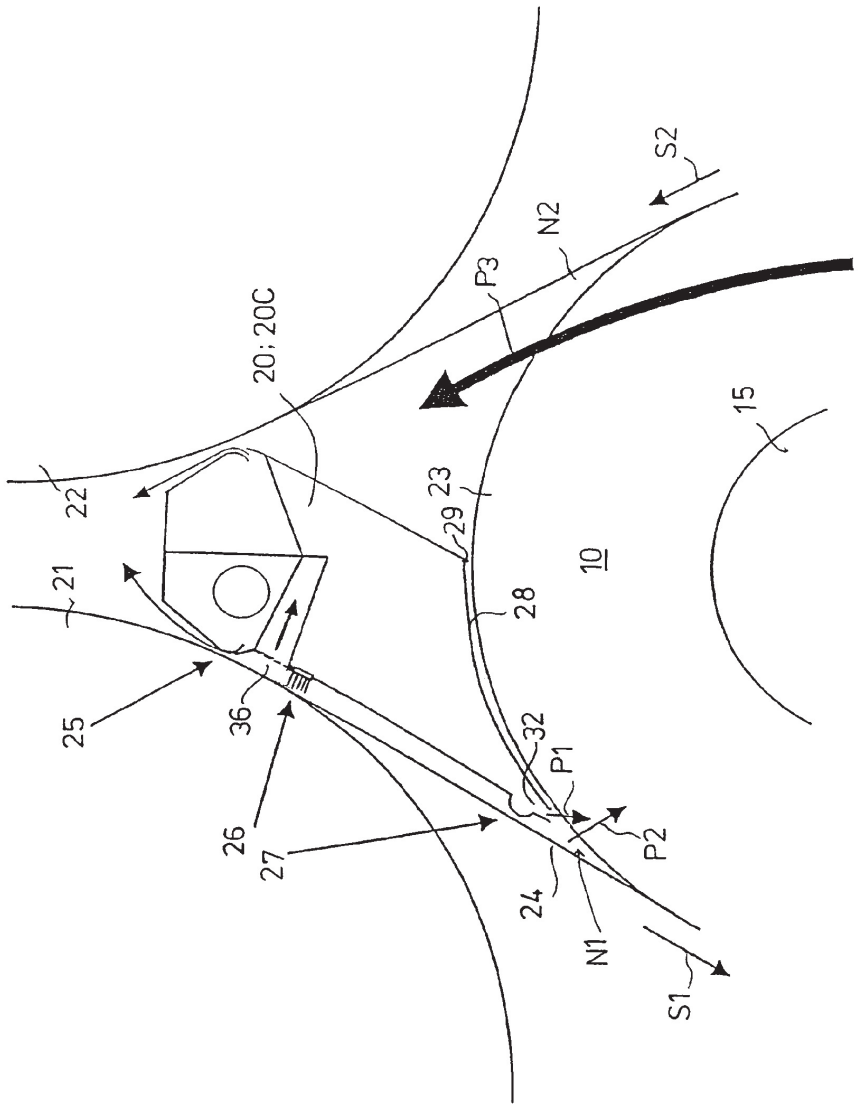

FIG. 6

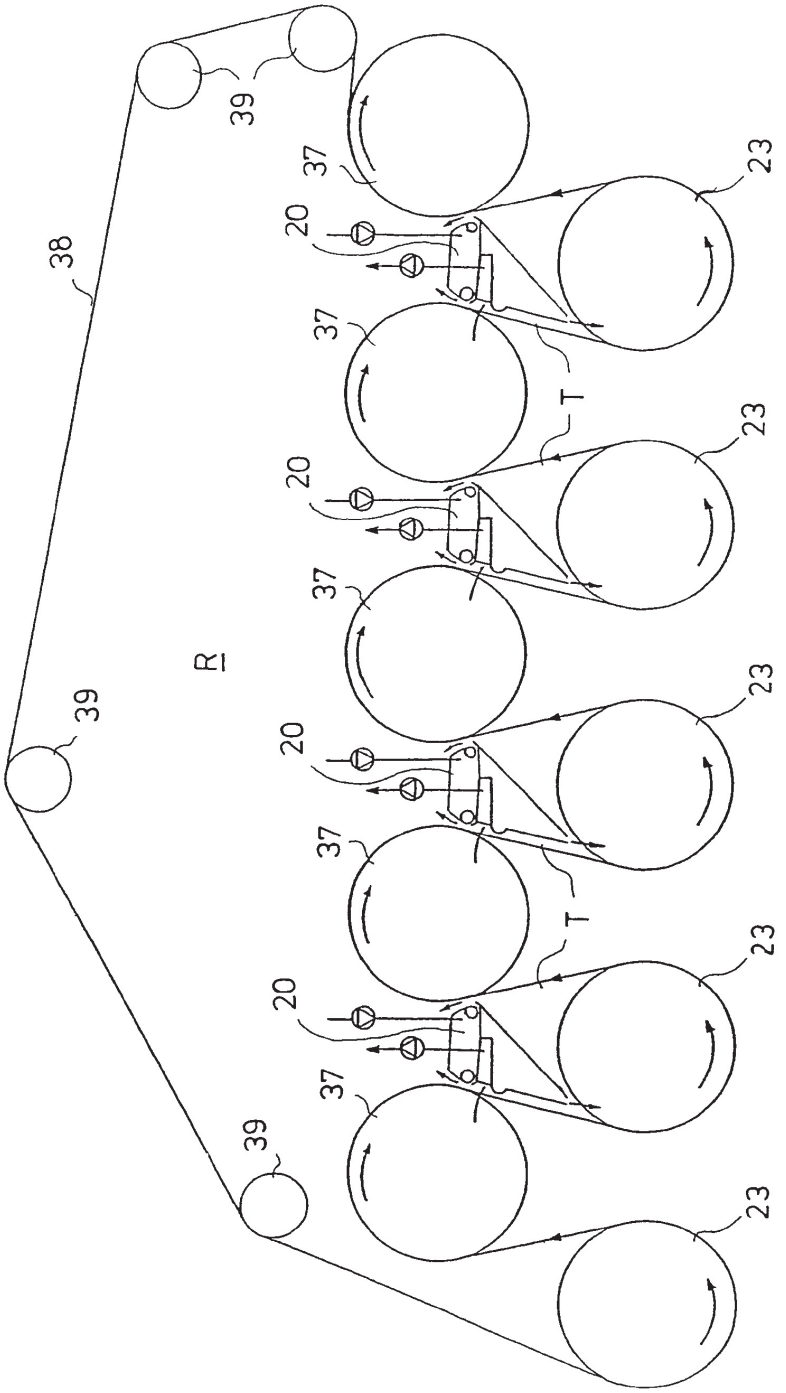

FIG. 7

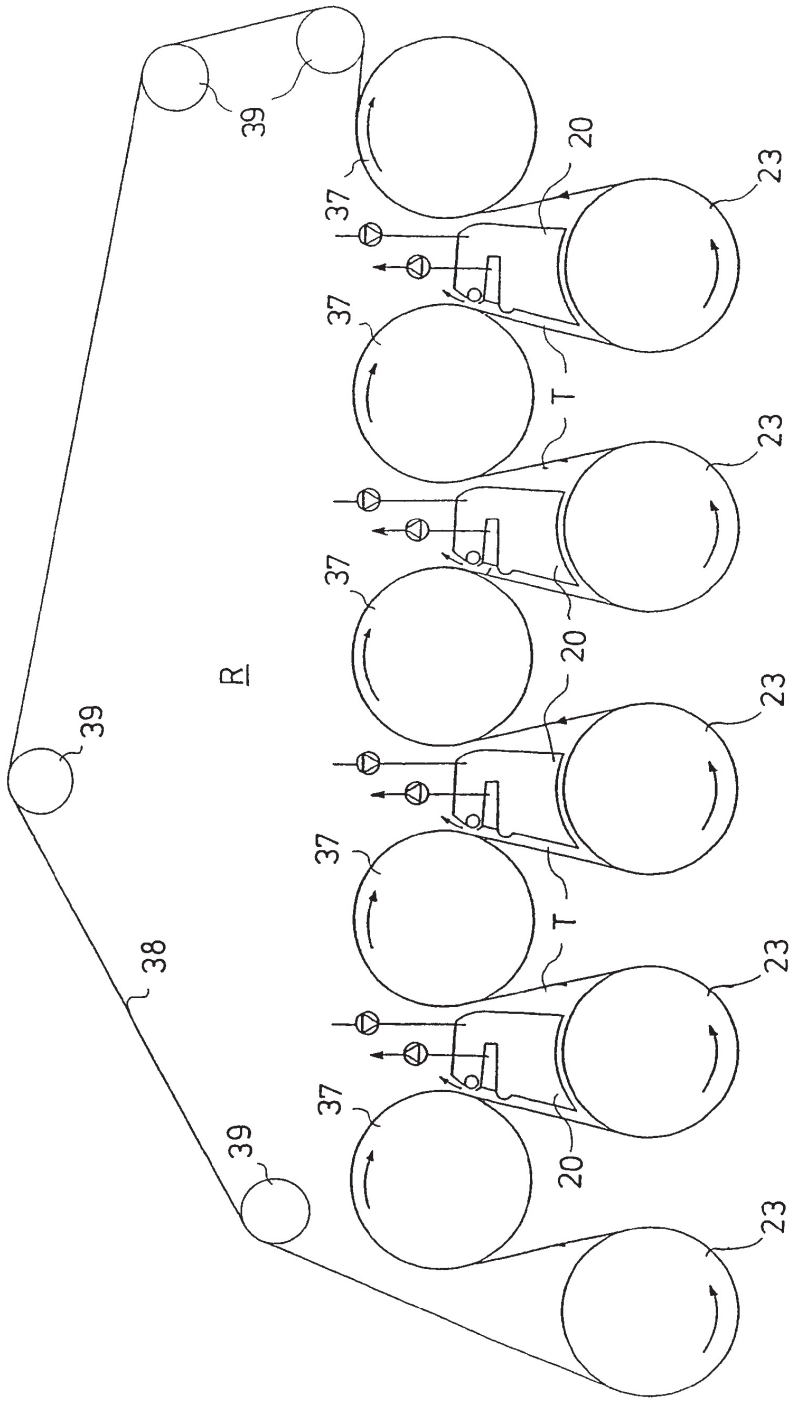

FIG. 8

ROLL IN A PAPER OR BOARD MACHINE AND A DRYER GROUP IN A PAPER OR BOARD MACHINE

CROSS REFERENCES TO RELATED APPLICATIONS

This application claims priority on Finnish Application No. 20031461, Filed Oct. 7, 2003, the disclosure of which is incorporated by reference herein.

STATEMENT AS TO RIGHTS TO INVENTIONS MADE UNDER FEDERALLY SPONSORED RESEARCH AND DEVELOPMENT

Not applicable.

BACKGROUND OF THE INVENTION

The invention relates to rolls and dryer groups in a paper or board machine.

The use of double fabric run and/or single fabric run arrangements in the dryer groups of multi-cylinder dryer sections of paper or board machines is previously known. In the double fabric run arrangement the dryer cylinder groups have two fabrics pressing the web one from above and the other from below against heated cylinder surfaces. Between the dryer cylinder rows, generally horizontal rows, the web has, in the double fabric run arrangement, free and unsupported draws, which are liable to fluttering, which may cause web breaks, particularly at such drying stages, in which the web is still relatively moist and therefore weak for its strength. Due to this, during several past years there has been increasing use of the said single fabric run arrangement, in which each dryer cylinder group has only one dryer fabric, supported by which the web travels through the entire group, the dryer fabric pressing the web against the cylinder surfaces heated by the dryer cylinders and the web remaining outside the outer curve at the turning cylinders or turning rolls located between the dryer cylinders. Thus, in the single fabric run arrangement, the dryer cylinders are positioned outside the fabric loop and the turning cylinders or turning rolls are located inside the loop. In so called normal single fabric run groups the dryer cylinders are in the top row and the turning cylinders or turning rolls are in the bottom row, and correspondingly, in so called turned single fabric run groups, the dryer cylinders are in the bottom row and the turning cylinders or turning rolls are in the top row.

In known dryer groups adapting the single fabric run arrangement the dryer fabric and the paper web are transferred from the previous drying element, such as a contact dryer cylinder, to a turning or suction cylinder or similar in a common straight run, whereby a closing wedge space, also referred to below as closing nip, is formed between the dryer fabric and the last-mentioned turning cylinder or suction cylinder surface. The dryer fabric and the cylinder surfaces moving towards this nip tend to generate positive pressure in the said wedge space by means of the boundary layer flows conveyed by them. This again produces a pressure difference over the paper web supported by the dryer fabric, the pressure difference having a tendency to detach the paper web from the dryer fabric causing runnability problems, wrinkles, and even web breaks. On the other hand, for improving the efficiency of dryer sections, the need arises for using dryer sections with a more compact construction than heretofore, in which the contact dryer cylinders and the mentioned suction cylinders are as close as possible to each other. All these aspects together with rising web speeds increase the overpressure problems of the said closing nip. It is previously known that the transfer of the paper web in the single fabric run arrangement on the contrary from the turning suction cylinder to the contact dryer cylinder takes place after a so called opening nip, supported by the dryer fabric. In dryer sections suitable for the single fabric run arrangement, the term pocket space is used to refer to the pocket-like space, which is limited by two parallel dryer cylinders and the turning cylinder and dryer fabric between them.

In the solutions known in the prior art technique, attempts have also been made to remove the problems occurring in the area of the closing nip by means of roll suction, roll sector suctions and various types of vacuum-generating boxes as well as by using combinations of rolls and suction boxes, which, however, have not necessarily been able to completely eliminate the problems in this area in an energy-efficient manner. At high machine speeds the requirement of energy used for web stabilization also strongly increases. Typically the power requirement increases to the power of three in relation to the web speed.

A solution for removing the problems in this area is set forth in the FI patent No. 105573 (corresponding U.S. Pat. No. 5,996,244), which discloses a roll in a paper machine, particularly in a paper drying device, and a dryer group in a paper machine, in which the roll in the paper drying device comprises a shaft, supported by which the roll is adapted to rotate, and a surface structure, connected to the shaft with support pieces or similar, in which the openness of the surface structure of the roll is more than 10% and the surface structure of the roll is open in a slot-like manner so that during the roll rotation an effect is produced that aspirates air to inside the roll, whereby an air flow-through is created through the roll. In a dryer group of a paper machine, in which dryer group the single fabric run arrangement is adapted, at least one of the turning rolls of the dryer group is an open roll of the type described above.

SUMMARY OF THE INVENTION

The object of the present invention is to develop further the above-described corresponding technique in order to principally solve the problems related to the web transfer in the mentioned closing nip area as well as in the turning roll area covered by the web.

Particularly at high speeds, e.g. exceeding 1,400 m/min, an extremely critical area for runnability at the beginning of a dryer section equipped with a single fabric run arrangement is the above-described closing nip area of the turning cylinder, and the object of the invention is therefore to set forth more efficient and more energy-saving new constructions for removing the drawbacks in this area prone to runnability problems.

The object of the invention is to set forth a roll during the use of which runnability problems in the closing nip area of the turning roll are eliminated or at least minimized.

Another object of the invention is to set forth a dryer group of a paper machine that is better for runnability than the known solutions.

The invention is based on a roll having a large open surface area, with its key characteristic being the capability to create a vacuum in the fabric wrap area together with the dryer fabric or the dryer fabric and paper. The generation of vacuum is based on

a) a change in the angular momentum of the in-going gas flow, such as airflow, taking place in the closing nip, which intensifies the inflow,

b) flow adjustment and pumping in the roll grooves and channels, which flows are influenced by the centrifugal forces created by the roll rotation, and

c) the vacuum effect of the opening nip, which aspirates gas, e.g. air, creating a vacuum, whose effect extends to the entire fabric wrap area.

Although the following description discusses airflows, air space, etc., this is not, however, intended to restrict the invention to such situations only, in which the flow is air. The flow can also be another gas (fluid).

The design of the roll according to the invention also allows increasing the vacuum-producing capacity of the roll along with a rising running speed, since the vacuum of the roll wrap area develops according to the formula

$$p=\zeta_f v^b [b=1.3\text{-}2],$$

where p=vacuum change,
ζ_f=fluid density, and
v=running speed.

According to the invention the roll comprises a surface structure having a large, most preferably groove-like open surface area, such as plate disks, and a center shaft and/or alternatively roll frame with grooves machined in it. According to the invention, both the vacuum produced by the roll and its profile on the roll surface are optimized to the maximum so that a contact exists, if required, between the surface structure, such as the plates, and the center shaft, i.e. there is no free air space between the roll frame and the grooves. According to the invention, a roll construction preferable for efficiency is provided for example by attaching plates with different diameters to a solid frame roll/shaft, the plates forming the grooving when placed at suitable intervals.

In the roll according to the invention the surface structure is so formed that most preferably a grooving is formed, in which the depth of each groove is approximately 10-155 mm, most appropriately 18-85, and the groove width is 1-50 mm, most appropriately 6-10 mm. The proportion of the groove width to the land width is most appropriately 0.6-2.0.

The most common form for the roll surface grooving is the U shape or one very much similar to it. The grooving can be straight or spiral. The grooving can be made by disk cutting and/or turning the frame roll surface. It can also be produced by welding, gluing or mechanically locking separate plate disks, made of metal, polymer or combinations of several materials, to the frame roll surface, in which case the part in contact with the fabric or otherwise the most external part is highly wear-resistant. The grooving can also be produced using a so-called G strip technique, in which the strip is applied directly on top of the smooth frame roll or in special mounting grooves in the frame roll surface. As a special application, the G strip is applied to an old or new frame roll by means of a support strip.

When the roll functions in the application placed against the fabric, the edges in the land supporting the fabric can be rounded, e.g. with a rounding radius of R=1-3 mm, or the whole land can be made to a slight circular arch, say with a radius of curvature of R'=100-500 mm, or the form can be selected in some other way so that the surface pressure between the fabric and the roll is optimal and the fabric wear is reduced.

The roll according to the invention can have a perforation at the bottom of the grooves, or the frame roll can have a perforation independent of the grooving geometry. In addition, according to a special aspect of the invention, the perforation can also appear at the groove peak/land so that the perforation opens to the contact surface of the fabric. This construction is particularly useful in a tail threading situation, since the tail can be stabilized to the fabric surface more efficiently with a higher vacuum.

When using a roll according to the invention, a dryer fabric that is normal for permeability is intended, such as a dryer fabric, whose permeability is 500 $m^3/(m^2h)$, preferably 1,000-35,000 $m^3/(m^2h)$, most appropriately 1,000-5,000 $m^3/(m^2h)$.

The advantages of the invention are its efficiency and simplicity. According to a preferable embodiment of the invention, the roll diameter is for example 1,500 mm. Separate plate disks have been attached for example by welding to a frame construction with a diameter of 1,300 mm, which does not need to be an actual frame roll, but a support construction similar to it. The height of the plate disks is 100 mm and their width is 6 mm. A 7-mm wide open groove remains between the plate disks. The peak of the plate disk is rounded with the radius of curvature R'=150 mm. A simulation model has provided results according to which the roll generates a good vacuum on its surface both in the closing and in the opening nip as well as a vacuum of almost the same level −500 to −900 Pa in the rest of the fabric-covered area on the roll surface. With the plate arrangement/grooving according to this preferable embodiment of the invention, the vacuum of the roll surface can be brought to a level of −500 to −900 Pa, based on the results achieved from the simulation, depending on the position of the wrap area. These pressure levels are for example of the same class as with the suction roll marketed with the trademark VacRoll™ of Metso Paper, Inc., in which the suction air volume is 400 $m^3/(hm)$ (2000 m/min). This vacuum in the fabric wrap area is achieved with the indicated power entirely without external aspiration or without runnability components in the pocket space.

The roll according to the invention, having a groove structure, such as lands of plate, preferably adapted around a solid center shaft or a frame roll, provides an inwardly air pumping phenomenon in the groove construction, which is generated when the air conveyed with the fabric hits against the roll surface and the groove walls, such as the plates. The airflow accelerates in the grooves and then exits from the opening nip. The inwardly pumping phenomenon in the roll according to the invention, providing a vacuum without special roll-external vacuum-providing equipment, is intensified with an increasing rotating speed. Thus, it automatically produces its own vacuum utilizing external boundary layer flows and/or blasting flows starting from the closing nip of the turning cylinder and continuing until to the opening nip, and this enables providing a preferable and efficient paper machine roll, which is particularly useful as a turning roll/cylinder of the dryer groups of a paper machine dryer section.

The roll creates the vacuum effect due to the fact that in the closing nip there occurs a change of angular momentum of the gas (fluid) flowing to the grooves. The gas flow directed to the roll grooves proceeds in the roll grooves to the area of the opening roll nip, whereby a vacuum effect is created, which extends over the entire fabric wrap area.

The roll surface structure is formed in such a manner that the vacuum effect and gas pumping are created by the friction between the structure and the fluid, the boundary layer, and accelerating movement of gas.

In the roll according to the invention, air hits against the surfaces of the groove walls, such as plates, placed around

the center shaft, whereby the groove walls tend to pump the air forwardly and particularly in a closing nip, also inwardly towards the shaft. Air circulates around the roll frame until to the opening nip. In this way the vacuum effect is created by a combined effect of three factors, i.e. the impact, flow and opening nip.

In connection with the invention it is possible to use a blow box according to a preferable embodiment of the invention described below in more detail, which is used to intensify the effect of the opening nip for example with trailing side aspiration, or on the other hand, a blow directed to a closing nip is used to intensify the impact and flow effect on the side of the closing nip. In addition, it is preferable to separate these areas of influence of the opening and closing nip from one other with a sealing in the roll axial direction/a blow box wall construction.

According to a preferable further characteristic of the invention, in a drying geometry based on the single fabric run design, besides the roll according to the invention, a box constructed on the leading side is used, built up of a separate blow box including a flexible nozzle solution and a passive box space attached below it, which has aspiration/an ejection blow, if required, and is open at the bottom part.

In this embodiment of the invention, aspiration is directed to the suction zone of the blow box using the passive box section. When this box is realized according to the blow nozzle/flow divider principle, it is possible to achieve a vacuum of approximately −1000 Pa in the high-vacuum zone (2.2 mm nozzle, blow air volume 900 m^3/(hm)).

This embodiment of the invention preferably also includes two flow divider/sealing elements in the box on the leading side, and by adjusting their distance to the fabric it is easy to adjust the vacuum of both the high-vacuum zone and the vacuum influencing in the open gap area, which keeps the web on the fabric surface before it comes to the influence area of the roll according to the invention. This allows efficiently preventing excessive bending of the fabric.

The total air volume requirement in the above-described system is 900 m^3/hm per blow box, which is 50% of the present blow box/VacRoll™ total air volume. Consequently, the blower power requirement also decreases by 50%, which in practice can mean a decrease of approximately 1 MW in the power consumption in the dryer section of a large modern paper machine. It is remarkable that the roll according to the invention preferably replaces this underpressurized turning roll, in which case runnability components (e.g. blow boxes) that are almost like the present ones are used in the pocket space, designed to improve/intensify the performance of the proposed roll.

The roll according to the invention is also easy to keep clean, because the airflows automatically created by it simultaneously prevent dirtying of the roll surface structure and grooving. Therefore, an advantage of the roll according to the invention is also in its operating principle, the flow direction changes during the rotation cycle whereby each point in the roll grooves is subjected to inflow and outflow, and the roll is then kept clean for a longer time.

According to a preferable further aspect of the invention, it is possible, if required, to arrange, in connection with the roll according to the invention, an adjustment/suction possibility through a connection placed on the roll hub for adjusting the vacuum effect as desired. This kind of connection can also be used in a situation in which at least one part in the roll axial direction is realized according to the known technique. The area of the tail or both edges, for example, could be constructed for this kind of adjustment, because the intensification of the vacuum effect by dividing the blow box in the cross-machine direction is not necessarily as efficient or easy to implement.

According to a preferable further characteristic of the invention, in the roll axial direction there is at least one part in which the air is adapted flowing through the openings in the roll shell to the roll interior.

The invention is described below in more detail by making reference to the figures in the enclosed drawing, to the details of which the invention is not intended to be strictly limited in any way.

BRIEF DESCRIPTION OF THE DRAWINGS

FIG. **1**A is a schematic view of the surface structure of an embodiment of the roll of this invention.

FIG. **1**B is a schematic view of the surface structure of an embodiment of the roll of this invention.

FIG. **1**B.**1** is an alternative partial enlargement A' of the region A in FIG. **1**B, showing the radius of curvature at the corners of a land.

FIG. **1**B.**2** is another alternative partial enlargement A" of the region A in FIG. **1**B, showing the radius of curvature formed large at a land.

FIG. **1**C is a schematic view of the surface structure of an embodiment of the roll of this invention.

FIG. **1**D is a schematic view of the surface structure of an embodiment of the roll of this invention.

FIG. **1**E is a schematic view of the surface structure of an embodiment of the roll of this invention.

FIG. **1**F is a schematic view of the surface structure of an embodiment of the roll of this invention.

FIG. **1**G is a schematic view of the surface structure of an embodiment of the roll of this invention.

FIGS. **2**A and **2**B illustrate examples of the effect of closing the open space between the plates and the center area in the roll according to the invention.

FIG. **3** is a schematic view of the flow behavior taking place in connection with the roll according to the invention.

FIGS. **4**-**6** show a schematic view of embodiments according to the preferable further characteristics of the invention, in which there is a blow box arranged in connection with the roll.

FIGS. **7**-**8** show a schematic view of preferable embodiments of the invention in connection with dryer groups adopting the single fabric run arrangement.

DESCRIPTION OF THE PREFERRED EMBODIMENTS

FIG. **1**A shows a surface structure **10** realized according to an embodiment of the roll according to the invention, in which the surface structure **10** is formed of turned or disk-cut grooves **11**, whereby lands **12** between the grooves **11** are simultaneously formed. In FIG. **1**B, on the contrary, the roll surface structure **10** is formed of separate plate disks **16**, attached with welds **13** or formed to the roll frame or center shaft **15** in another method known as such, which form the lands **12**, whereby the grooves **11** remain between them. In connection with FIG. **1**B, there are alternative partial enlargements A', A" of detail A indicated in FIG. **1**B.**1** and **1**B.**2**, in which according to the partial enlargement A', shown in FIG. **1**B.**1**, a radius of curvature R can be used in the corners of the lands **12**, such as plate disks **16**, which R is approximately 0.1-7 mm, or according to the partial enlargement A", shown in FIG. **1**B.**2**, the surface **17** of the

land **12**, such as a plate disk, can be formed large as to its radius of curvature R', with R' then being approximately 100-3000 mm.

According to the invention, regardless of the production method of the grooves, the edges **14**, **17** of the land **12** supporting the clothing shown in the partial enlargements A', A" can be rounded or shaped so as to reduce wear of the clothing, such as a fabric. In this case the open surface area of the roll can be slightly increased, which improves the roll performance particularly in the closing nip area. When the open surface area increases, the groove depth can be slightly reduced, if required, without deteriorating the roll performance.

FIGS. **1**C-**1**F illustrate the formation of the surface structure **10** of the roll according to the invention using the G strip technique, either without a support strip, FIG. **1**C, or with the support strip, FIGS. **1**D (grooved roll) and **1**E (smooth roll). According to FIG. **1**C, in the embodiment shown without a support strip, the G strip is applied slightly in a wedge form to the grooved roll shell **15**, and the bottom part of the G strip is slightly narrowing. According to FIGS. **1**D and **1**E, a grooved support strip **18** is applied to the roll surface with the strip **12** forming the lands, and the dimensions of the actual groove strip **12** are e.g. 45×5 mm and the dimensions of the grooved support strip **18** are 8×12 mm.

To form an open surface structure **10** of the roll according to the invention of the various embodiments shown in FIGS. **1**A-**1**G there are thus formed either grooves **11**, with the lands **12** remaining between them, or land sections **12** are attached to the roll center shaft or frame **15**, with the grooves **11** remaining between them. The depth S of each groove and thus the height of the land is approximately 10-155 mm, most appropriately 15-85 mm and the groove width L is 1-50 mm and the relation of the groove width L to the land width B is most appropriately 0.6-1.4.

According to a preferable embodiment shown in FIG. **1**B the roll diameter is for example 1,500 mm. Separate plate disks have been welded to a frame construction having a diameter of 1,300 mm, which does not need to be an actual frame roll, but a support construction similar to it. The height of the plate disks is 100 mm and their thickness is 6 mm. A 7-mm wide open groove remains between the plate disks. A simulation model has given results according to which the roll generates a good vacuum on its surface both in the closing and opening nip as well as a vacuum of almost the same level −500 to −900 Pa in the rest of the fabric-covered area on the roll surface. With the plate arrangement/grooving according to this preferable embodiment the vacuum of the roll surface can be brought to a level of −500 to −900 Pa, based on the results achieved from the simulation, depending on the position of the wrap area and the running speed.

In FIG. **1**F, according to a preferable embodiment of the invention, the open surface structure **10** of the roll has been formed by such land sections **12**, which comprise a metal part **12**A forming the frame construction **12**A of the land, and by a filler section **12**B, which is made for example of plastic or metal based material forming the other side wall of the groove **11**. In the embodiment according to FIG. **1**F the land sections **12** of the surface structure have been attached to the roll frame or center shaft with a support strip **18**. This structure according to FIG. **1**F has the advantage that the portions of metal and plastic can be optimized and the roll weight is also reduced and the renewal of the surface structure becomes easier.

FIG. **1**G shows a preferable embodiment of the invention in which separate plate units are attached to one another or to the center shaft using friction of form closing attachments. In the embodiment of FIG. **1**G plate disks **12** and **19** of different size have been attached to the roll frame for example by a shrink fit, whereby the alternately positioned plate disks form a surface grooving between them. It is also possible to produce plate disks comprising the structure of the disks **12** and **19**, which are then attached to each other using for example a form closing attachment. The use of plate disks of a different size also enables providing at least one roll part with a grooving of different depth, allowing to optimize the groove depth at the roll edges, for example, based on the generation of the maximum vacuum output.

FIG. **2**A shows the effect of closing the open space between the plates and the center shaft of the roll used in the embodiment according to FIG. **1**A. In the figure, X-axis represents the roll circle and Y-axis the pressure in the roll grooves. The top curve **40** in the figure illustrates an arrangement in which there is an open space between the plates and the center shaft, i.e. an arrangement according to the prior art technique, the center curve **41** and the bottom curve **42** represent situations in which the space interval between the plates and the center roll is closed, i.e. embodiments of the invention. Number **43** indicates a closing nip and number **44** an opening nip. The figure also shows pressure peaks present in the rotational pressure at the opening nip and at the closing nip. As shown in the simulation figure, the roll according to the invention can provide the above-mentioned rotational pressure on the roll surface. In the simulation the roll diameter was kept at 1,500 mm and the groove depth was 250 in the cases ofthe curves **40** and **41**, and 125 mm in the graph of curve **42**. The curves show that a groove closed at the center space generates greater vacuum than an open solution, and for the groove depths, 250 mm produces less vacuum than 125 mm.

FIG. **2**B illustrates measurement results of the effect of the running speed on the vacuum level of the roll circle showing that a speed increase increases the vacuum. This is preferable, because with a rising speed it is preferable that the forces keeping the web attached to the fabric surface at the turning roll also increase. Curve **45** represents the influence of the running speed 1,200 m/min on the vacuum level of the roll circle, curve **46** represents the influence of the running speed 1,400 m/min on the vacuum level of the roll circle, and curve **47** represents the influence of the running speed 1,600 m/min on the vacuum level of the roll circle. A closing nip is marked with number **43** and an opening nip with number **44**.

FIG. **3** depicts the flow behavior in the roll according to the invention for example in an embodiment according to FIG. **1**A, in which arrows are used to indicate the airflow. According to the invention, in the area of the closing nip N**1** the boundary layer airflow and a possible blasting flow hit against the roll plates. The impact produces airflows in the radial direction, and the flow between the plates accelerates being essentially an airflow in the tangential direction of the periphery. The flow continues until to the opening nip N**2** essentially in the direction of the tangential flow of the periphery.

In the embodiments according to FIGS. **4**-**6**, for preventing overpressurization of the pocket space T, a blow box **20**; **20**A, **20**B, **20**C is used. The blow box **20** is located in the pocket space T formed by the dryer cylinders **21**, **22** and the roll **23**, and it is provided with a flexible blow nozzle **25**, which is used to partly control the stream of the boundary layer flow conveyed with the fabric **24** to the closing nip N**1**. Further, the blow box is provided with projections **26**, **27** having a distance adjustment possibility, if required. This

can be used to prevent the fabric from conveying air with it and to seal the influence area of the vacuum zone restricted and thus more efficient. In boxes **20** producing a high vacuum it may also be preferable to use labyrinth sealing as shown in FIG. **6** for the sealing **26**. In the embodiment according to FIG. **4** the blow box **20** has a bottom surface **28** open towards the roll, from which the airflows P**1** are conveyed to inside the roll **23** according to the invention, intensifying in this way the in-pumping effect P**2** of the roll **23**. In the embodiments shown in FIGS. **5** and **6**, the bottom plate is without perforations, and, if required, inward pumping can be controlled with the nozzle **32** or even by using a blow nozzle in position **26**. This allows leading the blast air also through the interior of the box with adjustment of the air volume led to the roll **23** by removing part of the blast air. This prevents the canal between the box **20** and the fabric **24** from becoming overpressurized, which would hinder the runnability. Arrow P**3** indicates the airflow led outwardly from the roll **23** according to the invention in the area of the opening nip N**2**, which further intensifies the runnability. Arrows S**1**, S**2** indicate the travel direction of the fabric **24**. In the embodiments shown in FIGS. **4-6**, the sealing **29** separating the nip influence areas N**1** and N**2** is also shown in the boxes **20**.

FIG. **4** shows a so called half-pocket box **20**A, which fills the pocket space T on the side of the closing nip N**1** and leaving open the side of the opening nip N**2** of the pocket T, allowing the airflows of the trailing/up-going side to be freely removed form the pocket space without deteriorating the roll **23** performance.

FIG. **5** shows a so called box that fills the entire space, which fills the pocket space T and in which on the side of the opening nip N**2** there is created a blow that intensifies the airflow P**3** with the nozzle **30**, allowing thus to raise the vacuum production capability of the roll, while the aspiration **31** can still be used directly from the opening nip N**2**.

FIG. **6** shows a blow box **20**C, which in a sense represents an intermediate form between the blow boxes **20**A, **20**B illustrated in FIGS. **4** and **5**, and it has further a blow nozzle **32**, which can be used to adjust/intensify the vacuum production capability of the roll **23**.

Via the embodiments of FIGS. **4-8** it should be noted that the roll **23** functions as an active pump, in which case the blow boxes **20** and their use must be made in such a way that the flow-through air necessary for the roll operation exists. A preferable application principle is particularly the solution of FIG. **5**, which can be used to efficiently control the roll **23** operation.

The solutions illustrated in FIGS. **5**, **6** and **8** are preferable for the vacuum control of the pocket space T and for the intensification and control of the vacuum generated by the roll **23**. Particularly at the beginning stage of drying, higher vacuum is required especially for the runnability component of the pocket space (blow box), and the control of vacuum generated by the roll is also more useful in this case. At the final stage of drying it may be preferable to use a box according to FIG. **8** or even of FIG. **4**, the paper being then drier and easier to control.

FIGS. **7** and **8** show schematic views of dryer groups R adapting single fabric run arrangements, with rolls **23** according to the invention located as turning rolls and pocket spaces T, equipped with a blow box **20**, being used in connection therewith. The top row dryer cylinders are indicated with reference number **37** and the dryer fabric and its lead and guide rolls are referred to with numbers **38** and **39** respectively. FIG. **7** shows an embodiment, in which in the pocket spaces T of a dryer group R adapting a single fabric run arrangement, there is located a blow box **20**C, which corresponds primarily to the embodiment illustrated in FIG. **6**, allowing to optimize the vacuum production of rolls **23** considering the position of the group in the dryer section.

FIG. **8** shows an embodiment, in which the blow box **20** located in the pocket spaces T corresponds primarily to the embodiment illustrated in FIG. **4**, in which a plate without perforations **28** is applied and the suction at the opening nip of the cylinder is intensified with a separate suction connection **36**. Dryer groups R of the type illustrated in FIGS. **7** and **8** are particularly suitable for use as dryer groups at the beginning of the dryer section.

The invention is described above by making reference only to some of its preferable embodiments to the details of which the invention is not, however, intended to be strictly limited in any way.

We claim:

1. A dryer group in a paper or board machine comprising:

a first contact dryer cylinder, a second dryer cylinder and a turning cylinder positioned therebetween;

a single dryer fabric and a paper or board web arranged to travel over the first contact dryer cylinder with the paper or board web between the first contact dryer cylinder and the dryer fabric, and the paper or board web arranged to wrap around the turning cylinder supported by the dryer fabric to define a wrap area, and the dryer fabric and the paper or board web arranged to travel over the second dryer cylinder with the paper or board web between the second dryer cylinder and the fabric so that the paper or board web remains between the second dryer cylinder surface and the dryer fabric;

wherein the dryer group turning cylinder is a roll comprising a groove-like surface structure and a center shaft or a roll frame, wherein there is contact between the surface structure and the center shaft or roll frame so that a closed construction is formed except for a portion of the roll used for threading a tail;

wherein the turning cylinder roll is arranged with the dryer fabric to produce a vacuum that keeps the paper or board web attached to the dryer fabric at an outer surface within the wrap area of the turning cylinder;

wherein the groove-like surface structure has portions forming grooves 18-155 mm deep and 6-10 mm wide, and wherein lands of a defined width are formed between the grooves, and wherein the ratio of groove width to land width is 0.6 to 2.0, and the ratio of groove width to depth is 2.25 or greater.

2. The dryer group of claim **1**, wherein the lands have rounded edges with a radius of 1-3 mm.

3. The dryer group of claim **1**, wherein the lands have an outermost surface having a radius of curvature of 100-500 mm.

4. The dryer group of claim **1**, wherein the ratio of groove width to depth is 3.5 or greater.

5. The dryer group of claim **1**, wherein the ratio of groove width to depth is between about 2.25 and 16.

6. A dryer group in a paper or board machine comprising:

a first contact dryer cylinder, a second dryer cylinder and a turning cylinder positioned therebetween;

a single dryer fabric and a paper or board web arranged to travel over the first contact dryer cylinder with the paper or board web between the first contact dryer cylinder and the dryer fabric, and the paper or board web arranged to wrap around the turning cylinder supported by the dryer fabric to define a wrap area, and the dryer fabric and the paper or board web arranged to

travel over the second dryer cylinder with the paper or board web between the second dryer cylinder and the fabric so that the paper or board web remains between the second dryer cylinder surface and the dryer fabric;

wherein the dryer group turning cylinder is a roll comprising a groove-like surface structure and a center shaft or a roll frame, wherein there is contact between the surface structure and the center shaft or roll frame so that a closed construction is formed except for a portion of the roll used for threading a tail;

wherein the turning cylinder roll is arranged with the dryer fabric to produce a vacuum that keeps the paper or board web attached to the dryer fabric at an outer surface within the wrap area of the turning cylinder;

wherein the groove-like surface structure has portions forming grooves 18-155 mm deep and 6-10 mm wide, and wherein lands of a defined width are formed between the grooves, and wherein the ratio of groove width to land width is 0.6 to 2.0, and the ratio of groove width to depth is 2.25 or greater; and

wherein the depth of the of the grooves is selected to produce a vacuum on the surface structure of the turning cylinder which is wrapped by the paper or board web which is at least about 200 Pa when the dryer group is operated at a machine speed greater than 1200 meters per minute.

7. A dryer group in a paper or board machine comprising:

a first contact dryer cylinder, a second dryer cylinder and a turning cylinder positioned therebetween;

a single dryer fabric and a paper or board web arranged to travel over the first contact dryer cylinder with the paper or board web between the first contact dryer cylinder and the dryer fabric, and the paper or board web arranged to wrap around the turning cylinder supported by the dryer fabric to define a wrap area, and the dryer fabric and the paper or board web arranged to travel over the second dryer cylinder with the paper or board web between the second dryer cylinder and the fabric so that the paper or board web remains between the second dryer cylinder surface and the dryer fabric;

wherein the dryer group turning cylinder is a roll comprising a groove-like surface structure and a center shaft or a roll frame, wherein there is contact between the surface structure and the center shaft or roll frame so that a closed construction is formed except for a portion of the roll used for threading a tail;

wherein the turning cylinder roll is arranged with the dryer fabric to produce a vacuum that keeps the paper or board web attached to the dryer fabric at an outer surface within the wrap area of the turning cylinder;

wherein a pocket space is defined between the first contact dryer cylinder, the second dryer cylinder, the turning cylinder roll, and the fabric, and wherein a runnability component system is positioned within the pocket;

wherein the runnability component system has a lower portion arranged so that air is drawn from the runnability component system in to the grooves of the turning cylinder roll; and

wherein the pocket space is arranged to allow air from the grooves of the turning cylinder roll to pass out of the pocket space.

8. The dryer group of claim **7**, wherein the runnability component system in the pocket space of the dryer group is functionally divided into at least two parts.

9. The dryer group of claim **7**, wherein the runnability component system is arranged to produce a different vacuum in different functional parts utilizing the ejection or suction principle in a blow box.

10. A method of controlling runnability in a dryer group of a paper or board machine having a first contact dryer cylinder, a second dryer cylinder and a grooved turning cylinder positioned therebetween, the method comprising the steps of:

passing a paper or board web over the first contact dryer cylinder with the paper or board web between the first contact dryer cylinder and a dryer fabric;

wrapping the paper or board web around the turning cylinder supported by the dryer fabric to define a wrap area;

wrapping the dryer fabric and the paper or board web to travel over the second dryer cylinder with the paper or board web between the second dryer cylinder and the fabric so that the paper or board web remains between the second dryer cylinder surface and the dryer fabric;

wherein the paper or board web and the fabric travel over a grooved turning cylinder having a groove-like surface structure and a center shaft or a roll frame, wherein there is contact between the surface structure and the center shaft or roll frame so that a closed construction is formed except for a portion of the roll used for threading a tail, and wherein the paper or board web and the fabric travel at a running speed of at least about 1200 meters per minute, and wherein the grooves are selected with a configuration to produce a vacuum of at least about 200 Pa where the paper or board web and the fabric travel over the grooved turning cylinder at said least about 1200 meters per minute;

defining a pocket space between the first contact dryer cylinder, the second dryer cylinder, the turning cylinder roll, and the fabric, and positioning a runnability component system within the pocket;

drawing air from the runnability component system into the grooves of the turning cylinder roll; and

exhausting air from the grooves of the turning cylinder roll outwardly into the pocket space.

11. The method of claim **10** wherein the paper or board web and the fabric travel over the grooved turning cylinder at a running speed of at least about 1400 meters per minute, and wherein the grooves are selected with a configuration to produce a vacuum of at least about 300 Pa.

12. The method of claim **11** wherein the paper or board web and the fabric travel over the grooved turning cylinder at a running speed of at least about 1600 meters per minute, and wherein the grooves are selected with a configuration to produce a vacuum of at least about 400-900 Pa.

* * * * *